

LA-3412-MS

C.3-

REF ID: A66000

PUBLICLY RELEASABLE

Per Dill Polkings FSS-16 Date: 5-1-92

By Markus Lujan CIC-14 Date: 8-21-95

UNCLASSIFIED

# LOS ALAMOS SCIENTIFIC LABORATORY of the

## University of California

LOS ALAMOS • NEW MEXICO

CIC-14 REPORT COLLECTION  
**REPRODUCTION  
COPY**

VERIFIED UNCLASSIFIED

Per EMS 6-21-79

By Markus Lujan CIC-14 8/21/95

## Lectures on Nuclear Thermionic Electric Propulsion for Space

(Title Unclassified)

LOS ALAMOS NATIONAL LABORATORY  
3 9338 00362 4474

UNITED STATES  
ATOMIC ENERGY COMMISSION  
CONTRACT W-7405-ENG-36

REF ID: A66000

APP

UNCLASSIFIED

000000

000000

## LEGAL NOTICE

This report was prepared as an account of Government sponsored work. Neither the United States, nor the Commission, nor any person acting on behalf of the Commission:

A. Makes any warranty or representation, expressed or implied, with respect to the accuracy, completeness, or usefulness of the information contained in this report, or that the use of any information, apparatus, method, or process disclosed in this report may not infringe privately owned rights; or

B. Assumes any liabilities with respect to the use of, or for damages resulting from the use of any information, apparatus, method, or process disclosed in this report.

As used in the above, "person acting on behalf of the Commission" includes any employee or contractor of the Commission, or employee of such contractor, to the extent that such employee or contractor of the Commission, or employee of such contractor prepares, disseminates, or provides access to, any information pursuant to his employment or contract with the Commission, or his employment with such contractor.

All LA...MS reports are informal documents, usually prepared for a special purpose and primarily prepared for use within the Laboratory rather than for general distribution. This report has not been edited, reviewed, or verified for accuracy. All LA...MS reports express the views of the authors as of the time they were written and do not necessarily reflect the opinions of the Los Alamos Scientific Laboratory or the final opinion of the authors on the subject.

Printed in USA. Charge \$5.40. Available from the U. S. Atomic Energy Commission, Technical Information Service Extension, P. O. Box 1001, Oak Ridge, Tennessee. Please direct to the same address inquiries covering the procurement of other classified AEC reports.

000000

000000

~~SECRET~~ LA-3412-MS UNCLASSIFIED  
C-93b, ADVANCED CONCEPTS  
FOR FUTURE APPLICATION -  
CONVERSION DEVICES  
M-3679 (44th Ed.)

LOS ALAMOS SCIENTIFIC LABORATORY  
of the  
University of California  
LOS ALAMOS • NEW MEXICO

Report written: July 1965

Report distributed: July 8, 1966

Lectures on Nuclear Thermionic  
Electric Propulsion for Space

(Title Unclassified)

Compiled

by

Ernest W. Salmi

Classification changed to UNCLASSIFIED  
by authority of the U. S. Atomic Energy Commission,

Per *J. H. Kahn, AEC Wash, 6-20-72*

By REPORT LIBRARY *John Martini, 3-9-73*

UNITED STATES  
ATOMIC ENERGY COMMISSION  
CONTRACT W-7405-ENG. 36

LOS ALAMOS NATL. LAB. LIBS.  
3 9338 00362 4474

UNCLASSIFIED

UNCLASSIFIED

## INTRODUCTION

For the last four or five months, N-5 has been engaged in a system study looking at a thermionic nuclear electric propulsion system. We have been asked to present a series of indoctrination lectures on this subject to members of N-Division and other people in the laboratory interested in advanced propulsion. There are several LAMS documents which should be read along with these lectures to get all the meat, but the lectures should cover the essentials and give you a good feeling for the subject.

As you know, the important components of the system are the power supply, the radiator, the thruster, and the shield. Also, as you know, the lifetime and the specific power of the system determine its relative merit. Each talk will cover an aspect of the system. Also within the limits of the existing trajectory calculations available to us, a particular mission will be examined.

The lectures (arranged in the order and content as presented) were as follows:

1. Thermionic Cell Operation - Introduction
2. Heat Pipe Space Radiators
3. Thrust Motor and Related Systems
4. Key Materials Problems Encountered in Thermionic Reactor Construction
5. Part Two of Physics for Administrators
6. Moving Belt Radiators
7. Thermionic Cells

UNCLASSIFIED

UNCLASSIFIED

~~CONFIDENTIAL~~  
031713

8. Summary and Scaling Laws
9. Thermionic Space Reactors
10. Integrated System
11. Shielding
12. Manned Mars Mission Studies and Propulsion Time Requirements
13. Summary

Since the system study continued during the course of the lectures, it will be possible to find minor discrepancies in the numbers from one chapter to another. In addition, there will be specific points throughout on which one could debate at length. It is the general content which is of primary value and we hope this indoctrination series will stimulate further intensive effort in this field.

Los Alamos, New Mexico  
April 12 - July 6, 1965

UNCLASSIFIED

031713<sup>4</sup>

REF ID: A66666

UNCLASSIFIED

## TABLE OF CONTENTS

	<u>Page</u>
1. Thermionic Cell Operation - Introduction, Walter H. Reichelt . . . . .	9
2. Heat Pipe Space Radiators, Theodore P. Cotter . . . . .	17
3. Thrust Motor and Related Systems, T. F. Stratton . . . . .	26
4. Key Materials Problems Encountered in Thermionic Reactor Construction, William A. Ranken . . . . .	67
5. Part Two of Physics for Administrators, Ernest W. Salmi . . . . .	110
6. Moving Belt Radiators, Charles A. Fenstermacher . . . . .	127
7. Thermionic Cells, Walter H. Reichelt . . . . .	144
8. Summary and Scaling Laws, Ernest W. Salmi . . . . .	170
9. Thermionic Space Reactors, Richard C. Anderson . . . . .	191
10. Integrated System, Albert W. Blackstock . . . . .	203
11. Shielding, Samuel Robert Skaggs . . . . .	214
12. Manned Mars Mission Studies and Propulsion Time Requirements, Ernest W. Salmi and C. Dexter Sutherland . . . . .	223
13. Summary, George M. Grover . . . . .	238

REF ID: A66666

UNCLASSIFIED

~~CONFIDENTIAL~~ **CONFIDENTIAL**

LECTURES ON NUCLEAR THERMIONIC ELECTRIC PROPULSION  
FOR SPACE

7-8

**CONFIDENTIAL**

~~CONFIDENTIAL~~  
SECRET

## 1. Thermionic Cell Operation - Introduction

Walter H. Reichelt

In the following discussion, we are going to avoid some of the subtleties of thermionic conversion such as ionization processes and absorption mechanisms. We shall only be concerned with some of the more elementary descriptions of the physical processes involved.

The thermionic energy converter we will discuss is basically a cesium vapor-filled envelope which contains a hot emitter emitting electrons into a plasma and a cooler collector collecting electrons from the plasma. The emitter and collector are connected through an external circuit containing the load. Figure 1.1 illustrates a typical motive diagram for the converter electrons. Consider the emitter side of the diagram.  $\phi_e$  is the work function of the emitting surface. It could be that the surface is of bare, clean metal or has cesium, oxygen or other substance adsorbed on it. In the former case we will use the terminology "bare work function" while in the latter we will refer to the "effective work function" of the surface. When the emitter is heated, enough thermal energy is given to the electrons to enable appreciable numbers to escape from the surface. The Richardson equation describes this electron emission from a surface:

$$J = A T^2 e^{\frac{-\epsilon\phi}{kT}}$$

where

J is the electron current from the surface in amps/cm<sup>2</sup>

A is a constant

SECRET



CONFIDENTIAL

T is the emitter temperature  
 $\phi$  is the surface work function  
 $e$  is the electron charge  
 k is Boltzmann's constant.

The potential distribution in the interelectrode gap is characterized by an emitter sheath, plasma loss, and collector sheath. When the electrons enter the collector they lose energy to the collector equal to the collector work function,  $\phi_c$ , just as they take away energy equal to  $\phi_e + 2kT$  when leaving the emitter. The output voltage of the device is just the potential difference between the Fermi levels of the emitter and collector.

Cesium vapor in the cell serves several purposes:

1) It provides the source of positive ions necessary to reduce the electron space charge in the diode. Neutral cesium atoms are ionized at the emitter surface by contact ionization or in the interelectrode gap by volume ionization.

2) Adsorbed cesium on the collector surface reduces the collector work function to a value between that for the bare metal and that for bulk cesium:

$$\phi_{\text{metal}} \geq \phi_{\text{metal}} + \phi_{\text{cs}}$$

This results in an increased output voltage.

3) Adsorbed cesium on the emitter can also change its work function to advantage. As with the collector, adsorbed cesium can reduce the emitter work function, which results in increased cell currents.

The dependence of the effective work function of a tungsten emitter on cesium pressure and emitter temperature in a diode is shown in Fig. 1.2. The vacuum work function of bare tungsten is about 4.6 - 4.8 volts. As the emitter temperature is increased, the effective work function approaches that of the bare metal. As the temperature

10

~~CONFIDENTIAL~~

increases, the lifetime of the cesium on the surface decreases until, at a high enough temperature, the base metal is free of adsorbed atoms. If a diode were constructed with a tungsten emitter and collector to operate at 8 torr cesium pressure, the emitter work function would be 3.1 for a temperature of 2100°K. For a collector temperature of 1200°K, the collector work function would be 1.7 volts. We would have 18 amps/cm<sup>2</sup> electron emission from the emitter surface.

Because of the extreme pressure dependence of the effective work function of a tungsten surface, we might ask, "Does cesium pressure have the same effect on all materials considered for thermionic emitters?" The answer is no! Figure 1.3 illustrates the influence of cesium pressure on two diodes. One diode has a tungsten emitter representing high-valued, bare work function materials while the other has a uranium carbide emitter representative of low- or intermediate-valued, bare work function materials. The power output is given as a function of cesium pressure for the cell conditions indicated. It is immediately evident that cesium pressure has no significant influence on the uranium carbide emitter, while the changes are quite significant for the tungsten emitter. This latter dependence reflects the changing effective work function of the tungsten surface with cesium pressure as shown in Fig. 1.2.

The next figure, Fig. 1.4, indicates the effect of interelectrode spacing on cell output for the two emitters. As in the case of the cesium pressure, the influence of spacing is insignificant for the uranium carbide emitter while large for the tungsten emitter. We'll comment on this later.

Figure 1.5 illustrates the dependence of power output on emitter temperatures. The upper curve is that taken for a tungsten emitter with the collector temperature and cesium pressure optimized for maximum power output at each emitter temperature. The lower curve is that taken with a uranium carbide emitter. It should be noted that the cell spacings are quite different. In general, the high power outputs for the refractory

12  
~~CONFIDENTIAL~~

~~CONFIDENTIAL~~

~~CONFIDENTIAL~~  
03110

metals occur at high current densities -- of the order of 50 amps/cm<sup>2</sup> or higher. At these currents, the diode is not operating at maximum efficiency.

The tungsten emitters and other high, bare work function materials rely on cesium coverage to get reasonable power outputs. To maintain this coverage at normal emitter temperatures, it is necessary that the cesium pressure be high -- much higher than that necessary to supply ions for space charge neutralization. To avoid electron scattering and other losses at these high pressures, it is essential that the cell spacings be small. Reasonable cell outputs can be expected for the refractory metal emitters at spacings of 5 to 10 mils.

Up to this point we have considered some general properties of cesium diodes. Now we shall deal with a more specific topic: surface phenomena. This subject is of great importance for thermionic diodes. Possessing high melting points and low vapor pressures, the refractory metals are good candidates for emitters; and we might inquire into the differences between them. Figure 1.6 illustrates some of the differences. On this figure is plotted the effective work function versus the vacuum work function for several cesium pressures. The arrows indicate the bare work functions for the various refractories. If the work function of the surface were independent of cesium coverage, we would expect the effective work function to be equal to the bare work function, and the curve would have a slope of one. This is the case for the uranium carbide emitter. For the refractories which depend on cesium coverage, the trend is obvious. The higher the bare work function of a surface, the lower the effective work function when immersed in cesium vapor. This figure does not reveal the effects of surface structure. In general, surfaces are polycrystalline in nature, each crystal face having a different, characteristic work function. The data indicated in this figure are generally true and hold specifically for single crystal surfaces. The crystal planes having the highest vacuum work function will yield the highest electron emission when put in cesium vapor.

12  
03110

~~CONFIDENTIAL~~  
APPROVED FOR PUBLIC RELEASE

~~CONFIDENTIAL~~

SECRET

This leads into another requirement for emitters. It would be advantageous to have a surface with a uniform work function of the highest value. Considerable progress has been made in producing uniform surfaces by such techniques as etching and vapor deposition.

Within limits, cell output can be increased by reducing the collector work function. A good deal of effort has been extended in this area. Oxide coatings, for example, have been used in many instances. The results are rather startling; an oxide coating on a nickel collector revealed a work function of 1.13 volts compared with 1.8 volts for bulk cesium. Unfortunately, these coatings have proven unstable in the temperature and pressure ranges of interest.

Another means for advantageously altering the surface work function is through the use of additives such as CsF and barium. As has been indicated in the figures, we can already achieve rather high power densities. However, these are generally obtained at fairly close spacing. Additives permit the loosening of the tight spacing requirements.

The addition of CsF to an operating cell<sup>1</sup> has been used successfully to increase the power output of a molybdenum emitter from 7.2 to 24 watts/cm<sup>2</sup> at an emitter temperature of 2000°K and a cell spacing of 0.1 mm. With CsF it is possible to get the 7.2 watts/cm<sup>2</sup> at a spacing of 0.4 mm (compared to 0.1 mm without CsF). This increase in spacing make fabrication problems much easier. While the effects of CsF are quite good, one problem remains: that is the long-term corrosion effects in the cell of the F component. Tests in N-5 indicate that this could be rather serious.

Recently, there have been some data available on the addition of barium to an operating cell.<sup>2</sup> Apparently, adsorbed barium lowers the work function of the emitter surface to the point where cesium coverage of the emitter is not required. Operation is similar to that of a uranium carbide emitter; cesium in the cell merely provides the source for ions for space-charge neutralization. Consequently, lower cesium

SECRET

~~CONFIDENTIAL~~

~~CONFIDENTIAL~~

pressures can be used and the cell spacing can be opened up. Figure 1.7 illustrates the dependence of power output on spacing of two cesium cells, one with barium and one without. The power output of the cell without barium drops rather rapidly, while the output of the cell with barium stays fairly constant over the whole range of spacings.

Some of the remarks and figures used in the preceding text were taken from a paper given at the Third United Nations International Conference on the Peaceful Uses of Atomic Energy.<sup>3</sup>

#### References

1. A. Jester, Proceedings of the Thermionic Conversion Specialist Conference, p. 93, Cleveland, Ohio (Oct. 1964).
2. J. Psarouthakis, *ibid*, p. 100.
3. E. Salmi, et al., "Thermionic Diodes for Direct Conversion Reactors," presented at the Third United Nations International Conference on the Peaceful Uses of Atomic Energy, Geneva (Sept. 1964).

124  
CONFIDENTIAL

CONFIDENTIAL

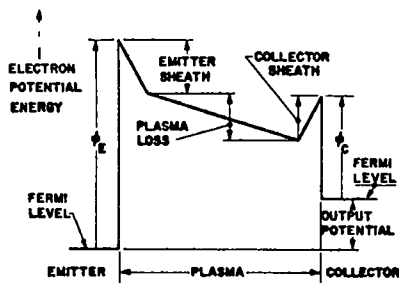


Fig.1.1. Thermionic Converter Potential Diagram

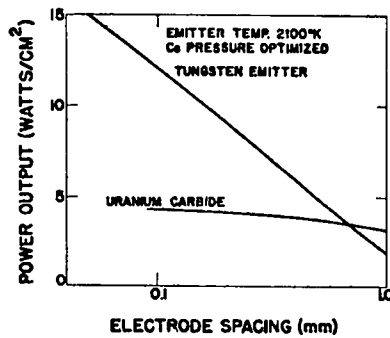


Fig.1.4. Power Output vs Electrode Spacing With 2100°K Emitter Temperature and Optimized Cesium Pressure

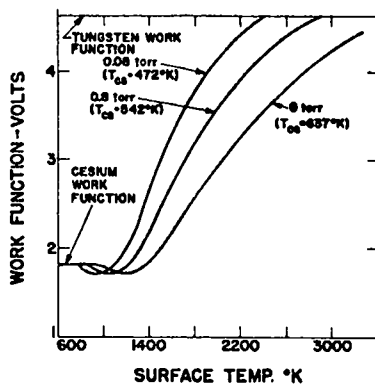


Fig.1.2. Tungsten Effective Work Function vs Temperature For Several Cesium Pressures

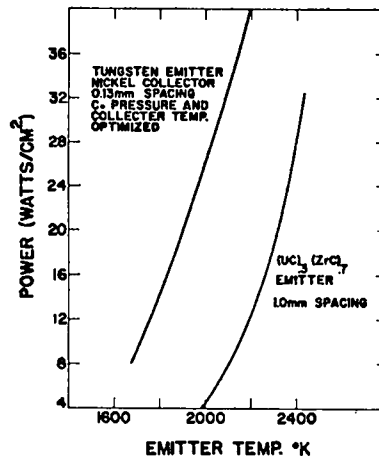


Fig.1.5. Power Output vs Emitter Temperature, 0.13 mm Electrode Space, Collector Temperature and Cesium Pressure Optimized

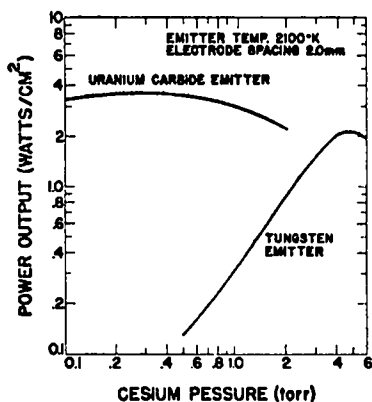


Fig.1.3. Power Output vs Cesium Pressure at 2100°K Emitter Temperature and 2.0 mm Electrode Spacing

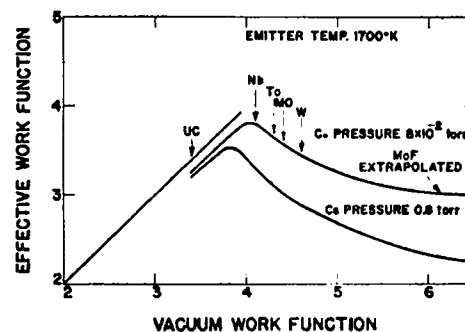


Fig.1.6. Effective Work Function vs Vacuum Work Function for Various Cesium Pressures

CONFIDENTIAL

03115

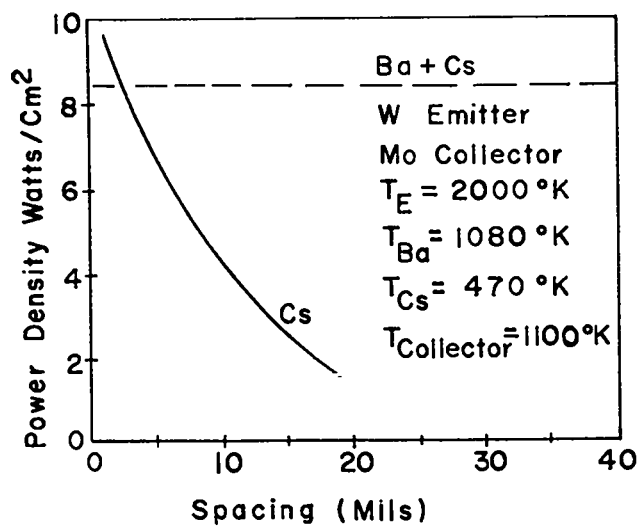


Fig. 1.7 Output Power Density  
Versus  
Interelectrode Spacing

03115

## 2. Heat Pipe Space Radiators

Theodore P. Cotter

Heat pipes are a general class of self-contained structures which achieve very high thermal conductance by means of two-phase flow and capillary circulation of a working fluid.<sup>1,2</sup> The potential advantages of the application of the heat pipe principle to the construction of low-mass space radiator systems come from its quite unique qualitative features. A heat pipe may be a nearly empty cavity transporting heat at almost uniform temperature, unrestricted in size and geometry, and capable of arrangement with other heat pipes in a variety of combinations of series and parallel. These properties suggest: first, that the maximum statistical advantage can be obtained from system redundancy in a direct and simple way; and second, that the bumper method of meteoroid protection can be employed without practical decrease of radiator efficiency.<sup>3</sup>

The estimate of the specific power of any space radiator system using circulating fluid is strongly dependent on the mass of armor required for protection against penetrating meteoroids. The present knowledge of the spatial, mass, velocity, and material density distributions of meteoroids is rather imprecise.<sup>4</sup> Further, the "scaling laws" for penetration of a target by a hypervelocity projectile in the ranges of variables appropriate to the meteoroid problem is, at present, so much conjectural that there is not even agreement about precisely which material properties and dynamical processes enter into these hypothesized



CONFIDENTIAL

laws.<sup>5</sup> We believe that estimates of armor mass using current data and theory are subject to uncertainties of at least a factor of two. In consequence, the comparison of alternative radiator systems which differ in basic principle, or even the assessment of the relative merits of alternative materials or configurations for a single type of radiator should not be accepted uncritically.

We give here some general design considerations for heat pipe space radiators, and preliminary semi-quantitative estimates for a case of current interest.

The total mass of the radiator,  $M$ , is the sum of the masses of the heat transport structure,  $M_h$ , and the meteoroid armor,  $M_a$ . The mass of vapor is assumed to be negligible. The size of the power supply will ordinarily be small compared to the size of the radiator. In good approximation we may then assume that all the heat travels radially (but not necessarily symmetrically) out from the power supply, which is regarded essentially as a point source of heat. We then need be concerned only with two geometrical properties of the radiator:  $A_c(r)$ , the total heat transport cross section at distance  $r$  from the power supply; and  $A_s(r)$ , the total radiator surface area lying at distance greater than  $r$  from the power supply. If  $\bar{\rho}$  is the mean density of heat transport structure, and  $\rho_a$  and  $\delta_a$  the density and thickness, respectively, of the meteoroid armor, we then have:

$$M_h = \int \bar{\rho} dv = \int \bar{\rho}(r) A_c(r) dr \quad (2.1)$$

$$M_a = \int \rho_a \delta_a dA = \rho_a \int \delta_a(r) dA_s \quad (2.2)$$

Our task is to determine  $\bar{\rho}$  and  $\delta_a$  so as to obtain a radiator of minimum total mass, subject to various system and mission requirements which will be introduced as we proceed.

In order to obtain the benefits of redundancy, the radiator must have a considerable number of heat pipes in parallel, so that the random

CONFIDENTIAL

CONFIDENTIAL

~~CONFIDENTIAL~~  
CONFIDENTIAL

puncture of some fraction of the pipes can be tolerated. (If the pipes are supplied with heat from a common, well-armored, intermediate heat exchanger, the only deleterious effect of the puncture of a pipe will be the loss of its working fluid to space, upon which it will cool and no longer contribute as a radiating element.)

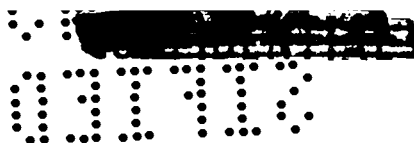
Several important advantages are obtained if the heat pipes are arranged in series as well as in parallel, so that the radiator has, in fact, a cellular structure. The immediate benefit is a decrease in the mass of capillary structure required for circulation of the working fluid, based on the following reasoning. The total pressure drop available within a single pipe for circulation of the vapor and liquid is fixed by the capillary pore size and the surface tension of the liquid. The pressure drop in the liquid is proportional to the total heat transport and to the length of the pipe, and inversely proportional to the cross sectional area of the wick, normal to the direction of liquid flow. For the same total heat transport, a short pipe may have a smaller wick cross section than a long pipe and, therefore, a smaller mass of wick per unit length.

If pipes are placed in series the heat must, of course, be transferred from one to another by ordinary conduction through the end walls. The resulting temperature drops are to be made small by using thin end walls. Furthermore, since there will be vapor condensation on one side of an end wall and evaporation on the other, this implies a drop in the pressure of the vapor from pipe to pipe. These are important effects which must be included in an accurate calculation. We will neglect them, however, in our present preliminary estimate.

In a cellular radiator the puncture of a cell should not cause a significant reduction in the temperature of those cells further from the power supply in the same series, for there will then be a compensating cross-flow of heat to them from their parallel neighbors.

The cell shapes must permit a volume-filling packing; but, for present convenience and with sufficient accuracy, we assume them to be

CONFIDENTIAL



right circular cylinders of diameter,  $d$ , and length,  $\ell$ . The wick is assumed to consist of grooves of equivalent capillary radius,  $r_c$ , parallel to the direction of liquid flow, in a wall of thickness  $\delta$ . If  $\ell/d$  is not large we may neglect the pressure drop in the vapor compared to total viscous pressure drop in the liquid,  $\Delta p_\ell$ . The limiting heat flux through the end wall of the cylinder,  $q$ , is determined by the condition:  $\Delta p_\ell = \gamma/r_v$ , where  $\gamma$  is the surface tension of the liquid. Accounting for both the radial liquid flow on the cylinder end and axial flow along the side we have:

$$\Delta p_\ell = \frac{b\eta d^2 q}{\rho \delta r_c^2 L} \left(1 + \frac{2\ell}{d}\right) = \frac{\gamma}{r_c} \quad (2.3)$$

where  $\eta$ ,  $\rho$  and  $L$  are, respectively, the viscosity, density and heat of vaporization of the liquid, and  $b$  is a dimensionless factor of order 2 to 4, which depends on the groove shape. According to this expression the limiting heat flux is proportional to  $r_c$ , so that the groove width should be large. We shall set  $r_c = \delta/2$ , as this is the largest that is geometrically possible. Then (2.3) can be written

$$q = \frac{q^*}{1 + \frac{2\ell}{d}} \left(\frac{\delta}{d}\right)^2 \quad (2.4)$$

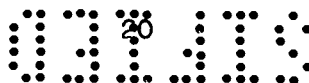
where  $q^* = \rho \gamma L / 2b\eta$  is a characteristic property of the working fluid with the units of heat flux. The very large magnitude of this  $q^*$  is chiefly responsible for the unique heat transport properties of heat pipes. For example, for lithium at  $900^\circ\text{C}$ ,  $q^* \approx 500$  megawatts/cm<sup>2</sup>.

The mean density of a cell is

$$\bar{\rho} = 2\rho_w \frac{\delta}{\ell} \left(1 + \frac{2\ell}{d}\right) \quad (2.5)$$

where  $\rho_w$  is the average density of the saturated wick.

Assuming that the flux of radiation from the external surface,  $q_R$ , is uniform over the radiator, then



$$q(r)A_c(r) = q_R A_s(r) \quad (2.6)$$

Using (2.4), (2.5) and (2.6) in (2.1) then yields

$$M_h = 2\rho_w \left( \frac{q_R}{q^*} \right)^{1/2} \int \frac{(1+2\ell/d)^{3/2}}{\ell/d} (A_c A_s)^{1/2} dr \quad (2.7)$$

In the integral, the factor  $(1+2\ell/d)^{3/2}/(\ell/d)$  has a minimum value of  $3^{3/2}$  for  $\ell = d$ . (One would expect that  $\ell > d$  for the optimum cell shape when the effects of temperature gradients are included in the analysis.) According to (2.7) the mass is minimized by making the radiator cross section  $A_c(r)$  as small as possible, but there are two limitations on the extent to which this can be done. First, there is a wick thickness which is the minimum that is feasible to fabricate,  $\delta_{\min}$ . Second, heat pipes are observed to develop hot spots and subsequent failure at heat fluxes through the wick in excess of a critical value,  $q_{\max}$ . (What in quantitative detail determines  $q_{\max}$  is not yet understood.) From (2.4) with  $\ell = d$ ,  $d$  thus has a minimum possible value determined by

$$q_{\max} = \frac{q^*}{3} \left( \frac{\delta_{\min}}{d} \right)^2 \quad (2.8)$$

and  $A_c$  a minimum value, using (2.6), of

$$A_c(r) = \frac{q_R}{q_{\max}} A_s(r) \quad (2.9)$$

Letting the total radiator power be  $Q$  and radiator area  $A$ , we then find

$$\frac{M_h}{Q} = \frac{M_h}{q_R A} = \frac{2 \cdot 3^{3/2} \rho_w \ell_R}{(q^* q_{\max})^{1/2}} \quad (2.10)$$

where  $\ell_R$  is the first moment of the radiating area about the power supply:

03110

$$\ell_R = \frac{1}{A} \int A_s(r) dr \quad (2.11)$$

Taking as a case of interest the following

$$\begin{array}{ll} Q \sim 20 \text{ MW} & T \sim 900^\circ\text{C} \\ q^* \sim 500 \text{ MW/cm}^2 & A \sim 250 \text{ m}^2 \\ q_R \sim 8 \text{ W/cm}^2 & \ell_R \sim 6 \text{ m} \\ q_{\max} \sim 500 \text{ W/cm}^2 & \rho_w \sim 2 \text{ gm/cm}^2 \end{array}$$

we estimate

$$\begin{array}{l} M_h \sim 0.02 \text{ to } 0.03 \text{ kg/kW} \\ d/\delta \sim 500 \text{ to } 1000 \\ \text{Volume} \sim 25 \text{ m}^2 \end{array}$$

If  $\delta_{\min} \sim 0.02 \text{ cm}$ , for example, then  $d \sim 10 \text{ cm}$ , and there would be a total of 25,000 cells in the radiator.

The armor might consist of a single layer; or, what is better but more difficult to analyse, the thickness  $\delta_a$  might be apportioned optimally between an outside protective bumper and the armor proper inside, with heat pipe wick and vapor spaces between the two. In the single layer case, the relation between the armor thickness and the flux of penetrating meteoroids,  $v$ , is usually described by a power law<sup>4</sup>

$$v = K \delta_a^{-k} \quad (2.12)$$

where  $K$  and  $k$  are empirical constants. The probability,  $p_1$ , that an individual pipe will survive penetration for a time,  $t$ , follows the Poisson distribution

$$p_1 = e^{-\frac{vAt}{N}} \quad (2.13)$$

03110

03110

~~CONFIDENTIAL~~  
 0110

The probability,  $p_m$ , that exactly  $m$  out of the  $N$  original pipes will survive is given by the binomial distribution

$$p_m = \binom{N}{m} p_1^m (1-p_1)^{N-m} \quad (2.14)$$

Then, the probability  $P_f$  that a fraction  $f$ , or more, of the original pipes will survive is given by the cumulative binomial distribution

$$P_f = \sum_{m=fN}^N p_m \quad (2.15)$$

The relation between  $P_f$  and  $\delta_a$  expressed by the equations (2.12) through (2.15) is too complex for direct use. We therefore obtain a simpler relation of adequate accuracy by several approximations. The distribution (2.14) has mean,  $\bar{m}$ , and variance  $\sigma^2$ :

$$\bar{m} = p_1 N; \quad \sigma^2 = p_1 (1-p_1) N \quad (2.16)$$

If  $N = \bar{m} > \sim 5$ , then (2.14) is not much different from the normal distribution with the same mean and variance, and we approximate (2.15) by the cumulative normal distribution

$$P_f = \frac{1}{\sqrt{2\pi}\sigma} \int_{fN}^{\infty} e^{-(m-\bar{m})^2/2\sigma^2} dm = \frac{1}{\sqrt{2\pi}} \int_{-\beta}^{\infty} e^{-\chi^2/2} d\chi \quad (2.17)$$

$$\beta = \frac{\bar{m} - fN}{\sigma} \quad (2.18)$$

Then  $\beta(P_f)$  is defined by (2.17). Some values of this function are:

$P_f$	0.80	0.90	0.95	0.98	0.99
$\beta(P_f)$	0.84	1.28	1.65	2.05	2.33

23  
 0110

~~CONFIDENTIAL~~

CONFIDENTIAL

Using (2.16) in (2.18) and solving for  $p_1$ , with the neglect of terms of order  $\beta^2$  compared to  $fN$ , one obtains

$$p_1 = f + \beta \sqrt{\frac{f(1-f)}{N}} \quad (2.19)$$

Expanding (2.13) to first order in the exponent and eliminating  $p_1$  and  $v$  from (2.12), (2.13) and (2.19), yields the desired expression for the armor thickness

$$\delta_a = \left[ \frac{KAt}{(1-f)N - \beta \sqrt{f(1-f)N}} \right]^{1/k} \quad (2.20)$$

Several features of the armor requirement for a multiple-segment redundant radiator are in favorable contrast to that of an unsegmented radiator, for which the expression equivalent to (2.20) is

$$\delta_a = \left[ \frac{KAt}{1-p_1} \right]^{1/k} \quad (2.21)$$

The leading term in the denominator of (2.20) is the dominant one, so that the armor thickness depends on the amount of redundancy,  $1-f$ , and the number of segments,  $N$ , both of which can be made large somewhat at the discretion of the designer. The allowed failure probability affects the thickness only weakly in the second term of the denominator, through the factor  $\beta(P_f)$ . The thickness of the unsegmented radiator, on the other hand, depends directly and fairly sensitively on the allowed failure probability,  $1-P_1$ . Conversely, however, an error in the estimate of the actual puncture rate in space has only a small effect on the survival probability of an unsegmented radiator, but a large effect on the survival probability of the redundant radiator. There is an important operational compensation for the latter. For the unsegmented radiator, the mean time between punctures will ordinarily be long compared to the mission time. An actual mission either succeeds or fails, neither of which events has much predictive value. For the redundant radiator, the mean time between punctures will be short compared to the mission time. An improved

CONFIDENTIAL

CONFIDENTIAL  
 0110

estimate of this quantity could, therefore, be obtained by measurement during the actual mission for use as the basis of an operational decision.

The optimum amount of redundancy depends on the whole radiator system. We may obtain a rough estimate of the optimum by considering the armor only. The armor mass is proportional to  $A\delta_a$ . If the supply power is fixed, as well as the maximum operating temperature of the radiator, then the product  $fA$  is fixed. Using the dominant term of (2.20), together with Whipple's estimate,  $k = 4$ , the armor mass must then be proportional to  $f^{-5/4}(1-f)^{-1/4}$ . This expression has a minimum for  $f = 5/6$ .

Taking as a case of interest the following

$A = 250 \text{ m}^2$	$N = 25,000$
$t = 1 \text{ yr}$	$P_f = 0.95$
$K = 1.5 \times 10^{-7} \text{ cm}^4/\text{m}^2 \text{ yr}$	$k = 4$
	$f = 5/6$

we find that  $\delta_a \sim 0.01 \text{ cm}$ , which for a 20-MW power supply implies  $M_a/Q \sim 0.01 \text{ kg/kW}$ .

#### References

1. G. M. Grover, T. P. Cotter, and G. F. Erickson, "Structures of Very High Thermal Conductance," J. Appl. Phys. 35, 1990 (1964).
2. T. P. Cotter, "Theory of Heat Pipes," LA-3246-MS.
3. F. L. Whipple, "The Meteoritic Risk to Space Vehicles," in "Vistas in Astronautics," Vol. 2, pp. 115-124, Pergamon Press, New York, 1958.
4. J. B. Neiger, "Physical Impact Phenomena," Chapter 8, "Space Materials Handbook," ML-TDR-64-40.
5. Proceedings of the Sixth Symposium on Hypervelocity Impact, Volume III, August, 1963.

25  
 0110



~~CONFIDENTIAL~~  
03713

## 3. Thrust Motor and Related Systems

T. F. Stratton

Introduction

The acceleration of plasmas to high velocity through an interaction with a magnetic field is in competition with electrostatic acceleration of ions as a method for propelling spacecraft. Electrostatic acceleration processes are well understood; and, consequently, ion engines are in a relatively advanced state of development. Cesium is a favorite material for electrostatic acceleration devices because of the high efficiency and ease of operation which exists by virtue of the circumstance that cesium atoms are ionized on leaving a hot, high work function surface. Subsequent focusing and acceleration of the ions in appropriate grid and electrode structures have been abundantly demonstrated. Most present work on electrostatic propulsion devices is concentrated on problems of long life, refinement of existing designs, and improvement in the operating efficiency. A principal defect of most electrostatic motors is associated with the fact that high direct current voltage is required to accelerate the ions. The weight of the appropriate power conversion equipment has so far proven to be excessive.

On the other hand, plasma propulsion engines are in a very early state of development and understanding. It is only appropriate to comment that the acceleration of plasma to velocities of interest with efficiencies which are competitive with electrostatic motors has not yet been conclusively demonstrated. There are reasons to believe, however,

03713<sup>26</sup>~~CONFIDENTIAL~~

SECRET

that magnetic plasma accelerators will eventually replace electrostatic systems, and some of these reasons are listed as follows:

1) The problem of neutralization of the emergent exhaust stream is automatically solved with plasma motors.

2) The thrust per unit area of motor is substantially greater for a magnetic motor than for an electrostatic (ion) engine. The advantage arises because of the following circumstance: the pressures exerted on a charged plate by an electric field and on a current sheet by an adjacent magnetic field are, respectively,  $E^2/8\pi$  and  $B^2/8\pi$  (in cgs units). Comparing pressures for typical large, but attainable values of  $E$  and  $B$ , we have Table 3.1.

Table 3.1

COMPARISON OF ELECTROSTATIC AND MAGNETIC PRESSURES

<u>E V/cm</u>	<u><math>E^2/8\pi</math> dynes/cm<sup>2</sup></u>	<u>B gauss</u>	<u><math>B^2/8\pi</math> dynes/cm<sup>2</sup></u>
10000	40	10000	$4 \times 10^6$

Expressed in other terms, the area required for the development of one pound of thrust from an electrostatic engine is about  $10^4$  cm<sup>2</sup>, i.e. one square meter. Well-developed plasma (magnetic) engines will deliver the same one pound from 0.1 cm<sup>2</sup>.

3) The class of magnetic engines designated as high-current, steady state arcs is specifically indicated as the most promising type of magnetic motor.<sup>1, 2, 3</sup> The reported efficiency of such motors far exceeds that of any other type; and the direct current, low-voltage power output of the thermionic reactor can be matched exactly to the plasma engine characteristic without addition of power conditioning equipment.

The following discussion shows that the selection of an optimum exhaust velocity for a maximum payload-to-initial mass ratio is intimately connected to the power-to-mass ratio of the power supply and engine

CONFIDENTIAL

03113

system. A mean-square velocity of the exhaust gas which is much in excess of the joules/kg available from the power supply results in a reduction of the payload fraction, particularly if the velocity increment of the spacecraft is a substantial fraction of the exhaust velocity.

The thrust developed by an engine may be expressed as

$$F = \dot{M} \langle v \rangle \quad (3.1)$$

where  $\dot{M}$  is the total mass flow-rate and  $\langle v \rangle$  is the average exhaust velocity. Taken alone, (3.1) would tend to imply that one should strive for as large a  $\langle v \rangle$  as possible in order to reduce the propellant mass. However, when consideration is also given to power expended in the propellant stream,

$$P = 1/2 \dot{M} \langle v^2 \rangle \cong 1/2 F \langle v \rangle \quad (3.2)$$

it is clear that large exhaust velocity means greater engine power, and power supply weight, for the same thrust.

The payload fraction for a power-limited propulsion system in gravity-free space is given by the relation<sup>4</sup>

$$\frac{M_L}{M_0} = e^{-u/v} - \frac{\alpha v^2}{2\eta_m t} (1 - e^{-u/v}) \quad (3.3)$$

where  $M_L/M_0$  is the payload fraction,  $u$  is vehicle speed at the end of the propulsion period of duration  $t$ ,  $v$  is the exhaust velocity,  $\eta_m$  is the efficiency with which electrical power is converted into "kinetic" energy in the propellant stream, and  $\alpha$  is the ratio of the mass of the power supply and propulsion engine to the available electric power. Equation (3.3) describes the characteristic in gravity-free space of a vehicle of mass  $M_0 = (M_P + M_F + M_L)$  at time zero (where  $M_P$  is the power plant propulsion system mass,  $M_F$  is the mass of the fuel, and  $M_L$  is the payload), and of mass  $(M_P + M_L)$  traveling with velocity increment  $u$  at

28

03113

SECRET

time  $t$ . The ratio  $\alpha$  is  $M_p/P_E$ , and the power in  $1/2 \dot{M} v^2$  is  $\eta_m P_E$ . Substituting  $x = u/v$  and  $u^2 = k \eta_m t / \alpha$  into (3.3), and letting  $M_L/M_O = f$ , we obtain:

$$f = e^{-x} - \frac{k}{2x^2} (1 - e^{-x}) \quad (3.3')$$

Differentiation of (3.3') shows a maximum in  $f$  which occurs at a value  $k = 2x^2$  in the limit  $x \rightarrow 0$ . Values of  $k/x^2$  which maximize  $f$  for larger values of  $x$  are plotted in Fig. 3.1. The variation of the ratio  $k/x^2$  which maximizes the payload fraction for values of  $x > 0$  is small; and, to good approximation,  $k/x^2$  may be set equal to 2. Therefore, the optimum exhaust velocity for a power-limited propulsion system is

$$v \approx \sqrt{2\eta_m t / \alpha} \quad (3.4)$$

The optimum exhaust velocity derived from (3.4) is plotted as a function of  $\eta_m/\alpha$ , with  $t$  as a parameter, in Fig. 3.2. Clearly,  $5000 \leq I_{sp} \leq 10000$  is indicated for optimum payload fraction. The only possible way of attaining such a large velocity in the exhaust stream is through some sort of electrical scheme.

#### Plasma Motor Performance

A detailed discussion of the coaxial arc plasma accelerator is the subject of the Appendix to this chapter. Further amplification of certain features of the performance of the arc accelerator is presented in the form of graphs showing efficiency, mass flow rate, thrust, and arc current and voltage as a function of  $I_{sp}$ . In this discussion lithium is chosen as the expellant fluid.

The efficiency of the magnetic plasma accelerator is given by the ratio of the power in the directed flow of the emergent propellant to the power input to the accelerator. Factors contributing to an efficiency of less than one are: the energy necessary to ionize the propellant, the energy in transverse (thermal) motion, and the kinetic energy

29  
SECRET

~~CONFIDENTIAL~~

031713

of electrons entering the arc anode (anode fall). Reasonable values for these parameters are:

Li ionization potential: 5.4 eV

$v_{\perp} = 1/2 v_{\parallel}$  ( $M^* = 2$ );  $W_{\perp} = 1/4 W_{\parallel}$

Potential through anode fall: 5 eV

The arc current is carried by ions in the plasma arc accelerator, and the arc power is

$$P_{\text{arc}} = I (W_{\parallel} + 1/4 W_{\parallel} + 10.4) \text{ watts} \quad (3.5)$$

where  $W$  is the directed energy of the emerging ions in eV. The accelerator efficiency,  $\eta$ , is

$$\eta = W_{\parallel} / (W_{\parallel} + 1/4 W_{\parallel} + 10.4) \quad (3.6)$$

which is plotted as a function of specific impulse in Fig. 3.3. For comparison, the efficiency of a hydrogen arc accelerator with appropriate values for the hydrogen potential and the anode fall is also plotted.

The arc current, voltage, and power in a lithium plasma accelerator are related to the  $I_{\text{sp}}$  by the following equations:

$$I = 3.5 I_{\text{sp}} \text{ amps} \quad (3.7)$$

$$V = 10.4 + 4.37 (I_{\text{sp}}/1000)^2 \text{ volts} \quad (3.8)$$

$$P = 0.0364 (I_{\text{sp}}/1000) + 0.0153 (I_{\text{sp}}/1000)^3 \text{ megawatts} \quad (3.9)$$

Arc current and voltage are plotted as a function of  $I_{\text{sp}}$  in Fig. 3.4. Arc power is plotted in Fig. 3.5 for both lithium and hydrogen expellant.

The mass flow rate,  $M$ , is related to the specific impulse through the arc current. The arc current is carried by ions between the anode sheath and the virtual cathode, and it is therefore necessary to supply

30  
031713~~CONFIDENTIAL~~

~~CONFIDENTIAL~~  
SECRET

sufficient heavy charge carriers (ions) to avoid starving the arc. Arc starvation results in serious electrode erosion. The lithium mass flow rate is given by

$$\dot{M} = 0.264 \times 10^{-3} I_{sp} \text{ g/sec} \quad (3.10)$$

where  $I_{sp}$  is the specific impulse in seconds, and is plotted as a function of  $I_{sp}$  in Fig. 3.6. The arc current, arc voltage, and mass flow rate are specified for a given  $I_{sp}$ ; and the mass flow rate for a given  $I_{sp}$  and input power level is properly determined only when the power for each arc engine is an integral submultiple of the total electrical power. For reference, the hypothetical  $\dot{M}$  for 2 MW(e) is plotted as a function of  $I_{sp}$  as the upper curve of Fig. 3.6.

The thrust,  $F$ , is plotted for a single arc motor and for 2 MW(e) (under the same conditions as in Fig. 3.6) as a function of  $I_{sp}$  in Fig. 3.7.

$$F = \dot{M}v = 0.26 (I_{sp})^2 \text{ dynes} \quad (3.11)$$

#### Plasma Motor Design

As indicated on Fig. 3.5, the input power to an arc plasma accelerator is related to the  $I_{sp}$  in a well-defined manner. The design criteria are summarized in Table 3.2.

Table 3.2

#### DESIGN DATA FOR ARC PLASMA ACCELERATORS WITH LITHIUM EXPELLANT

Power	V	I	$\dot{M}$	$I_{sp}$	Thrust	$\eta$	$1/2 \dot{M}v^2$	$P_{anode}$
MW	volts	Ka	g/s	s	dynes	%	MW	kW
0.5	48	10.2	0.76	2900	$2.2 \times 10^6$	0.62	0.31	92
1.0	74	13.3	1.00	3800	$3.7 \times 10^6$	0.69	0.69	120
2.0	114	17.1	1.30	4900	$6.2 \times 10^6$	0.73	1.46	154

31  
SECRET

~~CONFIDENTIAL~~  
APPROVED FOR PUBLIC RELEASE

~~CONFIDENTIAL~~

03113

The accelerator design is governed principally by power density considerations in the anode. Table 3.2 shows that the anode dissipation in a 2MW(e) accelerator is only 1.7 times that in a 0.5 MW(e) engine; and that the anode dissipation per 2 MW(e) at  $I_{sp} = 4900$  sec is 0.42 times that which it is at  $I_{sp} = 2900$  sec. For this reason a possible motor design for 2 MW(e) is examined for lifetime and weight.

Assume that the anode and cathode of the accelerator are tungsten. Also assume that the anode is radiation-cooled and will evaporate 20% of the wall material in 5000 hours =  $1.8 \times 10^7$  sec. Also assume that the anode wall thickness is so adjusted that the power in  $I^2R$  heating is 10% of the anode dissipation, i.e., 15 kW. Consider Fig. 3.8. The area of the anode through which the anode dissipation takes place is  $2\pi a^2$ . The area from which the anode power is radiated is  $7\pi a^2$ . The wall resistance is approximately  $\rho_r/4\pi d$ . The  $I^2R$  heating, 15 kW, then gives

$$d = 1.5 \times 10^3 \rho_r \text{ cm} \quad (3.12)$$

The anode power, 169 kW, is radiated. Hence

$$7\pi a^2 \phi = 169000 \text{ watts} \quad (3.13)$$

where  $\phi$  is the total radiation intensity in watts/cm<sup>2</sup>. The rate of evaporation  $\mu$  must be such that

$$1.8 \times 10^7 \mu / \rho_m = 0.2 d = 0.3 \times 10^3 \rho_r \quad (3.14)$$

The solution of (3.12) and (3.14) gives  $T = 2675^\circ\text{K}$  (see Fig. 3.9). Further, the wall thickness  $d = 0.12 \text{ cm} = 0.047 \text{ in.}$ , and the radiation is 90 watts/cm<sup>2</sup>. Now from (3.11)

$$a = 9.3 \text{ cm} = 3.7 \text{ in.}$$

The heat flux through the anode wall from the arc current is  $\phi$ .

$$\phi = 316 \text{ watts/cm}^2$$

03113<sup>32</sup>

~~CONFIDENTIAL~~

~~CONFIDENTIAL~~  
 31100

The anode mass may now be estimated. The volume of tungsten is  $12\pi da^2$ . Upon substituting  $a = 9.3$  cm,  $d = 0.12$  and multiplying by  $19.3$  g/cm<sup>3</sup>, the anode mass becomes 7.5 kg. The mass of the heat pipe working fluid, e.g. Au, may be estimated by supposing that there must be an Au film  $1/2$  the thickness of the wall, i.e., 0.06 cm. Then the mass of the fluid is 3.7 kg.

The accelerator cathode is shown as a right circular cylinder of tungsten of mass 6.0 kg. The cathode  $I^2R$  heating is 2.3 kW.

These are the heavy components of the arc head. Even by allowing an equal amount of mass for support structure and insulators the accelerator mass should not exceed 35 kg. If it should turn out that the anode cannot be operated at more than 2300°K, the present limit of heat pipe technology, the radiant flux  $\phi$  becomes 45 watts/cm<sup>2</sup>. The dimension  $a$  of Fig. 3.8 is increased by a factor 1.4 to radiate the anode power and  $d$  is left unchanged. The arc structure mass increases by a factor of 2 and becomes 70 kg.

It has been demonstrated that high-current arcs may be started directly with liquid metal expellant. There is no necessity of providing gas for starting fluid since the power dissipation in the anode and cathode with liquid metal in the arc gap is sufficient to vaporize the metal at a rate of 0.84 g/sec, adequate to insure startup.

#### Electrical Feed

Power must be conducted from the reactor current collector to the reaction motor. The voltage drop must not be excessive nor must the bus weight be large. By assuming the specific weight of the power supply to be  $\alpha_p$  kg/kW(e), the specific weight of the power supply plus electrical feed can be minimized with respect to the electrical bus cross sectional area.

The power supply specific weight is  $\alpha_p$ . The electrical feed has some length  $L$ , and each member has a thickness  $a$  and a width  $b$ . The bus has a mass  $2abL\rho_m$  and dissipates a power  $I^2\rho_e 2L/ab$ . The specific

33  
 31100

~~CONFIDENTIAL~~



~~CONFIDENTIAL~~

031713

performance of the power supply is thereby modified by the electrical feed to

$$\alpha'_p = \frac{\alpha_p P_e + 2L a b \rho_m}{P_e - 2\rho_e I^2 L / a b} \quad \text{kg/kW(e)} \quad (3.15)$$

where  $\rho_m$  and  $\rho_e$  are the density and electrical resistivity of the bus material, respectively. Minimizing  $\alpha'_p$  with respect to the product  $ab$ ,

$$ab = \frac{4LI^2 \rho_e}{P_e} \pm \frac{1}{2} \left( \frac{16L^2 I^4 \rho_e^2}{P_e^2} + \frac{4\alpha_p \rho_e I^2}{\rho_m} \right)^{1/2} \text{cm}^2 \quad (3.16)$$

The principal contribution to  $ab$  is contained in the second term beneath the radical, so that

$$ab \approx \left( \frac{\rho_e}{\rho_m} \alpha_p \right)^{1/2} I \text{ cm}^2 \quad (3.16')$$

Substituting  $ab$  from (3.16') into (3.15) and rearranging to find the minimum value of  $\alpha'_p$ , we obtain

$$\alpha'_p \approx \alpha_p \left[ 1 + \frac{4\sqrt{\alpha_p \rho_e \rho_m}}{\alpha_p P_e} IL \right] \quad (3.15')$$

showing that the appropriate figure of merit for the material from which the electrical feed is constructed is the product  $\rho_e \rho_m$ , which should be as small as is compatible with the bus operating temperature, stress, and other construction factors. The liquid alkali metals, especially sodium, actually exhibit the lowest  $\rho_e \rho_m$  product; but the advantage over solid copper is not great (see Fig. 3.10).

For purposes of illustration, the mass of a copper bus bar, 5 meters long carrying power from the reactor to the arc motor is estimated from (3.16'). The bus bar mass is

031713<sup>34</sup>

~~CONFIDENTIAL~~

~~CONFIDENTIAL~~

31100

$$M_B = 2\rho_m Lab = 2LI \sqrt{\rho_e \rho_m \alpha_p} \quad (3.17)$$

where  $I$  is the current transmitted to the plasma motor,  $L$  is the length, and  $\alpha_p$  is the specific weight of the power supply. By taking  $\alpha_p = 3.0 \text{ kg/kW(e)}$ ,  $I = 22000$  amperes (corresponding to the artificial situation of 1.3 plasma motors operating at an  $I_{sp}$  of 5000 seconds) and the product  $\rho_e \rho_m = 63 \times 10^{-6} \text{ g/cm}^2$  for copper at  $750^\circ\text{C}$ , (3.17) gives the mass of the bus bar as  $M_B = 303 \text{ kg}$ . The product of the bus bar width and thickness,  $ab = 34 \text{ cm}^2$  is given by (3.16'). The width-to-thickness ratio of the bus conductors may be adjusted to yield the radiation cooling required to dissipate the joule- and gamma-heating in the copper. Neglecting the gamma heating, the width of the bus bars can be calculated from the relation

$$b = I^2 \rho_e / 2ab\sigma\epsilon T^4 \text{ cm} \quad (3.18)$$

where all the quantities have their usual meaning. For copper, at  $750^\circ\text{C}$ ,  $\rho_e \approx 7 \times 10^{-6}$ , and for an emissivity  $\epsilon = 0.75$ ,  $b = 11.1 \text{ cm}$  and  $a = 3.06 \text{ cm}$ . The width-to-thickness ratio should be increased in the vicinity of the reactor where gamma heating is comparable to the joule heating in order to keep the entire electrical feed at approximately the same temperature.

### Propellant

The propellant mass flow (lithium) is related to the engine  $I_{sp}$  by (3.10). Plotted in Fig. 3.11 is  $\dot{M}t$  vs  $t$  with  $I_{sp}$  as the parameter. Inspection of Fig. 3.11 shows that propellant masses of the order of 30 tons are required. As the density of lithium is  $0.5 \text{ g/cm}^3$ , the tank volume must be  $\sim 1.5 \times 10^7 \text{ cm}^3$ . A sphere of this volume is 306 cm in diameter (10 ft).

The simple bursting strength of a sphere is proportional to  $r/d$ , where  $r$  is the radius and  $d$  is the wall thickness. The mass of a spherical shell is  $4\pi r^2 d \rho_m$  and the volume is  $4/3\pi r^3$ . Therefore since  $d \sim r$  for the same internal stress, the mass of a spherical shell scales directly as the volume of the sphere or as the mass of propellant.

35

31100

~~CONFIDENTIAL~~

03113

Titanium appears to be a reasonable choice for the propellant tank. It is compatible with lithium and possesses a high strength-to-weight ratio. A spherical shell of titanium, 10 ft in diameter, and having 0.1 in. wall thickness (10000 psi stress at 33 psi) weighs  $3.3 \times 10^5$  g or 1.1% of the propellant mass. Addition of internal and external bracing would probably bring the tankage mass up to 2% of the propellant, or 600 kg for  $3 \times 10^7$  g (30 metric tons) of lithium.

If it is intended to shield the reactor actuators and other sensitive components from the reactor neutron flux with the lithium propellant, the heat absorbed by the lithium shield is approximately 1 MW(th) (see Chapter 11, Shielding). The propellant tank of diameter 306 cm and temperature 1050°K will radiate 1 MW if all of the surface is free to radiate and the emissivity is 0.5. Therefore if the energy absorbed in the shielding is greater than 1 MW(th) provision must be made to remove heat from the propellant.

Other properties of lithium are:

Heat capacity	1 cal/g °K
Heat of fusion	158 cal/g
Melting point	179° C
Density	0.5 g/cm <sup>3</sup> .

The energy required to convert  $3 \times 10^7$  g of lithium from solid to liquid is therefore  $4.7 \times 10^9$  cal or  $2 \times 10^{10}$  watt sec. On the other hand, a mass of  $3 \times 10^7$  g of lithium radiating freely from a sphere of 306 cm diameter at a total emissivity of 0.1 will remain at the critical fusion temperature for 2700 hours.

#### Low-Voltage Electrostatic Motor

A survey of the present status of electrostatic motor technology may be found in a NASA-Lewis report.<sup>5</sup> Included are discussions of the various methods of ionizing the propellant, including contact ionization, appropriate to some of the alkali metals, and bombardment ionization of all types of vapors. Weight estimates for the electrostatic motor and

03113<sup>36</sup>~~CONFIDENTIAL~~

[REDACTED]

SECRET

the power conversion equipment, and engine efficiencies are discussed.

It has been pointed out in the discussion of the plasma accelerator that the weight of the plasma motor is appreciably less than the electrostatic engine because of the smaller size of the plasma motor and the ability of the magnetic accelerator to accept the output current and voltage of the thermionic power supply without power conditioning. Much of the present effort in electrostatic motors is directed toward the achievement of higher beam power densities by such expedients as post deceleration of ions and acceleration of charged colloidal-size particles in order to allow large electric fields without excessively large exhaust velocity. Since the space vehicle already possesses a very large component, namely the radiator, let us imagine that the electrostatic engine can somehow be supported on the radiator without any serious increase of the radiator weight, and that the electrostatic engine operates on low-voltage DC power direct from the thermionic power supply without the necessity of power conditioning equipment. What sort of regime do we find appropriate?

Assume that the area of the low-voltage electrostatic engine and the radiator area are in the ratio 1:2. Suppose that the power plant produces an electrical output  $P_E$  with an efficiency  $\eta$ . Then

$$P_E = \eta P_{th} \quad (3.19)$$

and the power to be radiated,  $P_R$ , is

$$P_R = (1-\eta)P_E/\eta \quad (3.20)$$

The radiated power and the characteristics of the radiator are related by

$$P_R = (1-\eta)P_E/\eta = 2 A \bar{\epsilon} \sigma T_R^4 \quad (3.21)$$

where  $A$  is the radiator area,  $T_R$  is the radiator temperature, and  $\bar{\epsilon}$  is the average of the front and back surface emissivities.

SECRET

~~CONFIDENTIAL~~

03113

The thrust produced by an electrostatic accelerator is somewhat modified from  $E^2/8\pi$  dynes/cm<sup>2</sup> because of space charge. A parallel-plate electrostatic acceleration structure, operating at the space charge limit current has a current density (in electrostatic units)

$$j_s = \frac{1}{9\pi} \sqrt{\frac{2e}{m}} \frac{V^{3/2}}{d^2} \quad (3.22)$$

where  $V$  is the applied voltage and  $d$  is the plate separation. The reaction per unit area is

$$F = \dot{M} v = \frac{m}{e} j_s \sqrt{\frac{2eV}{m}} = \left(\frac{4}{3}\right)^2 \frac{E^2}{8\pi} \frac{\text{dynes}}{\text{cm}^2} \quad (3.23)$$

The space charge has the effect of reducing the electrode spacing, increasing the force per unit area to  $(4/3)^2$  times  $E^2/8\pi$ .

The energy in the exhaust is composed of two parts. In addition to the kinetic energy in the flow there is the energy in ionization. By assuming that the ions can be formed exclusively in the first ionization state, with an ionization potential  $\phi_1$ , and defining a characteristic velocity  $v_{1c}$  by

$$1/2 M v_{1c}^2 = e \phi_1 \quad (3.24)$$

the total power in the exhaust may be written (per unit area)

$$P_E = P_{\text{exhaust}} = 1/2 \left(\frac{4}{3}\right)^2 \frac{E^2}{8\pi} \left( v + \frac{v_{1c}^2}{v} \right) \quad (3.25)$$

The radiator characteristics are related to the acceleration parameters by combining (3.21) with (3.25),

$$\frac{1}{2} \left(\frac{4}{3}\right)^2 \frac{E^2}{8\pi} \left( v + \frac{v_{1c}^2}{v} \right) = 2\bar{\epsilon}\sigma T_R^4 \left( \frac{\eta}{1-\eta} \right) \quad (3.26)$$

where  $E = V/d$ . Table 3.3 lists values of  $v_{1c}$  for the alkali metals.

03113<sup>38</sup>

~~CONFIDENTIAL~~

SECRET

Table 3.3

VELOCITIES CORRESPONDING TO ION KINETIC ENERGIES EQUAL TO  
THE FIRST IONIZATION POTENTIAL OF THE ALKALI METALS  
AND VOLTAGES CORRESPONDING TO ACCELERATION TO  
SELECTED SPECIFIC IMPULSE.

Metal	A	$\phi$ , eV	$v_{lc}$ cm/sec	Voltage for $I_{sp}$ (seconds)			
				3000	5000	7000	9000
Li	7	5.36	$1.21 \times 10^6$	31.5	88	172	283
Na	23	5.12	.67	104	288	564	932
K	39	4.32	.46	176	488	956	1535
Rb	85	4.16	.31	382	1060	2080	3450
Cs	133	3.87	.24	600	1660	3260	5400

The above table shows that there is very little energy in ionization compared to the kinetic energy, providing that only the first stage of ionization is reached. Higher ionization levels are expensive, especially with lithium, and must be avoided. Lithium, sodium and potassium appear to be the preferred propellant vapors if the acceleration voltage is so low that power conditioning machinery is unnecessary.

Plots of accelerating voltage, electrode spacing and current density are shown in Figs. 3.12, 3.13 and 3.14 for the following case:

$$\eta = 0.11$$

$$\bar{e} = (0.8 + 0.5)/2 = 0.65$$

$$T_R = 800^\circ\text{C} = 1073^\circ\text{K}$$

If the energy in ionization is neglected, the power in the accelerated beam is  $1.1 \text{ watt/cm}^2$ , and the power radiated off both surfaces of the radiator adds to  $9.8 \text{ watt/cm}^2$ . By the appropriate choice of alkali metal vapor it is still possible to obtain specific impulses between 3000 seconds and 9000 seconds with acceleration potentials less than 600 volts and electrode spacing greater than 0.1 cm. If the initial assumption can be

SECRET

~~CONFIDENTIAL~~

03713

fulfilled, viz, that the electrostatic motor can be fabricated as a part of the radiator without excessive weight addition, say 1 or 2 g/cm<sup>2</sup>, a low-voltage electrostatic accelerator becomes a possible engine design. The lower power density and low-voltage operation increase the probability of long-life operation. Problems connected with efficient ionization of the alkali metal vapor have not been considered, and represent a major problem with all types of electrostatic devices.

### References

1. A. C. Ducati, G. M. Giannini and E. Muehlberger, AIAA J. 2, 1452 (1964).
2. 1st Quarterly Progress Report, RAD-SR-64-239, Research and Advanced Development Division, AVCO Corporation, Wilmington, Massachusetts. October 1964 (Unpublished).
3. T. F. Stratton, Bull. Am. Phys. Soc. II, 10, 23 (1965).
4. R. D. Shelton, R. A. Potter, L. Lacy and E. Stuhlinger, AIAA J. 2, 682 (1964).
5. W. Mickelsen and H. Kaufman, NASA TN-7172, Lewis Research Laboratories (1964) (Unpublished).

03713<sup>40</sup>~~CONFIDENTIAL~~

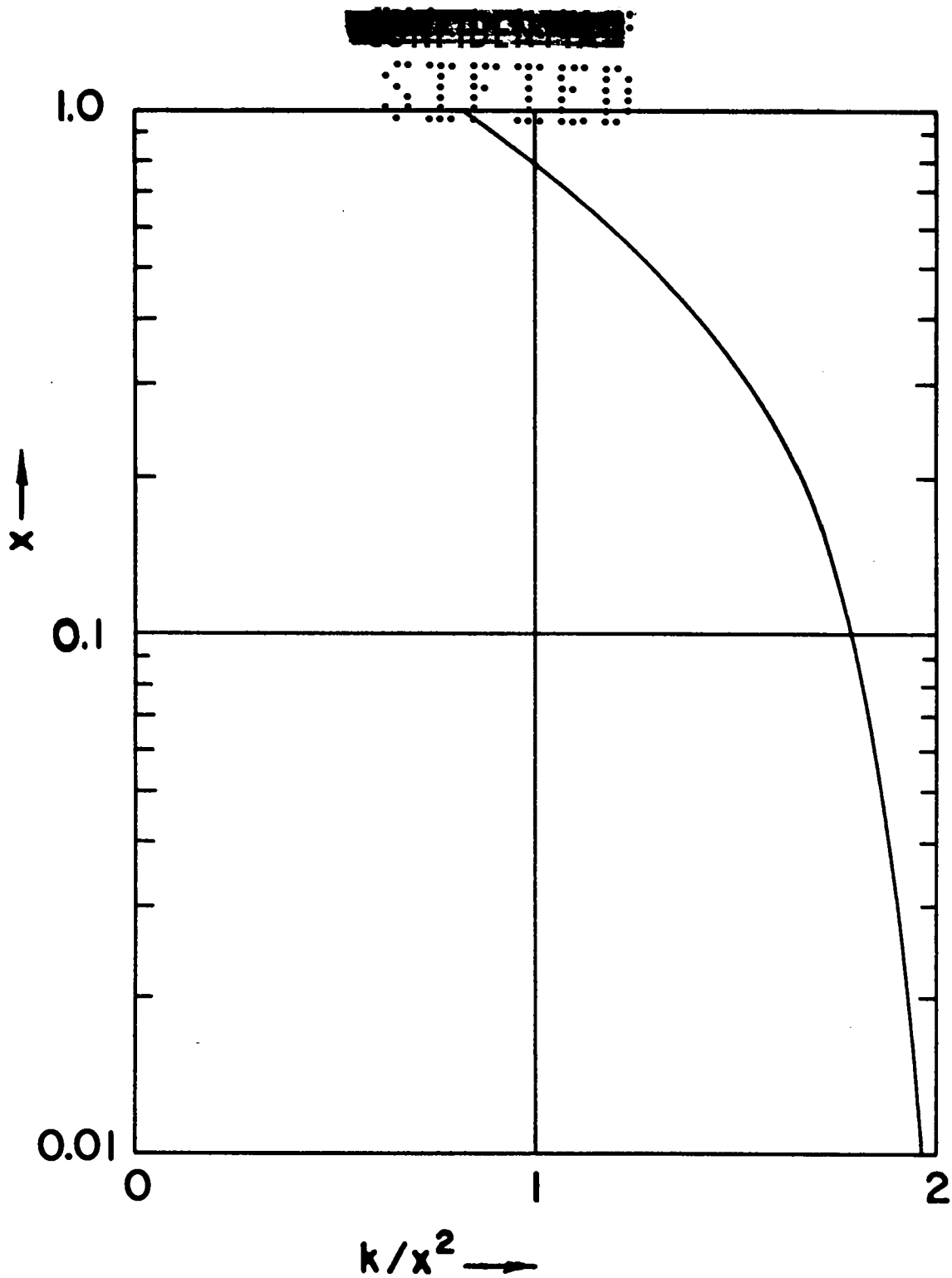


Fig. 3.1 Values of  $k/x^2$  which maximize  $f$  in the equation

$$f = e^{-x} - \frac{k}{2x^2} (1 - e^{-x}).$$

41  
SECRET



~~CONFIDENTIAL~~

03712

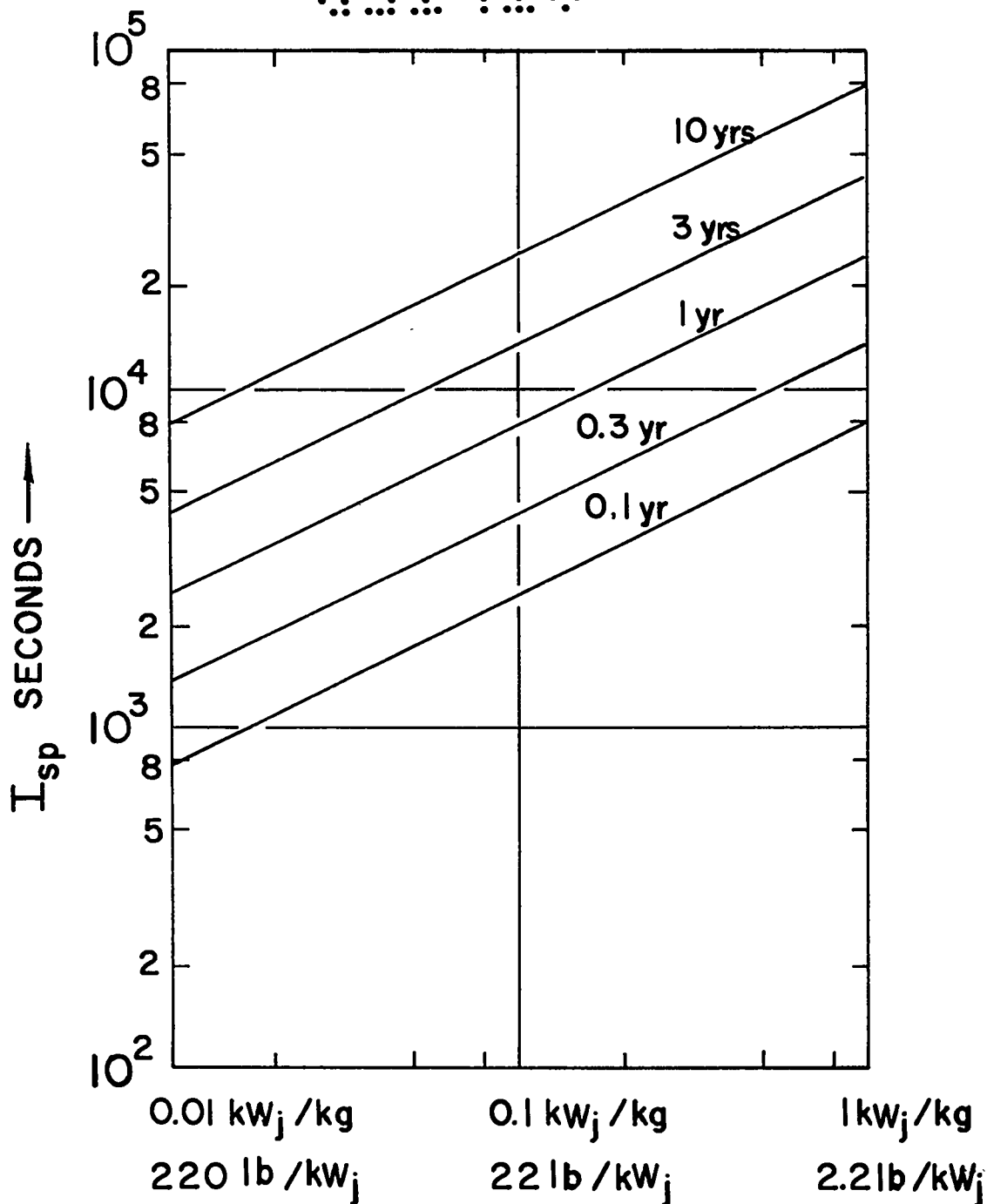


Fig. 3.2 Optimum exhaust velocity for maximum payload, as a function of power plant performance, with mission time in years as parameter.  $\text{kW}_j$  is power in jet.

03712 42

~~CONFIDENTIAL~~

~~CONFIDENTIAL~~  
 01100

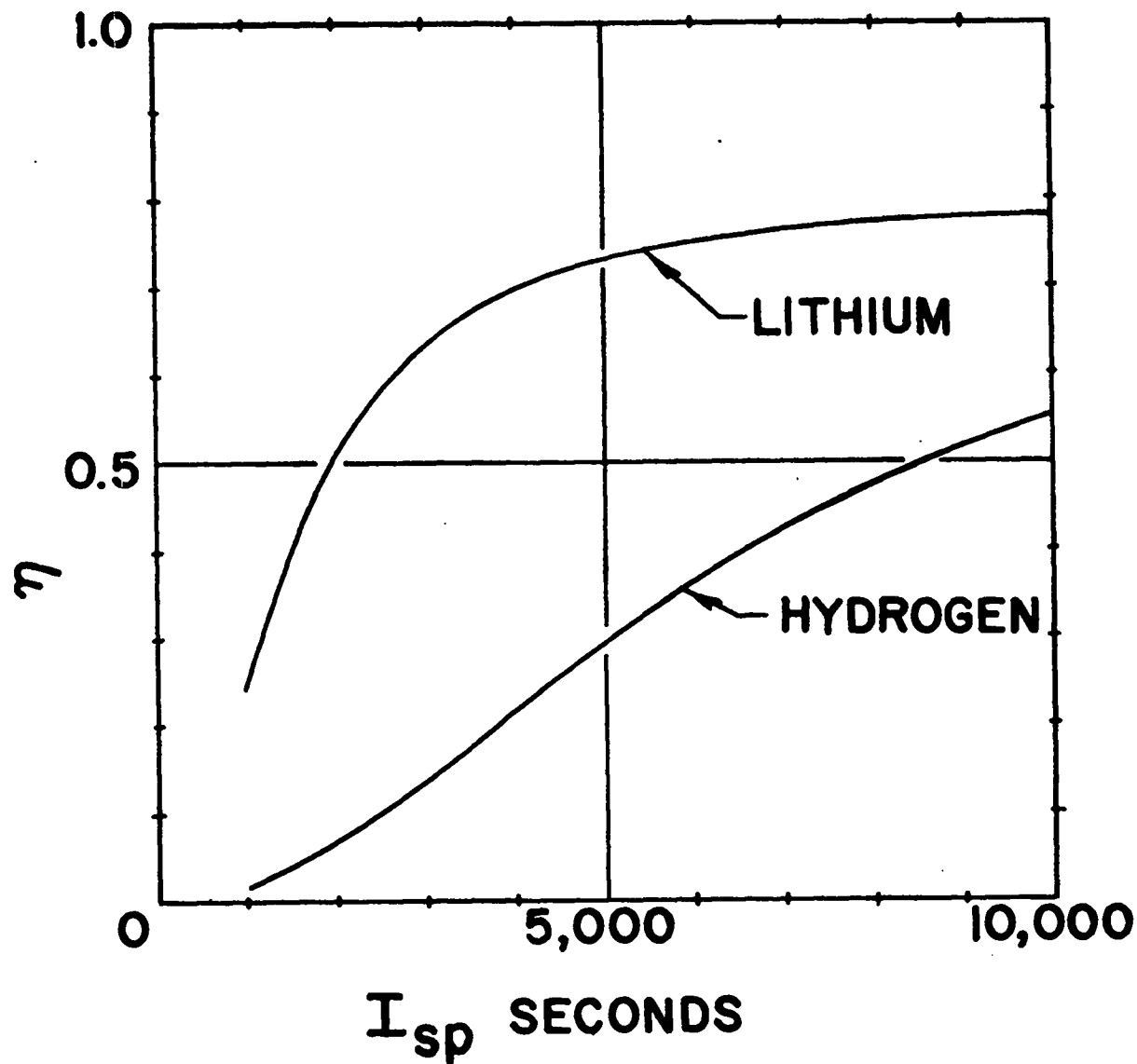


Fig. 3.3 Efficiency of conversion of electrical power into directed kinetic energy in thrust as a function of  $I_{sp}$ .  $v_{\perp}$  is assumed to be  $1/2 v_{\parallel}$ .

43  
 01100

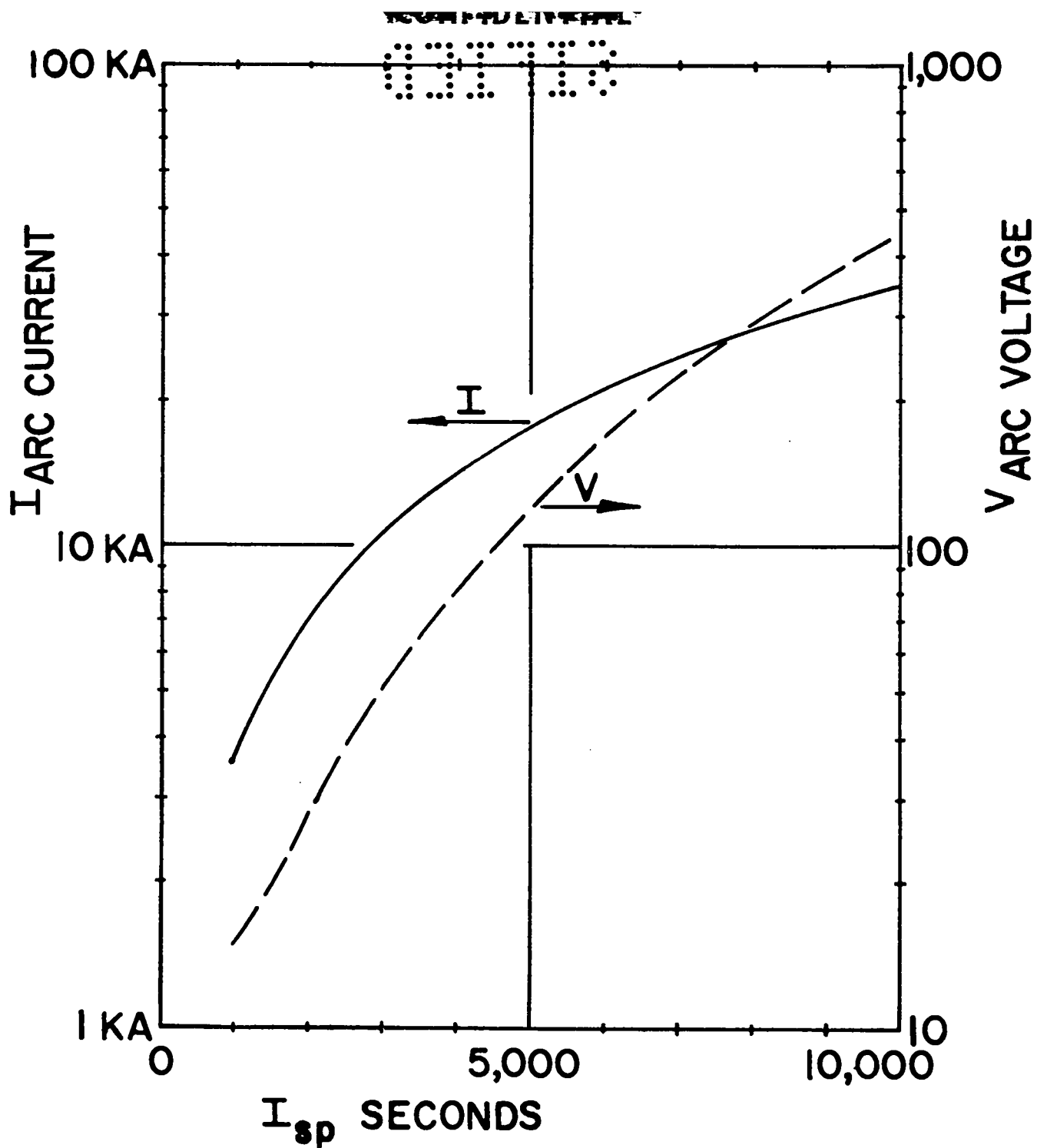


Fig. 3.4 Current and voltage as a function of  $I_{sp}$  for a lithium plasma accelerator.

44  
REF ID: A66144

SECRET

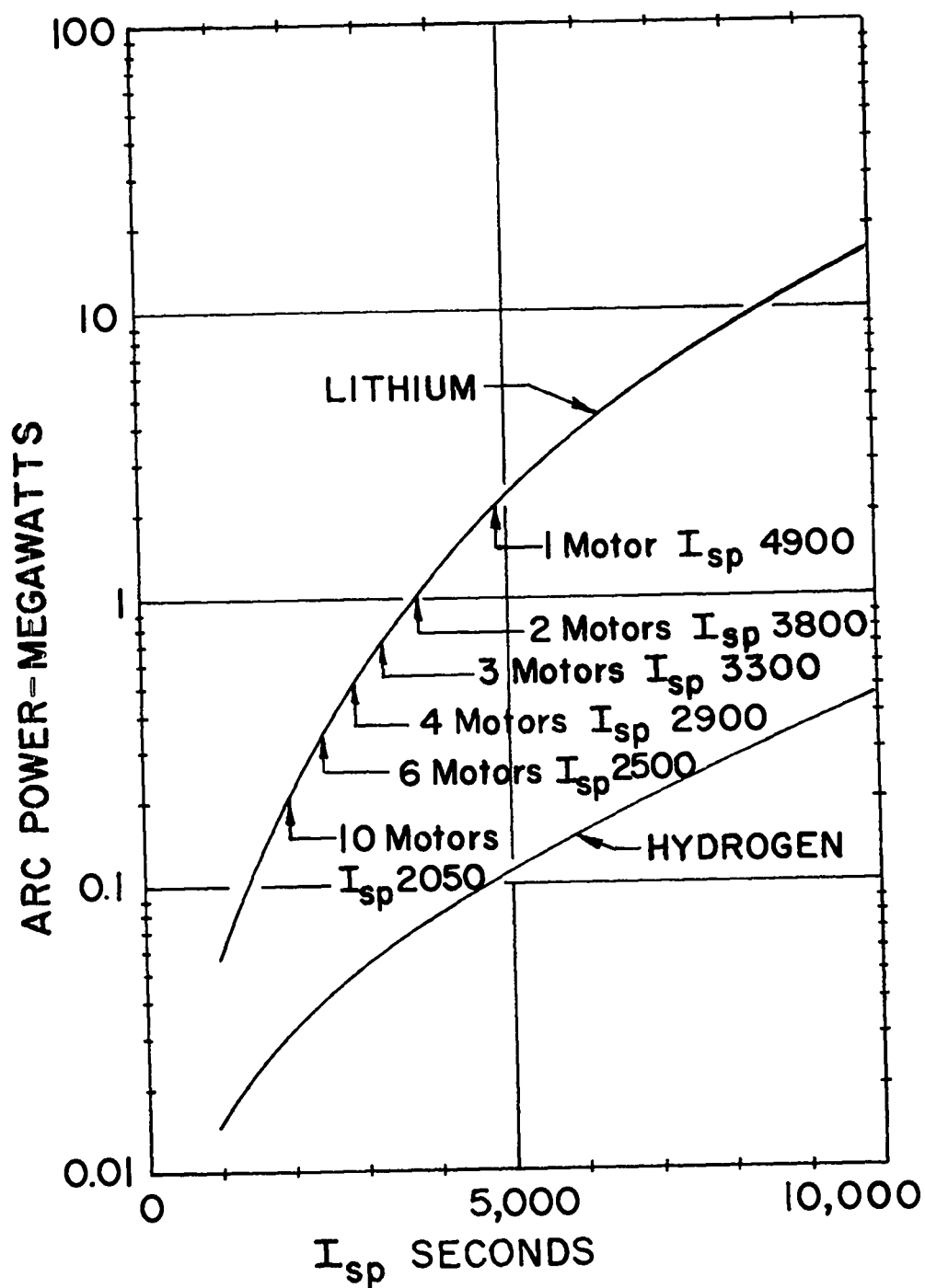


Fig. 3.5 Arc power vs  $I_{sp}$  for lithium and hydrogen expellent.  
Number of lithium arc motors, based on 2 MW(e) input.

SECRET

~~CONFIDENTIAL~~

031713

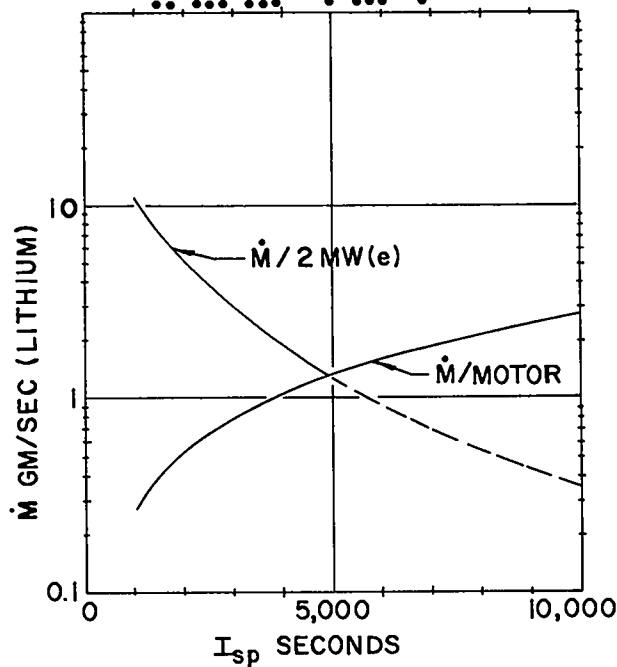


Fig. 3.6 Mass flow of lithium per motor and total mass flow for 2 MW(e) as a function of  $I_{sp}$ .

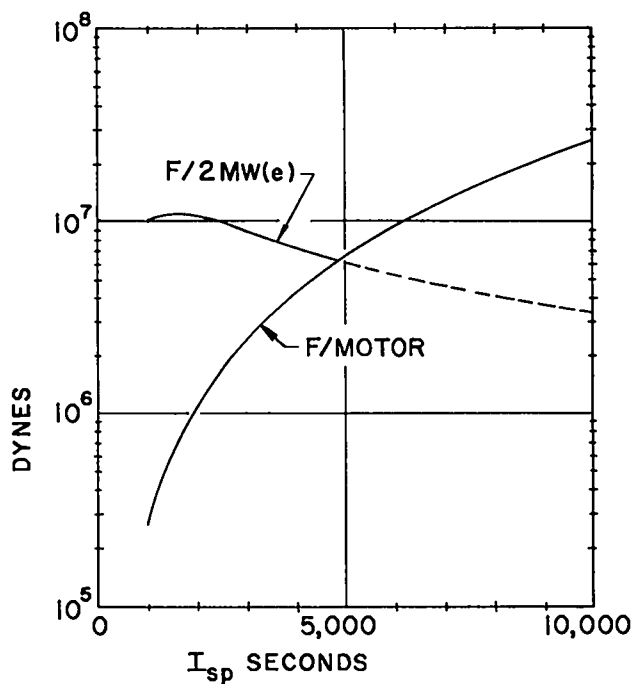


Fig. 3.7 Thrust developed by lithium arc engines per motor and for 2 MW(e).

031713

~~CONFIDENTIAL~~

~~CONFIDENTIAL~~  
 0110

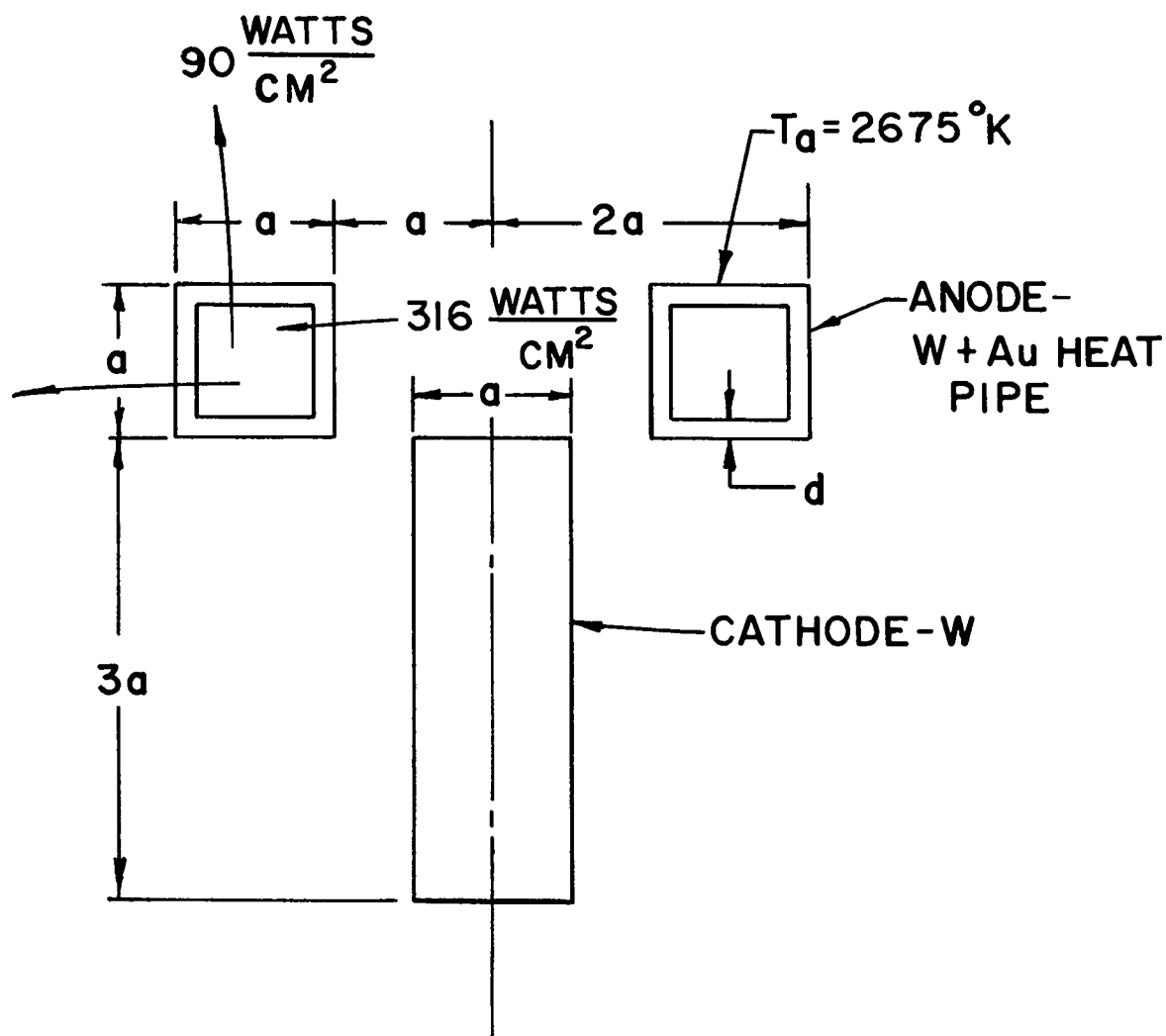


Fig. 3.8 Scale assumed for estimates of thruster dimensions. Total mass estimated at 35 kg for  $T_a = 2675^\circ\text{K}$ ; and 70 kg for  $T_a = 2300^\circ\text{K}$ . Power input to plasma motor: 2 MW(e).

47  
 0110

~~CONFIDENTIAL~~

031710

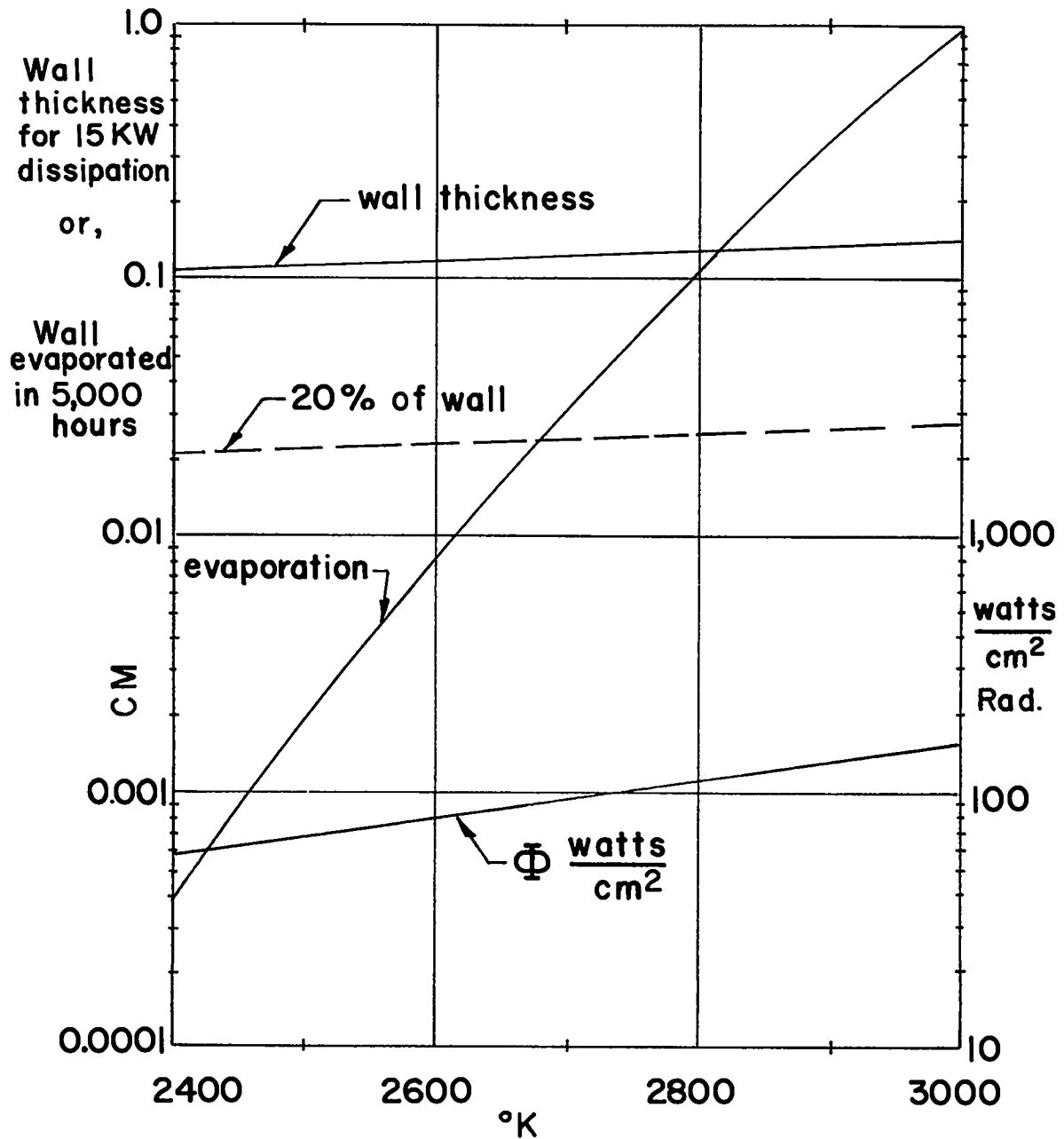


Fig. 3.9 Wall thickness, evaporation in 5000 hours and radiant flux for tungsten as a function of temperature.

031710 48

~~CONFIDENTIAL~~

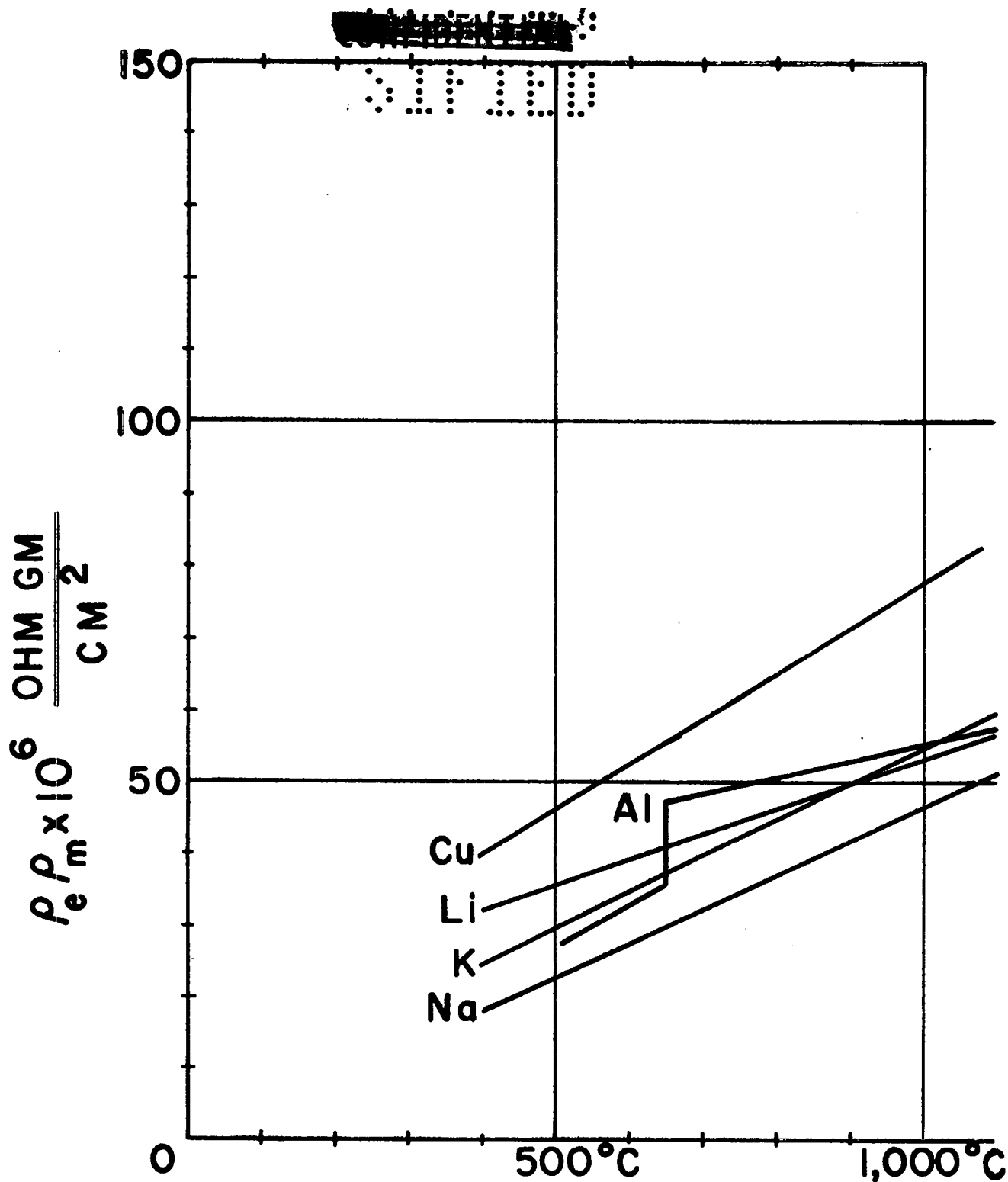


Fig. 3.10 Plot of the product  $\rho_e \rho_m$  for possible electrical bus bar materials as a function of the bus temperature.



~~CONFIDENTIAL~~

031710

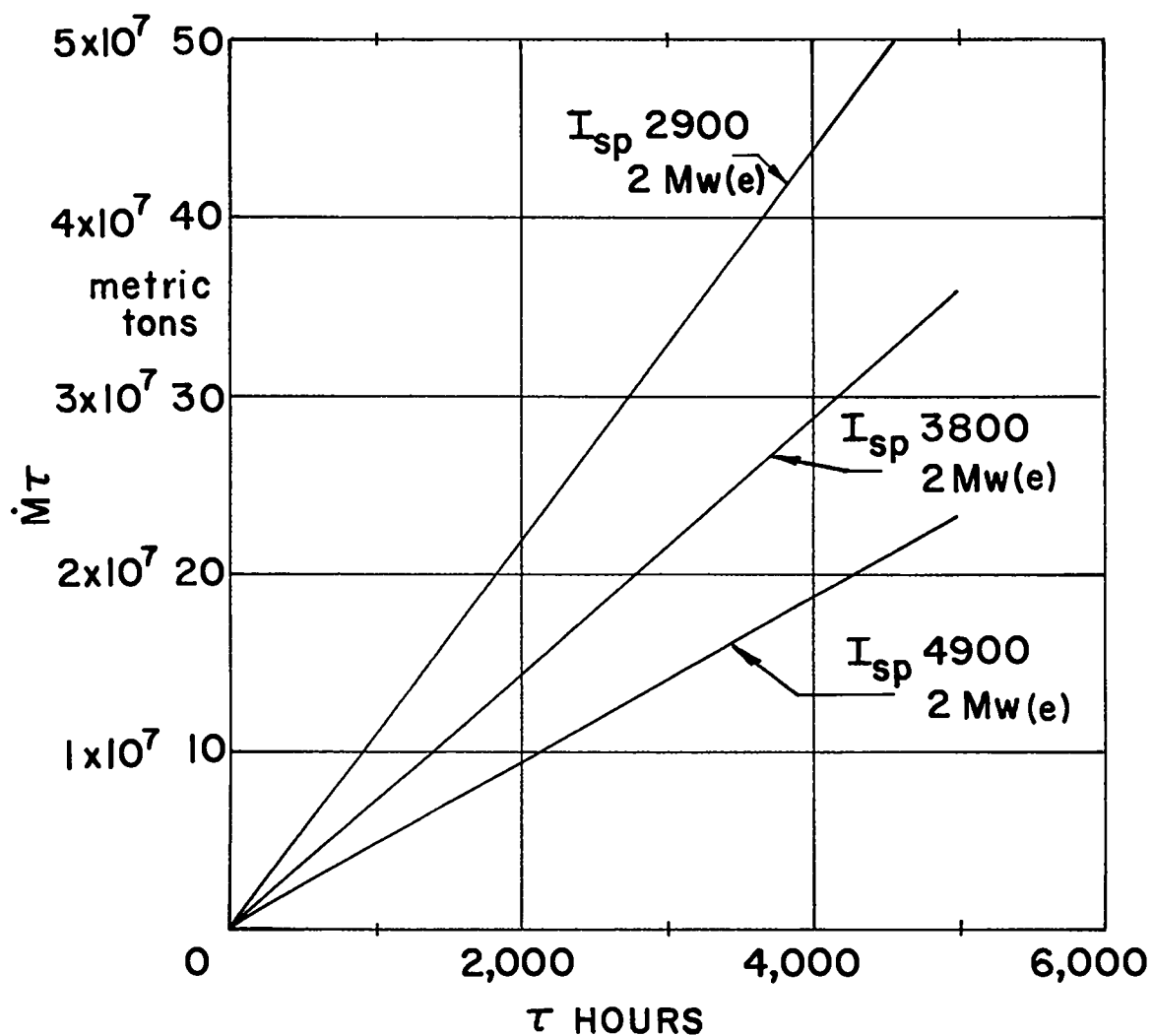


Fig. 3.11 Lithium propellant mass for 2 MW(e) power input to the plasma motor as a function of motor time.

031710

~~CONFIDENTIAL~~

CONFIDENTIAL

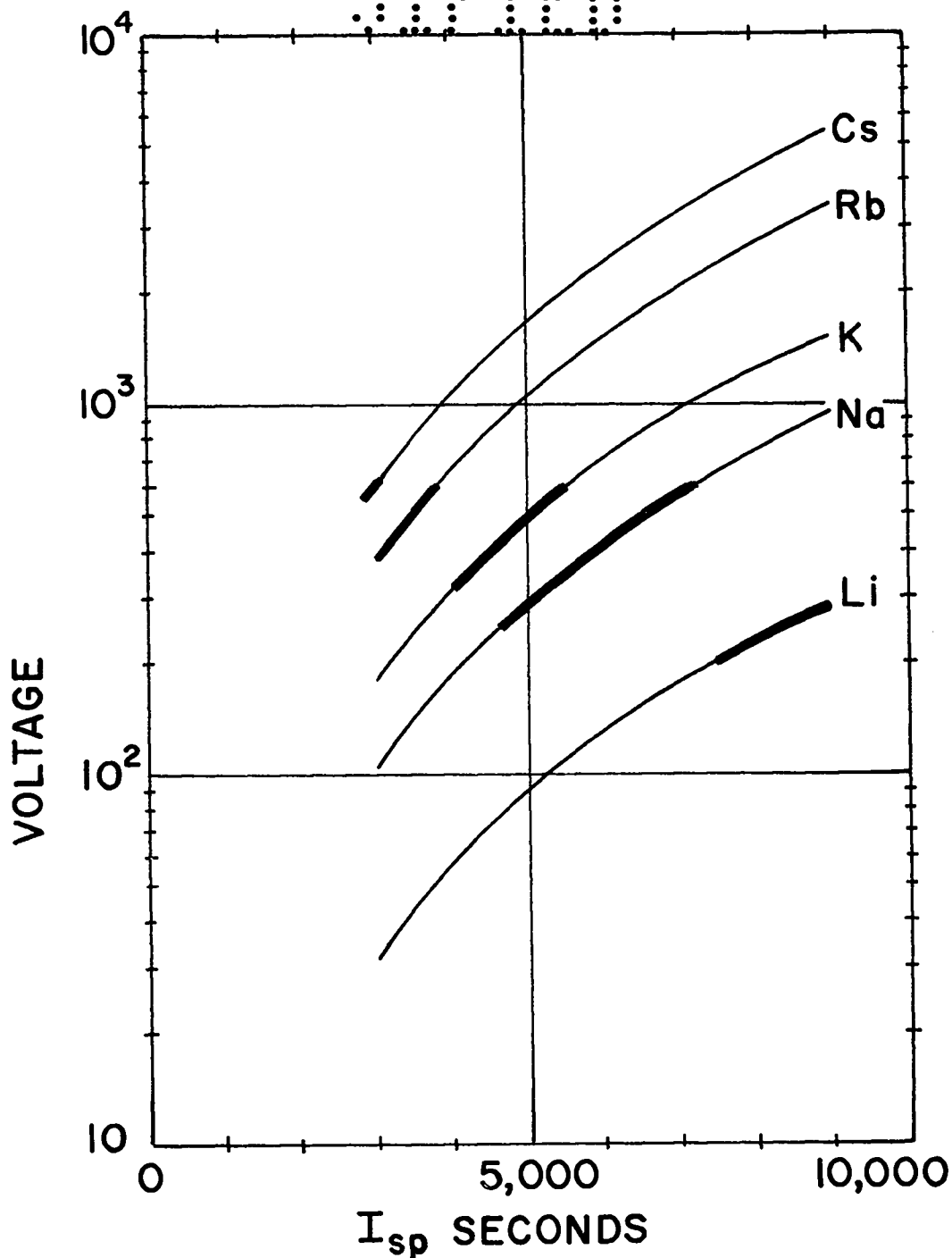


Fig. 3.12 Voltage vs  $I_{sp}$  for the alkali metals. The heavier portion of the curves shows where the voltage is less than 600 V and  $d$  is greater than 1 mm for space-charge-limited current. ( $P = 1.1 \text{ watt/cm}^2$ ).

51  
CONFIDENTIAL

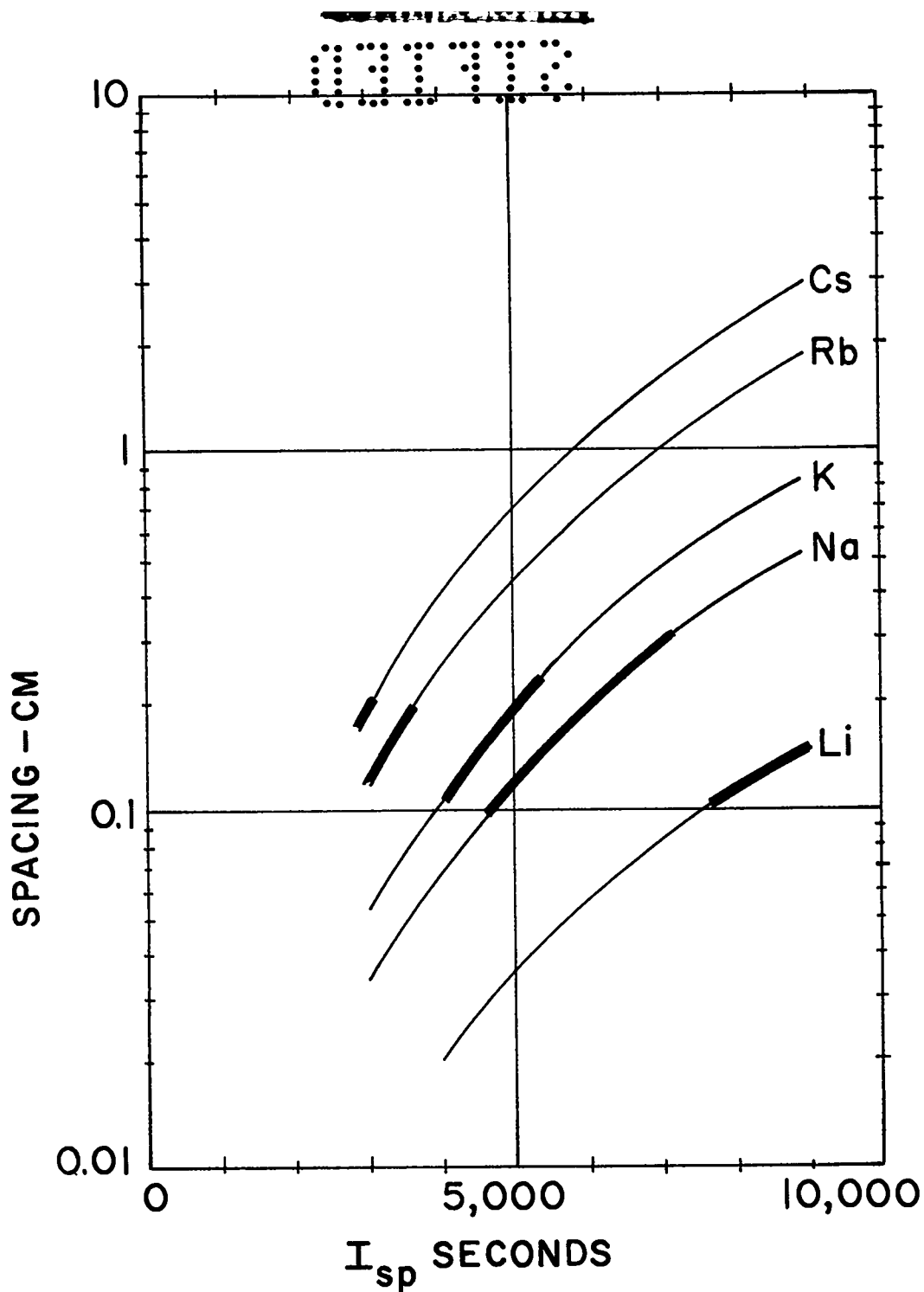


Fig. 3.13 Spacing vs  $I_{sp}$ . The heavier portion of the curves shows where the voltage is less than 600 V and  $d$  is greater than 1 mm for space-charge-limited current. ( $P = 1.1 \text{ watt/cm}^2$ ).

031713 52

~~CONFIDENTIAL~~  
 5110

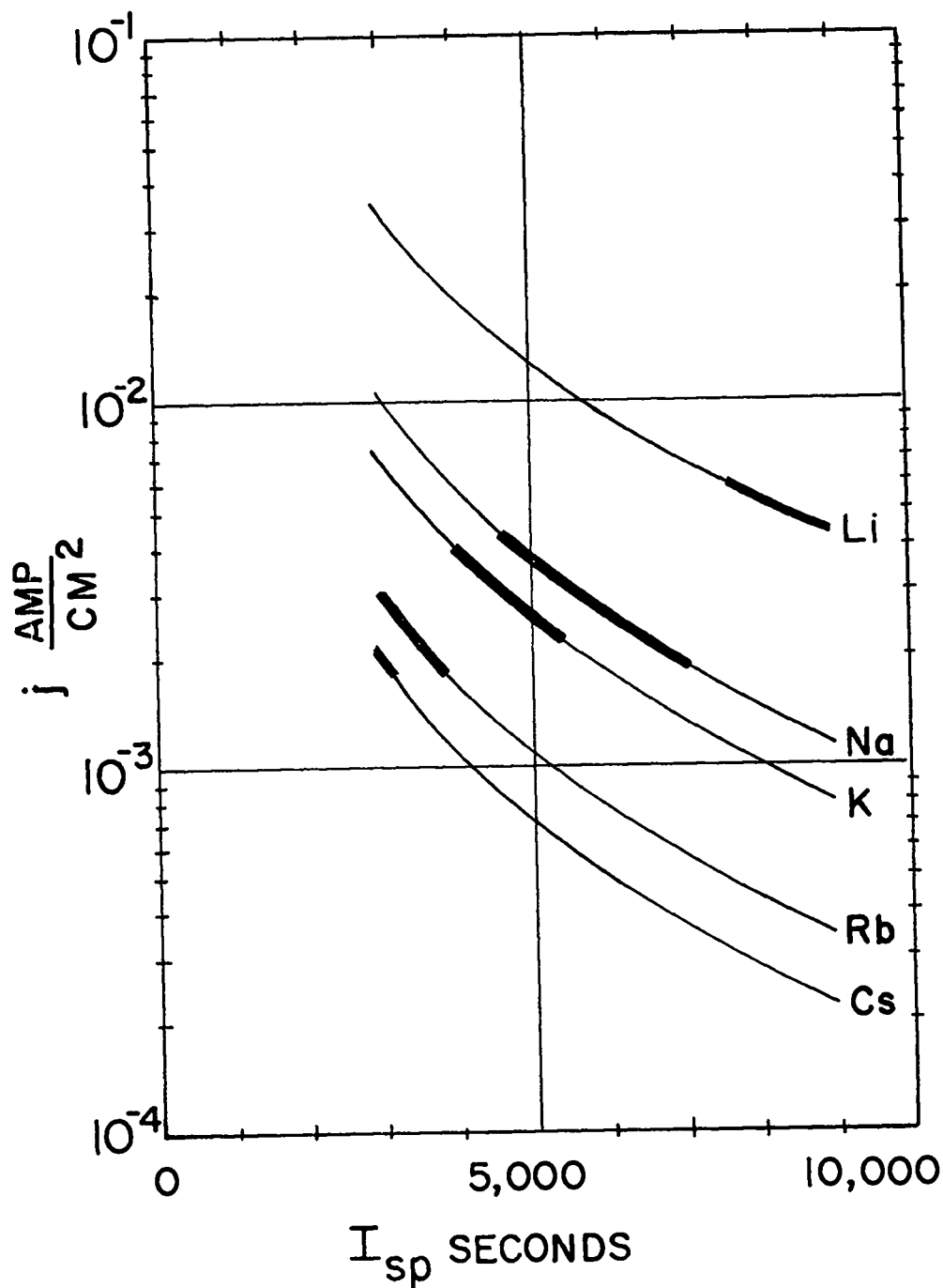


Fig. 3.14 Current density vs  $I_{sp}$ . The heavier portion of the curves shows where the voltage is less than 600 V and  $d$  is greater than 1 mm for space-charge-limited current. ( $P = 1.1 \text{ watt/cm}^2$ ).

53  
 5110

~~CONFIDENTIAL~~  
03713

Appendix to Chapter 3

HIGH-CURRENT, STEADY-STATE COAXIAL PLASMA ACCELERATORS\*

---

\*Originally published as LADC-7021.

03713 54

~~CONFIDENTIAL~~

~~CONFIDENTIAL~~  
XEROX

ABSTRACT

The performance characteristics of high-current arcs acting as plasma accelerators are predicted under the assumption that the arc current is carried by the ions in a nearly collisionless regime. In addition, it is assumed that the magnetic field due to the arc current must cause the ion gyro radius to be the same order of magnitude as the radial position. These two assumptions lead to the conclusion that (in cgs and emu): 1) the velocity of the emergent plasma stream is given by  $u = 2ZeI/m$ ; 2) the mass flow required to carry the current is  $M = mI/Ze$ ; and 3) the thrust is independent of  $Z/A$  and is  $F = 2I^2$ . It is a conclusion of the analysis that the energy of emergent singly charged ions is not greater than the applied voltage.

XEROX

CONFIDENTIAL

## 1. INTRODUCTION

Velocity and momentum measurements have been reported for the plasma streaming from high-current, coaxial, steady-state hydrogen arcs.<sup>1, 2, 3</sup> The hydrogen gas emerging to form the beam is fully ionized; the energies of the hydrogen ions are measured in tens of electron volts; and the power in the kinetic energy of the beam is a substantial fraction of the total power expended in the arc. These results represent a drastic departure from previous experience with arc jets and require an explanation which is based on considerations other than thermal behavior.<sup>4</sup>

The ensuing discussion presents a theory for the mechanisms which dominate the behavior of the arc and predicts with considerable accuracy the reported results. The ad hoc assumptions which are evoked encompass a complete and closed prediction of the properties of such arcs which is in substantial agreement with the results so far reported and which predicts the scaling properties of the arcs with respect to arc current, arc voltage, arc power, mass flow rate, and mass number and charge of the emergent ions. The predictions of the model are clear, and it should be easy to confirm or discredit the description with a few selected experiments.

## 2. OUTLINE OF MODEL

The arc jets under consideration differ from earlier work with coaxial arcs in that the operating pressures are lower and the arc currents are larger. In particular, pressures in the arc chamber of 10 torr and currents of 2000 amperes are typical. These two modifications suggest an acceleration mechanism in which collisional processes are not particularly important but in which the self-magnetic field of the arc current dominates the particle motion. Electron-atom collisions are necessary for the ionization process; but once ionization of the propellant gas has occurred the resulting ions suffer relatively few encounters, and the subsequent heavy particle motion is governed by the disposition

CONFIDENTIAL 56

CONFIDENTIAL

~~CONFIDENTIAL~~

SECRET

of the electric and magnetic fields. A schematic diagram of the appearance of the arc and the features of the model are shown in Fig. 3.A.1.

The coaxial geometry consists of a recessed center electrode, negative, surrounded by the anode. The structure of the arc is visualized as being divided into an anode sheath, a constricted current channel extending off the front of the cathode, and an ion acceleration region falling between the anode sheath and the virtual cathode. After the atoms become ionized, the ions gain velocity and move into a less restricted region toward the end of the cathode. The reduction in particle density and the increasing particle energy reduce the effect of collisions on the particle motion, and qualitative considerations of collisionless trajectories become increasingly valid. Electrons streaming off the front of the cathode form into a constricted channel and virtual cathode extending downstream from the real cathode. A substantial fraction of the ions move forward axially and inward radially toward the virtual cathode without striking the center electrode. The arc current is carried by ions between the anode sheath and the virtual cathode.

## 2.1 Mass Flow

The conclusion that ions carry the current follows from the supposition that collisions are infrequent. It is usual to find that ions carry the current across relatively strong magnetic fields because of the greater mobility of ions in the field. When a fraction  $f$  of the arc current is carried between the anode and cathode by ions, the following relation must hold:

$$fI = Ze\dot{M}/m \quad (3.A.1)$$

where  $fI$  is the current between electrodes carried by ions,  $\dot{M}$  is the mass flow through the coaxial jet, and  $Ze$  is the charge on the ions of mass  $m$ . (In this and all other equations in which numerical quantities have not been substituted the units are cgs and emu. In relations in which a numerical factor is quoted, current is in amperes.) By

57 SECRET

~~CONFIDENTIAL~~



03113

substituting for  $e$  and  $m$

$$\dot{M} = 10^{-5} (A/Z) \text{ fI g/sec} \quad (3.A.1')$$

where  $Z/A$  is the charge-to-mass ratio of the ions.

## 2.2 Exhaust Velocity

The magnetic field produced by the axial current is a field in the  $\theta$ -direction which falls off as  $1/r$  outside the virtual cathode and which also falls to zero in the axial direction because of current conduction between the electrodes. Ions formed in the region between the outer electrode (anode) and the constricted core move inward under the action of the radial electric field (also varying approximately as  $1/r$ ). As the ions gain speed they are directed forward by the bending action of the magnetic field. If there were no axial dependence of the magnetic field strength, the ions would be curved around to the radius at the point of origin and another cycle would begin. The fact that the magnetic field strength falls off in the axial direction means that the particles are not bent back so strongly and, in fact, emerge from the arc region with a forward component of velocity. The condition for this to happen is that the distance over which the magnetic field falls to zero in the axial direction is the order of the ion cyclotron radius. The axial requirement is automatically satisfied when the magnetic field is sufficiently strong to bend the ions with a radius of curvature approximately equal to the geometrical dimensions of the arc electrodes. As the ions join the electron beam streaming off the end of the cathode, the net axial current in the virtual cathode and the associated magnetic field fall to zero.

The radius of curvature of an ion in a magnetic field is

$$r_g = mu/ZeH \quad (3.A.2)$$

where  $u$  is the ion velocity. The magnetic field at a radius  $r$  outside the edge of a constricted current channel due to a current  $I$  in the

03113<sup>58</sup>

CONFIDENTIAL

CONFIDENTIAL

channel is

$$H_r = 2I/r \quad (3.A.3)$$

By substituting  $H_r$  for  $H$  in (3.A.3)

$$r_g = \mu r / 2ZeI$$

and rewriting,

$$u = 2ZeI r_g / r m \quad (3.A.4)$$

By assuming that the ion gyro radius is everywhere the same order of magnitude as the radial position in the arc and, therefore, letting  $r_g/r = 1$ , (3.A.4) becomes

$$u = 2 (Z/A) I \times 10^3 \text{ cm/sec} \quad (3.A.4')$$

upon substitution of numerical values.

A comparison of the predictions of (3.A.4') with the measured exhaust velocity of hydrogen plasma ejected from coaxial arcs at Giannini<sup>1,2</sup> and AVCO<sup>3</sup> is shown in Fig. 3.A.2. The experimental data shown in Fig. 3.A.2 are those for which (3.A.1') is satisfied, i.e.,  $\dot{M} \geq 10^{-5} \text{ I g/sec}$ . The magnitude and current dependence of the exhaust velocity are seen to be correctly predicted by (3.A.4').

### 2.3 Thrust

The reaction or thrust produced by the ejection of matter with velocity  $u$  at a rate  $\dot{M}$  is  $\dot{M}u$ . By substituting from equations (3.A.1) and (3.A.4),

$$F = 2fr_g I^2 / r \quad (3.A.5)$$

Setting  $fr_g/r = 1$ , and expressing  $I$  in amperes, we obtain

$$F = 0.02 I^2 \text{ dynes} \quad (3.A.5')$$

A comparison of (3.A.5') with the experimental measurements of Giannini and AVCO is made in Fig. 3.A.3. The agreement between theory and experiment is

59  
CONFIDENTIAL

~~CONFIDENTIAL~~

031713

again good, both with regard to absolute value and current dependence. The subtraction of a force of about 30 g from the experimental results in order to take account of the thrust due to the pressure change through the arc is reasonable and further improves the agreement between the experiments and the calculation.

The thrust produced by magnetic forces may also be calculated by integrating  $\vec{j} \times \vec{B}$  over the volume of the arc. This is equivalent to evaluating the integral of  $B^2/8\pi$  over the arc area. Evaluation of the integral for an axial position at which all of the current is carried with uniform density in the constricted core of radius  $r_c$  gives:

$$F = \int_0^{r_a} B^2/8\pi \, dA = 0.01 I^2 \left(1/4 + \ln \frac{r_a}{r_c}\right) \text{ dynes} \quad (3.A.6)$$

where  $r_a$  is the radius of the anode. From equations (3.A.6) and (3.A.5') one finds that

$$\left(1/4 + \ln \frac{r_a}{r_c}\right) = 2$$

or

$$r_a/r_c \approx 6 \quad (3.A.7)$$

The small size of the constricted current channel off the end of the cathode, which is predicted by (3.A.7), is in reasonable agreement with results reported by AVCO<sup>3</sup> for the size of the current channel. Reversing the polarity of the electrodes would be equivalent to setting  $r_c = r_a$  in (3.A.6) and would result in a magnetic component of thrust a factor of 8 less than with the center electrode negative.

#### 2.4 Arc Voltage and Power

The energy of the ions emerging to form the plasma jet is  $1/2 \mu v^2$ . In the model described above, ions gain this energy by falling through an electric field. The ions do not gain energy greater than that which

031713<sup>60</sup>

~~CONFIDENTIAL~~

APPROVED FOR PUBLIC RELEASE

~~CONFIDENTIAL~~

C I T I E D

corresponds to the voltage applied across the arc. When the fraction of the total current which is carried by the ions is large, the arc voltage must be somewhat greater than that corresponding to the directed ion energy, because some energy is put into ionization and sideways motion. There is also a voltage drop associated with the anode fall which is not available to the ions for acceleration but which causes current continuity between electrons carrying current into the anode and ions carrying current to the virtual cathode. The total arc power, if radiation and conduction losses are neglected, may be written

$$P = I (\mu^2/2e + \mu_{th}^2/2e + V_{IP} + kT_e/e) + I V_a \quad (3.A.8)$$

where  $u$  is the directed ion velocity,  $u_{th}$  is the sideways or thermal motion of the ions,  $T_e$  is the electron temperature in the exhaust,  $V_{IP}$  is the ionization potential of the ion species being accelerated, and  $V_a$  is the anode fall. In the limit that the voltage associated with the directed velocity is large compared with the other terms, the arc voltage should vary as  $I^2$ , since  $u \sim I$ .

### 3. DISCUSSION

The model discussed above suggests a way in which steady-state direct current and voltage are efficiently converted into directed plasma motion. The two assumptions upon which the model is based are: 1) ions carry the arc current between the anode sheath and the virtual cathode, and 2) the ion gyro radius is everywhere the same order of magnitude as the ion radial position. Some features of the arc which are essential to its successful operation have not been touched upon. One of these is the question of ionization. There must be set up in the arc a region in which ionization of the propellant material is accomplished efficiently. It is likely that a substantial fraction of the ionization occurs in the anode sheath. Another question centers about the electron emission from the cathode. It is likely that this must be thermionic in nature. The experimental arcs run at very high

C I T I E D

~~CONFIDENTIAL~~

031713

cathode temperature, and the necessary heat to overcome the Peltier cooling and the radiation loss must be supplied by ion bombardment. Arc stability is another matter which requires consideration. One would think that channeling of the arc into one or more spokes in the region of ionization would be very likely. Although some experiments have an axial magnetic field impressed upon them to rotate the arc, the magnetic field does not appear to be absolutely essential for stability. The fact that the current is carried by ions is probably sufficient to explain the stability of the acceleration region.

The velocity of the emergent plasma is proportional to the arc current and inversely to the mass of the ions. The acceleration of ions of mass number greater than 10 or so to velocities of several cm/ $\mu$ s ( $I_{sp}$  of a few thousand seconds) requires arc currents which are prohibitively large. It appears that lithium is the only possible expellant material, aside from hydrogen, which is of interest for propulsion applications of steady-state, coaxial-arc accelerators. Lithium is of special interest for  $I_{sp}$  of 2500 to 5000 seconds (22 to 88 eV) because the energy associated with the ionization loss (5.4 eV) is a small fraction of the total energy in the flow. The table below summarizes the predictions of the model for lithium accelerated to  $I_{sp} = 3000$  seconds and  $I_{sp} = 5000$  seconds. In the analysis, the voltage associated with the anode fall is taken to be 5 volts, and the anode work function is taken to be 4 volts. The jet is assumed to diverge with a 30° half-angle cone, corresponding to a mean transverse (thermal) velocity 1/2 that of the directed velocity.

031713 62

CONFIDENTIAL

~~CONFIDENTIAL~~

SECRET

APPENDIX TABLE I

Predictions of the model for the acceleration of lithium plasma to velocities corresponding to  $I_{sp} = 3000$  seconds and  $I_{sp} = 5000$  seconds.

Quantity		$I_{sp} = 3000$ seconds	$I_{sp} = 5000$ seconds
$V_{ke}$	Directed energy	32 eV	88 eV
I	Arc current	10500 amperes	17500 amperes
V	Arc voltage	50 volts	120 volts
P	Arc power	0.53 MW	2.10 MW
$P_a$	Anode dissipation	95 kW	158 kW
$\dot{M}$	Propellant mass flow	0.74 g/sec	1.22 g/sec
F	Thrust	2200 g = 4.9 lb	6100 g = 13.4 lb
$\eta$	Efficiency = $V_{ke}/V$	0.64	0.73

#### 4. ACKNOWLEDGEMENTS

It is a pleasure to acknowledge the many helpful discussions on this topic with C. Longmire and F. L. Ribe.

#### 5. REFERENCES

1. A. C. Ducati, G. M. Giannini, and E. Muehlberger, "Experimental Results in High-Specific-Impulse Thermo-Ionic Acceleration," AIAA J. 2, 1452 (1964).
2. A. C. Ducati, E. Muehlberger, and J. P. Todd, Interim Report IQS094-968, Giannini Scientific Corporation, Special Projects Group, Santa Ana, California, September 1964 (Unpublished).
3. 1st Quarterly Progress Report, RAD-SR-64-239, Research and Advanced Development Division, AVCO Corporation, Wilmington, Massachusetts, October 1964 (Unpublished).
4. T. F. Stratton, "High-Current Coaxial-Arc Thrusters," Bull. Am. Phys. Soc. II 10, 23 (1965).

SECRET

~~CONFIDENTIAL~~

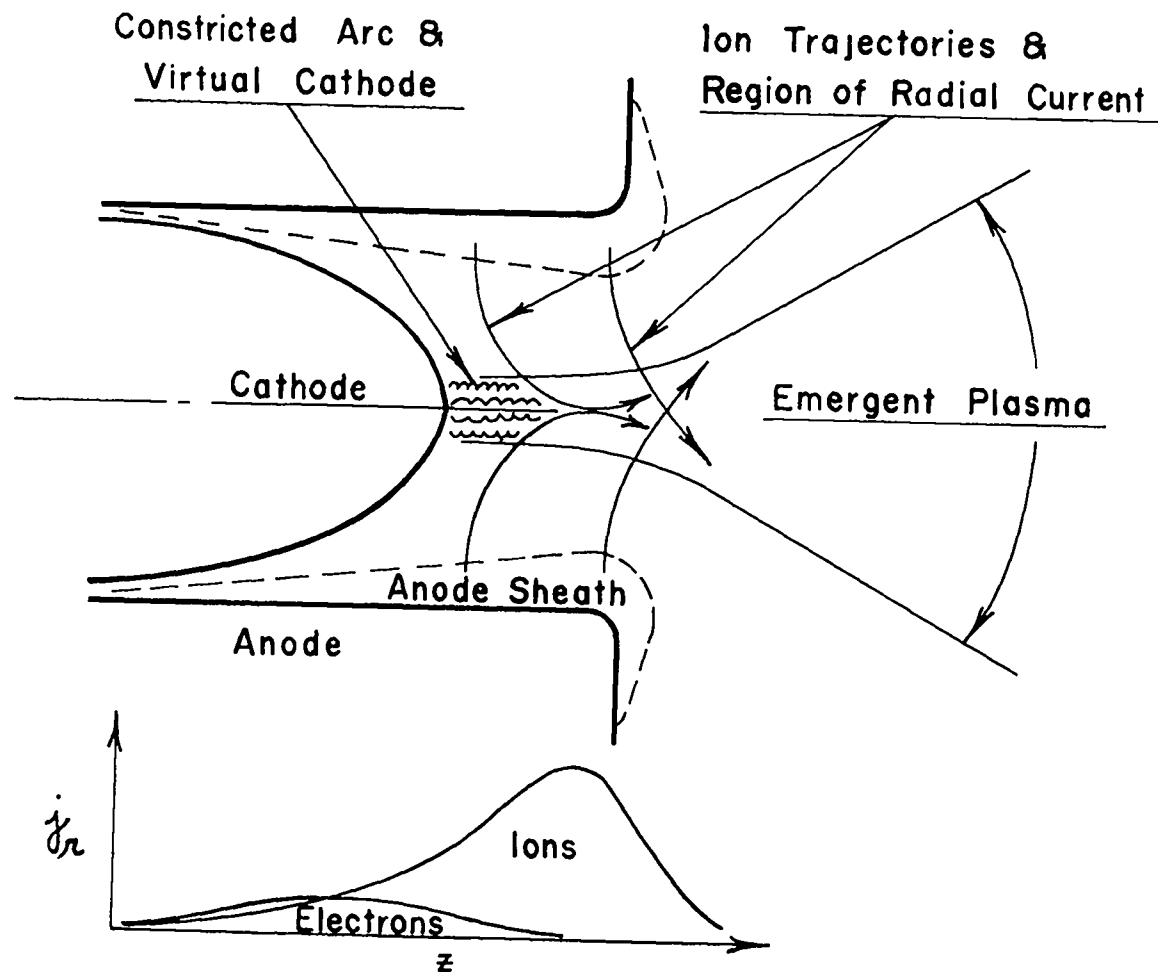


Fig. 3.A.1. A schematic diagram showing the features assumed for a description of the operation of the coaxial arc plasma accelerator. Electrons emitted from the cathode join with ions carrying current between the anode sheath and the constricted arc to form the emergent neutral plasma. Electrons formed by ionization of the propellant gas enter the anode to complete the electrical circuit.

~~CONFIDENTIAL~~  
CONFIDENTIAL

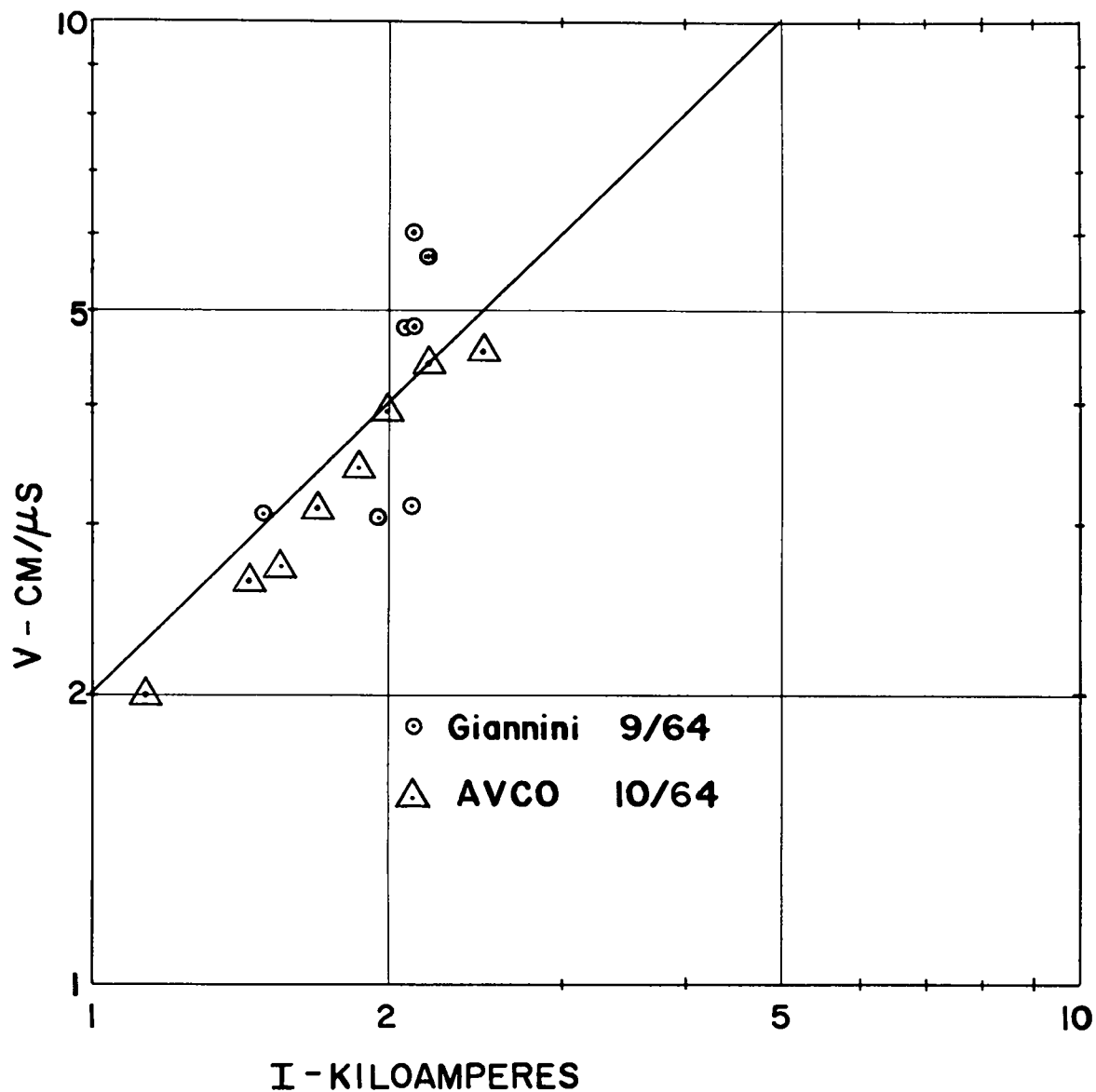


Fig. 3.A.2 A comparison of the prediction of the model with the measured exhaust velocity of hydrogen plasma formed in coaxial arcs at Giannini and AVCO.

69  
CONFIDENTIAL



~~CONFIDENTIAL~~  
03713

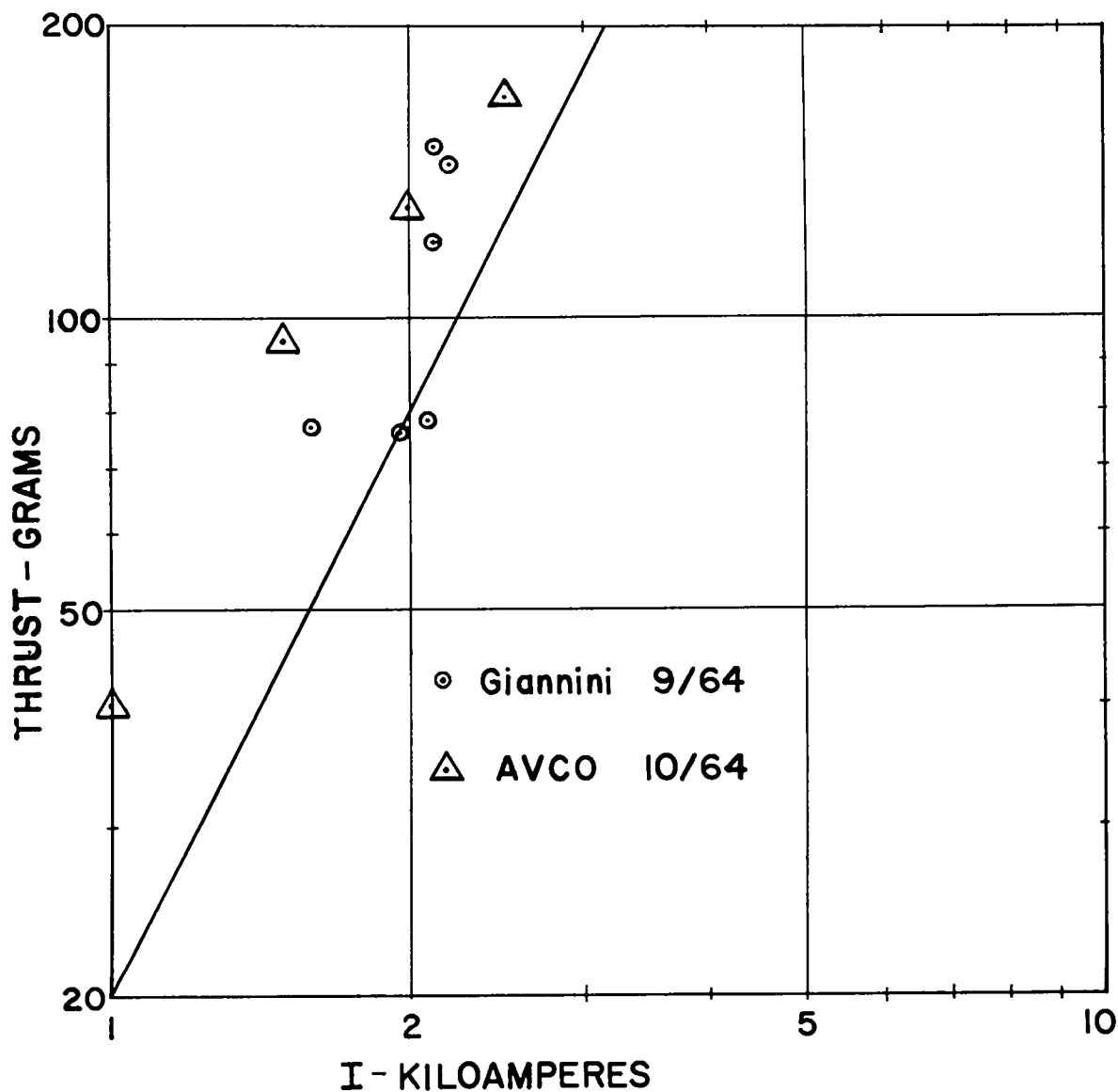


Fig. 3.A.3 A comparison of the prediction of the model with thrust measured in experiments at Gianni and AVCO.

03713 66

~~CONFIDENTIAL~~  
APPROVED FOR PUBLIC RELEASE

~~CONFIDENTIAL~~  
SECRET

#### 4. Key Materials Problems Encountered in Thermionic Reactor Construction

William A. Ranken

For the most part, the materials problems occurring in the design of a thermionic reactor are related to the fact that the minimum temperature encountered in such a reactor is likely to be in the range of 700° to 900°C. The effect of this temperature is to restrict the choice of structural, coolant and control materials because of such considerations as integrity and strength of structural materials, thermal expansion coefficient differences, and chemical compatibility of the coolant with structural materials. In general, the problems encountered are not qualitatively different from those encountered in the design of other high-temperature reactors such as SNAP 8 and SNAP 50 and appear to be quite amenable to solution. However, there are two components in the thermionic reactor for which problems arise which are not encountered in more conventional reactors. These components are the fueled emitter assembly and the interelectrode insulation.

##### The Fueled Emitter Assembly

The reason that the design of the fueled emitter assembly is a problem becomes apparent when one considers that this unit must contain a high loading percentage of U-235 at a temperature on the order of 1800°C for many thousands of hours during which time about one in every 300 - 400 atoms in the emitter structure is fissioned. While all this

SECRET

~~CONFIDENTIAL~~

~~CONFIDENTIAL~~

03113

is going on, the emitter structure must also fulfill its purpose -- the generation of electron emission currents on the order of 10 to 20 amp/cm<sup>2</sup>.

The consideration of the emitter can be divided into two categories, the bare emitter and the clad emitter. In the bare, or unclad emitter, the fuel material must serve the dual function of heat generation and electron emission. In the clad emitter, where the fuel material is encased by refractory metal, the functions of heat generation and electron emission can be separated. A list of some of the properties which the fueled emitter must have is shown in the table below.

Table 4.1

## PROPERTIES REQUIRED OF THE FUELED EMITTER

	<u>Bare Emitter</u>	<u>Clad Emitter</u>	
		<u>Clad</u>	<u>Fuel</u>
1. Fissionability	x		x
2. Useful work function	x	x	
3. Low vapor pressure	x	x	
4. Cesium compatibility	x	x	
5. Electrical conductivity	x	x	
6. Thermal conductivity	x	x	x
7. Low neutron absorption			
cross-section of diluents	x	x	x
8. High-temperature strength	x	x	
9. Temperature cycling capability	x	x	
10. Resistance to fission product damage	x		x
11. Fuel cladding compatibility		x	x

The first property listed is obvious enough; merely referring to the fact that the requirement that the fueled emitter structure must contain uranium is a major restrictive factor in emitter design. The useful work function requirement refers to the fact that efficient thermionic

03113

~~CONFIDENTIAL~~

~~CONFIDENTIAL~~  
SECRET

cells require an emitter work function either less than about 3.3 volts or greater than about 4.6 volts. The reason that high work function emitters are useful is that thermionic cell additives such as Cs and Ba are bound tightly to the emitter surface, forming a dipole layer which results in a low overall work function.

The requirement of low vapor pressure for the fuel material is to ensure that the fueled emitter does not evaporate over to the collector. In general, low vapor pressure at operating temperatures is a difficult criterion to satisfy for materials with a low inherent work function, because the electron work function of a material is related to the energy required to remove an atom of the material from the surface. Uranium carbide in solid solution with zirconium carbide is rather anomalous in this respect, in that the vapor pressure is sufficiently low at operating temperatures so that fuel mass loss rate is not prohibitively high.

The necessity that the fuel material be compatible with cesium is obvious enough, since a thermionic diode must contain cesium vapor at a pressure in the range of 0.5 to 10 torr. Good electrical conductivity is needed because the fueled emitter must be able to carry the current it emits without excessive voltage drop arising in the emitter structure. Good thermal conductivity is a less critical consideration which depends to some extent on the chemical stability of the fuel material. Poor conductivity can lead to very high temperature in the fuel interior. If the fuel does not dissociate at high temperatures -- which  $\text{UO}_2$ , for instance, does not -- then poor thermal conductivity of the fuel can be tolerated as long as gaseous fission products can be released from the emitter structure without excessive fuel loss.

Diluents are often added to uranium compounds to increase their strength. The seventh item in Table 4.1 emphasizes that the selection of such strengthening materials is limited by the neutron absorption cross section considerations. This is the reason that tantalum carbide and hafnium carbide are not used as strengthening agents for uranium carbide.

69  
SECRET

~~CONFIDENTIAL~~

03115

Since the thermionic emitter is not required to withstand external stress other than that resulting from its own weight (which in a space environment it does not have) the requirement of strength at high temperature is not set by external stress considerations. Rather it is set by internal stress considerations relating to the disposition of fission products. If the fuel material is both non-porous and plastic at operating temperature, then fission gases will tend to form bubbles and cause swelling to occur at a catastrophic rate. If the fuel material is sufficiently plastic, swelling can occur even if the material is filled with small interconnected pores which greatly reduce the distance fission gases must diffuse in the fuel material before being effectively free from the material. The catastrophic swelling phenomenon was observed for both dense and porous UCZrC bare emitters and is the reason that little work is currently being done on bare emitter configurations.

Temperature cycling capability is required of the fueled emitter structure primarily because of testing considerations. The thermionic reactor used in space propulsion will require very few temperature cycles, but research reactors used to test thermionic cells can be expected to scram on the average of once every one hundred hours of operating time.

Resistance to fission product damage is the most difficult property to attain in the fueled emitter structure and will be discussed in some detail later on.

Requiring a uranium-bearing compound to have all of the first ten properties listed in Table 4.1 is a rather tall order. UCZrC met the first nine adequately enough but, as mentioned above, has poor resistance to fission product damage. By cladding the fuel material with a refractory metal it is possible to divide the required properties between the fuel and the clad. When this is done most of the required properties of the fueled emitter are assumed by the clad as is shown in Table 4.1. The properties still required of the fuel, other than heat generation, are thermal conductivity, (mostly because of fission product venting considerations), low neutron absorption cross section of diluents, and

50  
03115

03115

~~CONFIDENTIAL~~

01100

resistance to fission product damage. Naturally, if one has a fuel with good electrical conductivity and high-temperature strength, some of the burden can be taken off the clad; and thinner clads are possible.

The price that must be paid for the separation of functions obtained by cladding the fuel is the last item shown in Table 4.1, the matter of fuel/clad compatibility. Just how restrictive this is is shown by some of the compatibility test results listed below in Table 4.2.

Table 4.2

## FUEL - CLAD COMPATIBILITY

Cladding	Fuel	Test
W	UO <sub>2</sub>	> 8500 hours, 1900°C <sup>a</sup> 1100 hours, 1800°C - No electron emission change <sup>b</sup>
Mo	UO <sub>2</sub>	> 6000 hours, 1700°C <sup>a</sup>
W25Re	UO <sub>2</sub>	> 2000 hours, 2000°C <sup>a</sup>
W	UC70a/oZrC	1100 hours, 1800°C - Slight electron emission increase <sup>b</sup>
Re	UCZrC	24 hours, 1800°C <sup>b</sup> - Ternary phase formation
Ir	UCZrC	24 hours, 1800°C <sup>b</sup> - Melting
W-Mo	UCZrC	24 hours, 1800°C <sup>b</sup> - Liquid phase formation

<sup>a</sup>See Reference 1 at the end of this chapter.

<sup>b</sup>See Reference 2 at the end of this chapter.

It can be seen that Re, Ir and W-Mo alloys are not compatible with UCZrC. In addition it has been found that Nb and Ta are incompatible with both UCZrC and UO<sub>2</sub>. However, as shown in Table 4.2, W, Mo, and W25Re are compatible with UO<sub>2</sub>, and W appears to be compatible with UCZrC. The

71  
01100~~CONFIDENTIAL~~

~~CONFIDENTIAL~~  
031710

measurements of the vacuum electron emission of tungsten-clad  $\text{UO}_2$  and UCZrC specimens indicate that less interaction occurs for W with  $\text{UO}_2$  than with W and UCZrC.

Baskin at ANL<sup>3</sup> has found US to be compatible at  $1980^\circ\text{C}$  with Mo, Ta, Nb and W25Re; and UP to be compatible at the same temperature with Mo, Ta and W. UN is compatible with tungsten at  $1800^\circ\text{C}$  but only if an over-pressure of 1 torr of  $\text{N}_2$  is present.<sup>4</sup> US and UP may prove to be useful in fueled thermionic emitter designs, but as yet very little work has been done toward effecting this application.

Thus, at the present time the three cladding materials which meet compatibility considerations are W, Re and Mo. Of these W and Re also satisfy the other requirements demanded of the cladding (Table 4.1) except for the low cross section; and this is why it is desirable to have a fuel which carries some of the cladding load, so that the clad can be as thin as possible. The vapor pressure of Mo is too high to allow its use as cladding; but, as will be discussed later,  $\text{MoUO}_2$  cermet clad with W show considerable promise. As mentioned earlier, the most difficult requirement that the fueled emitter must meet is resistance to fission product damage. The problem here is that one in every four atoms produced by fission of U-235 is either Xe, Cs, Rb or Kr, and these elements are all above their critical temperatures at  $1800^\circ\text{C}$ . Hence, when they collect in pockets in the fuel -- which they show a pronounced tendency for doing -- the pressure in the pocket will increase linearly with the number of atoms in the pocket. For instance, in a reactor running at  $1800^\circ\text{C}$  for 6000 hours with a fission energy generation rate of 200 watts per cc of fuel, enough gas atoms are formed so that if they collect in pockets forming 1% of the volume of the fuel, a pressure of 33,000 psi will exist in the pockets. This is a great deal of pressure to require a material to hold at  $1800^\circ\text{C}$ . Of course, if the void space is increased, the pressure attained will decrease; but even with 10% void the pressure will reach the uncomfortable level of 3300 psi. Because of this high pressure buildup, attention must be given to the possibility of venting the fission gases from the fuel.

031710

~~CONFIDENTIAL~~

~~CONFIDENTIAL~~

0110

The trick here is to get the gas to leave the fuel in the first place and then to keep the fuel from following the gas out, as  $\text{UO}_2$  is wont to do.

The three fueled emitter concepts which are currently receiving the most attention are the tungsten-clad UCZrC concept being studied by General Atomic, tungsten-clad  $\text{UO}_2$  being studied by General Electric at Vallecitos, and tungsten-clad  $\text{Mo}^{40}\text{V}/\text{oUO}_2$  which is being worked on here at LASL. All three of these concepts have been subjected to long-term irradiation tests -- which is the only way to find out if the fission product damage problem has been solved. In particular, GA has run tests on cylindrical samples of UC, UC10a/oZrC and UC70a/oZrC, clad in vapor-deposited tungsten so that the cladding-thickness-to-fuel-radius ratio was 0.12. These were irradiated to a fission density of  $4 \times 10^{19}$  fissions/cc at a temperature of  $1700^\circ\text{C}$ . The density of the fuel materials was in the range of 86% to 92% of theoretical and a void space equal in volume to that of the fuel was left in the tungsten capsule to collect fission gases released from the fuel. No change in dimensions of the cladding was observed in post test measurements, but some extrusion of the fuel into the capsule void space was observed. One long-term irradiation test of tungsten clad UCZrC has also been run at LASL. In the LASL tests cylinders of UC82a/oZrC and UC70a/oZrC were clad with vapor-deposited tungsten sleeves so that the cladding-thickness-to-fuel-radius was 0.10. The pin densities were in the range of 84% to 87% of theoretical, with most of the pores being observed by mercury porosimetry to be open to the exterior of the pin. Central holes in the pins theoretically enable fission gas released into the pores to be vented to a large gas collection chamber. Irradiation to a fission density of  $7 \times 10^{19}$  fissions/cc at a temperature of  $1800^\circ\text{C}$  resulted in cracking of the tungsten cladding, and the volume expansion of the fuel was identical to that measured for unclad pins irradiated to the same fission density at  $1900^\circ\text{C}$ . Radiographic inspections conducted periodically throughout the course of this test indicated that the cracking of the tungsten sleeve occurred after the fission density had reached about  $5 \times 10^{19}$  fissions/cc, although some

73

0110



031710

extrusion of the fuel out the open end of the tungsten sleeve was observed to have occurred prior to failure of the clad. It may be concluded from these tests that in order to reach the desired goal of  $1.5 \times 10^{20}$  fissions/cc either the UCZrC fuel cladding must be increased in thickness relative to the fuel radius, or better venting properties must be built into the UCZrC fuel.

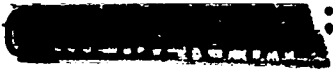
A number of irradiation tests of the tungsten-clad,  $UO_2$ -fueled emitter have been conducted by GE. In the most successful test to date, an operating thermionic converter was run in-pile for approximately 2500 hours without degradation of output power. Failure apparently occurred because of a weld in the tungsten cladding cracking and letting a mixture of helium and fission product gases into the collector emitter interspace of the converter. The fact that fission gas did escape the emitter indicates that venting does take place when the emitter temperature is reduced sufficiently for  $UO_2$  cracking to occur.

The clad, fueled emitter concept which has been the subject of the most irradiation testing is the W-clad  $Mo^{40}V/oUO_2$  concept being worked on at LASL. In general, one can say that the principal advantages in thermionic use of a dispersion fuel of this type are its relatively high thermal and electrical conductivity as well as an expected resistance to fission product damage which results from the fact that the diluent structure is relatively free from direct fission product damage, since only a small fraction of the fission products recoil into the diluent -- in this case molybdenum.

The disadvantage of the dispersion fuel is that the diluent decreases the fuel density; and this can cause criticality problems for small reactors and control problems for any reactor, since the percentage burnup is larger for a given reactor lifetime and, hence, larger reactivity changes must be provided for.

The work on  $MoUO_2$  which has been done at LASL demonstrates that fuel pins can be constructed from this cermet which will have the long lifetimes required for space propulsion applications. The pin configuration

031710  
71

  
SECRET

which has been tested at LASL is shown in Fig. 4.1. It consists of a  $\text{Mo40v/oUO}_2$  cermet cylinder clad with W by means of a vapor deposition process. Initially this cladding was 0.015 inch thick, but the thickness of more recently manufactured pins has been reduced to 0.005 inch. The central hole in the pin provides for the release of fission gases. The achievement of long lifetime for the tungsten-clad  $\text{Mo40v/oUO}_2$  fuel is keyed to the release of fission gases from the cermet without concurrent loss of  $\text{UO}_2$ . How this can be accomplished can be understood by considering what the cermet structure is like.

Figure 4.2 is a photomicrograph showing the appearance of the  $\text{MoUO}_2$  cermet when the  $\text{UO}_2$  has been driven out of the molybdenum matrix. This figure demonstrates that both the molybdenum and the  $\text{UO}_2$  are essentially continuous phases, since the fact that a negligible amount of  $\text{UO}_2$  remains in the depleted region means that very little  $\text{UO}_2$  is completely encased in molybdenum. From this one gets a picture of the cermet which says that the molybdenum is in the form of a sponge - filled with interconnecting channels. These channels, in a 90% dense cermet, are about 80% filled with  $\text{UO}_2$ . This leaves 20% of the volume of the channels unfilled, and it is this unfilled volume which is termed "pores" in the cermet. It is possible to manufacture the cermet in such a way that these pores are essentially all interconnected.

In this circumstance, fission gases can escape from the cermet by diffusing through the  $\text{UO}_2$  particle in which they are generated until they reach an open pore. Once in the pores, the gases can readily escape from the cermet, since the impedance for gas flow in the pore structure is much less than the effective impedance for diffusion through the  $\text{UO}_2$  particles even though the latter are very small. One might expect that increasing the amount of porosity would decrease the average distance fission gases would have to diffuse before reaching a pore and, thus, enhance the fission gas release characteristic of the cermet. Figure 4.3 demonstrates the expected effect. The top portion of this figure illustrates the configuration of  $\text{UO}_2$  in the channels in the molybdenum for a

75  
SECRET

CONFIDENTIAL

relatively low-porosity cermet. As more porosity is introduced, one might expect to approach the situation in the lower part of the figure where the  $\text{UO}_2$  is distributed in the channels in the form of spheres, and the average distance the gases must diffuse before reaching a pore is greatly reduced.

Evidence that increasing the porosity of the cermet does indeed increase fission gas release has been obtained from post-irradiation diffusion measurements on fuel pins of the type shown in Fig. 4.1. In these tests fuel pins representing several cermet manufacturing techniques were irradiated in the IASL Water Boiler reactor to a fission density of about  $10^{11}$  fission/cc. All but one of the pins was heated for a period totaling 500 hours, and the fractional escape of  $\text{Te}^{132}$  was determined as a function of time by comparing the gamma spectra of the heated pins with that of the unheated pin.

Figure 4.4 shows the retained fraction versus time for a high-porosity pin versus a low-porosity pin. In general, the pins termed "low-porosity" had porosity values in the range of 8% to 10% while the pins termed "high-porosity" had porosity values of 12% to 13%. It can be seen that the porosity change has a marked effect on the release of  $\text{Te}^{132}$ .

The solid lines in Fig. 4.4 are the fits obtained by applying simple diffusion theory for the escape of fission products from a sphere. The theory predicts that the release fraction will follow the behavior shown in Fig. 4.5. Here the calculated fractional release of fission products is plotted as a function of the parameter  $Dt/a^2$ , where  $t$  is the time at temperature,  $D$  is the diffusion coefficient, and  $a$  is the effective radius of the  $\text{UO}_2$  spheres. The two curves shown in Fig. 4.5 are for the case where the pin is heated after irradiation and for the case where the pin is heated during irradiation.

Fission gas release measurements have also been made for pins subjected to long-term irradiation tests. These tests, varying in duration from 400 to 3000 hours, were conducted in both the OWR and the MTR.

CONFIDENTIAL

CONFIDENTIAL  
APPROVED FOR PUBLIC RELEASE

~~CONFIDENTIAL~~

CONFIDENTIAL

Figure 4.6 shows the configuration of a typical MTR test capsule. The interior wall of the nickel capsule is threaded so as to provide for increased heat transfer rate at a given emitter temperature and thus mock up more closely the actual thermionic diode where heat transfer occurs both by thermal radiation (to a shiny collector) and by electron cooling of the emitter.

The OWR test units are similar in design, differing primarily in that a high-temperature thermocouple is introduced into the top pin and a 20-foot pole is attached to the test unit so that the thermocouple leads can be brought out of the reactor.

The fission gas release results obtained for the pins in the long term irradiation tests are shown in Fig. 4.7. Here the open circles denote the percentage of Xe plus Kr formed during the tests which was released from the pins for various irradiation times. For the low-porosity pins, the percentage release is rather constant with irradiation time at a value in the neighborhood of 16%. Failure to obtain a good measurement of Xe plus Kr release from the only high-porosity pin for which such measurements have been attempted thus far was compensated for by a measurement of the percentage of cesium released from the high-porosity pin and a comparison measurement of cesium release for a low-porosity pin from the same test unit. These two values appear as open squares in Fig. 4.7. The high release value obtained for the high-porosity pin indicates that the excellent gas release characteristics of pins of this type are retained after 400 hours of irradiation.

Less direct evidence of the difference between the low- and high-porosity pins has recently been obtained from inspection of fuel pins which were irradiated for 5080 hours in the MTR at an average temperature of 1800°C. The appearance of these pins following irradiation is shown in Fig. 4.8. Visual observation revealed no sign of cracking of the tungsten cladding. However, the tungsten surfaces were considerably rougher than they were prior to irradiation. This was especially true for the three low-porosity pins in the test unit. As can be seen in the

77

CONFIDENTIAL

CONFIDENTIAL

photograph, one pin, the high-porosity pin, was considerably more glossy in appearance than the other three. This difference is presumably caused by the relative lack of swelling which occurred for this pin. Dimensional measurements showed that the average diametral increase for this high-porosity pin of 1.5% was only half as much as occurred for the low-porosity pins, and no increase in length occurred, whereas the latter pins increased in length by 6%. Although fission gas release measurements have not as yet been completed for this test, one can assume that the difference in swelling behavior results from the difference in fission gas release characteristics.

The 5080-hour irradiation test demonstrates that the tungsten-clad, high-porosity Mo40v/oUO<sub>2</sub> fuel pins have the lifetime required to be used in thermionic reactors for space propulsion, since the amount of swelling observed is quite tolerable. Thus it can be said that the problem of fission product damage has a solution and can no longer be considered a deterrent to the construction of a thermionic reactor. It is also true that a great deal more long-term irradiation testing of fueled emitters and of operating thermionic cells is required to prove fabrication techniques and to improve further on the results obtained in the 5080-hour irradiation.

#### Restriction of UO<sub>2</sub> Loss from Mo40v/oUO<sub>2</sub> Cermet

In the first part of this lecture, the necessity of venting fission gases from the Mo40v/oUO<sub>2</sub> dispersion fuel was discussed. Evidence was presented which demonstrated that such release is indeed possible and also necessary. The next question that arises is whether this gas release can be accomplished without a concurrent release of UO<sub>2</sub>. Referring to the cermet model discussed earlier, one can see that the escape of fission gases from the cermet is a qualitatively different process than UO<sub>2</sub> loss. In the case of fission gas release, the rate-determining factor is the diffusion of the gases through the UO<sub>2</sub> to an open pore. Once the gases are in the pores of the cermet, the impedance they see in

CONFIDENTIAL

~~CONFIDENTIAL~~  
 5110

traveling to the escape hole is negligible compared to the effective impedance involved in reaching the hole. For  $\text{UO}_2$  molecules the case is different, primarily because the driving pressure for  $\text{UO}_2$  escape is limited by the vapor pressure of  $\text{UO}_2$  to values less than  $10^{-3}$  torr at thermionic emitter temperatures.

The manner in which the  $\text{UO}_2$  loss rate from a cermet surface varies with time and with  $\text{UO}_2$  vapor pressure can be calculated with simple diffusion theory. The greatly simplified model of the cermet which is shown in Fig. 4.9 illustrates how the calculation is done. Here the cermet is considered as an array of cylindrical channels in the molybdenum which are 80% filled with  $\text{UO}_2$ . As the  $\text{UO}_2$  evaporates from the free surface at  $x = 0$ , the solid  $\text{UO}_2$  interface recedes back into the cermet and the impedance for  $\text{UO}_2$  molecules escaping increases. The  $\text{UO}_2$  molecular flow from the solid  $\text{UO}_2$  interface to the free surface of the cermet at  $x = 0$  can be expressed by Fick's diffusion law:

$$D \frac{dN}{dx} = J \quad (4.1)$$

where  $D$  is the diffusion coefficient characterizing the cermet,  $N$  is the  $\text{UO}_2$  number density and is a function of  $x$ , and  $J$  is the  $\text{UO}_2$  diffusion current in the negative  $x$  direction.  $J$  is evaluated by assuming that once the  $\text{UO}_2$  molecules reach the vacuum they go away and do not come back. Hence:

$$J = \epsilon \frac{N_0 v}{4} \quad (4.2)$$

where  $N_0$  is the  $\text{UO}_2$  number density at  $x = 0$ ,  $v$  is the mean  $\text{UO}_2$  molecular velocity, and  $\epsilon$  is the fraction of the cermet surface ( $x = 0$ ) which consists of holes. (It also is the volume fraction in the cermet which is not molybdenum.)

Integration of the first equation is simple enough and gives

$$N_0 = N_p / (1 + \epsilon v x_1 / 4D) \quad (4.3)$$

79  
 5110

~~CONFIDENTIAL~~  
 5110

~~CONFIDENTIAL~~  
03700

where  $N_p$  is the  $UO_2$  number density at the solid  $UO_2$  surface and is determined only by the vapor pressure of  $UO_2$  for the temperature at which the cermet is maintained, and  $x_1$  is the distance of the solid  $UO_2$  interface from the free surface of the cermet.

The diffusion coefficient  $D$  can be evaluated for straight cylindrical pipes with the following result:

$$D = \frac{2 \epsilon v r}{3 \tau}$$

where  $r$  is the radius of the cylindrical channel, and  $\tau$  is the fudge factor, which in this case is called tortuosity, and takes into account the fact that the actual channels in the molybdenum are neither straight, nor of uniform diameter, nor cylindrical, and furthermore are interconnected. This evaluation of  $D$ , incidentally, is the only real use made of the cylindrical channel model.

Multiplying the molecular diffusion current,  $J$ , by the mass of the  $UO_2$  molecule,  $M$ , gives the mass loss rate of  $UO_2$  per square cm of cermet surface, thus:

$$\frac{dm}{dt} = MJ = M \epsilon N_p v / 4(1 + \epsilon v x_1 / 4D) \quad (4.4)$$

To find the integrated mass loss per unit area,  $m$ , as a function of time one notes that:

$$m = u \rho x_1 \quad (4.5)$$

where  $u$  = fraction of cermet which is  $UO_2$ ,  $\rho$  is  $UO_2$  density, and  $x_1$  is thickness of  $UO_2$ -depleted cermet.

If equation (4.5) is used to evaluate  $x_1$  in equation (4.4) the latter may be integrated with the following result:

$$m = (8 u r \rho / 3 \tau) [(1 + \epsilon \tau v M N_p t / 16 \rho u r)^{1/2} - 1] \quad (4.6)$$

Here  $m$  is taken as zero at  $t = 0$ . For the 90% dense cermet  $u \cong 0.36$ ,  $\epsilon \cong 0.45$ , and the average value of  $r$  is about  $7 \times 10^{-4}$  cm. At  $2100^\circ K$ ,

03700  
~~CONFIDENTIAL~~  
APPROVED FOR PUBLIC RELEASE

~~CONFIDENTIAL~~  
 31100

$v$  is  $4 \times 10^4$  cm/sec. When these values are substituted into equation (4.6) and the constants in the equation are evaluated, one finds that for  $t > 10^4$  seconds the term  $(\epsilon \tau v M N_p t / 16 \rho u r)^{1/2}$  is much greater than unity so that one may write

$$m = 0.71 (pt/\tau)^{1/2} \quad (4.7)$$

where  $m$  is in gm/cm<sup>2</sup>,  $t$  is in hr, and  $p$  is in torr.

A few experiments have been done which can be used to check the validity of this expression. In one case an unclad cermet pin was heated in vacuum and the mass loss,  $m$ , was determined periodically. The results are shown in Fig. 4.10 where the  $UO_2$  mass loss is plotted as a function of time. The fit of the data points is a curve that has the square root of time dependence. The poor fit of the initial point probably occurs because some of the  $UO_2$  was torn out of the surface when the pin was ground during fabrication.

The variation of  $UO_2$  loss rate with temperature (i.e. with  $UO_2$  vapor pressure) was determined by measuring the loss rate from the central holes of the standard fuel pin configuration (Fig. 4.1). In Fig. 4.11 the  $UO_2$  loss rate divided by the square root of heating time is plotted as a function of pin temperature. The dashed line is proportional to the square root of  $UO_2$  vapor pressure and its magnitude is given by equation (4.7) for a value of  $\tau$  of 8.5.

In another experiment, a direct demonstration of the contention that the  $UO_2$  loss and fission gas release are qualitatively different mechanisms was attempted. In this case, a combined fission gas release and  $UO_2$  loss measurement was made on both the standard fuel pin with venting in the central hole and on a fuel pin configuration shown in Fig. 4.12. Here, the central release hole has been plugged by a molybdenum rod brazed to the support tack, as shown; and a small hole has been cut in the tungsten cladding at the free end of the fuel pin.

The results of this comparison experiment showed that placing the hole in the end reduced the  $UO_2$  mass loss rate by a factor of five,

81  
 31100



~~CONFIDENTIAL~~  
03170

while the fission gas release rate was essentially unaffected by the change in configuration. Thus, it appears that the  $\text{UO}_2$  loss and fission gas escape mechanisms are virtually independent and that by introducing diffusion barriers or smaller escape areas into the fuel pin design it will be possible to make the  $\text{UO}_2$  loss very small without affecting the fission gas release rate.

#### Interelectrode Insulation

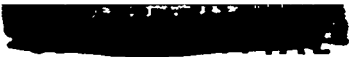
The second major problem area which arises in the design of a thermionic reactor involves the interelectrode insulation. Every thermionic cell in the reactor must have an insulator separating its emitter and collector; and, for most thermionic reactor designs, a thin insulation layer must also be wrapped around the collector so that cells may be stacked in series and yet not be shorted out by the liquid-metal reactor coolant. This report will deal specifically with the insulator between the emitter and collector, but many of the considerations discussed will apply equally well to any other insulation used in the reactor design. In the discussion, the assumption is made that hermetic seals are required between the insulator and the metal parts which it separates, even though it may be possible to design a reactor configuration in which pressure contact is all that is required.

Some of the things that one worries about in choosing insulator materials and designing insulator-to-metal seals are:

- 1) Cesium compatibility
- 2) Time at temperature
- 3) Temperature cycling
- 4) Fast neutron damage
  - a) Swelling
  - b) Strength changes
  - c) Resistivity changes

Of these the most serious is the fast neutron damage problem; fast neutrons scatter off atoms in the insulator's crystal lattice and in so

03170 82  
~~CONFIDENTIAL~~  
APPROVED FOR PUBLIC RELEASE

  
CONFIDENTIAL

doing transmit a portion of their energy to these atoms. For instance, a 2-MeV neutron that is elastically scattered in a  $180^\circ$  angle by an  $O^{16}$  atom will transmit 440 keV of its energy to that atom. The recoiling atom, which is termed a primary knock-on atom, takes off through the lattice. It gives up most of its energy in stripping electrons from the atoms in the lattice, forming electron-hole pairs in the process. But this primary atom may also collide elastically with another lattice atom which may, in turn, do the same to yet a third, so that depending on the initial energy of the primary knock-on, a number of atoms may be displaced from their original locations in the crystal lattice. What this leaves is a number of sites in the lattice called vacancies, where atoms are supposed to be but are not. It also leaves a number of displaced atoms trying to squeeze into the lattice where there is no room for them -- and these are termed the interstitials. The presence of the interstitials leads to expansion of the lattice -- and, worse yet, this expansion is frequently anisotropic so that grain boundary separation or microcracking may take place.

If vacancies and interstitials manage to get together they recombine. Because the mobility in the lattice of both these species increases rapidly with increasing temperature, the recombination rate also rises with temperature. Therefore a steady state situation between the rate of production, which depends on the neutron flux, and the rate of recombination will eventually be reached. For a given fast neutron flux, the higher the temperature the sooner this saturation level of vacancy and interstitial density will be reached, and the lower will be its magnitude; hence, the lower will be the damage to the crystal lattice. This is one area in which the high temperature at which thermionic reactors must run promises to be more of a help than a hindrance.

From the description of the cascade process by which a fast neutron damages the lattice it is easy to see that the amount of damage this neutron does is related to its initial energy. In fact, it is possible

86  
CONFIDENTIAL

~~CONFIDENTIAL~~  
03113

to derive a damage coefficient for a given neutron flux distribution which is

$$D = K \int_0^{\infty} \phi(E) \sigma(E) E dE \quad (4.8)$$

where  $\phi(E)$  is the neutron spectrum,  $\sigma(E)$  the differential neutron-atom elastic scattering cross section, and the number of displacements produced by the collision of a neutron with a lattice atom is taken to be proportional to the neutron energy,  $E$ . This damage coefficient becomes useful when an insulator has been tested in a reactor having one flux distribution and one wishes to predict how it will behave in a reactor having quite a different neutron flux distribution.

The minimum energy that a lattice atom must be given before it can be displaced from its location in the crystal lattice is approximately 25 eV. This means that for an alumina lattice, a neutron having an energy of less than 113 eV will not be able to displace even the oxygen atoms, and hence thermal neutrons can damage the lattice only by transmutation of lattice atoms. Displacements can also be caused by electrons and by gamma rays, which do the job by first generating a Compton, or photoelectron or pair-production electron. However, the electrons can transfer such a very small fraction of their energy to a lattice atom that the damage they do is negligible compared to the fast neutrons, since the fluxes in a reactor are roughly equivalent.

Some of the ceramics which at first sight appear of most interest for use as thermionic cell insulators are:  $\text{Al}_2\text{O}_3$ ,  $\text{BeO}$ ,  $\text{MgO}$ ,  $\text{ThO}_2$ , and  $\text{Y}_2\text{O}_3$ . All of these are cesium-compatible; but  $\text{MgO}$  and  $\text{Y}_2\text{O}_3$ , as will be shown later, do not look good from a neutron damage standpoint, and  $\text{ThO}_2$  has poor electrical resistivity at 1200°K and also seems to be susceptible to thermal shock. This leaves  $\text{Al}_2\text{O}_3$  and  $\text{BeO}$  as the prime candidates for thermionic cell insulators.

Figure 4.13 shows the type of ceramic-to-metal seal which has been investigated at LASL. It is made by applying a thin tungsten coat to an alumina cylinder and brazing thin-lipped Nb cylinders to it with a

03113<sup>84</sup>  
~~CONFIDENTIAL~~  
APPROVED FOR PUBLIC RELEASE

~~CONFIDENTIAL~~  
SECRET

high-temperature braze. At the present time, vanadium seems to work the best as a braze material, since test assemblies utilizing this braze have been heated to 1370°K for as long as 2300 hours and with 46 temperature cycles without developing leaks in the joints. Those assemblies which failed during this test did so by developing a leak in the ceramic body rather than at the seal. This type of failure has been ascribed to stresses induced by grinding and has led to changes in the method of manufacture of the ceramic bodies.

Since resistance to fast neutron damage is really the property that makes or breaks a given material in so far as its use in thermionic reactors is concerned, much of the LASL effort in the field of insulators has been devoted to irradiation testing of insulators and ceramic-to-metal seals. A number of different ceramic materials and ceramic-to-metal seal concepts have been tested in the MTR to integrated fast flux values in the range of  $1.5$  to  $3.2 \times 10^{20}$  neutrons/cm<sup>2</sup> and with temperatures nominally in the range of 500° to 900°K. (As used here the term "fast" refers to neutrons having an energy of  $\geq 1$  MeV.) The integrated thermal flux values which the units in these tests saw were about 9 times as high as the fast flux values.

The test units were cylindrical stainless steel capsules shown in Fig. 4.14. These were loaded with the samples to be tested and outgassed for 24 hours at 900°C before being welded shut in one atmosphere of argon. The specimen temperatures were calculated on the basis of known MTR gamma heating rates and the conductivity of the argon.

The tests revealed that some insulating materials do not withstand fast neutron damage very well. Figure 4.15 shows a series of MgO disks which saw  $1.5 \times 10^{20}$  nvt of fast flux. Extensive cracking is plainly visible in all six of the samples. The volume increase for these samples amounted to 30%.

Figure 4.16 shows some yttria discs which also experienced  $1.5 \times 10^{20}$  nvt of fast flux. Cracking took place in these samples also and is

85  
SECRET~~CONFIDENTIAL~~

~~CONFIDENTIAL~~  
03713

quite obvious for one of the disks. However, the actual volume increase which occurred for these samples was only 2.5%.

In general, all of the alumina insulators that were tested held up well under the irradiation treatment. Figure 4.17 shows an Al-300 insulator made by Western Gold and Platinum Co. which has seen  $3.2 \times 10^{20}$  neutrons/cm<sup>2</sup> integrated fast flux at 700°K.

Figure 4.18 shows a ceramic-to-metal seal which was subjected to  $3 \times 10^{20}$  neutrons/cm<sup>2</sup> at 900°K. This seal was made by brazing a tungsten-metallized Al-300 insulator to niobium with a palladium/cobalt braze. This did not work well because the braze material ate its way through the thin lips of the Nb pieces and, as a result, the assemblies leaked.

Figure 4.19 depicts a tungsten-metallized Al-14 insulator (99.5% Al<sub>2</sub>O<sub>3</sub>, 0.5% Y<sub>2</sub>O<sub>3</sub>) which was irradiated to  $3.2 \times 10^{20}$  nvt of fast flux at about 700°K. Insulators of this type were also vanadium-brazed into niobium test pieces and irradiated to  $2.0 \times 10^{20}$  nvt at 970°K. One of these is shown in Fig. 4.20. Three of the four assemblies thus tested were helium leak-tight following the irradiation. The leaking assembly was sectioned and examined metallographically. As shown in Fig. 4.21 both the ceramic and seal do not appear damaged by the irradiation exposure, and it is speculated that the leak may have resulted from the same type of failure that was observed in the long-term heating and temperature cycling tests mentioned earlier.

In general the alumina test bodies increased slightly in volume and in some instances decreased in resistivity. Test results are presented in Table 4.3.

86  
03713  
~~CONFIDENTIAL~~  
APPROVED FOR PUBLIC RELEASE

~~CONFIDENTIAL~~  
 5110

Table 4.3

FAST NEUTRON IRRADIATION EFFECTS  
 Temperature Range 500°-900°K

Sample	Fast nvt	Volume Increase %	Remarks
MgO	$1.5 \times 10^{20}$	30	severe cracking
$Y_2O_3$	$1.5 \times 10^{20}$	2.5	cracking
Al-13	$2.8 \times 10^{20}$	1.4	
(98% $Al_2O_3$ , 2% $Y_2O_3$ )	$2.5 \times 10^{20}$	0.3	$\rho \sim 6 \times 10^3$ to $5 \times 10^4 \Omega \text{ cm}$
Al-300	$3.2 \times 10^{20}$	1.2	$\rho \sim 6 \times 10^6$ to $> 10^9 \Omega \text{ cm}$
Al-14	$2.8 \times 10^{20}$	1.0	
(99.5% $Al_2O_3$ , 0.5% $Y_2O_3$ )	$2.5 \times 10^{20}$	0.2	$\rho \sim 2 \times 10^4$ to $> 10^9 \Omega \text{ cm}$
	$3.2 \times 10^{20}$	1.3	

Unfortunately, the test temperatures are not well established, and it is quite likely that considerable temperature gradation occurred in the individual samples. As a result it has not been possible to correlate swelling and resistance change with irradiation temperatures. However, the post irradiation electrical conductivities of the alumina samples appear to increase with the degree of blackening of the samples.

This is not too surprising, since both effects are dependent on the number of vacancies introduced into the crystalline structure. In the case of the coloring, one can attribute the effect to electrons trapped in negative ion vacancies. The increased conductivity also results from this trapping of electrons, because they are removed from

87  
 5110

~~CONFIDENTIAL~~  
 5110

~~CONFIDENTIAL~~  
03712

the normally full conduction bands in the perfect insulator. When the bands are less than full, conduction can take place; and the conductivity will be proportional to the number of electrons removed and, hence, to the density of the vacancy defects. Both the coloring and conductivity change may be expected to go away with sufficient post-irradiation annealing. A trend in this direction was observed when a piece of irradiated  $\text{Al}_2\text{O}_3$  was heated for 8 hours at  $1000^\circ\text{C}$ , and its color changed from black to reddish brown while its resistivity increased by a factor of 1000.

It is important to distinguish the conductivity changes which develop during fast neutron irradiation because of vacancy formation from those which occur during irradiation in an intense gamma flux. In the latter case, the normal conductivity of the insulator is increased by the formation of electron-hole pairs. The amount of increase is proportional to the equilibrium density of these pairs which is, in turn, proportional to the gamma flux. Since these pairs recombine rather quickly, no residual effects are observed when the insulator is removed from the gamma flux. Dau and Davis<sup>5</sup> have measured the amount of increased conductivity for alumina as a function of temperature and reactor power, and find that for thermionic reactors of typical design the increase is negligible compared to the normal conductivity for temperatures above  $900^\circ\text{K}$ .

The alumina irradiation results discussed above are somewhat erratic but they demonstrate that alumina-to-niobium seals can be made which will survive integrated exposures in excess of  $2 \times 10^{20}$  neutrons/cm<sup>2</sup> of fast neutrons for an MTR flux distribution. In order to determine what this means in terms of thermionic reactors where the flux distribution is quite different from the MTR and varies with uranium-to-Be ratio, it is necessary to calculate a damage coefficient in the manner indicated earlier. This has been done, and the results are presented in Chapter 8.

88  
03712~~CONFIDENTIAL~~

~~CONFIDENTIAL~~  
CONFIDENTIAL

References

1. A. I. Kaznoff and B. Weidenbaum, International Conference of Thermionic Electrical Power Generation, London, Sept. 1965.
2. Yang, et al., GA-4769, Part 1 (1964).
3. Y. Baskin, ANL-6856 (1964).
4. Melvin Bowman, LASL, Private communication.
5. G. Dau and M. Davis, Nuc. Sci. & Eng. 21, 30-33 (1965).

89  
CONFIDENTIAL



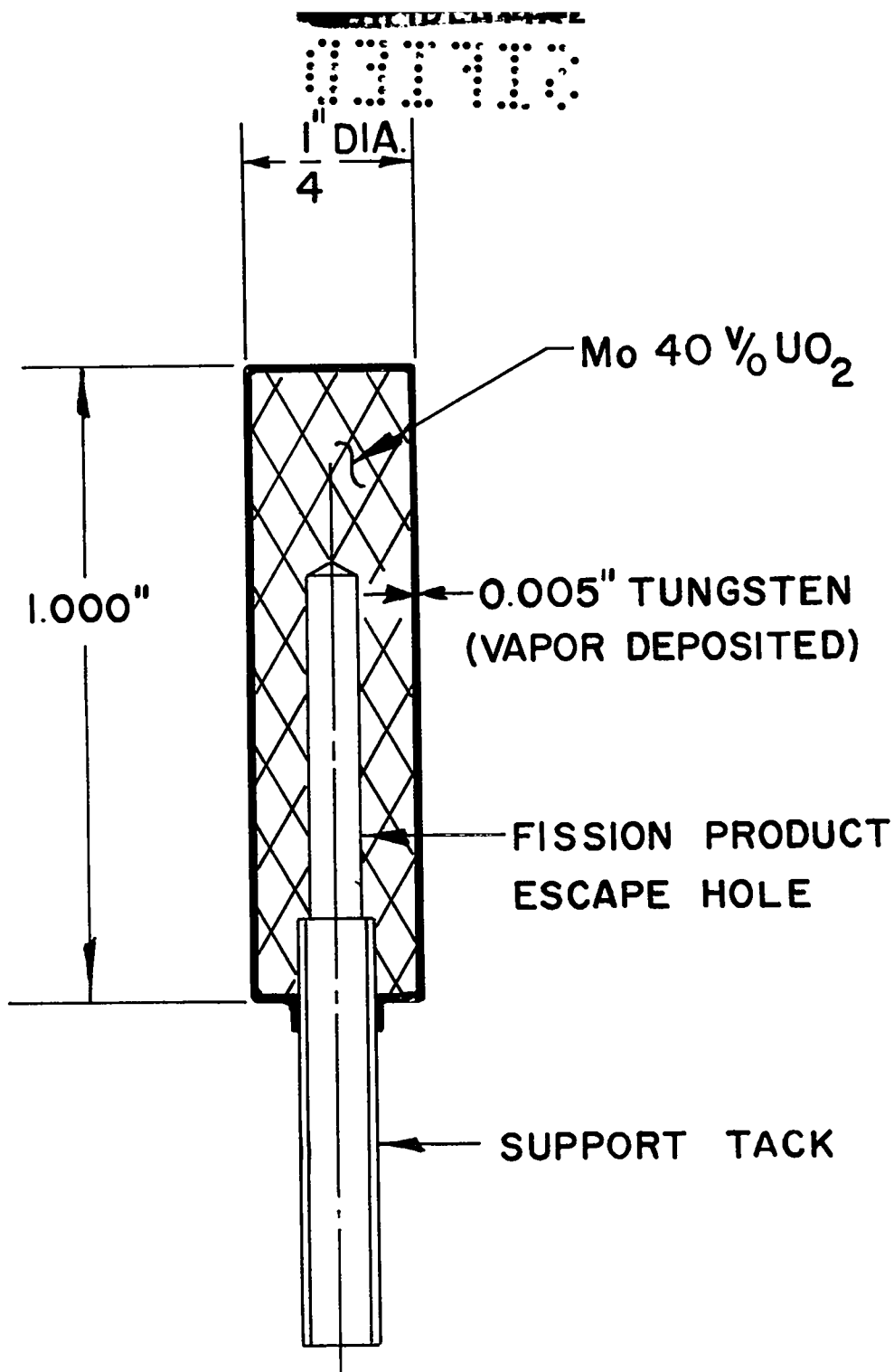


Fig. 4.1. Configuration of LASL cermet fuel pin.

~~CONFIDENTIAL~~

01100



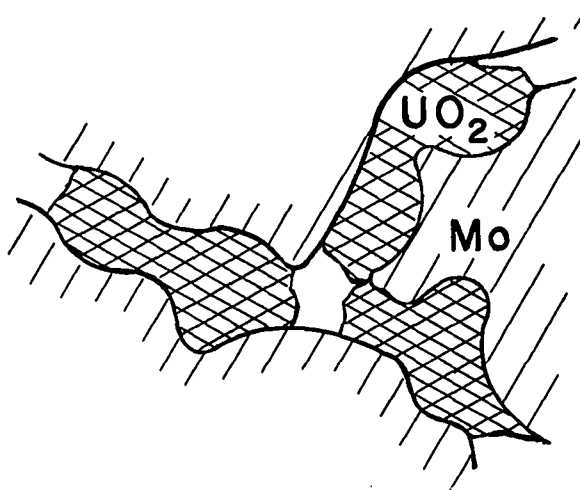
←200μ→

Fig. 4.2. Photomicrograph of Mo40v/oUO<sub>2</sub> cermet showing a region depleted of <sup>235</sup>UO<sub>2</sub>.

01100

~~CONFIDENTIAL~~

03110

Low Porosity Cermet

b.

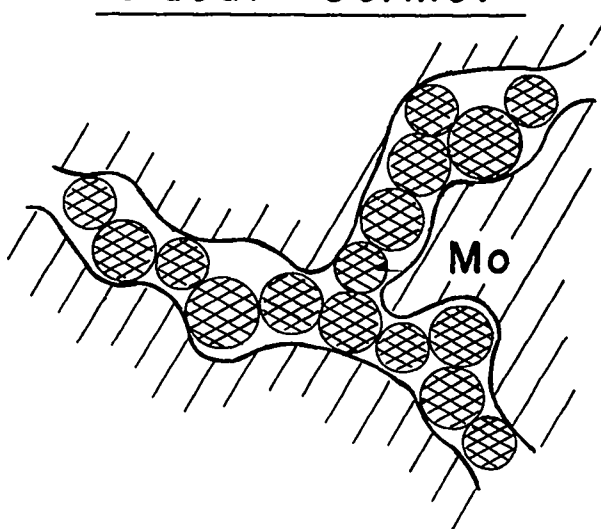
"Ideal" Cermet

Fig. 4.3. Model demonstrating the effect of introducing porosity into the MoUO<sub>2</sub> cermet.

03110

[REDACTED]

SECRET

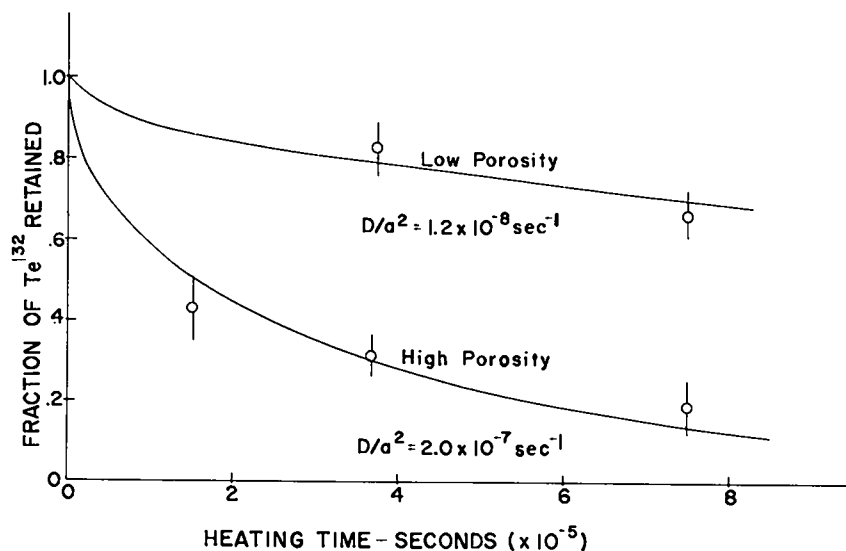


Fig. 4.4 Retention of  $\text{Te}^{132}$  in irradiated cermet fuel pins versus time at  $\sim 2200^\circ\text{K}$ . Curves are those calculated for diffusion from spherical and  $\text{UO}_2$  particles for the  $D/a^2$  values shown.

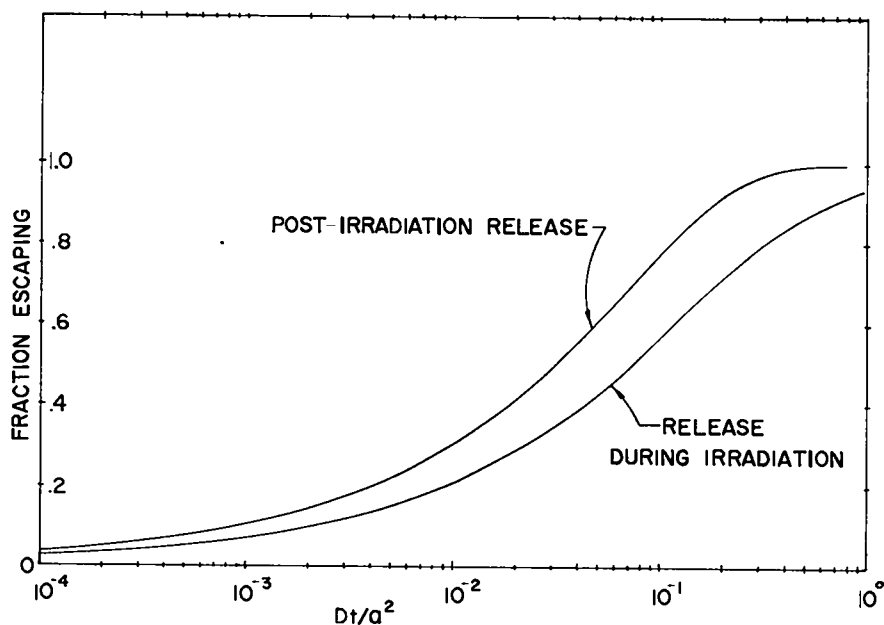


Fig. 4.5 Fractional release of fission products by diffusion from spherical particles as a function of diffusion coefficient,  $D$ , particle radius,  $a$ , and heating time,  $t$ .

93  
SECRET

CONFIDENTIAL

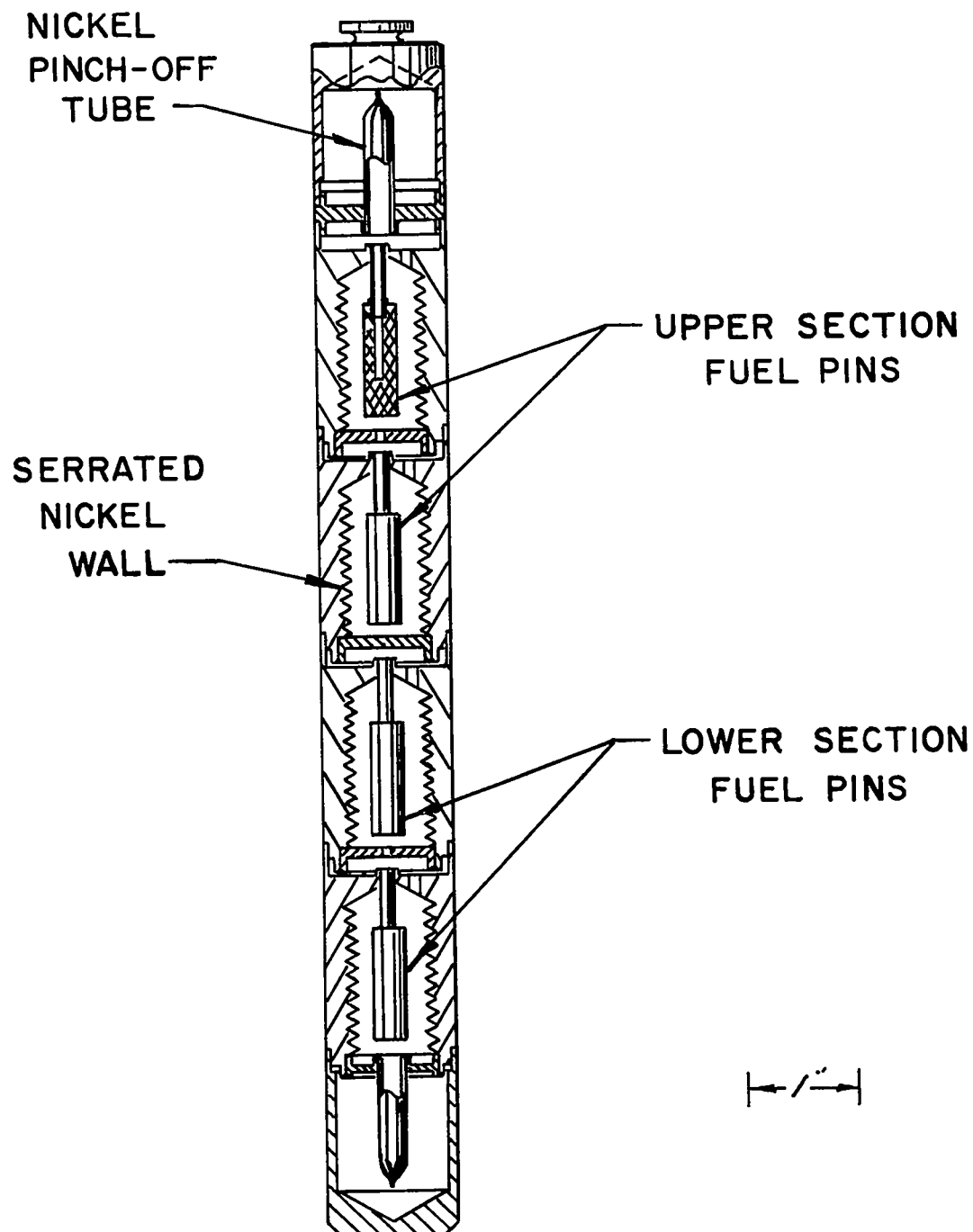


Fig. 4.6. Capsule design used in long term fuel pin irradiation tests conducted in the MTR.

CONFIDENTIAL

CONFIDENTIAL

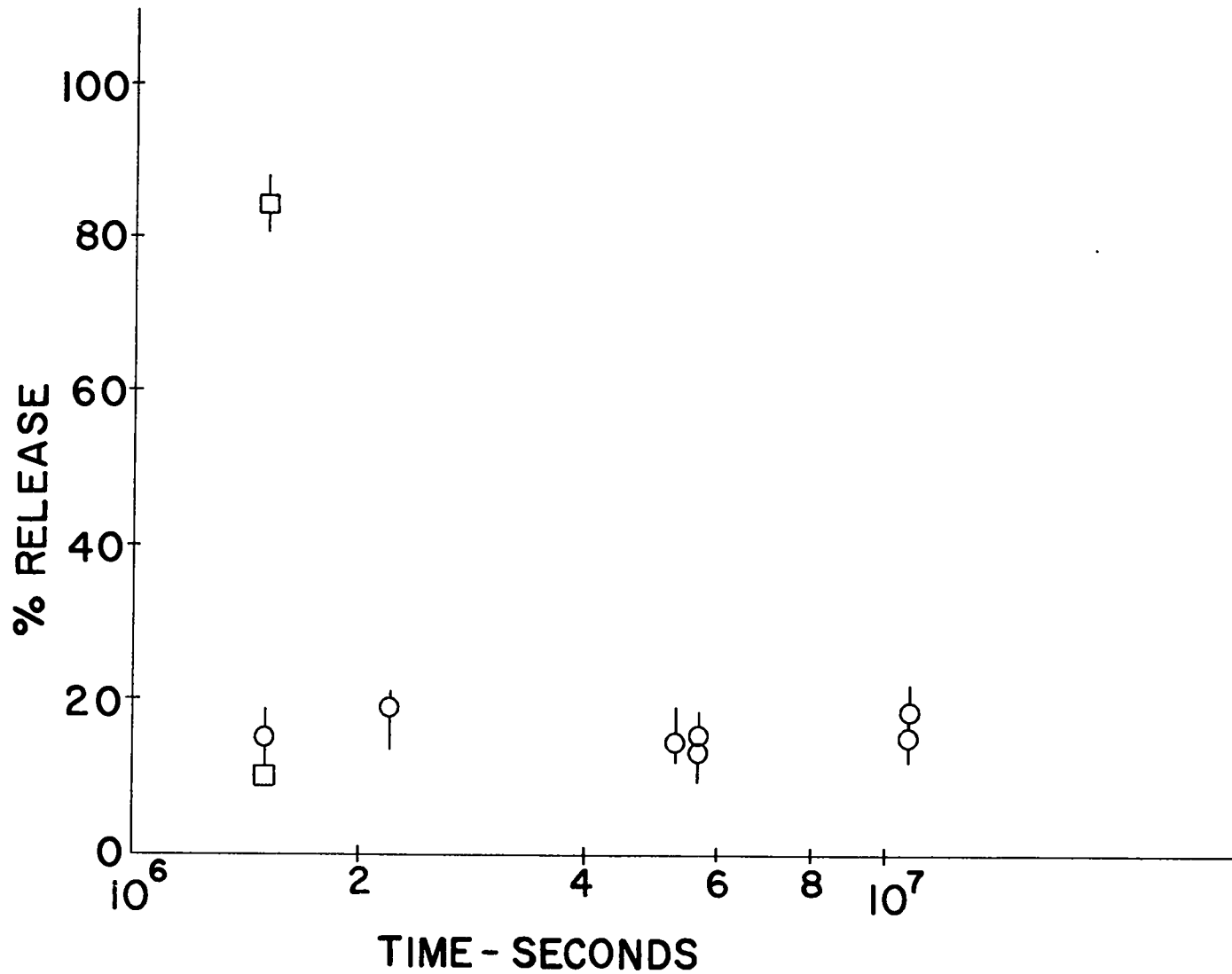


Fig. 4.7. Release of gaseous fission products from fuel pins versus logarithm of irradiation time. Open circles are values for Xe plus Kr release obtained for low porosity fuel pins. Open squares are values of Cs release.

CONFIDENTIAL

CONFIDENTIAL

031710

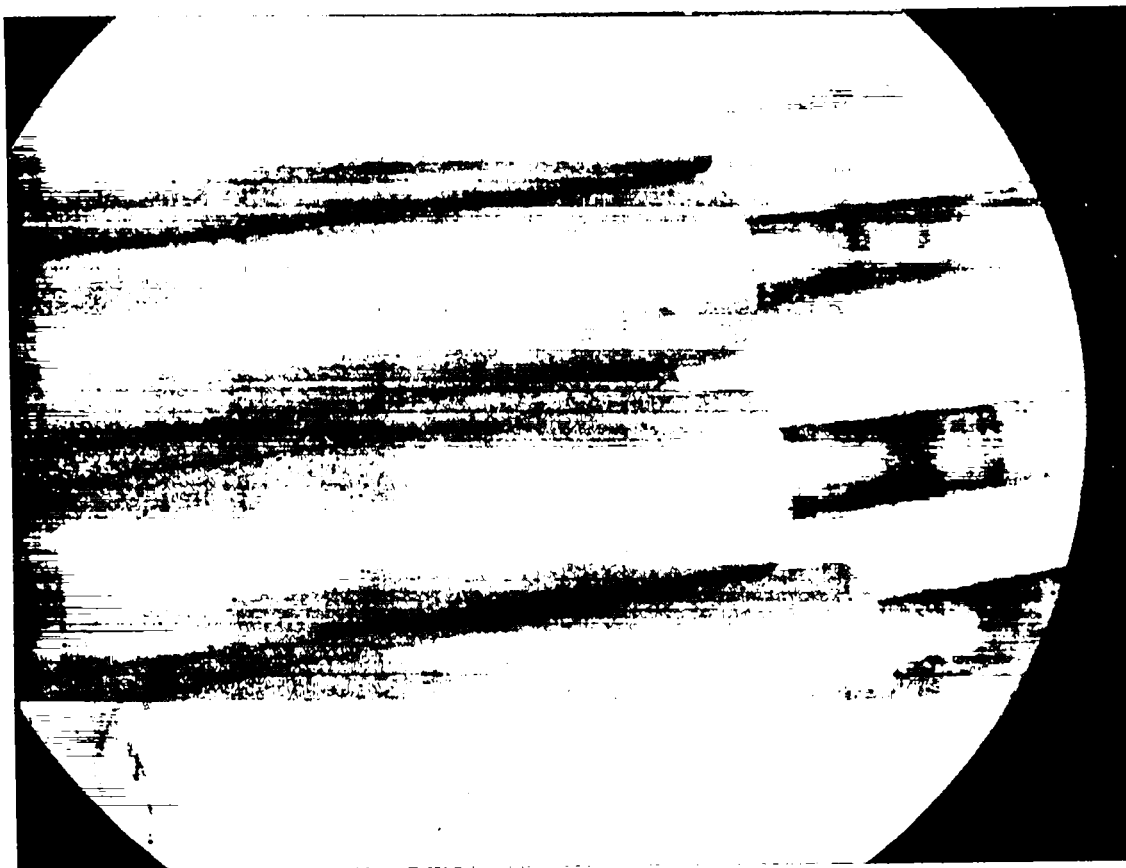


Fig. 4.8. Photograph of fuel pins irradiated for 5080 hr at  $\sim 1800^{\circ}\text{C}$ . Fission power density averaged 290 watts per  $\text{cm}^3$  of cermet.

031710

CONFIDENTIAL

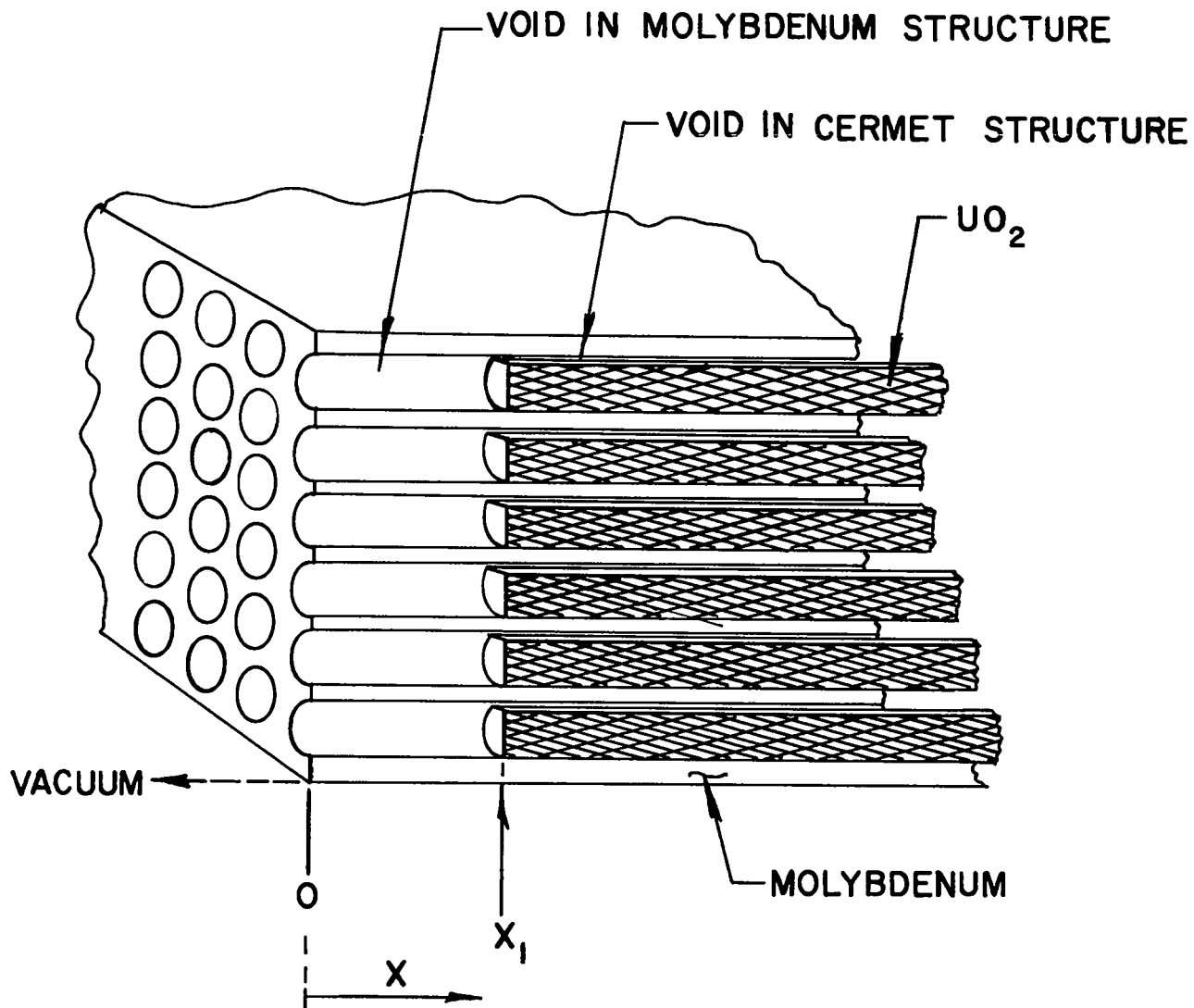


Fig. 4.9. Simplified model of MoUO<sub>2</sub> cermet structure used to calculate UO<sub>2</sub> loss rate as a function of time.

CONFIDENTIAL



031713

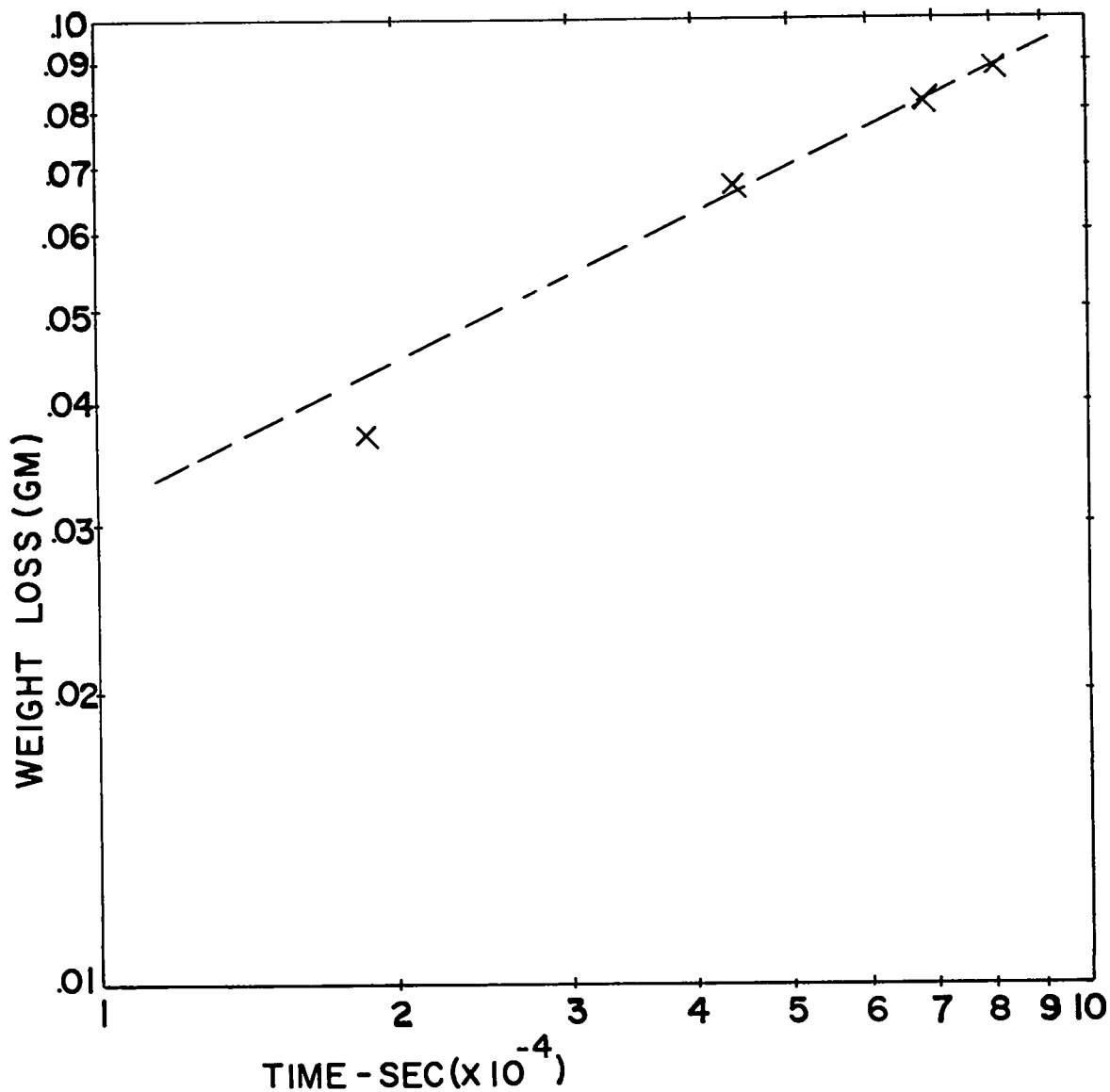


Fig. 4.10. Integrated loss of  $\text{UO}_2$  from uncoated cermet fuel pin heated at  $2170^\circ\text{K}$  versus heating time. Dashed line is proportional to the square root of heating time.

031713<sup>98</sup>

CONFIDENTIAL  
3110

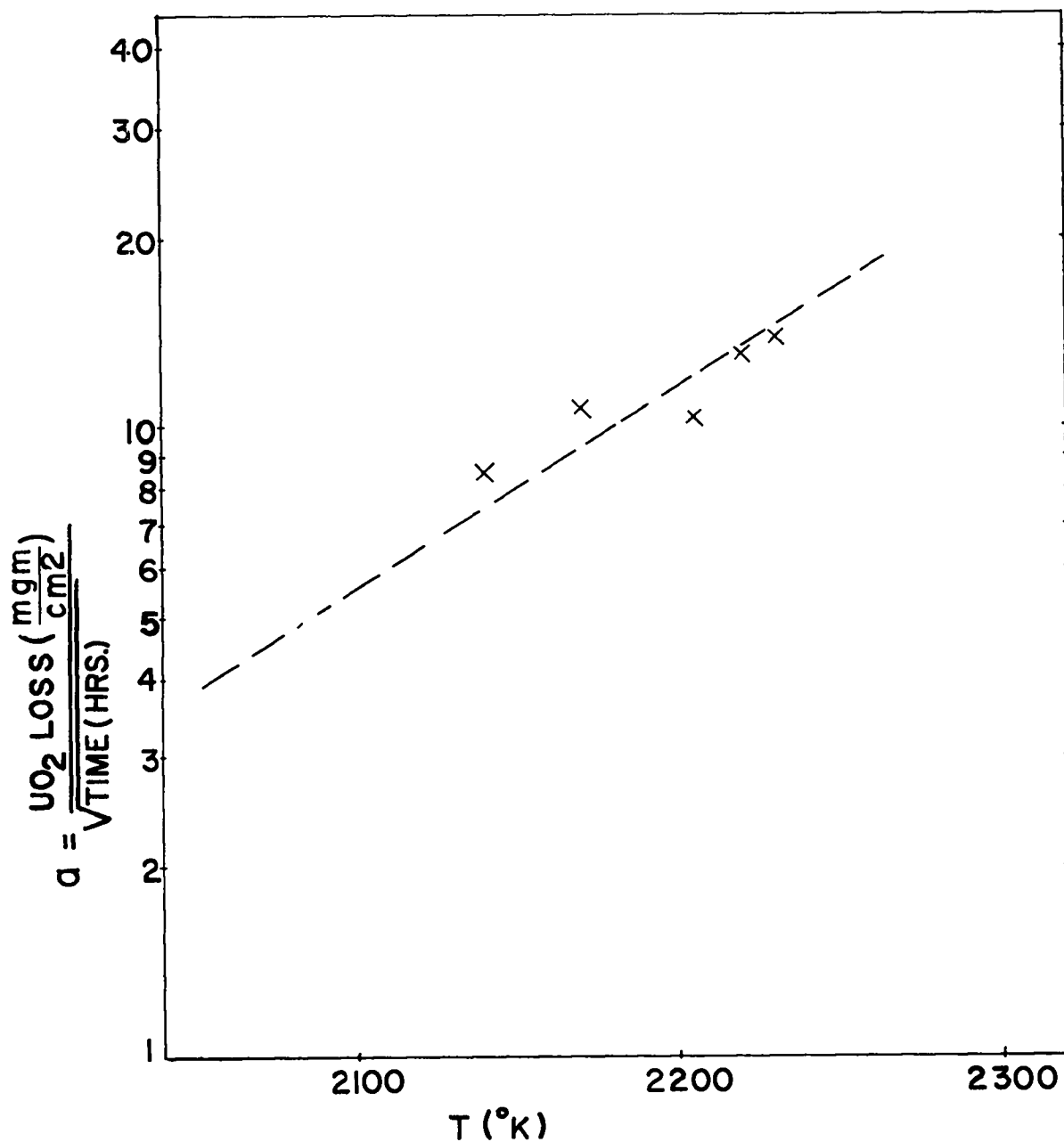


Fig. 4.11. Magnitude of  $\text{UO}_2$  weight loss parameter,  $a$ , for various fuel pin temperatures. Dashed line is proportional to the square root of  $\text{UO}_2$  vapor pressure.

CONFIDENTIAL  
3110

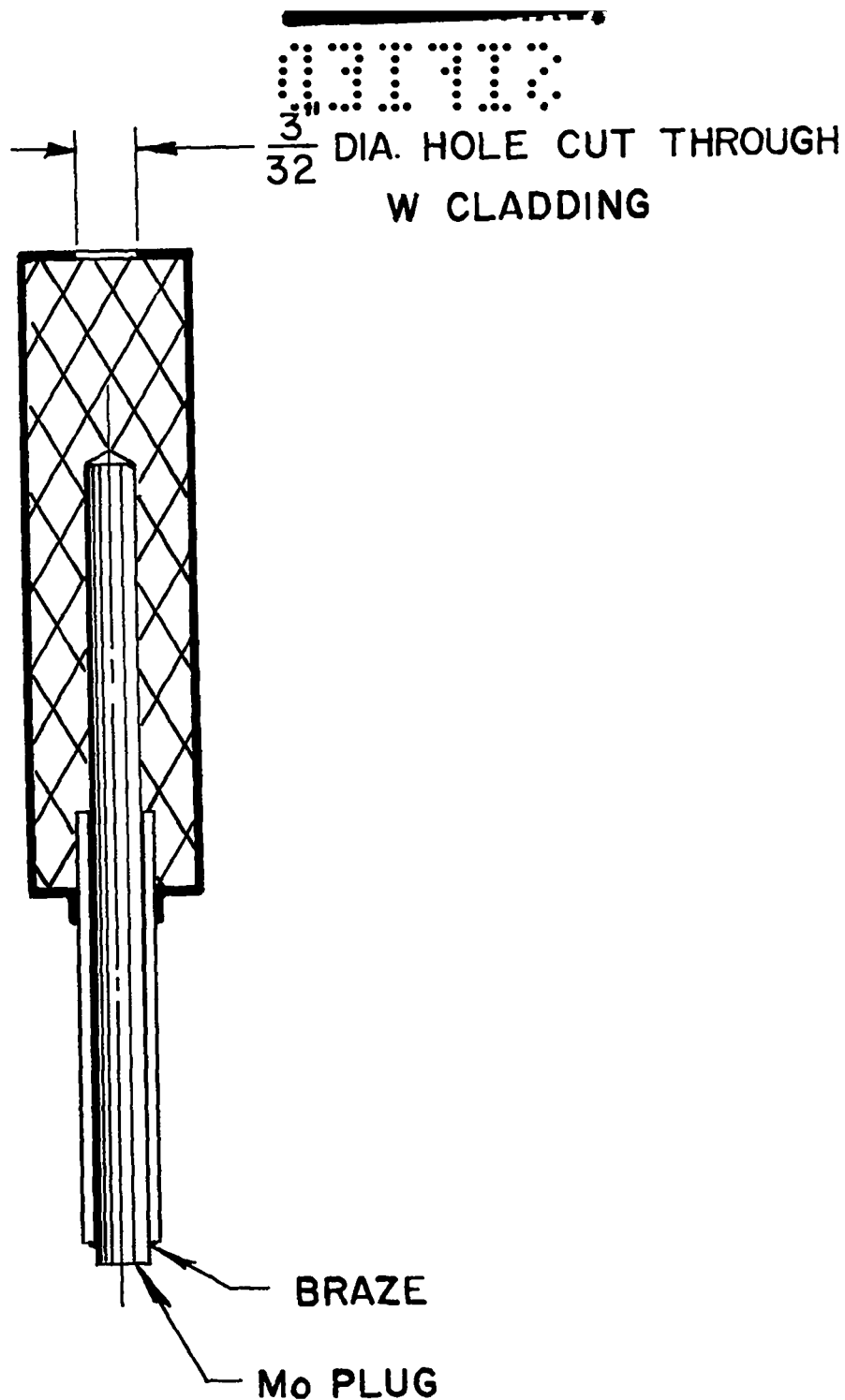


Fig. 4.12. Configuration of fuel pin used to demonstrate the possibility of reducing  $\text{UO}_2$  loss rate without reducing escape fraction of fission gases.

100  
 03113  
 00000

SECRET

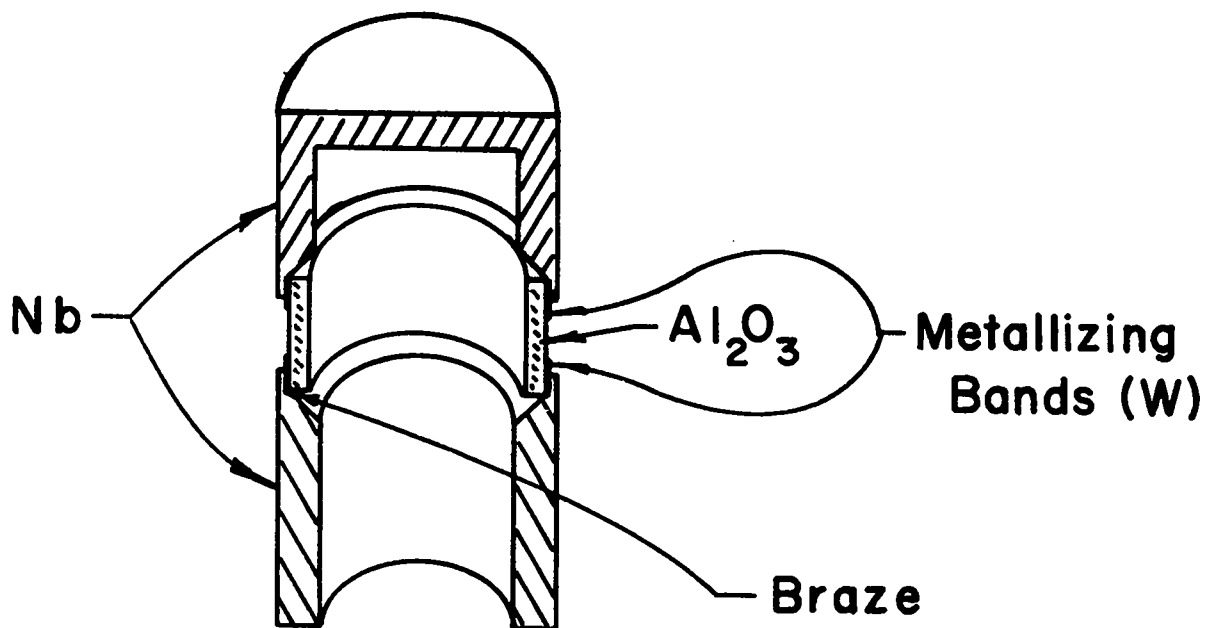


Fig. 4.13. Configuration of ceramic-to-metal seal test pieces.

SECRET

CONFIDENTIAL

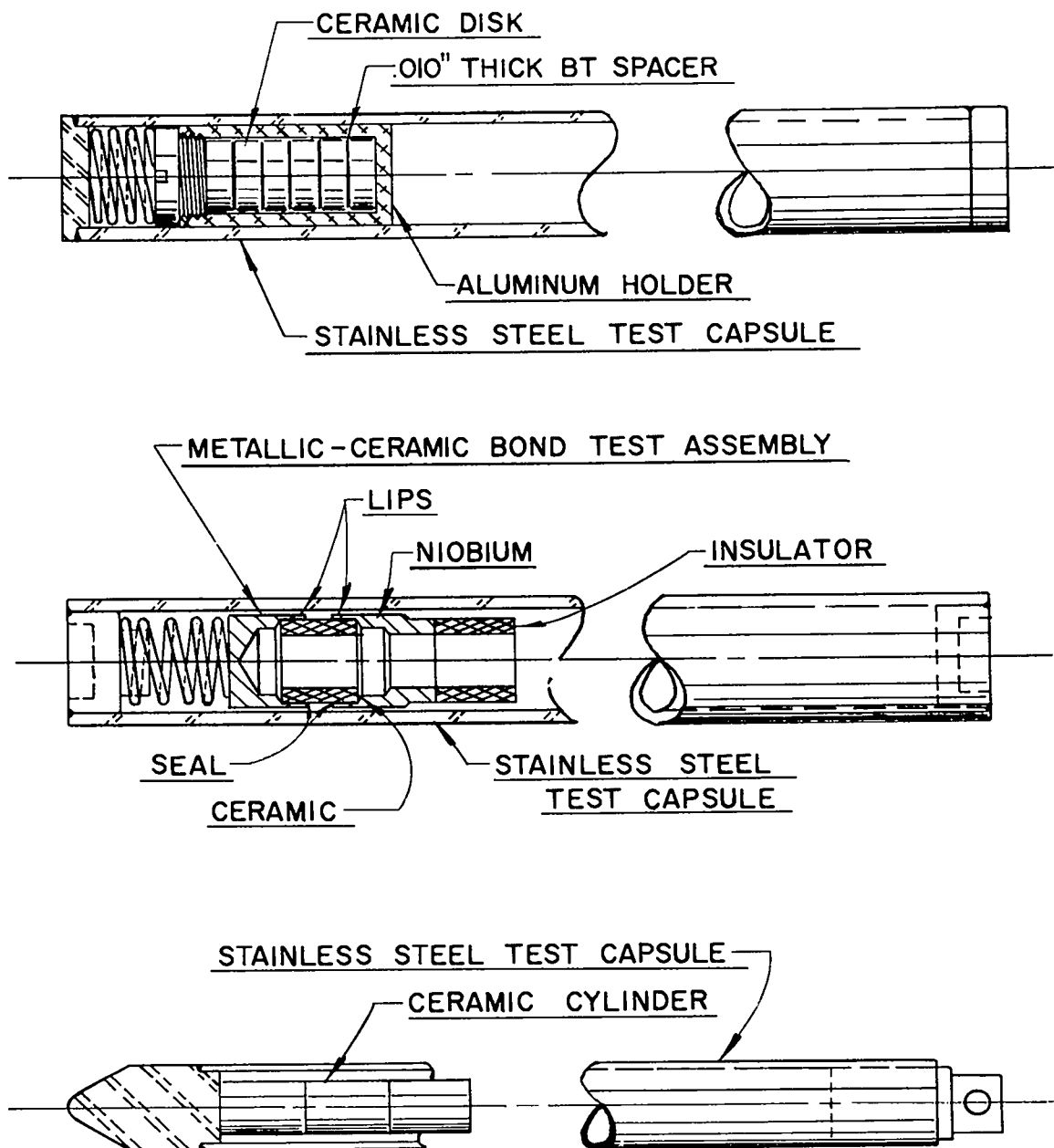


Fig. 4.14. Capsules used for neutron irradiation tests of ceramics and ceramic-to-metal seals.



Fig. 4.15. MgO discs irradiated in the MTR to  $1.5 \times 10^{20}$  nvt integrated fast flux ( $\geq 1$  Mev).

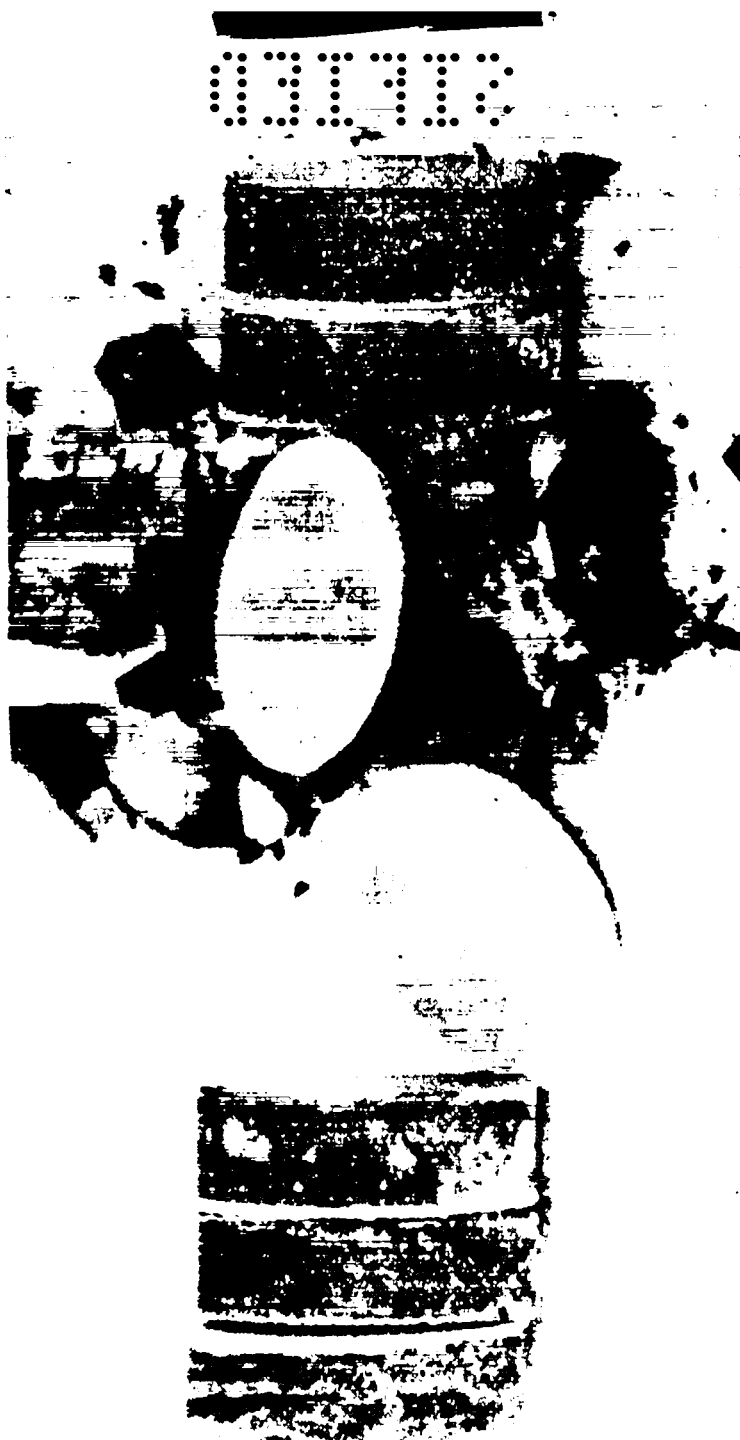


Fig. 4.16. Yttria discs irradiated to  $1.5 \times 10^{20}$  nvt integrated fast flux.

104

SIFTED

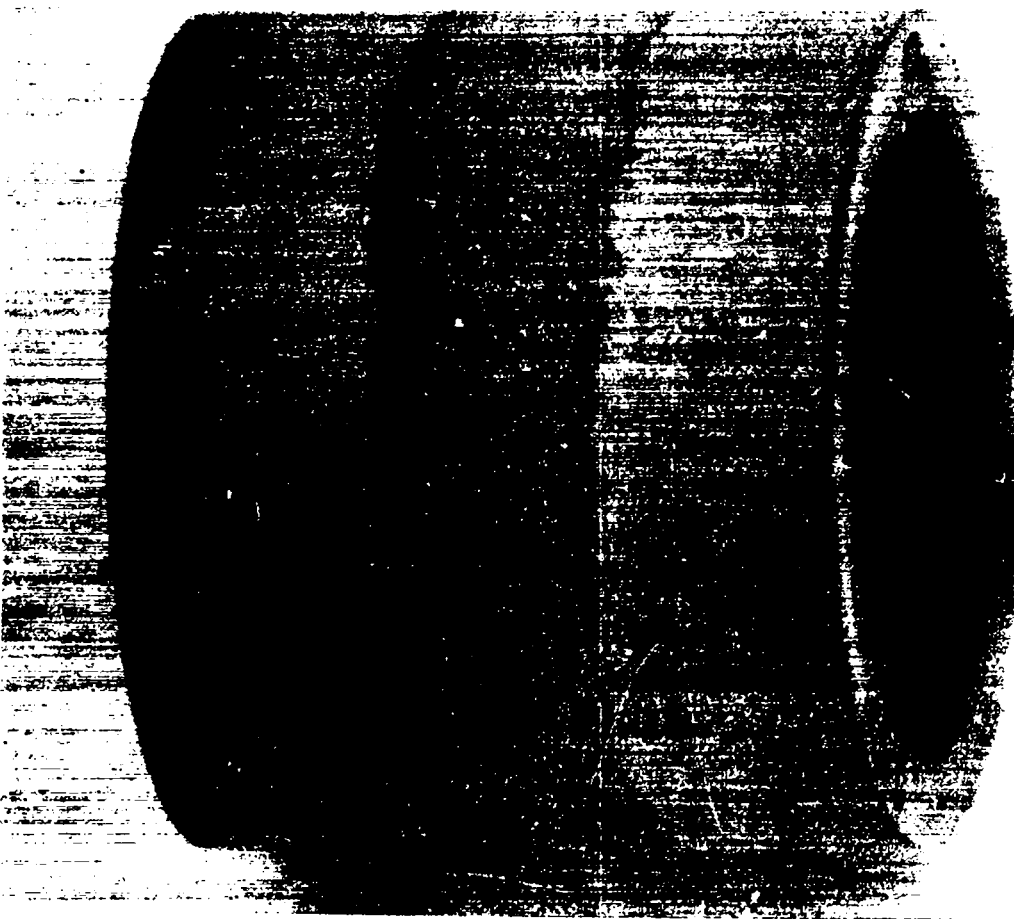


Fig. 4.17. Al-300 insulating bushing after exposure to  $3.2 \times 10^{20}$  nvt fast flux at  $\sim 700^\circ\text{K}$ .

105  
SIFTED



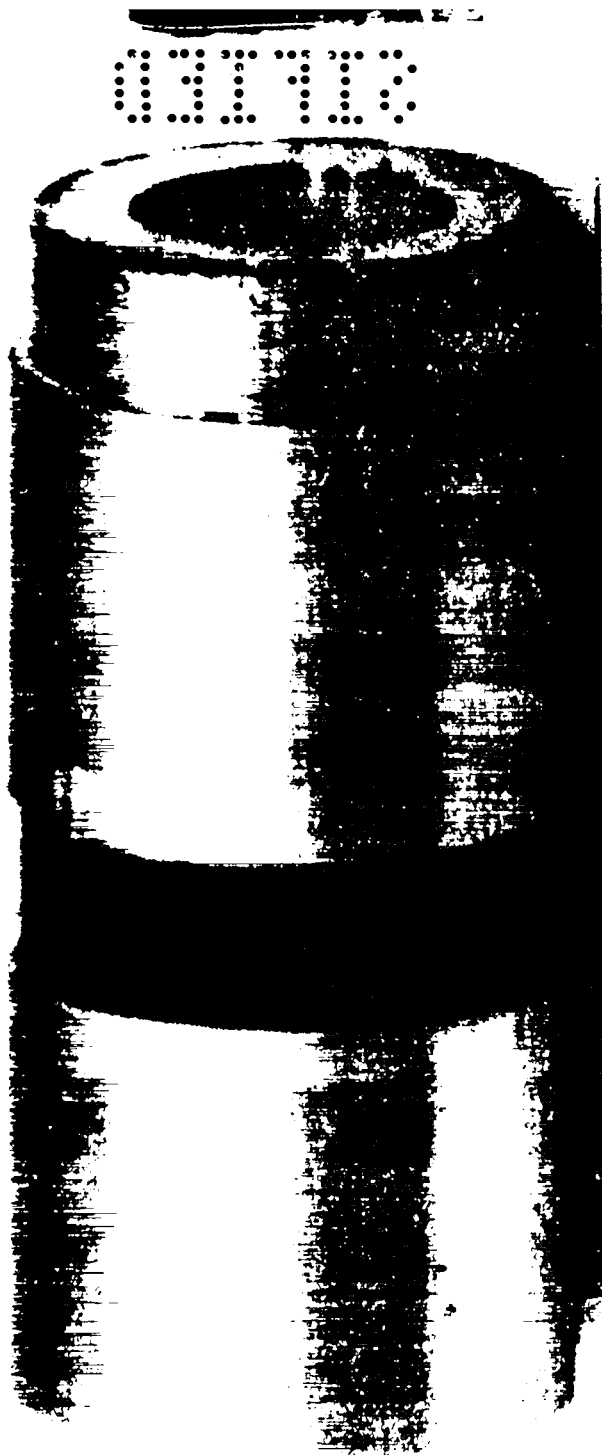


Fig. 4.18. Tungsten metallized Al-300 ceramic to niobium seal made with palladium/cobalt braze after  $3 \times 10^{20}$  nvt fast neutron irradiation at  $\sim 900^\circ\text{K}$ .

106  
03712

~~CONFIDENTIAL~~  
SECRET

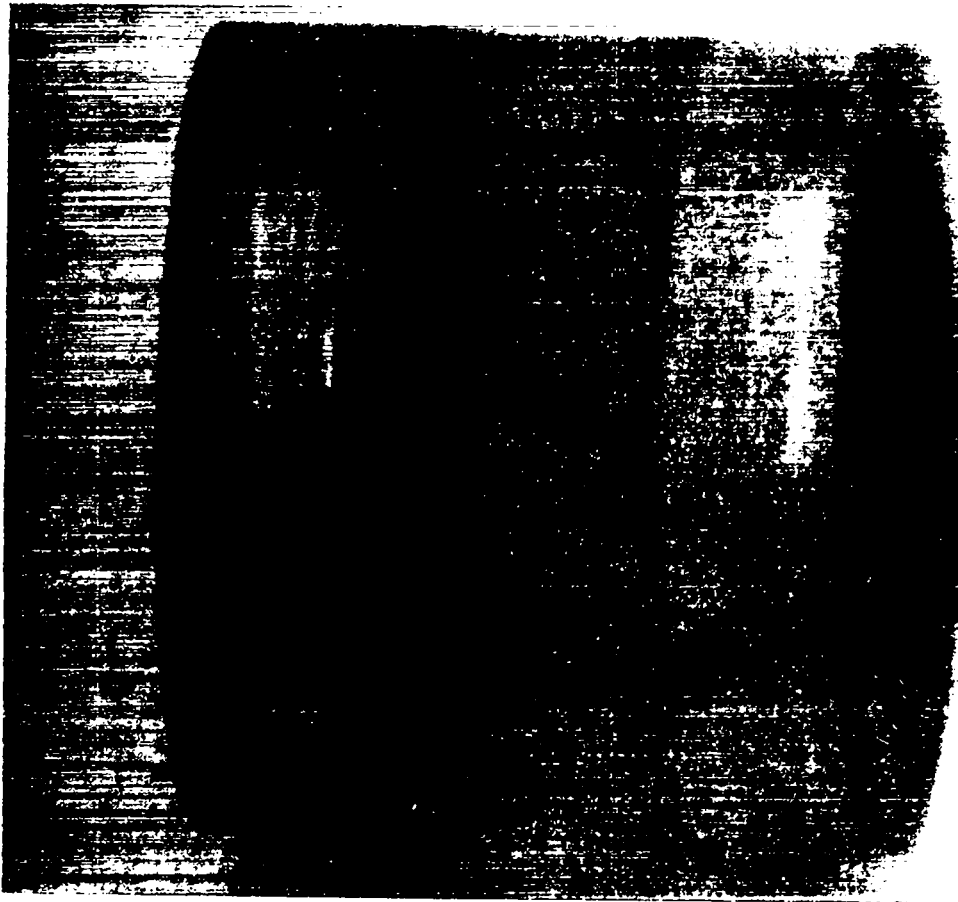


Fig. 4.19. Tungsten metallized Al-14 insulating bushing  
after  $3.2 \times 10^{20}$  nvt fast neutron irradiation  
at  $\sim 700^\circ\text{K}$ .

107  
SECRET

031710



Fig. 4.20. Tungsten metallized Al-14 ceramic to niobium seal made with vanadium braze. Fast neutron exposure was  $2.0 \times 10^{20}$  nvt at  $\sim 970^\circ\text{K}$ .

031710 108

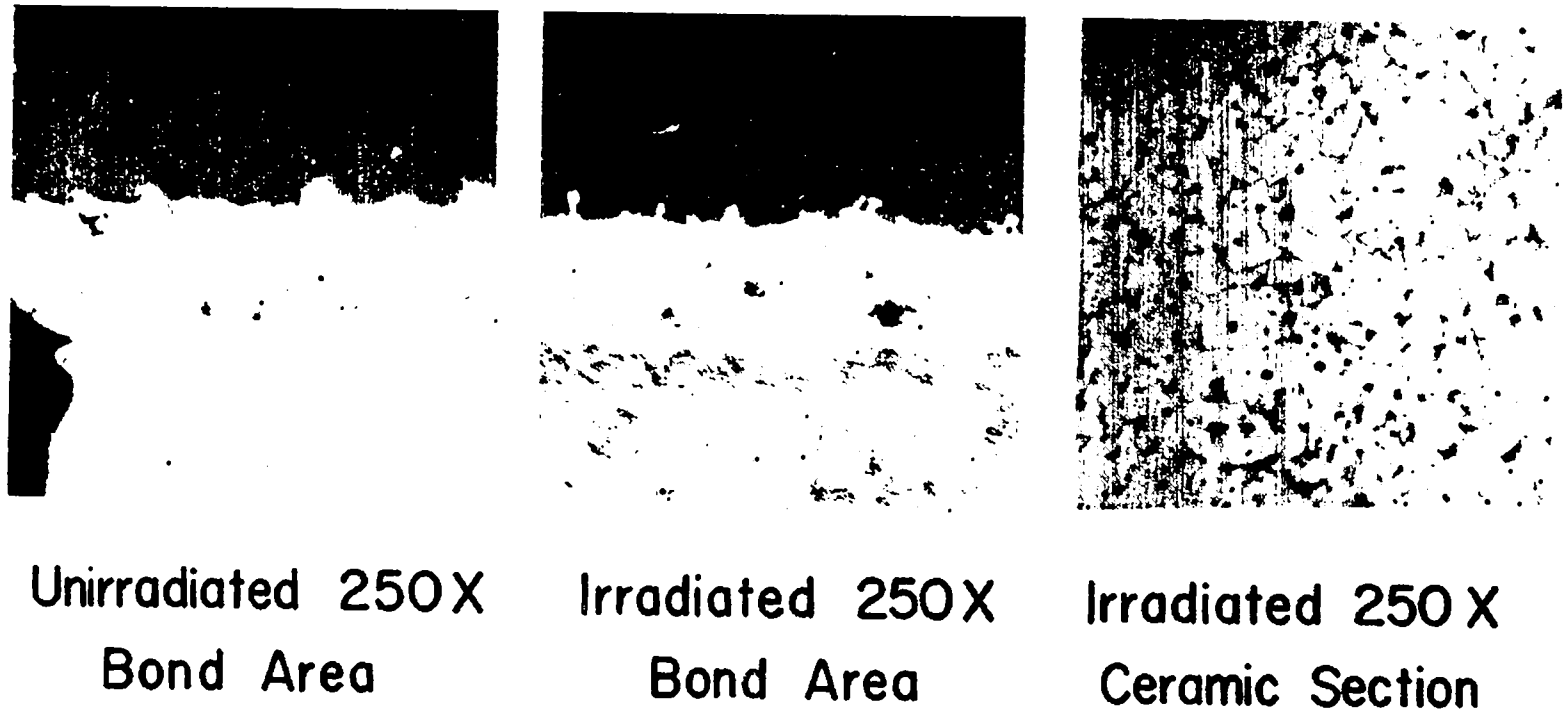


Fig. 4.21. Photomicrographs of Al-<sup>14</sup>W-V-Nb test assembly. Irradiated sample experienced  $2.0 \times 10^{20}$  nvt of fast neutrons at  $\sim 970^\circ\text{K}$ .

03113

## 5. Part Two of Physics for Administrators

Ernest W. Salmi

This lecture has been billed as "Part Two of Physics for Administrators," however, there will be very little physics involved. We shall first develop a rather simplified model of a thermionic converter. This model will then be optimized for maximum power density and then for maximum efficiency. The results will then be compared to experiments, and then a rather broad generalization will be made.

Since work function, plasma potentials, and sheath drop will be turning up all the time we will begin our discussion with these subjects. If one has a metal box which is at a uniform high temperature, and inside the box is a high-pressure (approximately 1 torr) plasma in equilibrium with the metal box, then one will have the potential distribution shown in Fig. 5.1.

The definitions of the quantities shown are:

$W$  is the work function of the metal

$\phi_1$  is the plasma potential with respect to the metal  
Fermi level

$\phi$  is the sheath potential drop

$N_e$  is the electron density in the plasma

$N_e v/4$  is the random current in the plasma

$A$  is a constant equal to  $120 \text{ amps/cm}^2 (\text{°K})^2$ .

The sheath potential drop,  $\phi$ , is present in order to establish equilibrium between the Richardson current emitted by the metal and the electrons entering the metal from the plasma. One therefore has the

03113

03113

SECRET

equation

$$J_e = AT^2 \exp\left(\frac{-eW}{kT}\right) = N_e ev/4 \exp\left(\frac{-e\phi}{kT}\right)$$

solving for  $W-\phi$ , one has

$$\phi_1 = W - \phi = \frac{k}{e} T \ln\left(\frac{AT^2}{N_e ev/4}\right)$$

The plasma potential  $\phi_1$  is independent of the work function of the metal and depends mainly on the properties of the plasma.

If the plasma pressure is varied, one can obtain the potential diagrams shown in Fig. 5.2. The low pressure case has a potential sheath drop of the opposite sign from the example above. In this case, the sheath potential reduces the Richardson emission.

Suppose that the high-uniform-temperature metal box is cut in half and the materials changed so that one half has a high work function and the other half has a low work function. Also assume that the two halves are isolated electrically. This situation is shown in Fig. 5.3. Since no current is allowed to flow, there will be a uniform potential in the center of the plasma. Therefore, the difference in potential of the Fermi level of the two parts of the container will be

$$\Delta V = \phi_1 - \phi_2$$

However, above, it was shown that the plasma potential depends only on the plasma properties, therefore

$$\phi_1 = \phi_2$$

and

$$\Delta V = 0$$

This is surely a trivial case; however, many inventions have been dreamed up which are supposed to get past this solution.

In the above case, equilibrium was established between the electrons emitted and received by the metal. An interesting non-equilibrium situation is established if the right-hand side of the box is cooled so

SECRET

CONFIDENTIAL

that only a trivial number of electrons are emitted. Then the potential diagram has the shape shown in Fig. 5.4. On the left, the value of the plasma potential,  $\phi_1$ , has not changed. On the right-hand side, since the total current is zero, at the cold metal interface the ion and electron current must be equal. The random electron current,  $N_e v_e/4$ , is larger than the random ion current,  $N_i v_i/4$ , because the electron velocities are much higher than the ion velocities. A sheath potential is therefore developed to reduce the electrons arriving at the metal. This is shown in Fig. 5.4 as a potential  $\phi_2$ . The ion current and electron currents are set equal by the equation

$$N_i v_i/4 = N_e v_e/4 \exp\left(\frac{-e\phi_2}{kT}\right)$$

and since

$$N_i = N_e$$

then

$$\phi_2 = \frac{k}{e} T \ln\left(\frac{v_e}{v_i}\right)$$

The ratio of velocities is proportional to the square root of the mass ratio, and using the mass ratio of an electron to a cesium ion one obtains the value

$$\phi_2 = 6.2 kT$$

The voltage difference set up between the hot and cold sides of the box is given by

$$V = \phi_1 + \phi_2 - W_2$$

Since  $\phi_1$  and  $\phi_2$  are independent of the work function of the hot side or emitter, then one finds that the open-circuit voltage of a thermionic diode is independent of the emitter work function. This statement may need a second-order correction.

If the value of  $V$  is now reduced by interconnecting the two halves of the box through an external impedance, there will be a resultant

112  
CONFIDENTIAL

[REDACTED]

SECRET

current of electrons from the hot emitter to the cold collector. If the voltage difference,  $V$ , is set equal to zero, then one can see how the potential diagram varies with plasma pressure. This is shown in Fig. 5.5. In Fig. 5.5a, the pressure is very low so that the electron current is less than the Richardson emission limit. The main potential drop occurs at the collector side. In Fig. 5.5b, the pressure is very high. There exists a very large potential drop at the emitter resulting in very high electron temperatures. The electron current is at the emission limit. In Fig. 5.5c, one has an intermediate pressure. The electron current is almost emission-limited. At the collector there exists a potential drop. In order to develop power, the voltage,  $V$ , could be increased to eliminate this potential drop at the collector, and one would obtain a resultant power output. What would be the situation for the maximum power output? A very much idealized potential diagram is shown in Fig. 5.6 in which it is assumed that

$$\begin{aligned} V &= W_1 - W_2 \\ I &= AT^2 \exp \left( \frac{-eW_1}{kT} \right) \\ P &= I (W_1 - W_2) \end{aligned}$$

It is admitted that this situation is very idealized and perhaps never exists in practice. The equation for power is surely an overestimate. However, because of its simplicity, it shall be assumed as the model for maximum power output for a converter with an emitter work function of value  $W_1$  and a collector work function of value  $W_2$ . Throughout the following discussion the emitter temperature will be held constant at  $2100^\circ\text{K}$ .

If one assumes that both  $W_1$  and  $W_2$  can be adjusted arbitrarily, one can ask what value should they be for maximum power. As for  $W_2$ , it is obvious that the smaller  $W_2$ , the higher the power output; however, we shall for the moment assume that  $W_2$  is 1.7 eV. As for the optimum  $W_1$  value, one can set the derivative of  $P$  equal to zero as below:

173  
SECRET



031713

$$\frac{dP}{dW_1} = 0 = \exp\left(\frac{-eW_1}{kT}\right) - \frac{e}{kT} (W_1 - W_2) \exp\left(\frac{-eW_1}{kT}\right)$$

or

$$W_1 = W_2 + \frac{k}{e} T$$

Inserting the value of

$$W_2 = 1.7 \text{ eV}$$

$$kT = .184 \text{ eV}$$

one obtains

$$W_1 = 1.884 \text{ eV}$$

$$V = .184 \text{ volts}$$

The power output for these conditions and this model would then be  $3 \times 10^3 \text{ watts/cm}^2$ . This could be called a high-performance cell but, as will be shown below, entirely unrealistic.

Another type of optimization can be performed. Instead of asking for maximum power, assume that one desires maximum efficiency. Assuming for the moment that there are no thermal losses, one can write the following equations.

$$\text{Power input} = I(W_1 + 2 kT)$$

$$\text{Power output} = I(W_1 - W_2)$$

$$\text{Efficiency} = \frac{\text{Power output}}{\text{Power input}} = \frac{I(W_1 - W_2)}{I(W_1 + 2 kT)}$$

It is obvious that the maximum efficiency occurs for very large values of  $W_1$ . So, for maximum power, the emitter work function should be about 1.9 eV; however, for maximum efficiency the emitter work function should be infinite. Of course, this latter condition gives zero power

031713

[REDACTED]

SECRET

output; and, since there are thermal losses, this is not a correct answer. Therefore, one can assume a constant thermal loss,  $H$ , which then gives the following:

$$\text{Power input} = I (W_1 + 2 kT) + H$$

$$\text{Efficiency} = E = \frac{I(W_1 - W_2)}{I(W_1 + 2 kT) + H}$$

For a maximum in  $E$ , one has

$$\frac{dE}{dW_1} = 0 = W_1 + 2 kT + \frac{H}{I} - (W_1 - W_2) \left(1 + \frac{1}{kT} \frac{H}{I}\right)$$

or

$$\frac{H}{I} = \frac{kT(W_2 + 2 kT)}{W_1 - W_2 - kT}$$

A typical value of  $H$  is about 20 watts/cm<sup>2</sup> which results in an electron current of about 30 amps/cm<sup>2</sup> or 30 watts/cm<sup>2</sup>. The efficiency would be about 30%. The interesting point to be made is that the maximum efficiency is very far from the maximum power point. When one adds other losses such as connector losses, this current density value will be reduced still further.

Before comparing these results with experiment, a few words will be added concerning the assumed collector work function value of 1.7 eV. It has been assumed that the application will be in space. This application requires a high collector temperature which is assumed to be 1000°K. If the work function is reduced from 1.7 eV, the collector will start to emit a considerable amount of current. The potential diagram at the collector will therefore have the shape shown in Fig. 5.7. One sees that the reduction of the work function results in a sheath potential drop which reduces the collector emission. The electrons enter the collector with extra kinetic energy picked up while falling through the

15  
SECRET

03113

sheath potential. The result is that the reduced collector work function has not produced any useful effect. For this application, a collector work function of about 1.7 eV is the best one can do.

For comparison between the above results and experiment, it was decided to use the very recently published data of V. C. Wilson.<sup>1</sup> This is a fine piece of work on a thermionic converter which had a tungsten emitter, nickel collector, and a 0.005-inch cesium gap. The collector temperature gave a maximum power output at about 1050°K. The cesium pressure was optimized to give maximum power at various emitter temperatures. In Fig. 5.8, the maximum power has been plotted as a function of current. One sees that the maximum power occurs at 55 amps/cm<sup>2</sup>. The maximum power at 2100°K is 30 watts/cm<sup>2</sup>. Wilson also presents some curves of efficiency versus current at various emitter temperatures. He has introduced some losses for an optimized connector. These curves are shown in Fig. 5.9. The dotted lines are simple extrapolations. As Wilson points out in his article, the maximum efficiency occurs at about 15 amps/cm<sup>2</sup> and is almost independent of the emitter temperature. The fundamental point to be made is that maximum efficiency occurs at a much lower current than maximum power. This is in accord with the interpretation obtained from the above simple theoretical model.

Although Wilson has introduced an optimized connector loss, there are still a few more resistive losses to be considered in an actual cell design. For this reason, it is assumed that the maximum efficiency will occur at about 10 amps/cm<sup>2</sup> and restricting ourselves to emitter temperatures of about 2100°K, the following is stated as a proposition. "All thermionic converters for space reactor applications when designed for maximum efficiency will optimize at 10 amps/cm<sup>2</sup>.

The above proposition has some very interesting ramifications, a few of which will now be considered. One interesting example is supplied by some data published by Kitrilakis, et al. in 1962.<sup>2</sup> They measured the optimized power output of cells which had various emitter materials and emitter-collector spacings. In Fig. 5.10, the power output has been

03113 116

CONFIDENTIAL

CONFIDENTIAL

plotted as a function of emitter work function. The scale on the abscissa is arbitrary in spacing. The materials are listed in order of their vacuum work function. The materials shown span a variation in work function of about 1.2 eV. On the top curve, labeled "maximum power," is the maximum power output for a 2-mil spacing as reported in this reference. One sees that the type of material used as an emitter has a great influence on the maximum power output. The point at the top of the graph is the value taken from Wilson. One sees that there has been an increase of 50% in maximum power output while the spacing has increased from 2 to 5 mils. This represents tremendous progress in maximum power density in these few years.

Next, suppose one takes the above proposition seriously and considers only the "10 amps/cm<sup>2</sup>" points. Using the same Kitrilakis, et al. and Wilson data, one can plot power output at the 10 amps/cm<sup>2</sup> point for various materials and spacing. These two curves are shown in Fig. 5.10 and labeled "2-mil" and "10-mil." The dotted curve labeled "20-mil" is only an estimate. Wilson's value for power output at 10 amps/cm<sup>2</sup> is also shown.

One sees that the situation is now entirely different from the case for maximum power. The 2-mil, 10 amps/cm<sup>2</sup> data show that power output is almost independent of the emitter material. Probably, thermal emissivity and other questions are more important in determining the choice of emitter material than their thermionic characteristics.

The case of a tungsten emitter and 10-mil spacing is reduced about 30% from the maximum expected value. The spacing dependence is much less critical than the case for maximum power.

The important point to be made here is that in reactor design requiring maximum efficiency of thermionic converters using small cesium gaps of about 10-mils and a tungsten emitter, one can conclude that spacing variations and long-time variations in the emitter work function are not too critical. If one used one of the foreign gases, such as CsF or barium - as discussed in a previous lecture - then the above statement may be extended further.

137  
CONFIDENTIAL

03113

Another problem to be considered is the effect of collector materials on the thermionic power output. As mentioned above, the desired value is 1.7 eV when the collector operating temperature is about 1000°K. For cells with small spacings, the optimum pressure is several torr, while in cells with a foreign gas the optimum will be at a few tenths of a torr, and the spacing will be large. In Fig. 5.11, the work function of various materials are plotted for a high and a low cesium pressure. It must be admitted that this curve is not exact; however, the point to be noted here is that one should avoid using niobium for a collector. The use of either Mo, W, Re, or Ni for the collector in the high-pressure cases appears to have little effect. This statement is probably in doubt for the low-pressure case, since there is a greater sensitivity of work function to the type of material as shown in Fig. 5.11. The result to be noted here is similar to the emitter material question. If one constructs the converter out of high-vacuum work function material, long-term variations in the operating work function should have very little effect on the cell performance.

The conclusion is that for maximum-efficiency thermionic converters, the output has reached a point at which one does not expect substantial changes through further refinement of the physics. The main problems with a reactor thermionic converter are concerned with the design and fabrication, which will be discussed in Chapter 12.

#### References

1. V. C. Wilson and J. Lawrence, "Operating Characteristics of Two Thermionic Converters Having Rhenium-Nickel and Tungsten-Nickel Electrodes," Advanced Energy Conversion, Vol. 4, pp. 195-221, Pergamon Press, 1964.
2. S. S. Kitrilakis, M. E. Meeker, and N. S. Rasor, "Annual Technical Summary Report for the Thermionic Emitter Materials Research Program, 1 July 1961 through 30 June 1962," TEE-4015-3.

03113 113

~~CONFIDENTIAL~~

[REDACTED]

SECRET

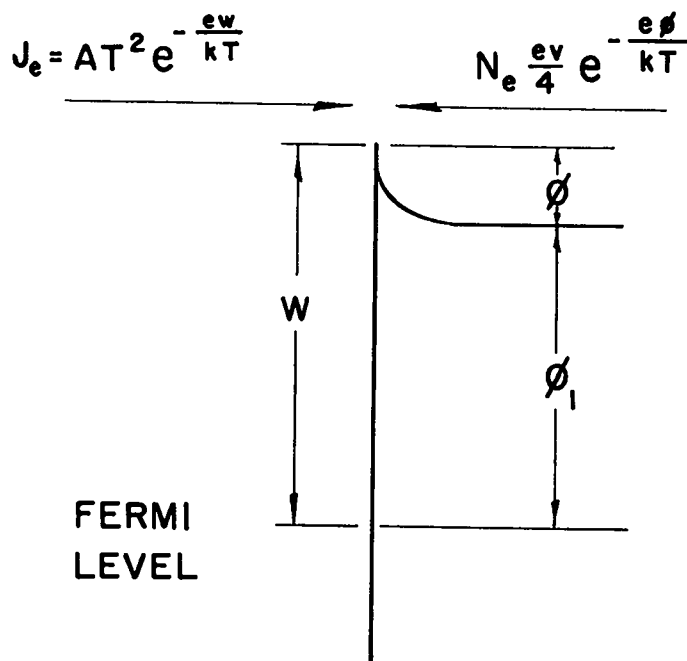


Fig. 5.1. Potential distribution in metal and plasma at high temperature equilibrium.

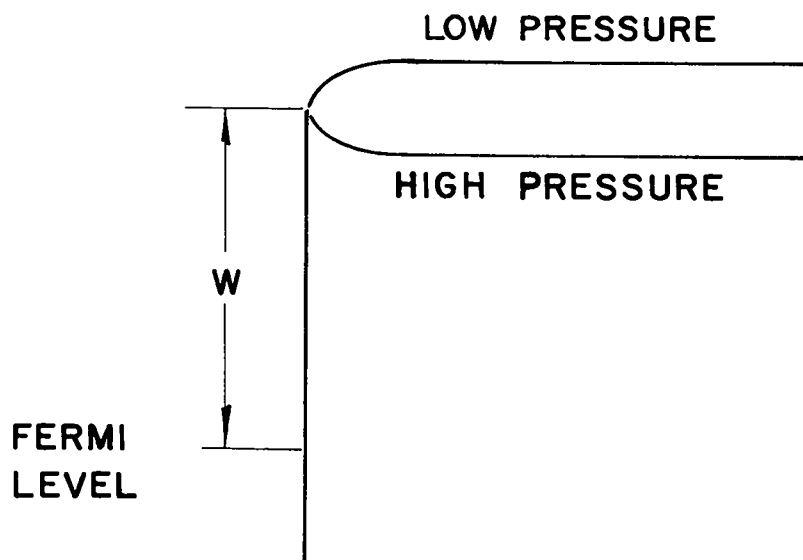


Fig. 5.2. Effect of plasma pressure on potential distribution.

119 SECRET

[REDACTED]

03713

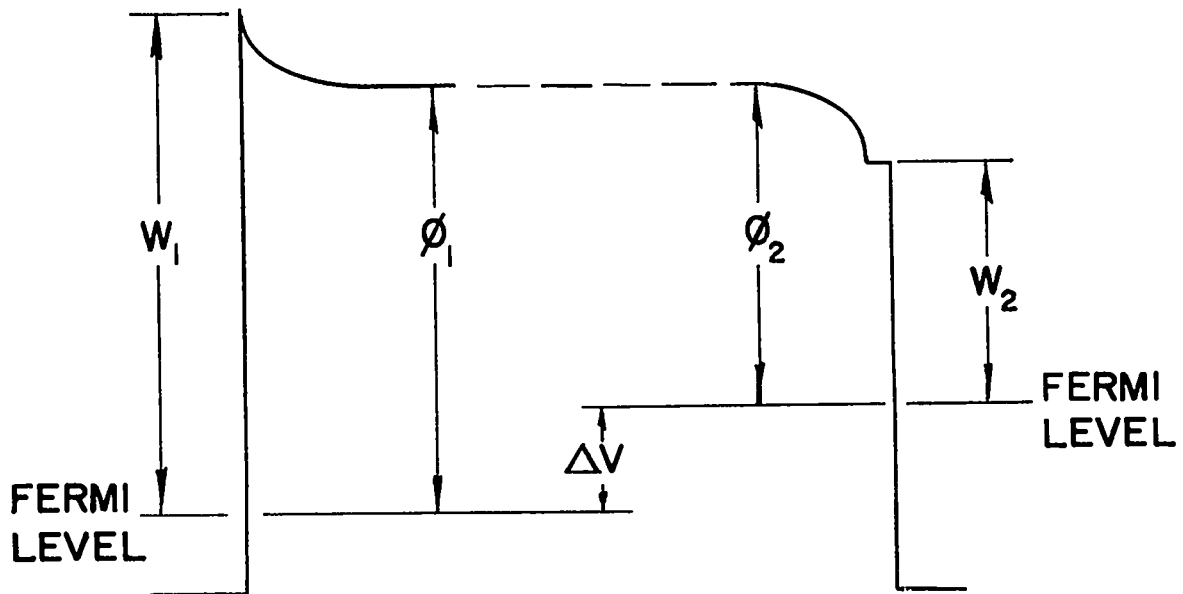


Fig. 5.3. Effect of work function on potential distribution at high temperature equilibrium.

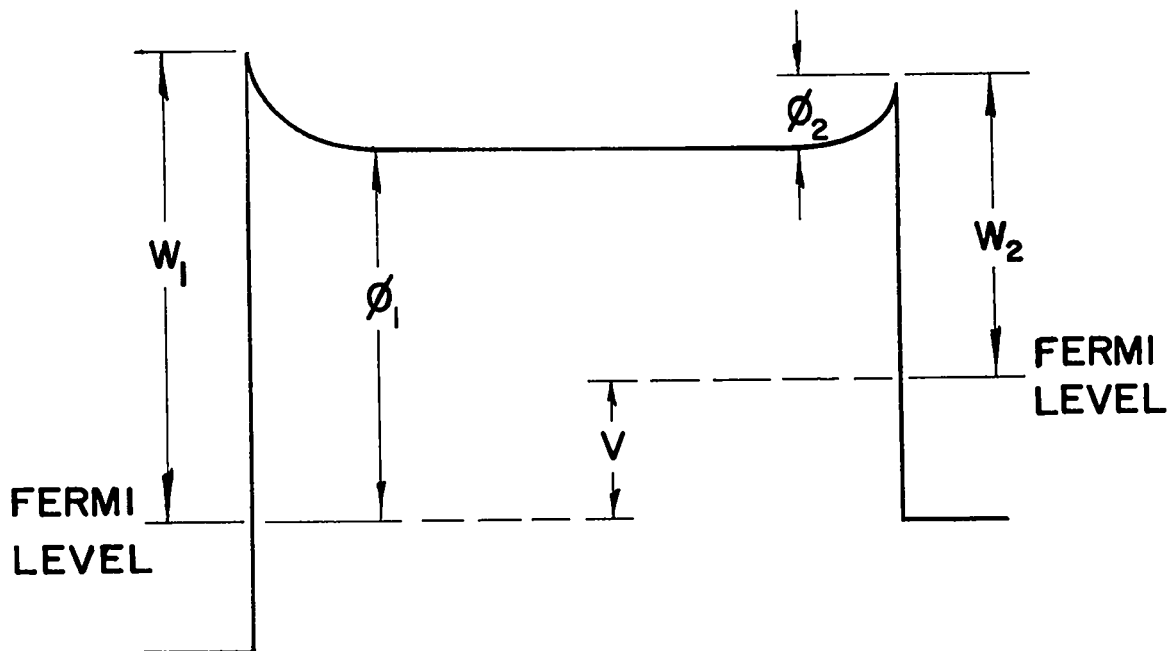


Fig. 5.4. Potential distribution for case of non-uniform temperature distribution.

03713 120

~~CONFIDENTIAL~~  
SIFTED

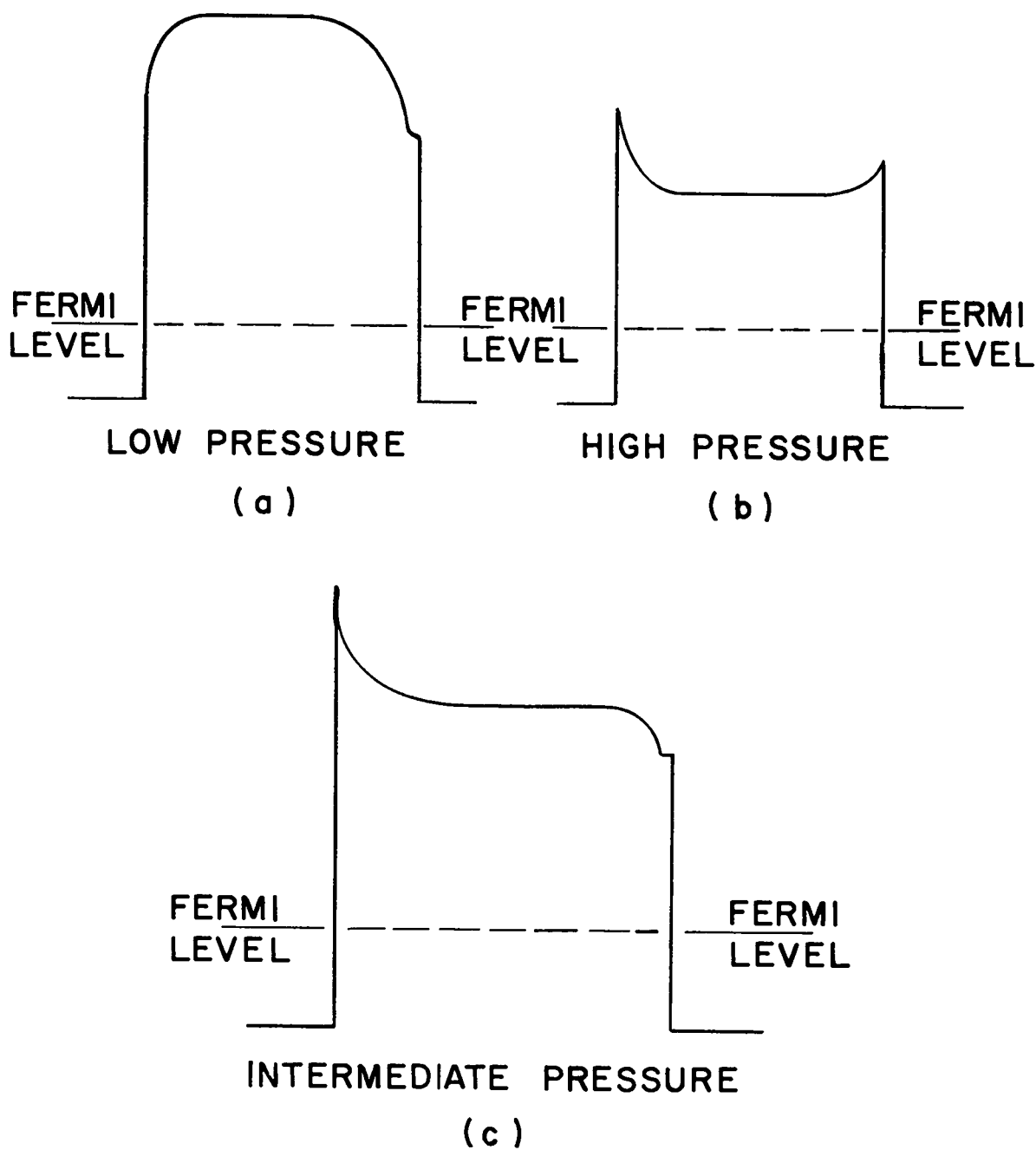


Fig. 5.5. Pressure effects on potential distribution for case of non-uniform temperature.

121  
SIFTED



031710

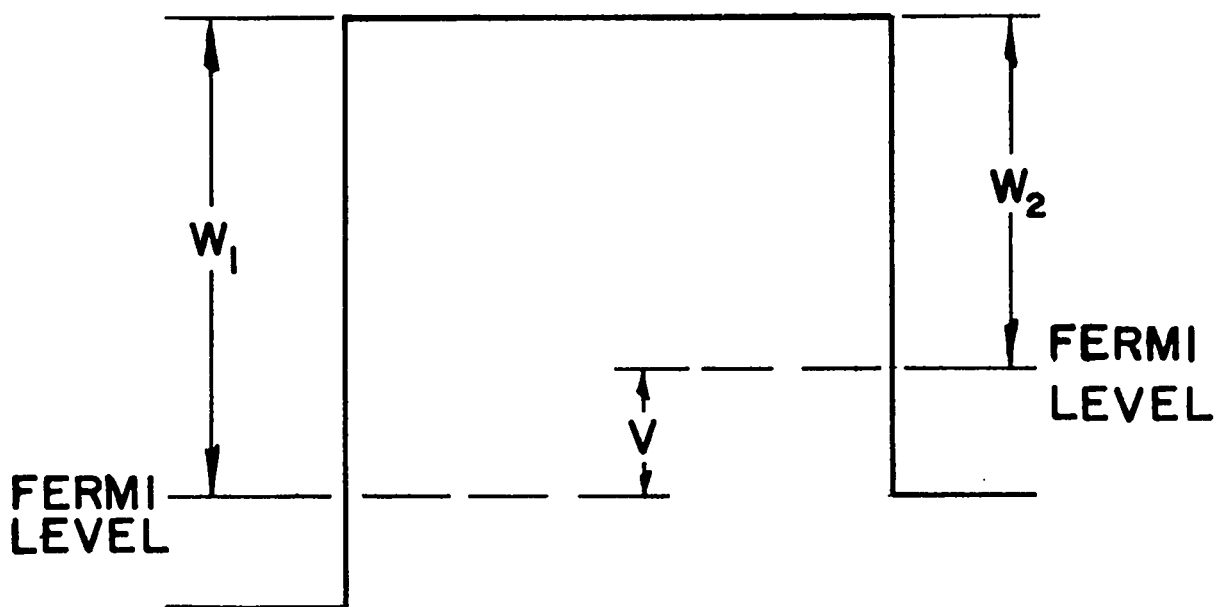


Fig. 5.6. Idealized potential distribution for maximum power output.

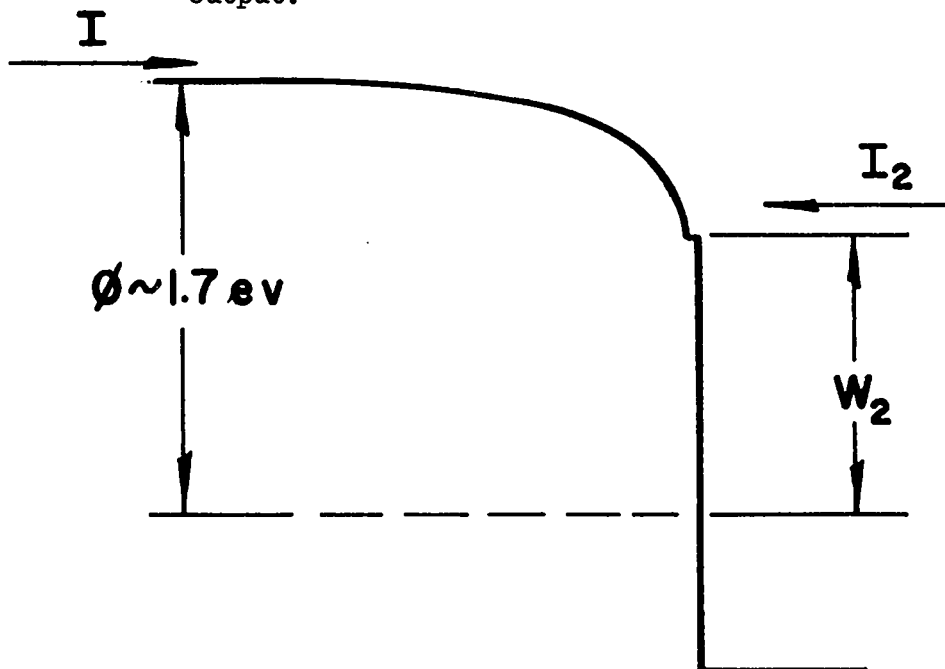


Fig. 5.7. Potential distribution near collector when collector emits electrons.

031710

122

CONFIDENTIAL

[REDACTED]

SECRET

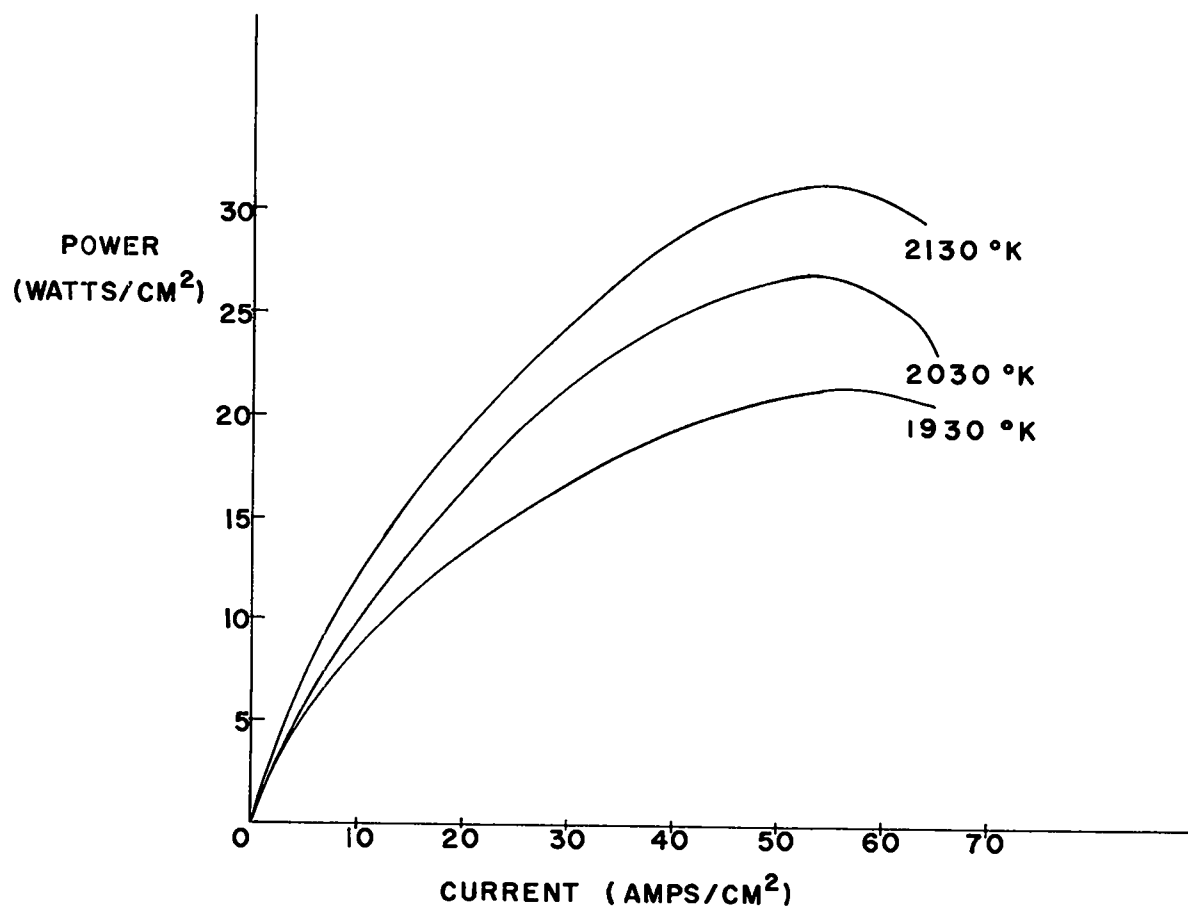


Fig. 5.8. Experimental powers vs current curves.

123  
SECRET[REDACTED]  
APPROVED FOR PUBLIC RELEASE

031713

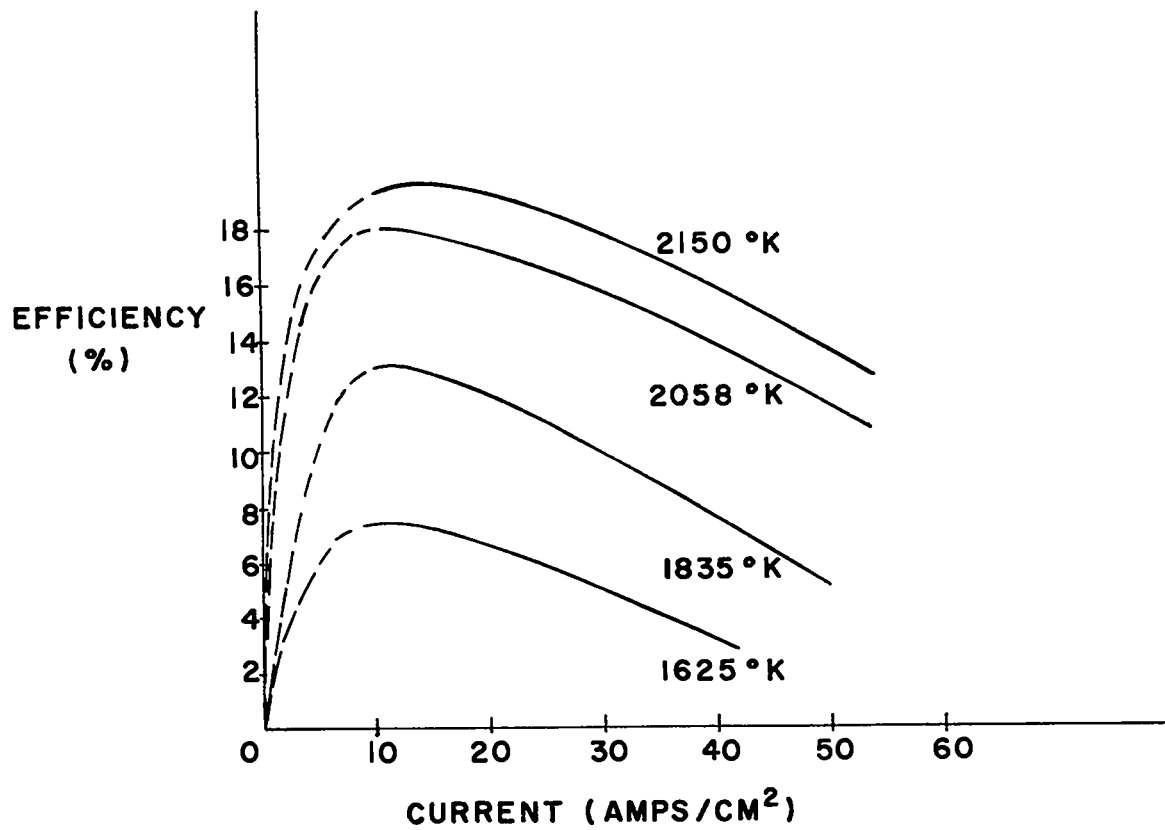


Fig. 5.9. Efficiency vs current.

031713 124

~~CONFIDENTIAL~~

SECRET

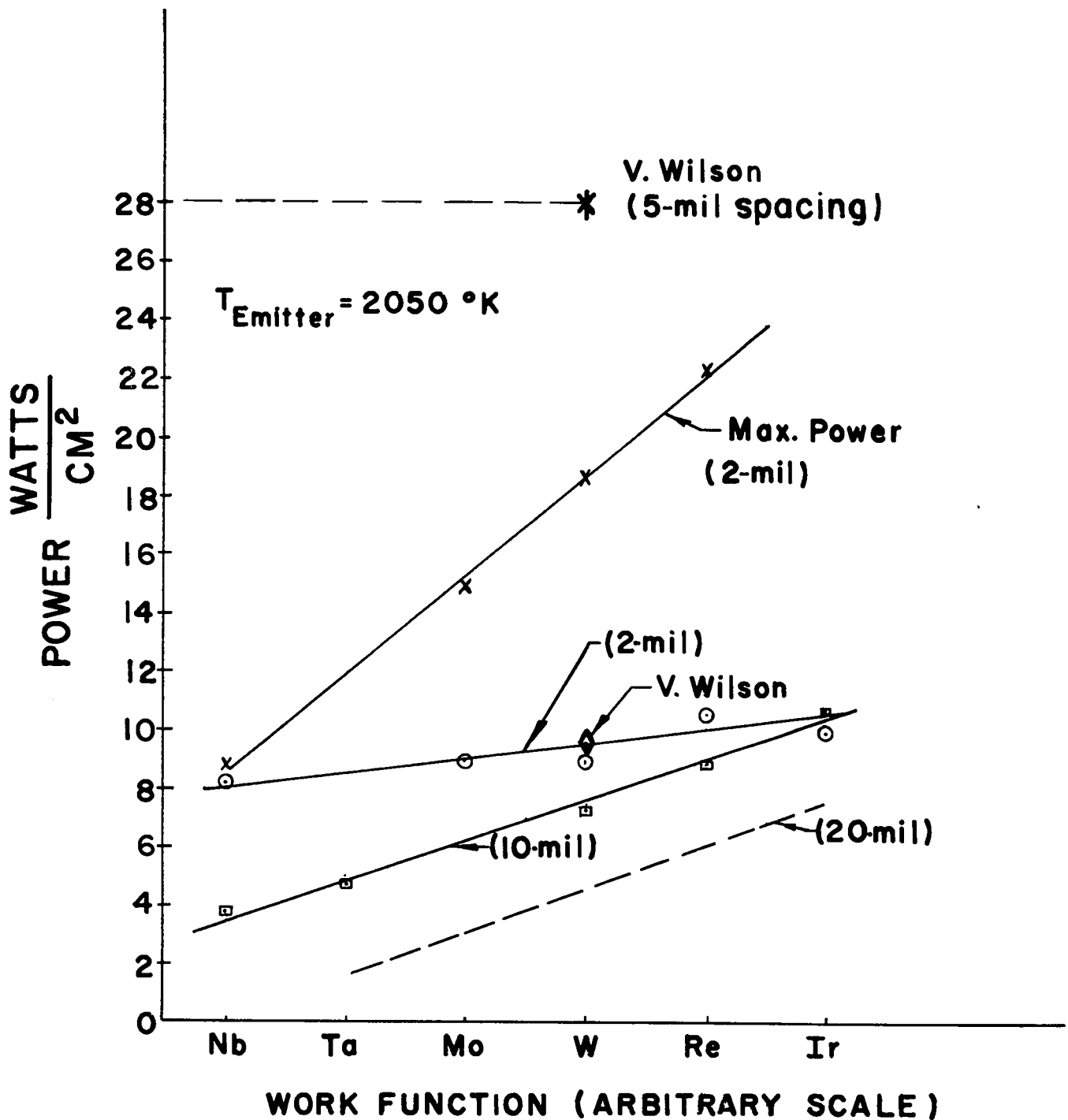


Fig. 5.10. Power output for cases of maximum power and maximum efficiency for various emitter materials.

~~CONFIDENTIAL~~  
 $T_{\text{collector}} = 1000^\circ\text{K}$

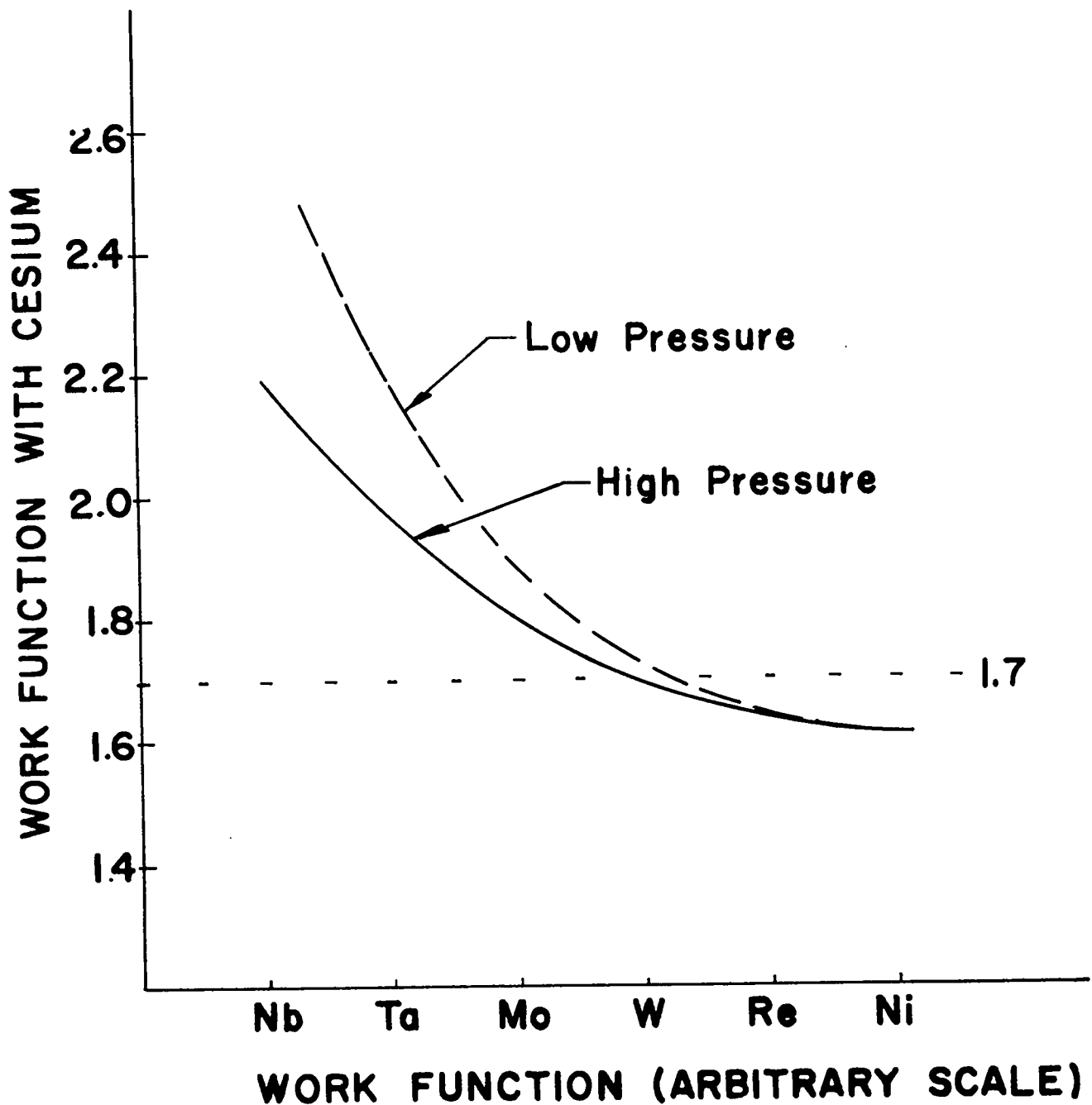


Fig. 5.11. Collector work function at realistic operating condition for various materials.

~~CONFIDENTIAL~~  
SECRET

## 6. Moving Belt Radiators

Charles A. Fenstermacher

The information presented here is based on the two references<sup>1,2</sup> and private communication with the Power Conversion System Group of the Rocketdyne Division of North American Aviation Corporation. The purpose of this monograph is to describe the moving belt radiator concept and to summarize the optimization analysis given in Reference 2, indicating the important parameters. An application to the thermionic system is made.

### Concept

The first published report describing the moving belt radiator concept was Reference 1. This brief paper described the concept and applied it to a 20,000 kW(e) space power supply to indicate the possible reduction in radiator weight. The reduction was greater than a factor of two; the 42,750-pound conventional radiator was compared with a 16,000-pound moving belt radiator.

The concept is simple and straightforward. The rejected heat from the engine cycle is transferred to a drum which acts as a receiver or condenser for the working fluid. The heat is transferred from the drum to a metallic belt loop which is rotated about the drum. After picking up heat, an element of the belt moves away from the drum and radiates the energy to space (see Fig. 6.1).

127  
SECRET

CONFIDENTIAL

Variations in the design concept include the possibility of a rotating drum with stationary belt configuration and a revolving belt slung around a stationary drum; and, of course, the number of loops is a variable.

### Analysis

The first aspect of the system to be considered is the mechanism of heat transfer from the drum to the belt. This will determine the size of the drum and the temperature of the belt and, hence, influence the weight of the system.

Consider the heat transfer as shown in Fig. 6.2. The total thermal resistance is

$$r = \frac{1}{h} + \frac{1}{H} + \frac{S}{kD} + \frac{b}{2k_b} \quad (6.1)$$

For working fluids and materials under consideration,  $h \sim 10^5$  Btu/ft<sup>2</sup>-hr-°R, and  $(s/k_b + b/2k_b)^{-1} \sim 2 \times 10^4$  Btu/ft<sup>2</sup>-hr-°R, whereas  $H$  is  $\sim 100$ -5000 Btu/ft<sup>2</sup>-hr-°R. So it is clear that the contact conductance is controlling. The conductance depends on the surface contact area which in the usual cases may be only 1% to 2% of the apparent area because of surface roughness. Perfect contact would produce an  $H = \infty$ .

If one considers the case of a thin, wide belt and a thin-shelled drum, i.e., the case for  $S + b \ll D$ , the heat transfer rates can be found by applying the one-dimensional heat transfer equation to the regions involved.

$$\frac{\partial^2 T}{\partial x^2} = \frac{1}{k/c_p} \frac{\partial^2 T}{\partial t^2} \quad (6.2)$$

$k$  and  $c_p$  being the thermal conductivity and specific heat of the regions in question.

Flaherty<sup>2</sup> has obtained an exact solution in parametric form, the parameters being  $T_{\text{wall}}$  of the drum, and  $T_2$  minimum temperatures on the belt. For the local temperature through the drum wall, he finds:

128  
CONFIDENTIAL

[REDACTED]

CONFIDENTIAL

$$\frac{T - T_2}{T_w - T_2} = 1 - \sum_{n=1}^{\infty} \exp \left( -(\lambda_d)_n^2 \gamma_d^2 t_{c_n} \right) \sin(\lambda_d)_n x \quad (6.3)$$

$$0 \leq x \leq X$$

and for the belt

$$\frac{T - T_2}{T_w - T_2} = 1 - \sum_{n=1}^{\infty} \exp \left( -(\lambda_d)_n^2 \gamma_b^2 t \right) F_n \cos 3(\lambda_b)_n (s-x) \quad (6.4)$$

$$S \leq x \leq x + b$$

The various constants being determined, of course, by the initial boundary conditions.

Flaherty points out that this complex exact solution of the problem can be replaced by a simple approximation if one assumes uniform temperature for the drum wall and uniform temperature through the belt, and that this approximate solution agrees with the exact solution within several percent over a wide range of values of H.

The heat transferred to the belt at a time dt produces a change in average belt temperature given by:

$$dq = \frac{A(T_w - \bar{T}_b)}{r} dt = A_p bc(dT_2) \quad (6.5)$$

- A = area of a strip across the belt
- $T_w$  = wall temperature of the drum
- $\bar{T}_b$  = average belt temperature of the element in question
- r = thermal resistance
- $\rho$  = belt density
- b = belt thickness
- c = belt heat capacity

129  
CONFIDENTIAL



03113

Integration of this expression over the contact time  $t_c$  gives

$$\frac{T_w - T_{b1}}{T_w - T_{b2}} = \exp(-t_c/rpcb) \quad (6.6)$$

where  $t_c$  is the contact time. This expression can be rearranged to give an expression of the form of the exact solution

$$\frac{T_{b1} - T_{b2}}{T_w - T_2} = 1 - \exp(-t_c/rpcb) \quad (6.7)$$

Where  $t_{b2}$  and  $T_{b1}$  are incoming and outgoing temperatures of the belt.

### System Weight

Having examined the heat transfer mechanism, one uses the results to obtain an expression for the weight of the belt and the drum in terms of temperature and to see what the important parameters of the system are.

### Belt Weight

For the equations of the belt, one notes first that heat transferred to the belt equals the heat radiated by the belt

$$\dot{M}_c(T_1 - T_2) = 2\sigma\bar{\epsilon}\bar{T}^4LB \quad (6.7)$$

where

$$\dot{M} = \frac{MN}{L/V}$$

$M$  = total mass of belt

$N$  = number of loops

$L$  = total belt length

$V$  = belt velocity

$\sigma$  = Stefan-Boltzmann constant

$\bar{\epsilon}$  = average emissivity times a view factor for the two sides of the belt

$$= \frac{1}{2}(\epsilon v_f) \text{ inside} + \frac{1}{2}(\epsilon v_f) \text{ outside}$$

$\bar{T}^4$  = average value of  $T^4$  over the belt

03113

CONFIDENTIAL

Note that at each roller the mass of the entire belt passes by in a time  $L/V$ ; and, for  $N$  loops, this gives the mass rate shown above.

For a unit area, one also finds that the heat radiated in a time  $dt$  causes a temperature change given by

$$2\sigma\bar{\epsilon}T^4 dt = -\rho cb dT \quad (6.8)$$

Noting that

$$dt = dL/V \quad (6.9)$$

one finds

$$L/N = \int_0^{L/N} dL = -\frac{1}{K} \int_{T_1}^{T_2} \frac{dT}{T^4} K = \frac{2\bar{\epsilon}\sigma}{cV\rho b} \quad (6.10)$$

which relates the length of the belt to inlet and outlet temperatures and belt speed.

The average value of  $T^4$  can be calculated using this result

$$\bar{T}^4 = \frac{1}{L} \int_{T_1}^{T_2} T^4 dL = \frac{3T_1^4 (1-\tau)}{(1/\tau^3 - 1)} \quad (6.11)$$

where

$$\tau = T_2/T_1 \quad (6.12)$$

The weight of the belt

$$W = \rho bLB \quad (6.13)$$

can now be expressed in terms of  $T_1$ ,  $\tau$ ,  $V$ , etc.; or, since the specified weight is the parameter of interest in optimizing space power systems, and the total power radiated is

031713

$$q = 2\sigma \bar{\epsilon} T_1^4 L B$$

(6.14)

$$\alpha_b = \frac{W}{q} = (\rho b \sqrt{\epsilon}) \frac{(1/\tau^3 - 1)}{b \tau T_1^4 (1 - \tau)} \quad (6.15)$$

for fixed belt thickness.

If one permits varying belt thicknesses, which might be the case for a revolving belt system in which centrifugal stresses exist, one finds, using

$$q = N V B c \rho T_1^4 (1 - \tau) b = M c (T_1 - T_2) \quad (6.16)$$

that

$$\alpha_b = \frac{q}{6 \tau \bar{\epsilon} N V B c T_1^5} \frac{(1/\tau^3 - 1)}{(1 - \tau)^2} \quad (6.17)$$

#### Drum Weight

Drum weight is calculated in an analogous fashion. The weight is expressed as

$$W_D = \beta G \pi B D \quad (6.18)$$

$W_D$  = weight of the drum

$\beta$  = specific weight/area ratio -  $W_d$ /belt contact area  
(assumed constant)

$G$  = fractional area of contact

$\pi B D$  = total drum area

and remembering

$$\frac{T_W - T_1}{T_W - T_1} = \exp(-t_c / r c \rho b) \quad (6.19)$$

031713

~~CONFIDENTIAL~~

CONFIDENTIAL

and

$$t_c = \pi G D / V N \quad (6.20)$$

so that

$$D = \frac{N V r \rho b c}{\pi G} \ln \frac{(T_w - T_2)}{(T_w - T_1)} \quad (6.21)$$

Combining with

$$q = N V B c \rho T_1 (1 - \tau) b \quad (6.22)$$

and setting

$$u = T_w / T_1 \quad (6.23)$$

$$\alpha_D = \frac{W_D}{q} - \frac{\beta}{(1 - \tau)} \frac{r}{T_1} \ln \frac{(u - \tau)}{(u - 1)} \quad (6.24)$$

### Specific System Weight

The specific system weight

$$\alpha_T = \alpha_b + \alpha_D \quad (6.25)$$

is now expressed in terms of system design parameter  $u$  and  $\tau$

$$\alpha_T = \frac{\beta r}{T_w} \left( \frac{u}{1 - \tau} \right) \ln \frac{(u - \tau)}{(u - 1)} + \frac{1}{b} \left( \frac{\rho b}{\sigma T_w} \right) \frac{u^4}{\sigma T_w} \frac{(1/\tau^3 - 1)}{(1 - \tau)} \quad (6.26)$$

(b fixed)

$$\alpha_T = \frac{\beta r}{T_w} \left( \frac{u}{1 - \tau} \right) \ln \frac{(u - \tau)}{(u - 1)} + \frac{1}{6 \epsilon \sigma} \left( \frac{q}{N V B} \right) \frac{u^5}{c T_w^5} \frac{(1/\tau^3 - 1)}{(1 - \tau)} \quad (6.27)$$

[(q/NVB) fixed]

Whether one used 6.26 or 6.27 depends on whether there is some fixed minimum value of  $b$ , or whether the value of  $(q/NVB)$  is fixed by some system constraint.

031710

System Optimization

For optimization by variation of  $u$ ,  $\tau$  one notes that:

- 1) Large  $u$  implies a small drum large belt; and, conversely
- 2) Large  $\tau$  implies a large drum, small belt

The optimization consists of trading off drum weight which scales as  $\frac{1}{T_w} f(u, \tau)$  against belt weight which goes as  $\frac{1}{T_w} g(u, \tau)$ .

One also notes that  $\alpha_T = \alpha_T(r)$ , specifically the drum weight is linear in  $r$ . If  $b$  is fixed, then it can be seen that since

$$q = NVB\rho e \frac{T_w}{u} (1-\tau)b \quad (6.28)$$

$\tau$  is not an independent variable and

$$\alpha_T = \alpha_T(u) \quad (6.29)$$

For this case

$$\frac{\partial \alpha_T}{\partial U} = 0 \quad (6.30)$$

Leads to:

$$\xi \equiv \frac{\rho b}{6r\beta\sigma e T_w} = \frac{\frac{u(1-\tau)}{(u-\tau)(u-1)} - \ln \frac{(u-\tau)}{(u-1)}}{4u^3 (1/\tau^3 - 1)} \quad (6.31)$$

( $\tau$  fixed)

where  $\xi$  is a design parameter, and  $\tau$  is picked to give minimum belt weight, e.g.,  $\tau = 0.69$  (see equation 6.15).

Flaherty gives minimum values of  $(u-1)$  versus  $\xi$  and his plots are reproduced here as Fig. 6.3.

031710

CONFIDENTIAL

SECRET

The case for variable  $b$ , i.e.,  $u$  and  $\tau$  both variable, leads to minimum values of  $u$  and  $\tau$  as functions of another design parameter:

$$\xi\sigma = \frac{1}{432} \sqrt{\rho/2g\sigma_a} \left( \frac{G\pi}{N\sigma\epsilon} \right)^2 \frac{D}{\beta r^3 T_w^6 c} \quad (6.32)$$

where all symbols are as previously defined and

$g$  = acceleration due to gravity

$\sigma_a$  = allowable stress of the belt material

This second optimization takes into account stress limitations imposed by allowable stress values for a revolving belt system.

Flaherty's plots of minimum values of  $u$  and  $\tau$  versus  $\xi\sigma$  are reproduced in Figs. 6.4 and 6.5.

### Conclusions

Plots of  $\alpha_T$  versus  $T_w$  for minimum-weight values with the parameter  $H$  are reproduced in Fig. 6.6. It can be seen the  $\alpha_T$  scales as approximately  $1/T_w^2$  for low  $H$  and as  $1/T_w^4$  for  $H \infty$ .

It might also be pointed out that for meteorite protection,  $W_{\text{armour}} \sim A^{1.3}$ ; and for the system, it is believed that only the drum need be protected. It is this feature of the system that makes it appear advantageous.

The choice between a revolving belt system and a stationary belt system would be made after taking into account the following considerations:

- 1) The revolving belt system provides greater contact pressure and, hence, higher value for  $H$ .
- 2) The revolving belt eliminates a high temperature rotating seal.
- 3) The revolving belt leads to increased belt thickness.

The feasibility of this concept remains to be proved. The power conversion group of Rocketdyne has an experimental program under contract

135

SECRET

03113

with the Air Force to the tune of about \$500,000 to \$1,000,000 a year. They have investigated material properties to determine best material compatibility for a belt/drum combination. These investigations, in hard vacuum ( $\sim 10^{-9}$  mm Hg and less), examined vacuum welding, fatigue life, and heat transfer properties. Rocketdyne has found several materials which appear compatible. These include molybdenum for a drum material, and stainless steel and columbium for both belt and drum. They have achieved values of  $H$  greater than 5000 Btu/ft<sup>2</sup>-hr-°R by using liquid metal film to increase contact area. In addition to the experimental program, Rocketdyne has developed a computer code to optimize belt radiation systems, taking into account engineering realities.

#### Applications to Thermionic Converter System

To get some idea of the comparison of this concept with heat pipes, system design parameters were worked out for the same conditions. These conditions were:

$$T_w \text{ (collection temperature)} = 900^\circ\text{C}$$

$$q_{\text{rejected}} = 18 \text{ MW}$$

Drum material: Molybdenum,  $s = 0.050$  in.

Belt material, stainless steel,  $b = 0.005$

$$\beta = 16 \text{ lb/ft}^2 \text{ contact area}$$

$$H = 5000 \text{ Btu/ft}^2\text{-hr-}^\circ\text{R}$$

$$\tau = 0.69$$

#### Results

For the above conditions, and considering a stationary drum system, the following design resulted:

$$L = 650 \text{ ft}$$

$$N = 2$$

$$B = 10 \text{ ft}$$

$$D = 1.73 \text{ ft}$$

$$V = 25 \text{ ft/sec}$$

031136

~~CONFIDENTIAL~~  
CONFIDENTIAL

$$T_1 = 2000^\circ\text{R}$$

$$T_2 = 1380^\circ\text{R}$$

$$\alpha T \approx 0.1 \text{ lb/kW(r)}$$

No claim is made as to the realism or feasibility of this application, the object here being to demonstrate that for the assumption made for the concept, specific weights and temperatures are attained which are within reason and competitive. If one is interested in the concept, it would, of course, be necessary to do a more detailed investigation to get more accurate estimates of  $\alpha_T$ ,  $T_1$ , etc.

#### References

1. R. Weatherston and W. Smith, ARS J. 30, 268-269 (March 1960).
2. Richard S. Flaherty, NASA TN-D-1990 (Lewis Research Center, August 1964).

137  
CONFIDENTIAL



~~CONFIDENTIAL~~  
03713

$L$  = total belt length

$B$  = belt width

$b$  = belt thickness

$V$  = belt linear speed

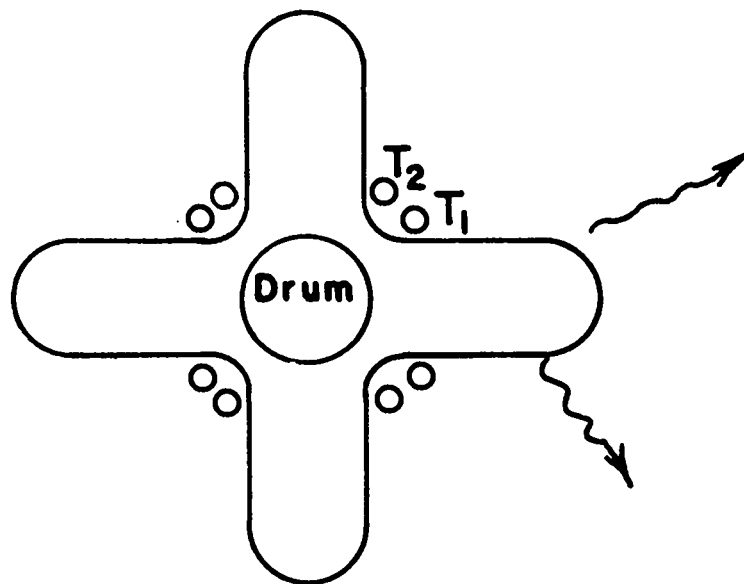


Fig. 6.1. Drum belt configuration schematic.

[REDACTED]

REF ID: A66000

$h$  = condensing heat transfer coefficient on the inner drum wall  
 $k_D$  = drum thermal conductivity  
 $k_b$  = belt thermal conductivity  
 $H$  = contact conductance defined as  

$$\frac{\text{heat transfer rate between drum and belt}}{\text{apparent contact area per Temp. difference}}$$

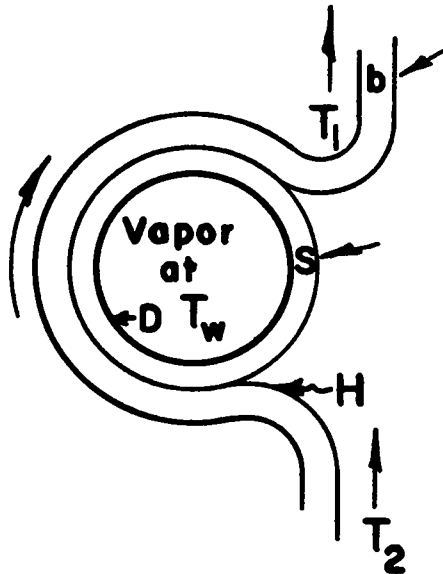


Fig. 6.2. Drum belt heat transfer schematic.

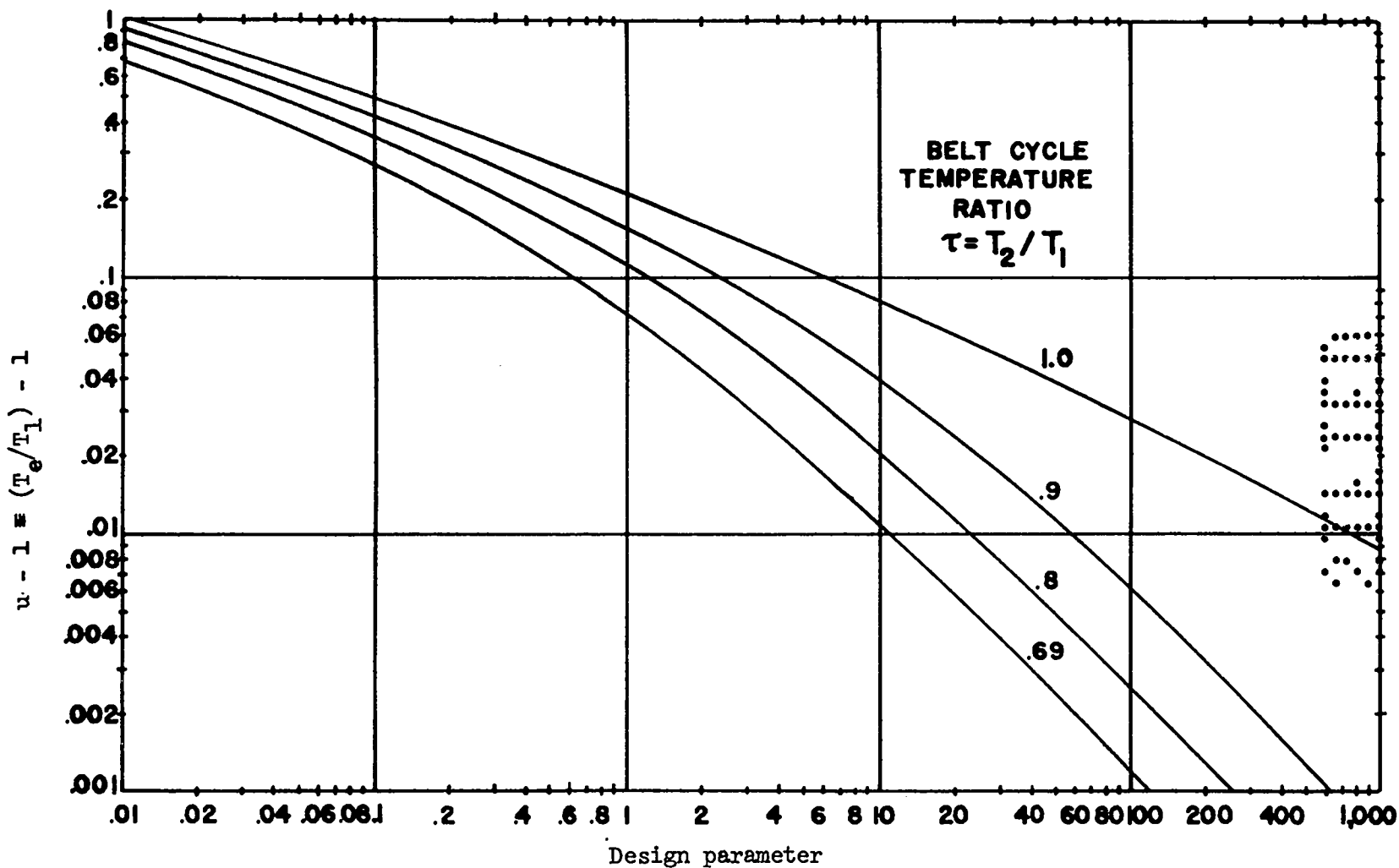
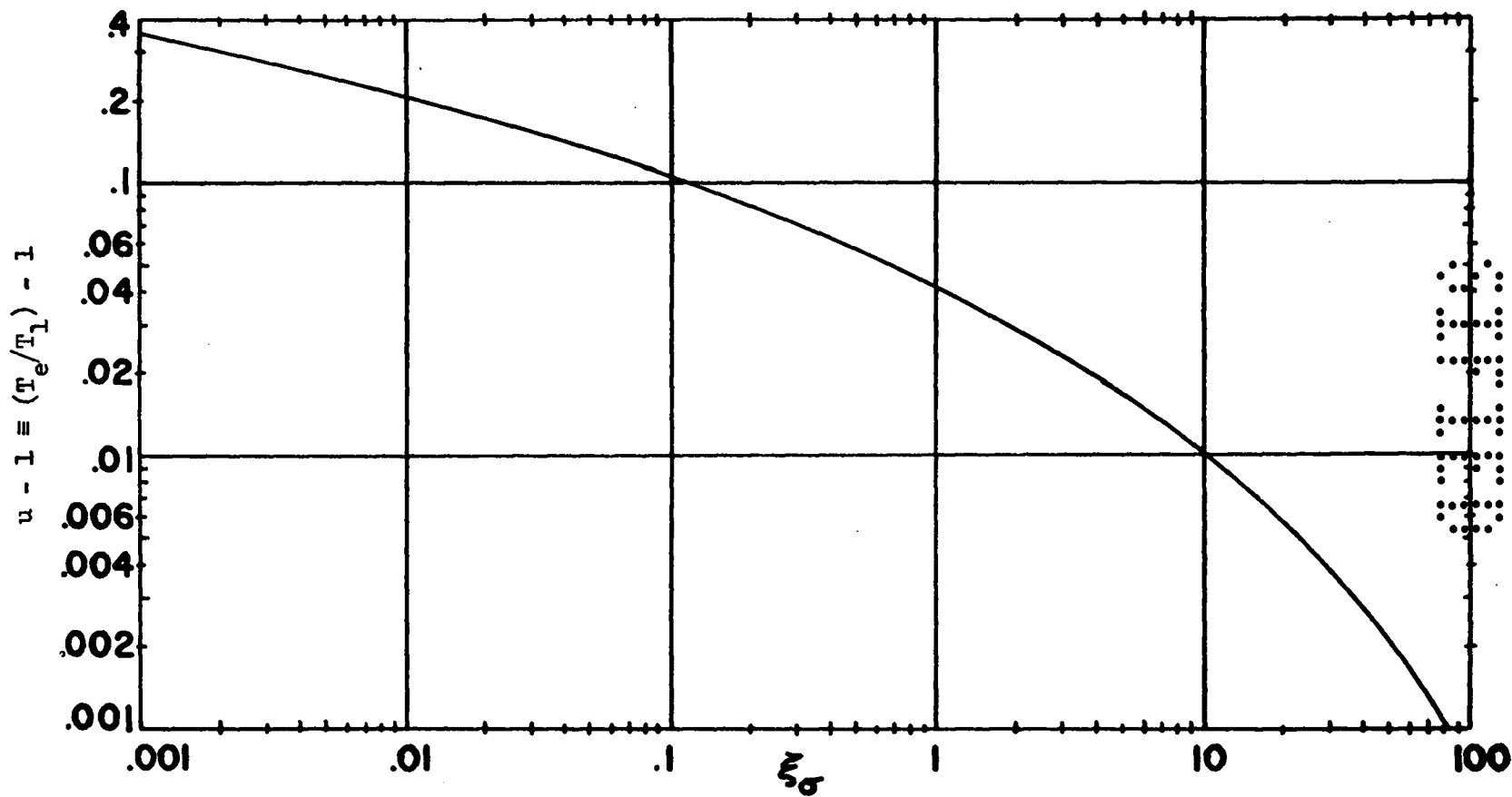


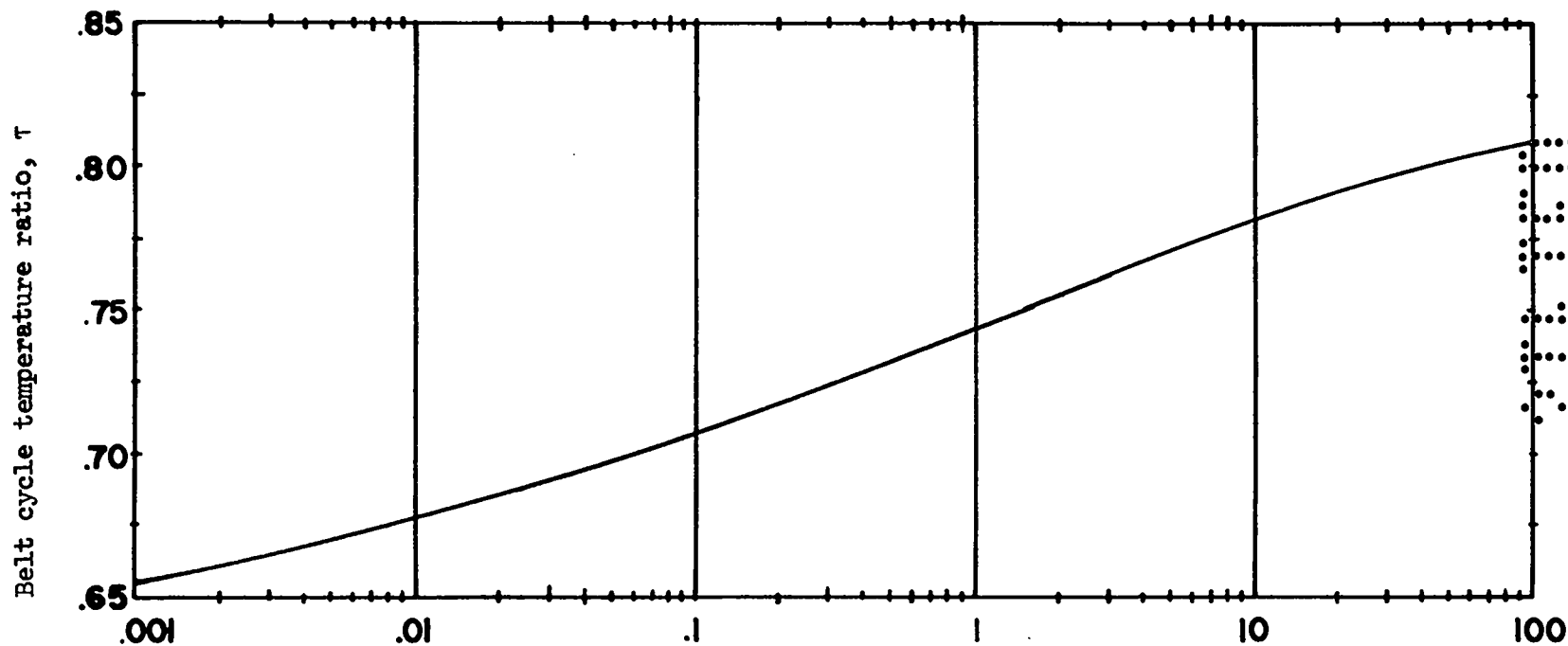
Fig. 6.3. Value of  $u - 1$  that gives minimum total weight as a function of  $\xi = \rho_b b / 6r\beta v \bar{T}_e^3$  for constant belt cycle temperature ratios.



Minimum weight values of  $\tau$  and  $u-1$  for revolving-belt radiators as a function  
of design parameter  $\xi_\sigma = \frac{1}{432} \sqrt{\frac{p_b}{2g\sigma_a}} \left( \frac{G\pi}{N\sqrt{e}} \right)^2 \frac{D}{Br^3 T_{ecb}^6}$

Fig. 6.4. Minimum weight value of  $u - 1$ .

000000  
142



Minimum weight values of  $\tau$  and  $u - 1$  for revolving-belt radiators  
as a function of design parameter  $\xi_\sigma \equiv \frac{1}{432} \sqrt{\frac{\rho_b}{2g\sigma_a}} \left( \frac{G\pi}{N_{ve}} \right)^2 \frac{D}{\beta r_{ec_b}^3}$

Fig. 6.5. Minimum weight value of  $\tau$ .

~~CONFIDENTIAL~~

01130

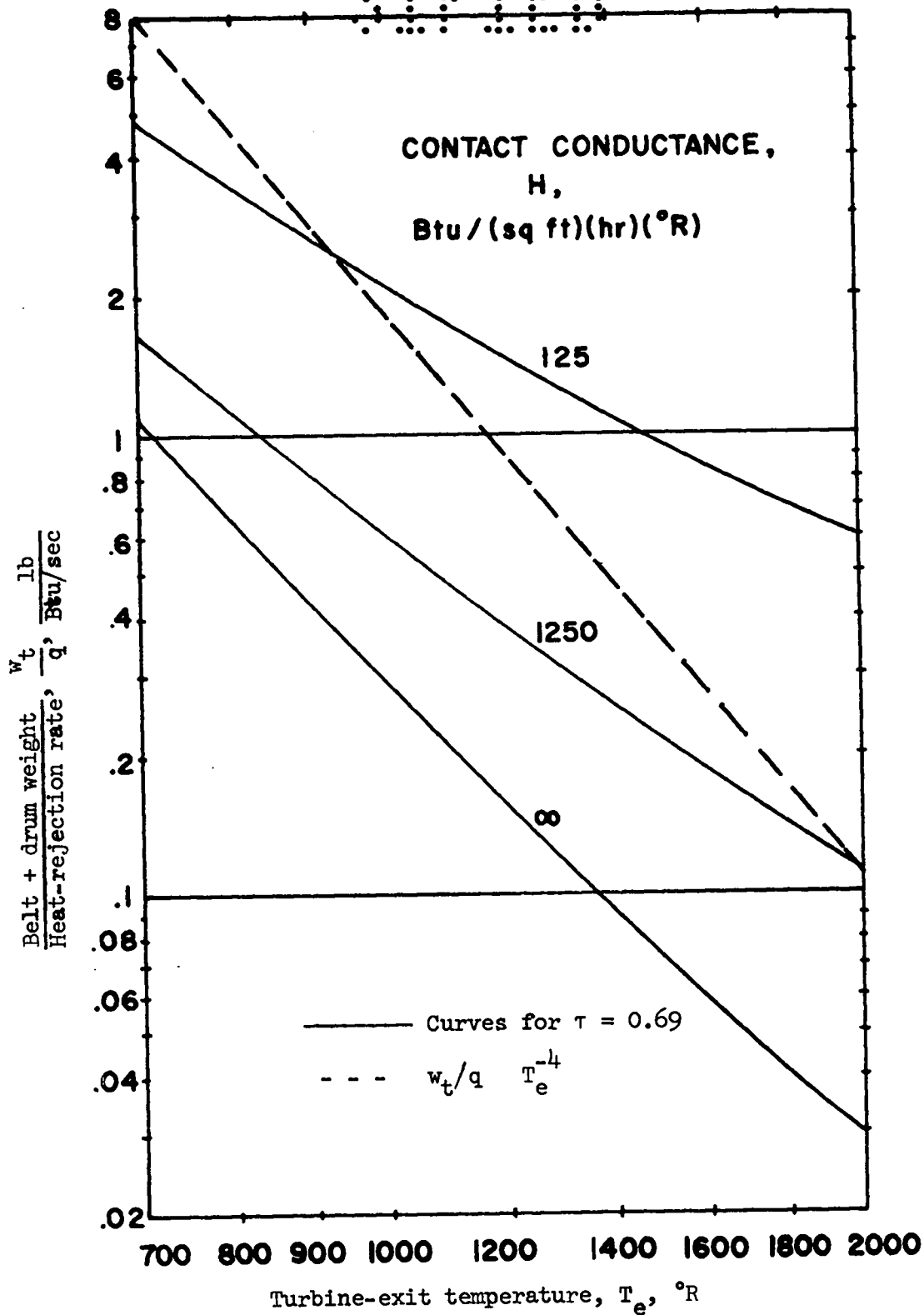


Fig. 6.6. Variation of radiator-system weight with temperature.

01130

~~CONFIDENTIAL~~

01130

031710

## 7. Thermionic Cells

Walter H. Reichelt

Introduction

The thermionic cells that will be discussed in the following sections are in-pile cells, that is, cells which are an integral part of the reactor core. As with almost any manufactured item, the design and fabrication of these cells is not a haphazard affair but one governed by certain rules or guide lines and state-of-the-art knowledge. These rules may be no more than "educated guesses" (for example, the extrapolation of lifetimes) but nevertheless do provide design inputs.

In this discussion, enough state-of-the-art knowledge and other considerations will be given to permit the design of a practical thermionic cell. In fact, this design has been successfully built and operated here at the Laboratory and at other places. Once having demonstrated that such a design can be built and recognizing that no one particular design represents a unique approach to in-pile conversion, a second design will be discussed, one that is quite different in concept.

Cell Design Considerations

Design inputs are generally derived from three sources: experiments, theory of the physical principles involved, and the practical and total reactor aspects. Each category will be briefly discussed in the following text:

1) Experiments reveal the power generation in the fuel, 300 watts/cm<sup>3</sup> for the case at hand, radiation resistance of the components of the thermionic cell, and whether or not the fission products have to be

031710

~~CONFIDENTIAL~~

CONFIDENTIAL

vented. In the design to be discussed the fission products will be assumed to be retained in the fuel or vented into the operating cell. If it is necessary to separate the fission products from the inter-electrode gap, the design is somewhat more complicated but not overwhelming so.

Experimental data also provide information on the dependence of cell output on cesium pressure and cell spacing, both of which are considerations in the design, as will be demonstrated later.

For the purpose of this discussion, a spacing of 0.010 in. will be assumed with a power output density of 10 watts/cm<sup>2</sup>, 10 amps/cm<sup>2</sup> at 1 volt.<sup>1, 2</sup> The spacing is reasonable from a fabrication standpoint. The efficiency is assumed to be 13% which is consistent with the experimental data and calculations<sup>3, 4, 5</sup> and perhaps a little more conservative than need be. Later, calculations will indicate the range of efficiency values.

2) Theoretical calculations lead to physical sizes of the components. Of course, experimental data are used to get final results. The converter is basically a high-current, low-voltage device which implies that voltage losses due to IR drops in the components could be a problem if not considered properly. At the same time, thermal losses could be a problem if the voltage drops were minimized. In the final design, voltage drops and thermal losses must be balanced to arrive at component sizes which minimize the combined effect. Calculations also indicate the temperature gradients in the fuel.

3) The practical aspect of cell design is that once it is designed, can it be built reasonably? Spacing considerations are a good example of this: a practical cell with a 0.001 inch spacing is much more difficult to build than is one with a 0.010 inch spacing. The proper mating of components must be another area of practicality. One total aspect of the system is that a choice must be made between a fast or a thermal reactor system. For the thermal case, a moderator must be included in the design. The moderator as well as the cells must be cooled. The

CONFIDENTIAL



03710

coupling of the reactor to the radiator is another problem area in the overall design.

### Typical Cell Design

The cell which will be discussed in some detail has a cylindrical emitter, and the design is one which has been the basis of almost every proposal extended for an in-pile-thermionic reactor. This type of in-pile cell, that is, the cylindrical geometry, has been built and operated successfully by LASL, GE, GA, and RCA.<sup>6, 7, 8</sup> Two of these groups, GA and GE, have demonstrated lifetimes of well over one thousand hours with the maximum of twenty-five hundred hours demonstrated by the group at GE.

The cell is shown in Fig. 7.1 which illustrates a conceptual fuel rod containing many cells. In this design the emitter is a cylinder of  $\text{MoUO}_2$  supported at one end by a tack of refractory metal. The tack is mounted or brazed to the collector of the adjoining cell. A vapor deposited layer of tungsten 0.005 inch thick is put on the fuel to form the emitter surface. This layer also prevents evaporation of the  $\text{UO}_2$  at operating temperatures. The collectors are separated by high-purity alumina insulators. A vanadium braze is used between the tungsten metallizing on the insulator and the collector. The radiation shield is employed to reduce the pin end radiation losses which reduce the efficiency. Holes in the collector ends provide a passage for cesium vapor migration to all units in the stack.

The layers of metal collector, insulating layer, and metal clad are collectively known as the triple layer. Since liquid metals will be used for cooling, the cooling liquid would short out the cells without the presence of the insulating layer. The ceramic prevents this. The clad of niobium-1% zirconium prevents corrosion of the ceramic insulating layer by the coolant. This triple layer presents quite a problem area. The bonding between all surfaces must be complete since there is a large heat flux across it. If there are sections that are non-contacting, hot

03710<sup>146</sup>

~~CONFIDENTIAL~~

SECRET

spots could develop which might result in cell failure. The ceramic layer must also have enough resistance to prevent break-down when a potential difference of about 200 volts exists across it. While this layer has been successfully built, it has not had adequate testing under cycling and reactor environments. The ceramic layer can be sprayed on, vapor-deposited on, or poured in place in a molten state. In one case, a ground tube of ceramic is used. The cladding is vapor-plated or is a close-fitting tube which is swagged in place. Care must be taken, in any case, to insure that the bonding is complete.

This discussion of the cell will revolve about one unit in the stack, consisting of an emitter, collector, and tack. In Fig. 7.2 some of the voltage and thermal losses are given. There are radiation losses from the pin on all sides. The radiation shield reduces these at the free end of the pin. Thermal conduction results in losses down the tack. The voltage drops result from the finite resistivity of the components in which cell currents exist.

There are three physical sizes to be determined: pin diameter, pin length, and collector thickness. These are derived from physical principles, while the remainder of the cell dimensions are governed by good design practices. Examples of this latter category are the insulator size and shape, and collector-pin base configuration.

The easiest of the three design parameters to determine is the pin radius. Power generation in the fuel ( $300 \text{ watts/cm}^3$ ), efficiency (13%) and power density ( $10 \text{ watts/cm}^2$ ), are used to determine the radius. All of these quantities are experimental values. A simple power balance between the power generated in a volume of fuel and the power that must leave the pin surface gives the radius:

Power generated = total power output

$$\pi r^2 \ell \rho = 2\pi r \ell \sigma \quad (7.1)$$

$$r = \frac{2\sigma}{\rho} = 0.5 \text{ cm}$$

147  
SECRET~~CONFIDENTIAL~~

031710

where

$r$  = pin radius

$\ell$  = pin length

$\rho$  = power generated = 300 watts/cm<sup>3</sup>

$\sigma$  = power leaving surface = 77 watts/cm<sup>2</sup>

The value of  $\sigma$  is determined from a value of 10 watts/cm<sup>2</sup> output (electrical) and the efficiency value of 13%. From the relationship above, the radius of the fuel pin has been determined.

The pin length and collector thickness are all that remain to be determined. As discussed in the last chapter, the quantity of interest in the space thermionic power supply is the maximum efficiency. From a calculation which maximizes the efficiency will come the optimum pin length and the collector thickness. The detailed equations and computer code will not be discussed because of their complexity. Instead, the starting equations and boundary conditions will be indicated; these show how resistivity, collector thickness, and pin radius enter the equations. After this brief introduction to the analysis, the results of the computer code will be given in graphical form.

The efficiency for the thermionic diode is not merely the ratio of output to the power input. Many factors must be included:

- 1) Resistance in the components
- 2) Losses from the pin, radiative and conductive
- 3) Temperature gradients along the pin
- 4) Contributions from joule-heating arising from currents
- 5) Collector losses
- 6) Power generation in the pin

The starting point for the efficiency calculation is shown in Fig. 7.3. The current pattern in the pin and collector are indicated schematically along with the appropriate boundary conditions. At  $x = 0$ , the emitter current is equal to the total cell current; and at  $x = \ell$ , the collector current is equal to the total cell current. The analysis assumes a current density, ( $j_e$ ), equation of the form:

03148

~~CONFIDENTIAL~~

~~CONFIDENTIAL~~

01100

$$j_e = -b + a (V_e - V_c) \quad (7.2)$$

where  $a$  and  $b$  are constants determined from experimental I-V curves, and  $(V_e - V_c)$  is the emitter-collector potential difference. The change in emitter current,  $(J_e)$ , for a length  $dx$  is given by

$$dJ_e = -2\pi r dx j_e \quad (7.3)$$

while the change in emitter potential,  $(V_e)$ , is given by

$$dV_e = - \frac{\rho_e dx}{\pi r^2} J_e \quad (7.4)$$

where  $\rho_e$  is the resistivity of the emitter material. A similar set of equations pertains to the collector:

$$dJ_c = 2\pi r dx j_e \quad (7.5)$$

$$dV_c = \frac{\rho_c}{2\pi r t} dx J_c \quad (7.6)$$

where  $\rho_c$  is the collector resistivity, and  $t$  is the collector thickness. These equations illustrate how the material quantities enter the equations. The computer code is based on the reasoning just illustrated and includes inputs from the experimental data.

The code is set up so that the pin length is fixed, and the heat flux from the tack end of the pin is varied. This gives a maximum in the efficiency curve, as illustrated in Fig. 7.4. The maximum efficiency is consistent with the assumed 13% conservative estimate given earlier in determining the pin radius. Similar calculations can be made for different pin lengths, and the maximum efficiency can be plotted as a function of pin length, as shown in Fig. 7.5. There is an optimum pin length for the maximum efficiency. The reason for this maximum point is simple. At long pin lengths, the voltage drops in the pin and collector become excessive, and the efficiency decreases. At short pin lengths, the thermal and radiative losses from the pin ends dominate,

01100 149

03113

and the efficiency again drops. Somewhere in between these two extremes, the efficiency must go through a maximum as Fig. 7.5 demonstrates. An optimum pin length has been determined. In the course of the efficiency analysis, the collector thickness is also determined so that all three design parameters - pin radius, length, and collector thickness - are determined. It might be noted that the efficiencies given in Fig. 7.5 are well in line with those determined by other groups working in the field.

The temperature profile down the pin and tack are also calculated by the computer code. A typical case is shown in Fig. 7.6. The calculated efficiency takes this gradient into account. The temperature drop at the tack end of the pin is the result of the conduction loss down the tack. The code does not include a radial temperature gradient. However, one does exist and is shown in Fig. 7.7. In this figure the radial change in temperature is shown for two fuels in a thermal neutron flux. The larger gradients for the UCZrC are a consequence of its relatively poor thermal conductivity. A comparison between the fast and thermal fluxes indicates that the gradients are about 13% greater for the fast case.

The important dimensions of the cell have been determined, and the remainder of the dimensions are chosen consistent with good design practices. All that remains then is the fabrication and assembly of the components. The fabrication and assembly problems are not to be underestimated in building a stacked fuel rod. From the experiences here at Los Alamos and at other laboratories, the first multiple-cell assemblies present a vast array of problems. Once overcome, however, the cells could be turned out on a production basis with little problem.

The discussion on the cylindrical geometry cell is now complete. It has been demonstrated that critical dimensions are determined from physical principles and experimental data. Brazes, insulators, and the like exist which are radiation-resistant. The triple layer can

03113

150  
[REDACTED]

~~CONFIDENTIAL~~  
SECRET

be fabricated in several ways. Briefly, the stacked cell can be, and has been, built.

It might be noted that a change in the power generation in the fuel would not create any problems in the design. If the power generation were  $600 \text{ watts/cm}^3$  or  $150 \text{ watts/cm}^3$ , the computed dimensions would change; but the cell could still be fabricated. This observation also holds for the design to be discussed later.

#### Cesium Reservoir

The experimental data shown in Fig. 7.8 indicate that at a cell spacing of 0.010 inch, the power output of the converter is fairly independent of the reservoir temperature for a rather broad range of temperatures -- of the order of  $25^\circ\text{K}$ . The reservoir heat source can be electric heaters, radioisotopes, or the gamma flux from the reactor. It is a relatively simple matter to design and build a reservoir which operates within the temperature limits described above. In fact, several utilizing gamma heating have been built by LASL and have been operated in the Omega West Reactor.

#### Alternate Design

Figure 7.9 illustrates the emitter shapes of interest. The cylindrical emitter has been discussed in some detail. Flat-plate emitters, as shown in Fig. 7.9-b and -c form the basis for the alternate design. The current pattern in Fig. 7.9-b is the same as that for the cylindrical emitter where the emitter is supported from one end, and the voltage drop is across the width of the emitter. If the emitter is supported by pins on one flat side, as illustrated in Fig. 7.9-c, there is a different current pattern, and the voltage drop is now across the thickness of the pin. To be sure, the current pattern radiates from each pin, and the drop is a little more complicated than indicated in the sketch. The flat-plate emitters will be discussed in the following text.

151  
~~CONFIDENTIAL~~  
SECRET  
APPROVED FOR PUBLIC RELEASE

~~CONFIDENTIAL~~

03710

### Flat-Plate Thermionic Cells

The first configuration shown under this heading is the so-called "pancake" reactor (Fig. 7.10). The reactor was invented at LASL and in design goals was a low-power reactor with electrical outputs in the tens of kilowatts. While not of immediate interest because of its low power, it is shown because of its simplicity and because it illustrates several features which are both novel and attractive.

The emitter and collector are large discs; the collectors are separated by large ceramic ring insulators. As in the previous design, the fuel is  $\text{MoUO}_2$  coated with tungsten. The emitter is supported by refractory metal pins which also electrically connect the emitter to the collector of the adjoining cell. The current pattern is that shown in Fig. 7.9-c. Because of the relatively large emitting surface, each emitter has an output which can be at least an order of magnitude greater than that produced by the cylindrical geometry.

In the pancake cells, the collectors are flat pillbox heat pipes which remove the rejected heat to separate radiators. Separate radiators are used since the collectors are at different potentials, and the power level of the reactor is low enough to make the use of multiple radiators feasible.

In the pancake concept, the seals between the cell sections are merely the polished metal and ceramic surfaces pressed tightly together. The cell is "leaky"; that is, the seal is not vacuum tight, and the cesium can leak out. The pressure for sealing may come from an external yoke surrounding the stack of cells; or, if the cells are constrained by an external structure, the collector walls at the seals may be made thin enough so that the internal vapor pressure of the heat pipe fluid deflects the collector walls and makes the seal. To be sure, the leaks may not be too large. In addition, the cesium reservoir must contain enough excess cesium to make up for that lost. In the leaky cell concept, vacuum seals are not necessary.

03710

~~CONFIDENTIAL~~

~~CONFIDENTIAL~~

SECRET

With the pancake reactor in mind, the next flat-plate reactor to be discussed is one capable of 2MW(e) output and is a much-modified version of the pancake reactor. The design is shown in Fig. 7.11. As indicated, the emitter is a rectangular plate 5 cm wide by 100 cm long. The emitter is located between two collectors, one for each side of the emitter. The current pattern through the cell is that indicated in Fig. 7.8-b. As in the case of the pancake reactor, the collectors are heat pipes and have a rectangular cross section. Coolant tubes are located in the collectors. These coolant tubes are triple-layered assemblies; that is, there is an inner metal tube, insulator, and outer metal tube. The outside tube of the triple layer is welded into the end walls of the collector, and the inner metal tube carries the liquid metal coolant. The ceramic layer isolates the collector from the liquid metal cooling and prevents shorting of components. Complete bonding of the triple layer is not as important in this case as it was for the cylindrical diode. The long collector and triple-layered tube permit local variations in temperature with no detrimental effects. Waste heat entering the collector is transferred to the coolant by heat pipe action. The wick in the collector interior must be intimately connected to the coolant tube as well as to all parts of the collector. Ceramic blocks separate the collectors as indicated. Again, the concept is leaky. The collector edge facing the emitter can be thinned down enough so that the internal vapor pressure of the working fluid would force the metal against the ceramic, sealing the system. Sodium would probably be used as the working fluid at approximately 800°C, so that the pressure would be about one-half an atmosphere. Thin sections can be used, since the current carrier is the working fluid in the heat pipe. Ceramic strips are also used to electrically isolate adjoining collectors.

The emitter thickness is again determined from the power generated in the fuel. For 300 watts/cm<sup>3</sup>, an efficiency of 13% at 10 watts/cm<sup>2</sup>, and emission from both sides, the thickness turns out to be approximately 0.5 cm. The overall emitter size, then, is 0.5 cm x 5.0 cm x 100 cm.

SECRET



031713

It is supported between the dual collectors, and the cell spacing is maintained by refractory-metal-insulated pins fastened to the collector. Pin spacing must take into account the creep rate of the collector material at the temperature of and pressure in the collector. The internal pressure in the collector will tend to deflect the surface in which the pins are mounted and will tend to maintain the cell spacing. Molybdenum screen connectors connect the emitter to the collectors of the adjoining cell.

Figure 7.12 illustrates how the flat-plate cells may form an array as in a reactor core. The cells are lined in a series connection in layers. Between layers are slabs of Be moderator and thin sheets of alumina for electrical insulation. It may be necessary to provide separate cooling of the moderator if thermal conduction is not adequate. The whole system is constrained by an external frame. As the internal pressure in the collector increases, the system tends to seal itself because of the expansion of the collectors. The cesium reservoir has enough excess capacity to make up for the losses that occur because of leaks.

It should be noted that this design could also be used with a single-sided emitter so that the current pattern would be that shown in Fig. 7.9-c.

#### Reactor Concepts

Incorporating the cells into a conceptual reactor will illustrate what the final system might look like and where some of the problem areas are.

A conceptual reactor using the cylindrical emitter fuel rods is shown in Fig. 7.13. The reactor might be looked at in two sections. One section to the right of the bulkhead is that section which requires cooling. The cell sections of the fuel rods are located here. Consequently, this section must have provisions for removing the rejected heat from the collectors as well as that deposited in the materials by

03175413

~~CONFIDENTIAL~~

SECRET

the gamma field. Since the reactor is thermal, the moderator also requires cooling. Section "A-A" represents a cross section through several cells and moderator. Each rod is located in the moderator in a cylindrical hole, several of which are connected to a coolant channel - in this case, a heat pipe. All the rejected heat flow is down the coolant channel to the radiator. The wicks extend around both cell stack and moderator, since the latter must be cooled also. The series cell is "U"-shaped so as to separate the electrical connections and cesium vapor source from the section requiring cooling.

To the left of the bulkhead - which is also a Be reflector - the electrical connections, the cesium vapor source, and the control rod actuators are located. Shielding may be necessary for the actuators, since the reflectors are quite thin. The control rods are located in the reflector as indicated.

For the cylindrical stacked cell in the configuration just discussed, the whole core must be included in a shell to prevent the loss of heat pipe coolant.

When the flat-plate cells are placed in a reactor core, there exists a different set of problems. Since the cells are leaky, there can be no closed shell surrounding the core. Instead, the reflector must have provisions for the escape of cesium to prevent shorting. The cells are stacked in layers and held in position by an open support structure. Be plates surround the whole core. Since a triple-layer construction is used in the coolant tubes at the collector, a single radiator can be used.

#### References

1. V. C. Wilson and J. Lawrence, "Operating Characteristics of Two Thermionic Converters Having Re-Ni and W-Ni Electrodes," Advanced Energy Conversion, Vol. 4, pp. 195-221, Pergamon Press, London, 1964.
2. Thermo Electron Engineering Company Report TEE-4015-3 (July 1961).
3. J. W. Holland, Proceedings of the Thermionic Conversion Specialist Conference, p. 88, Gatlinberg, Tenn. (Oct. 1963).

155  
SECRET

~~CONFIDENTIAL~~

031710

4. J. Psarouthakis, Proceedings of the Thermionic Conversion Specialist Conference, p. 100, Cleveland, Ohio (Oct. 1964).
5. Douglas Aircraft Company, Inc., Douglas Report SM-46275, (Feb. 1965).
6. W. Reichelt, et al, "Operating Characteristics of a Cesium Diode Utilizing Fission Heating of the Emitter," Los Alamos Scientific Laboratory Report, LAMS-2598 (Sept. 1961).
7. General Atomic Division, General Dynamics Corporation Report GA 5103 (April 1964).
8. General Electric Co. Report GESR-2034 (Nov. 1963).

031710<sup>156</sup>

~~CONFIDENTIAL~~

SECRET

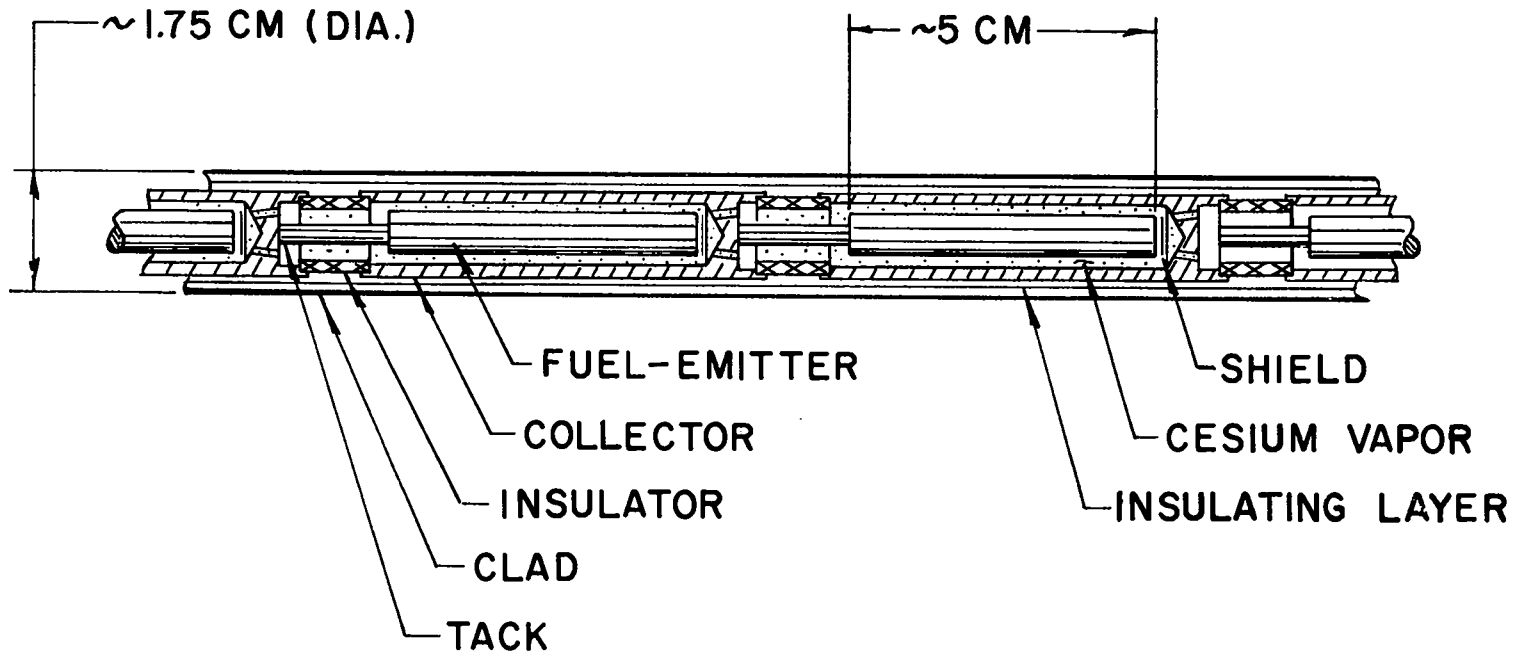


Fig. 7.1 Stacked Cell Assembly

SECRET

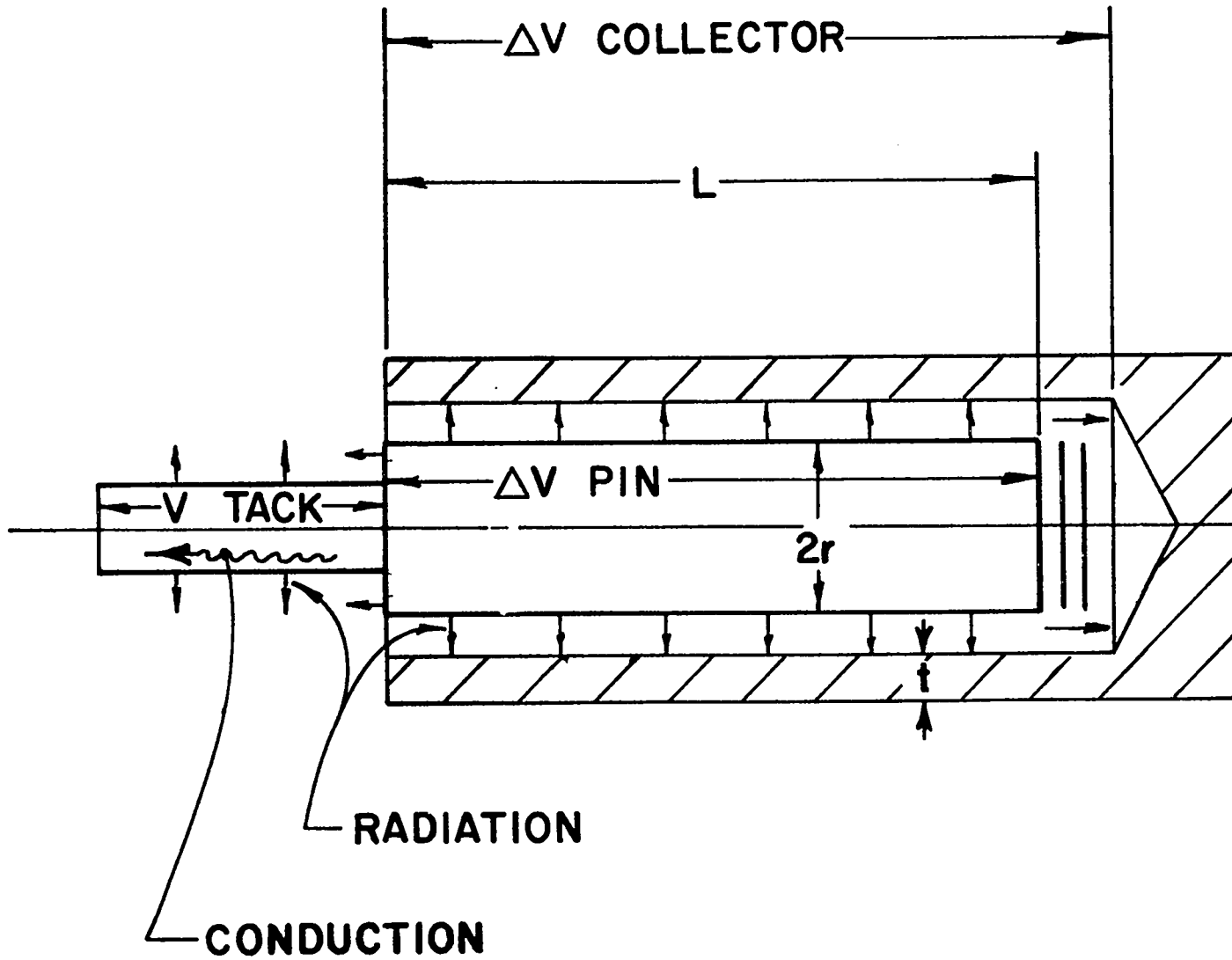
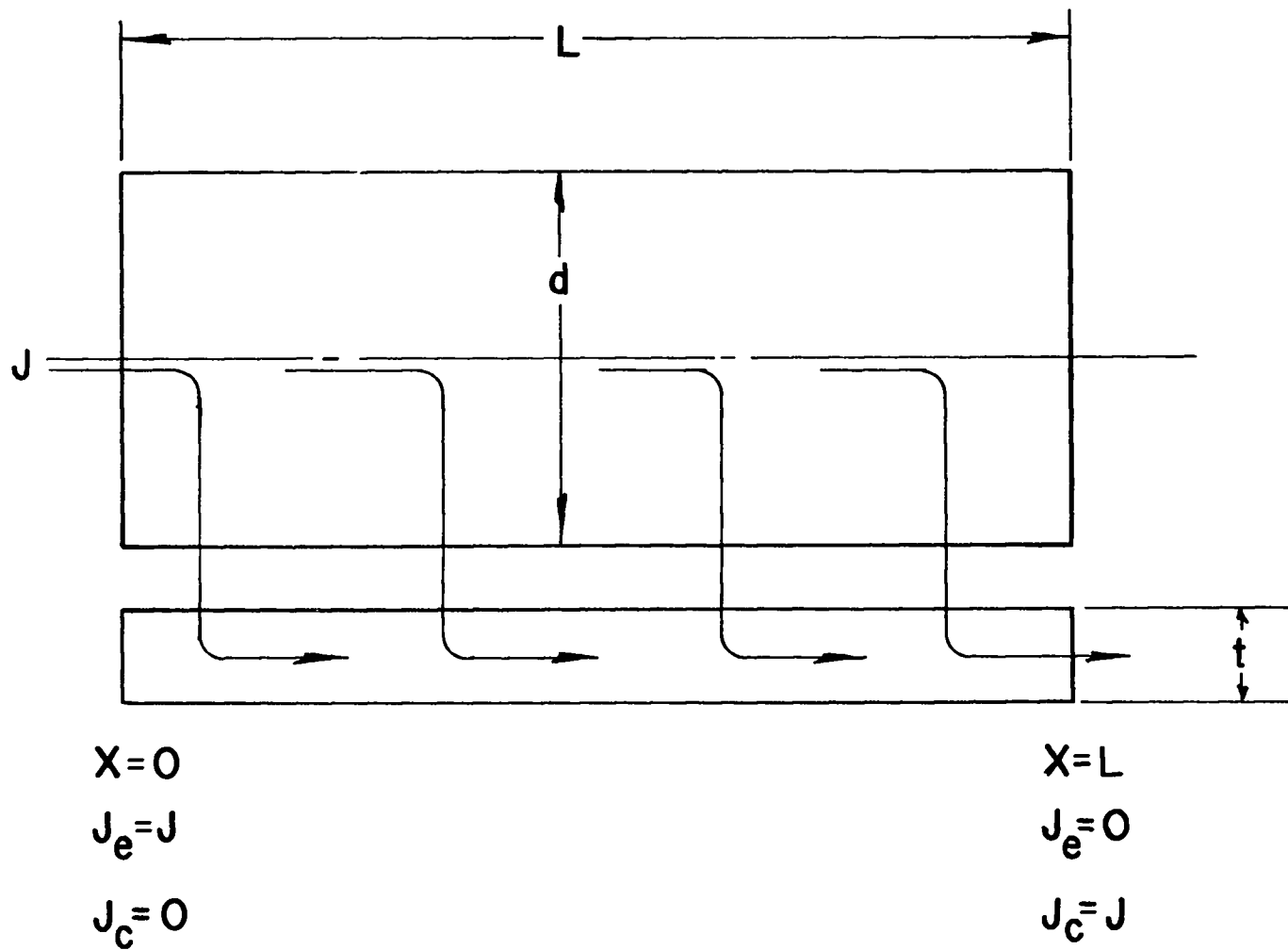


Fig. 7.2 Thermal and Voltage losses in fuel pin.

SECRET



$$+j_e = -b + a(V_e(x) - V_c(x))$$

Fig. 7.3. Current path in emitter and collector.

SECRET

SECRET

000000

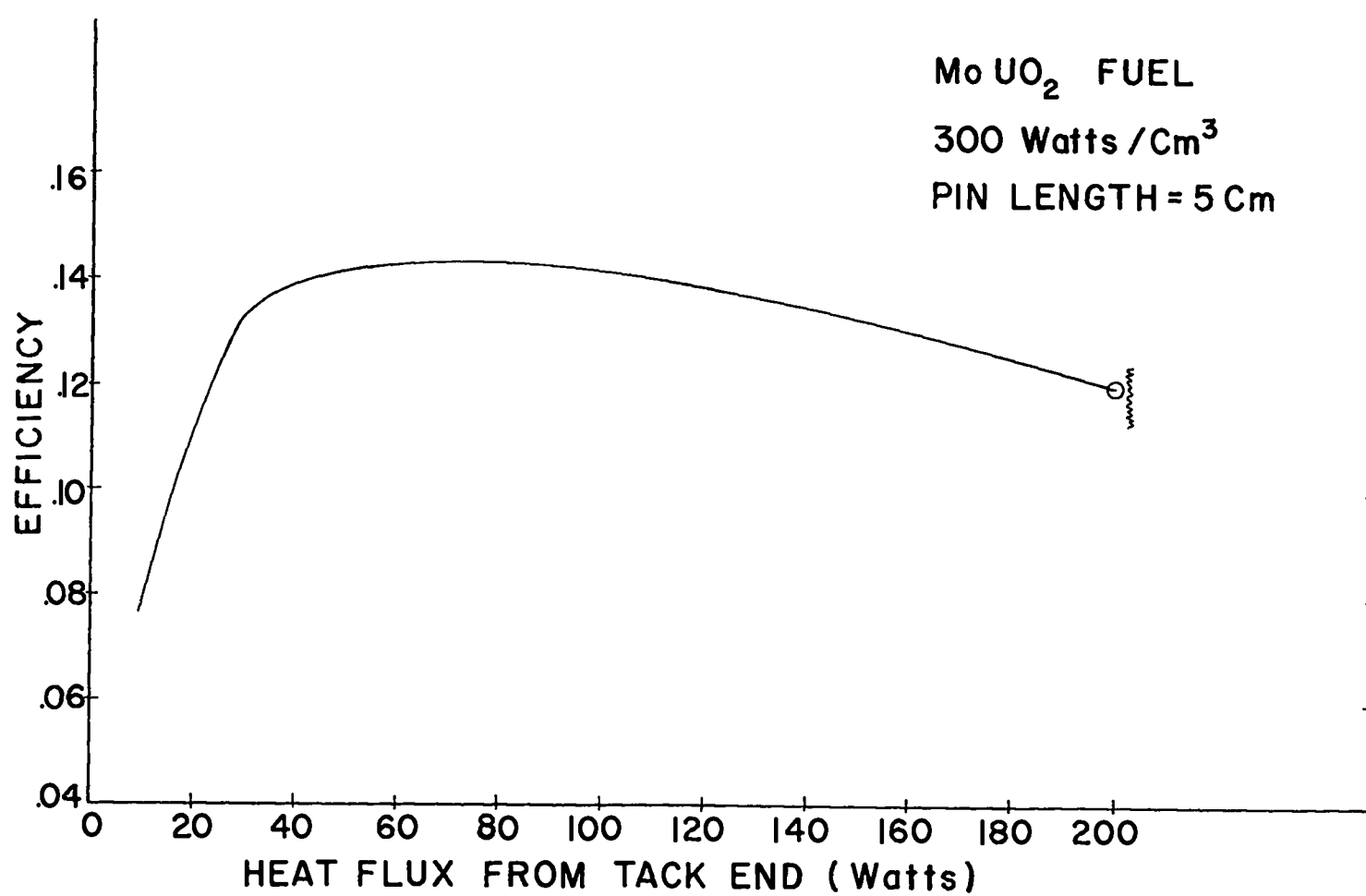


Fig. 7.4. Calculated efficiency vs. heat flux from tack end of fuel pin.

000000

CONFIDENTIAL

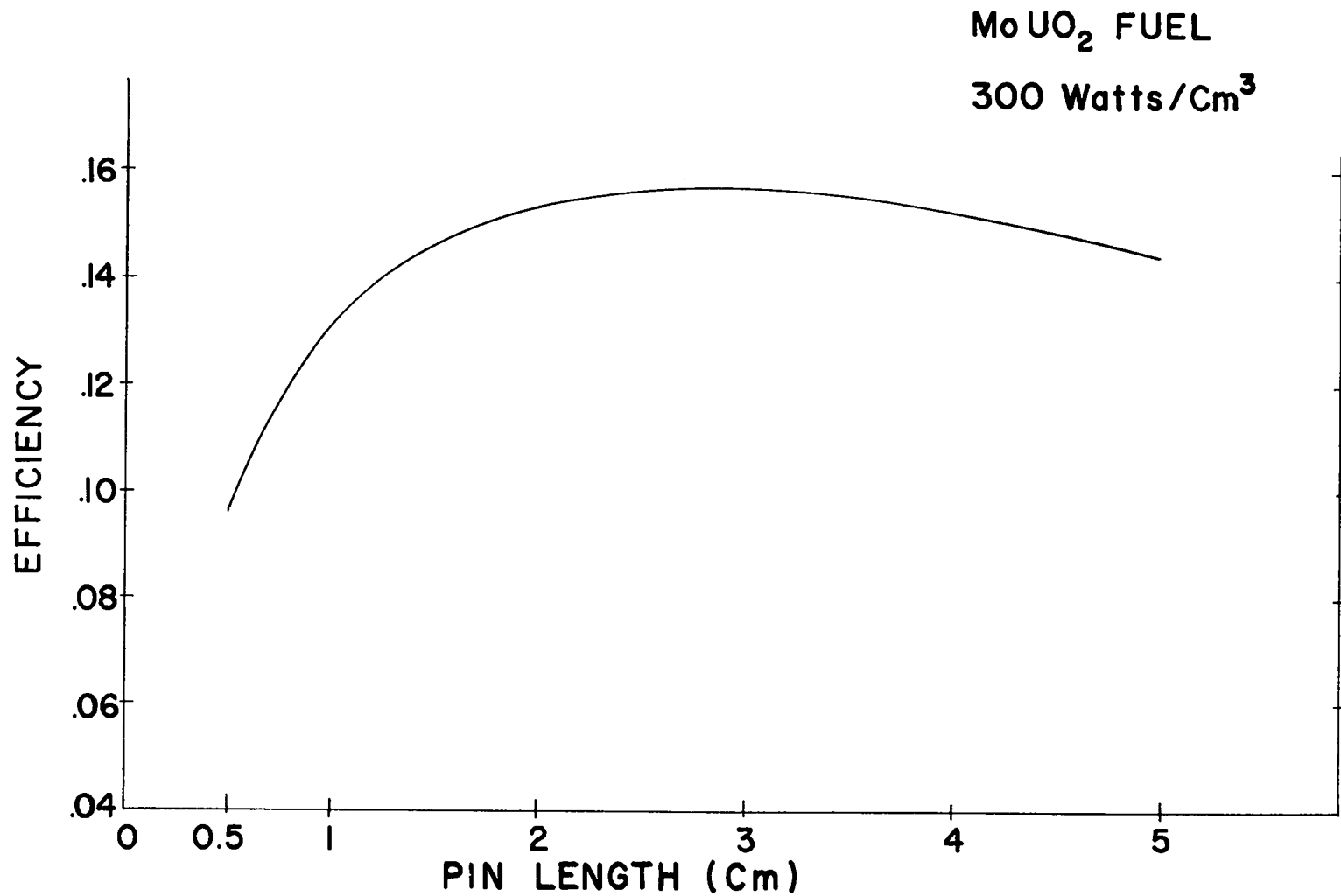


Fig. 7.5. Calculated efficiency vs. fuel pin length.

CONFIDENTIAL



000000

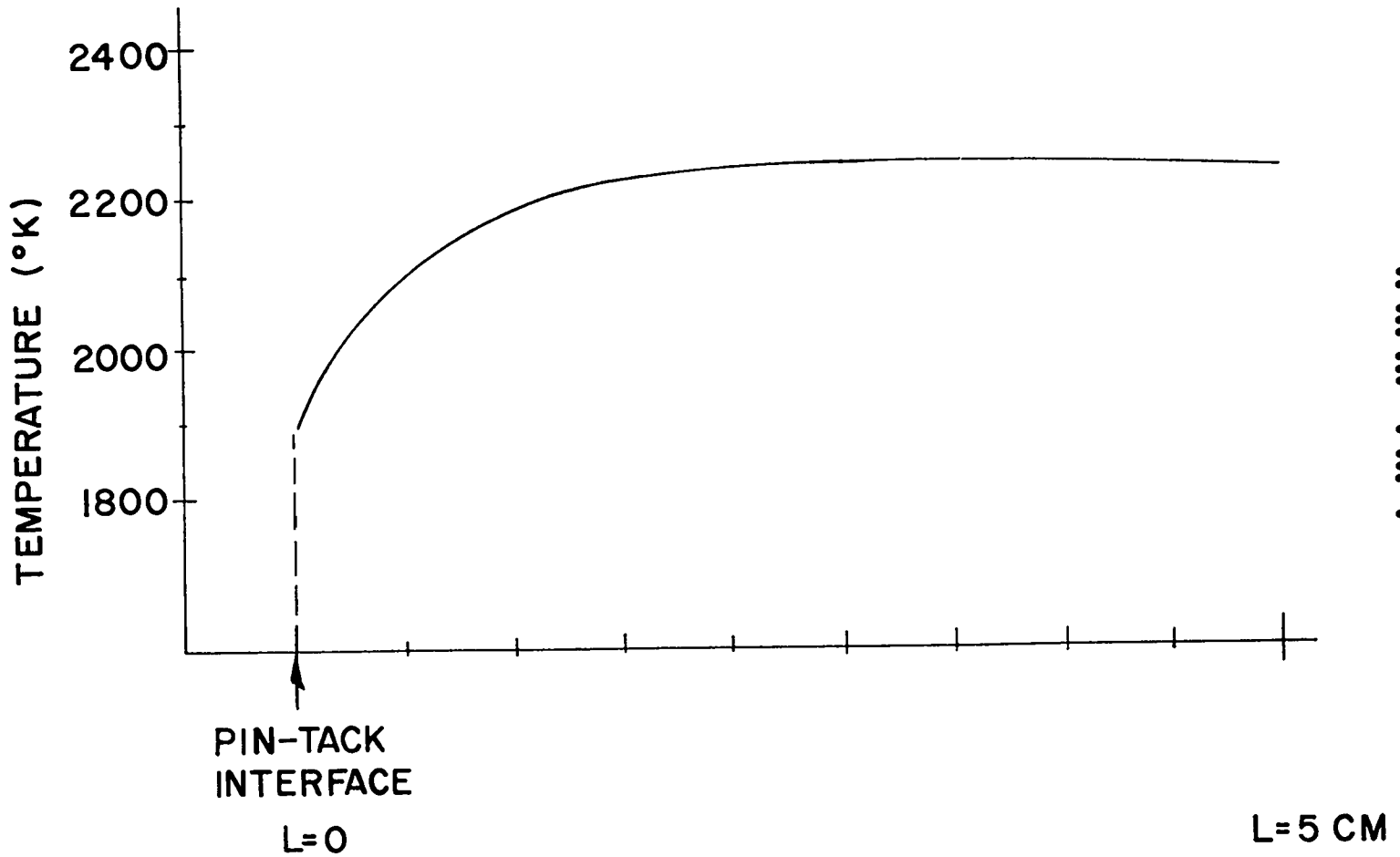


Fig. 7.6. Temperature distribution along fuel pin axis.

000000

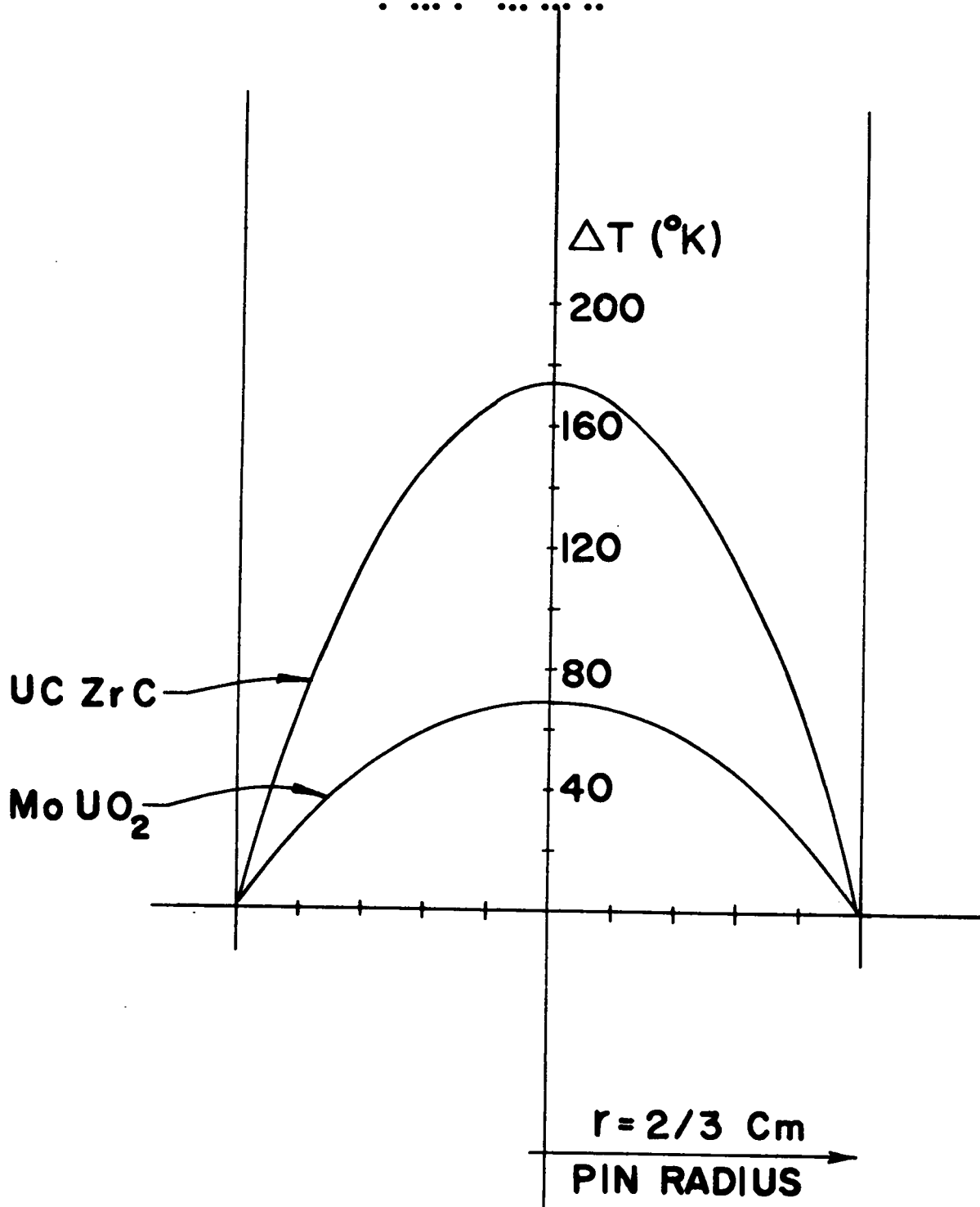
~~CONFIDENTIAL~~  
CONFIDENTIAL

Fig. 7.7. Radial temperature gradient (thermal neutron flux)

163  
CONFIDENTIAL

CONFIDENTIAL

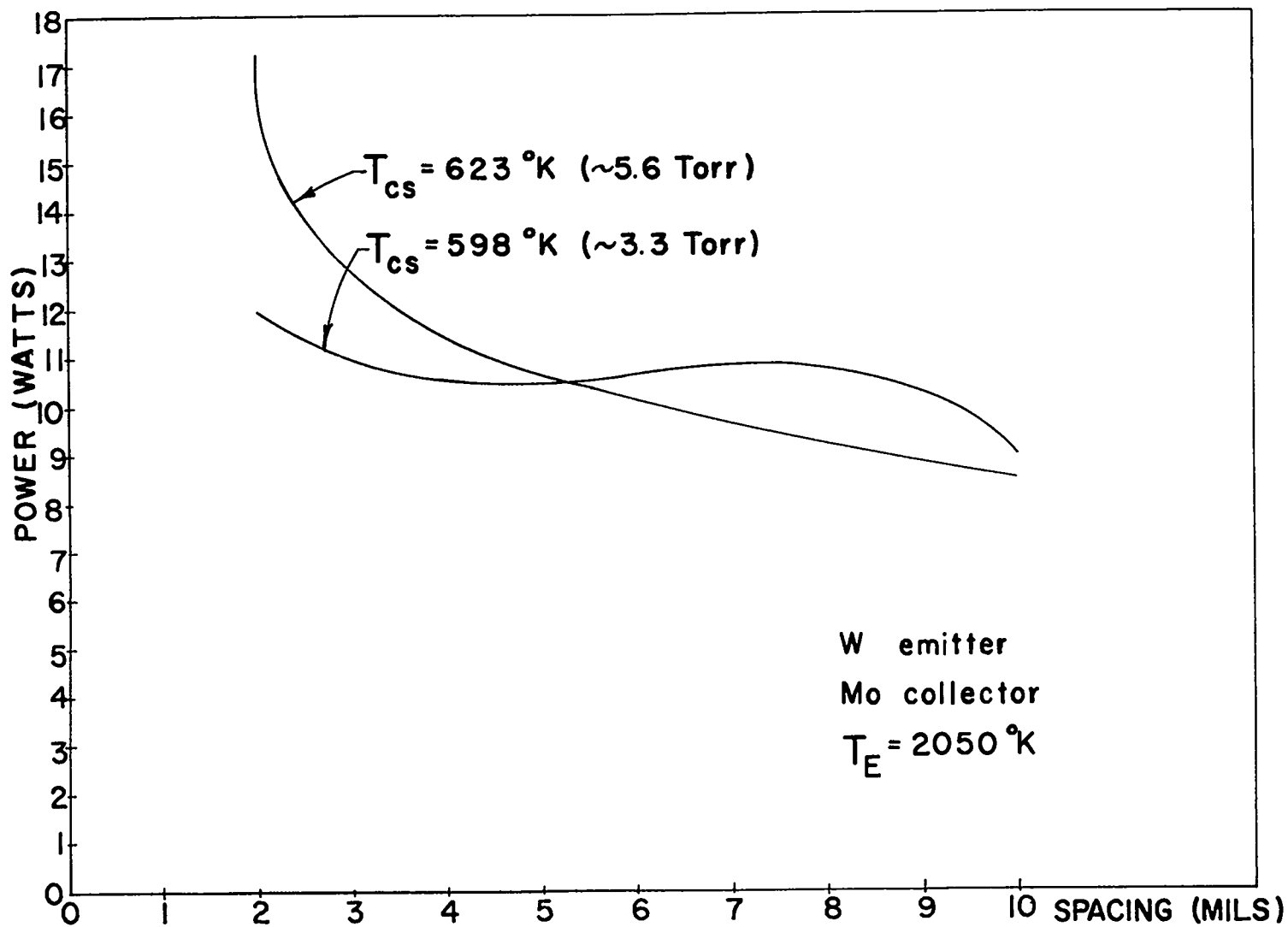


Fig. 7.8. Power output vs. interelectrode spacing.

CONFIDENTIAL

SECRET

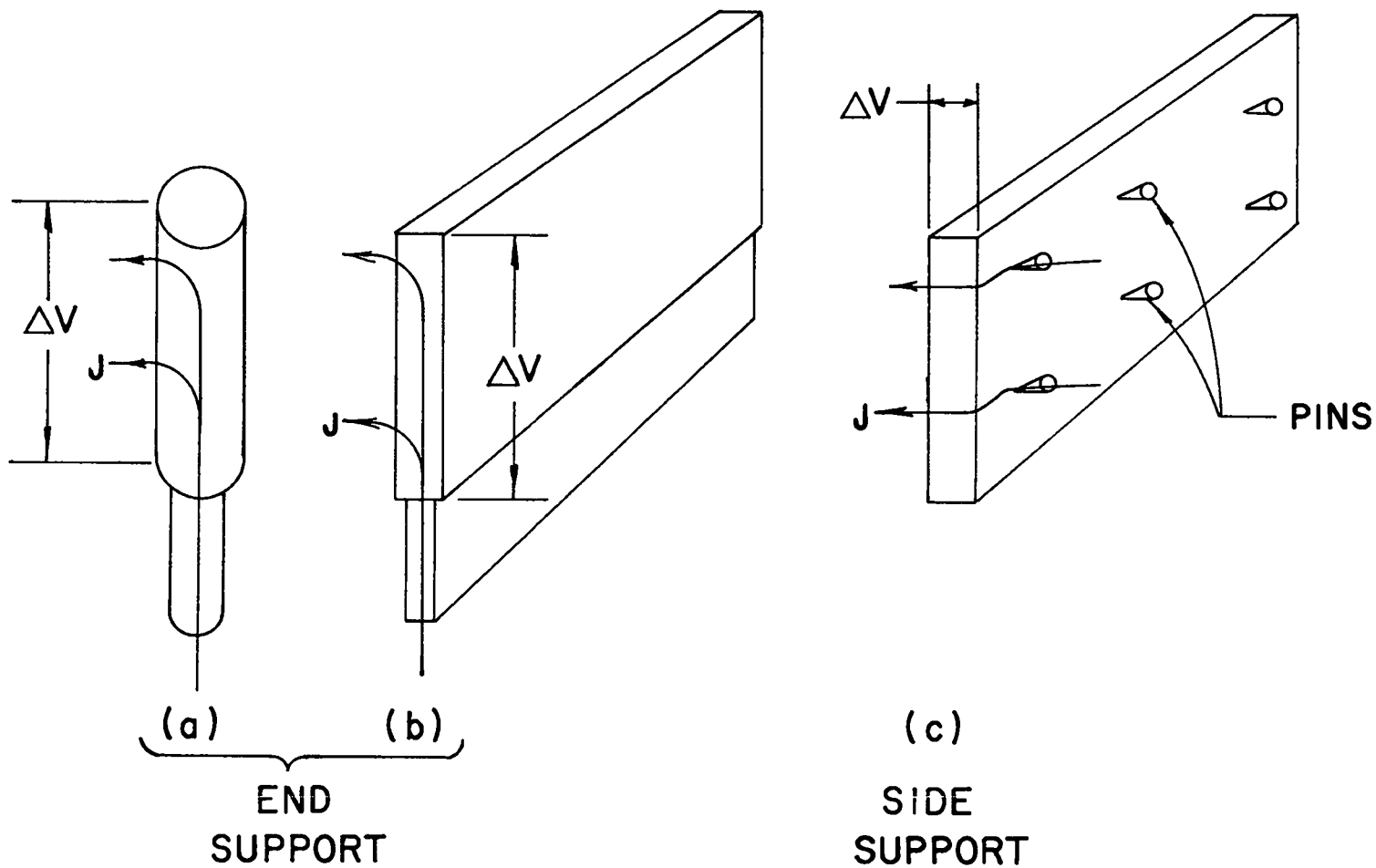


Fig. 7.9. Typical pin support configurations.

SECRET

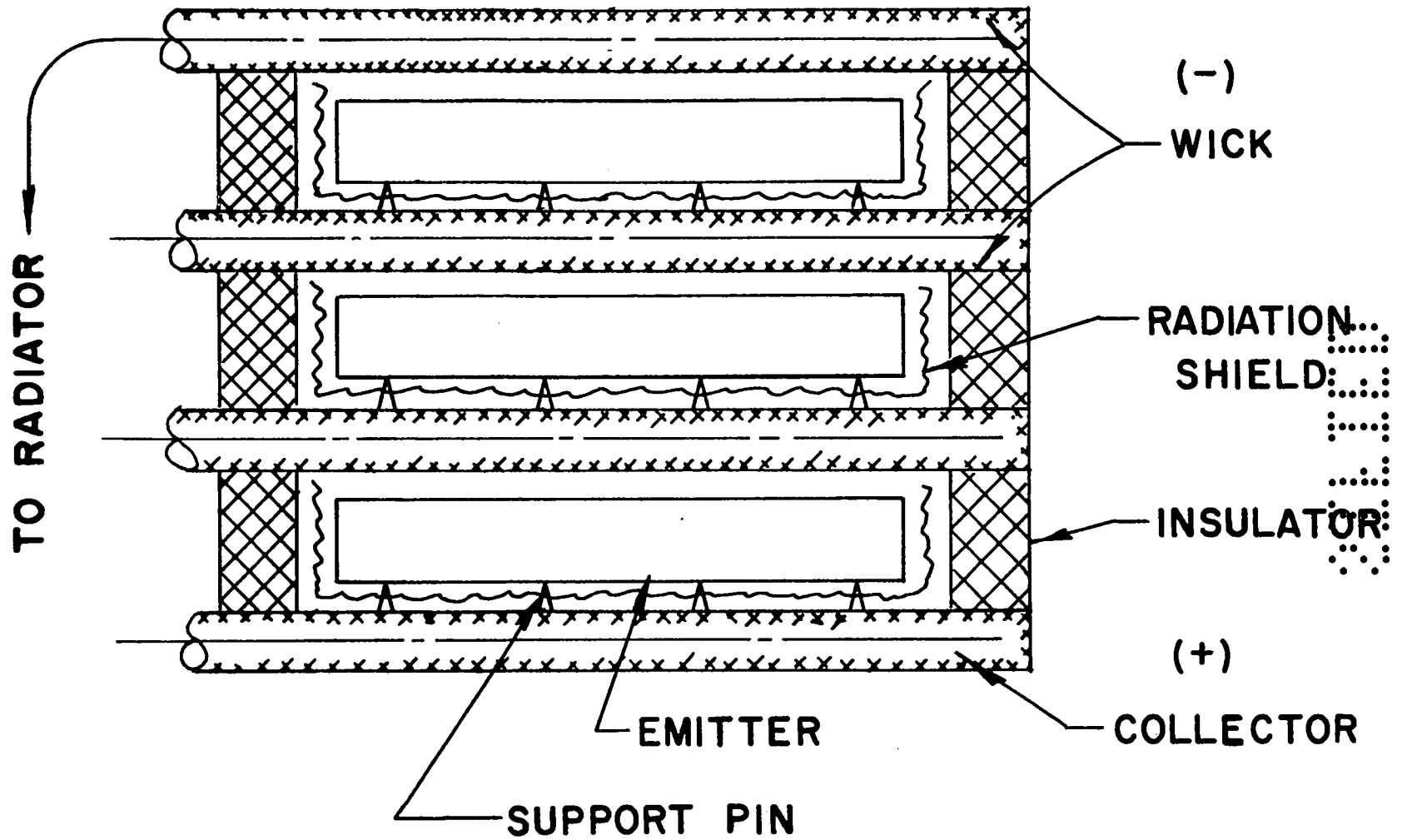


Fig. 7.10. "Pancake" reactor.

SECRET

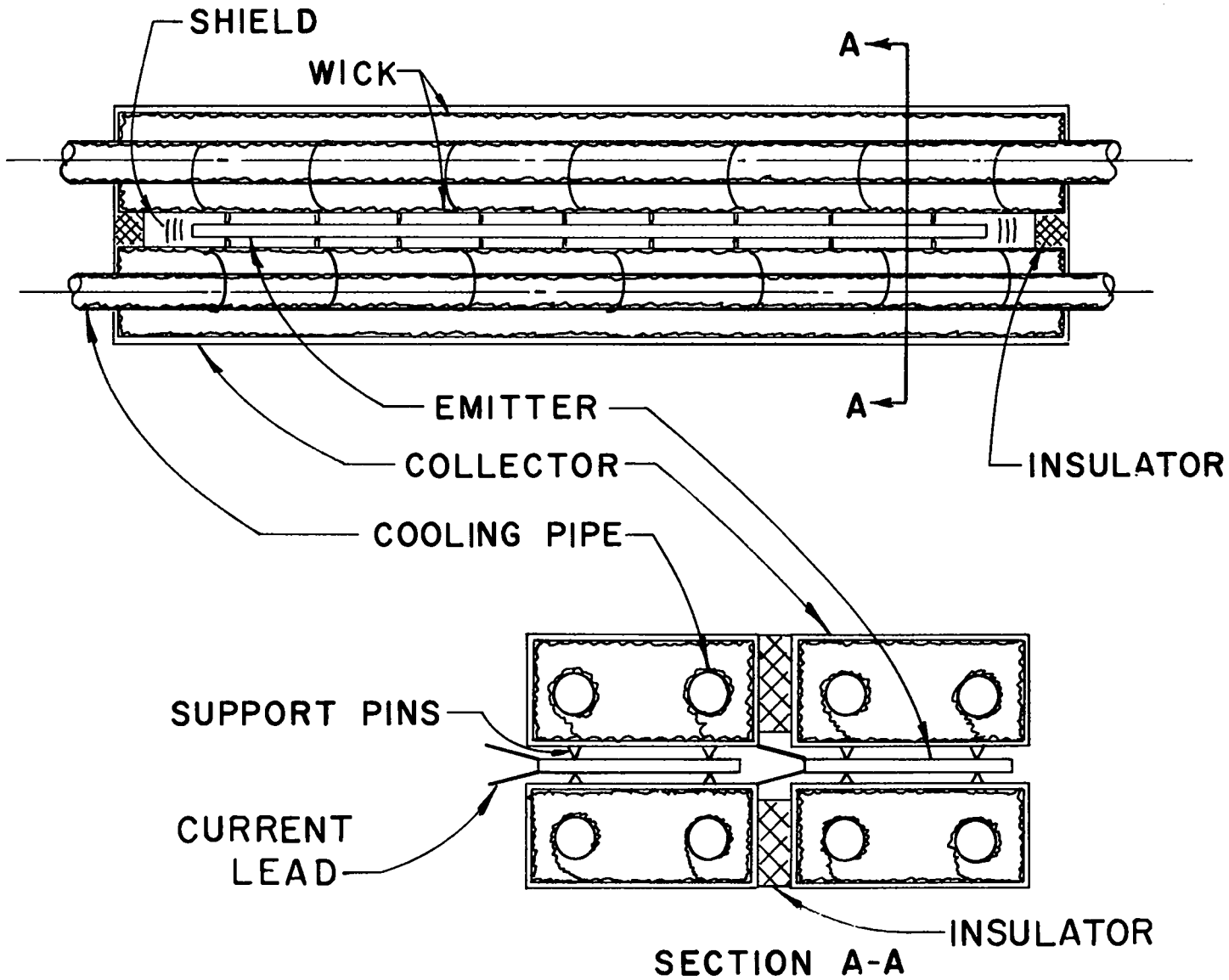


Fig. 7.11. Flat-Plate Cell.

SECRET

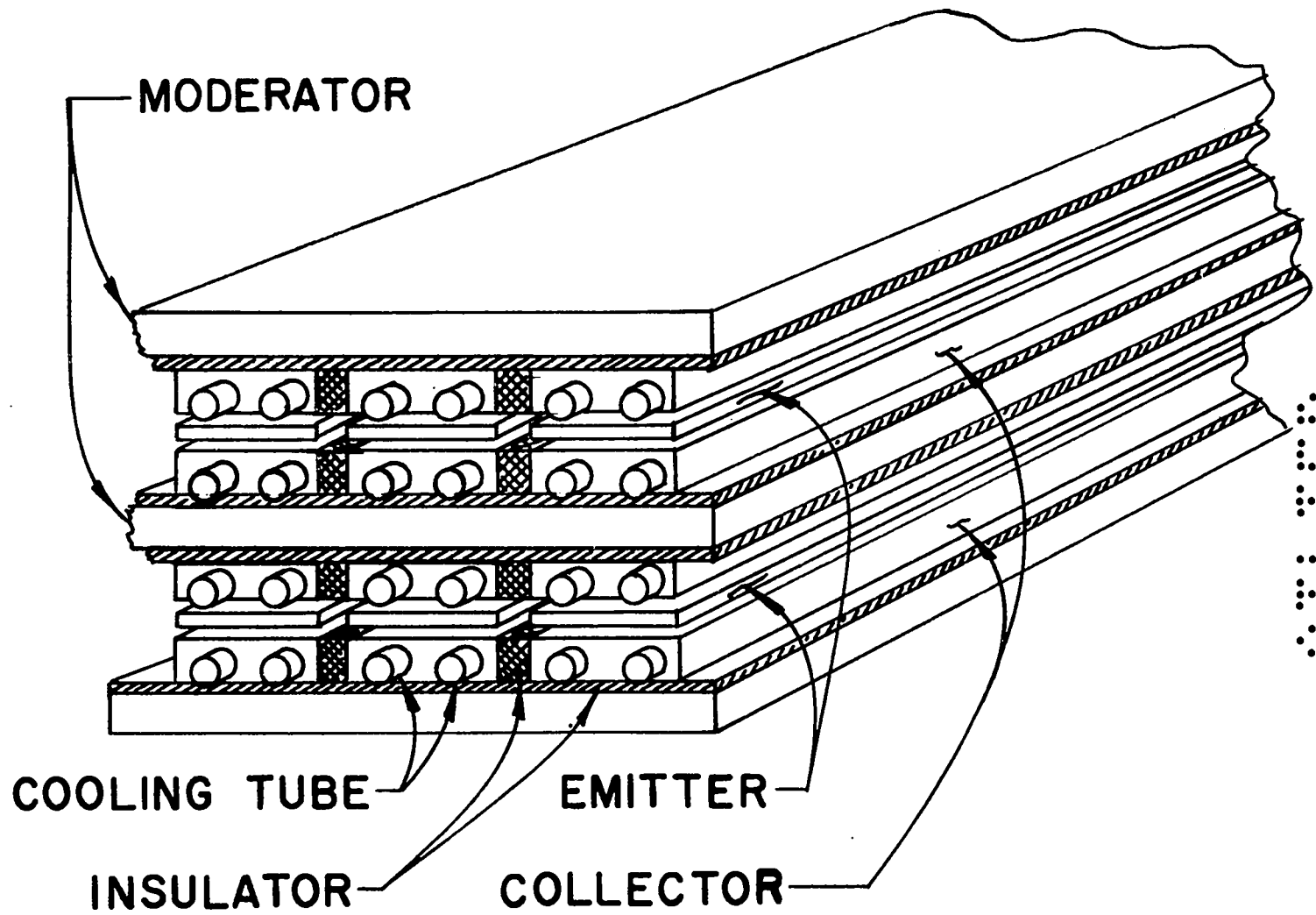


Fig. 7.12. Flat plate cell stacking.

SECRET

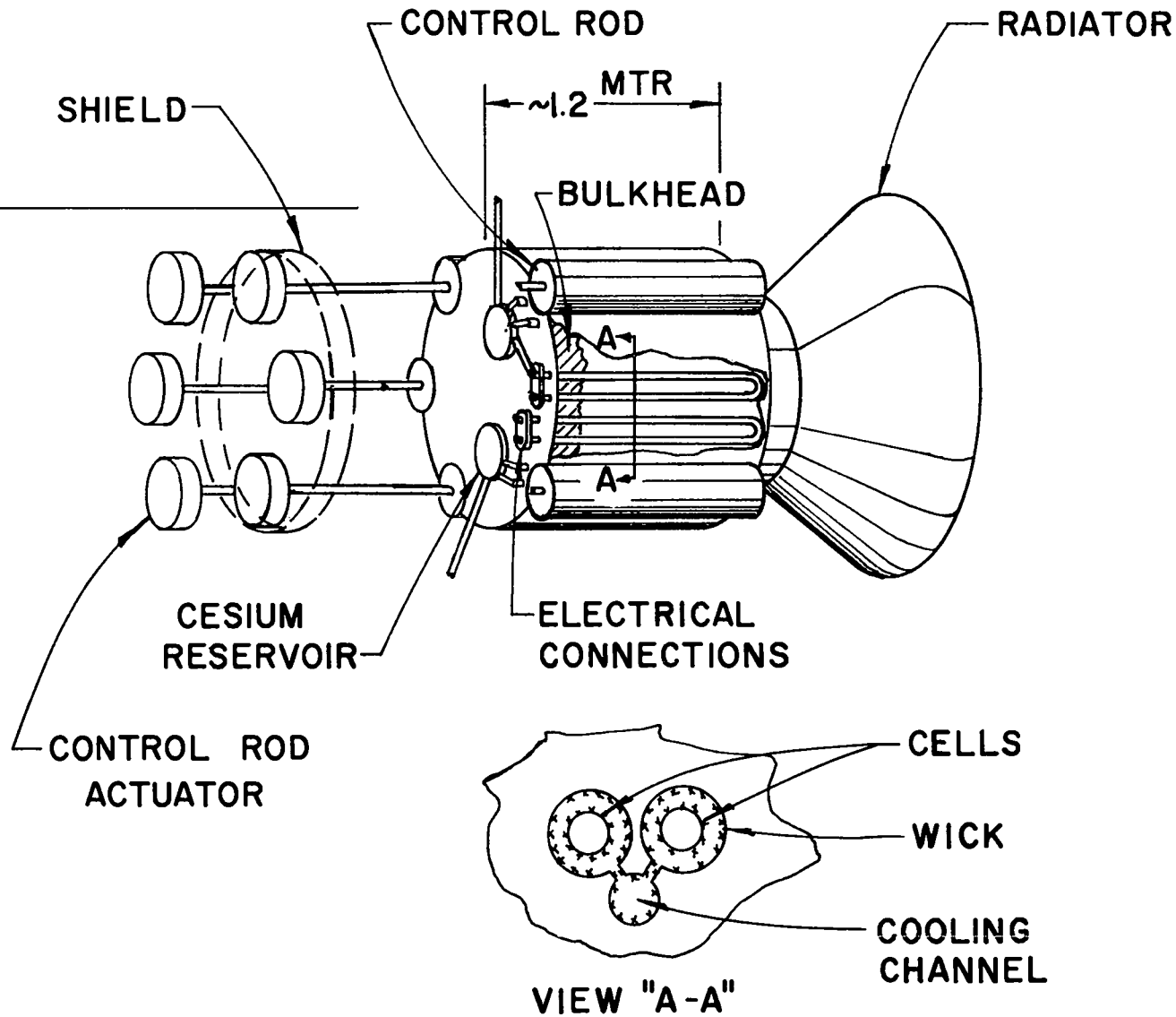


Fig. 7.13. Thermionic reactor system.

SECRET

SECRET



~~CONFIDENTIAL~~  
031710

## 8. Summary and Scaling Laws

Ernest W. Salmi

This lecture will be an accumulation of various subjects, none of which require the standard lecture time; however, they should be discussed because of some rather interesting conclusions. The subjects are:

- 1) Preliminary reactor designs
  - a) Material limitations
  - b) Criticality
  - c) Future advances and their effect on weight to power ratio.
- 2) Shield for equipment and control actuators
  - a) Flux from reactor
  - b) Present damage limitation
  - c) Future damage limitation
  - d) Shield weight
- 3) Summary of past talks and final weight to power ratio and scaling law
- 4) Some comments on mission studies

In Chapter 4 it was predicted that the present  $\text{Mo}^{40}\text{v}/\text{oUO}_2$  fuel being tested here at LASL would have a life of 10,000 hours. Unfortunately, to prove this point takes a very long time. Fuel pins have been run to 5,000 hours, and data should be available on these pins shortly. The power density has been roughly  $300 \text{ watts/cm}^3$  in these experiments. For the present study instead of assuming the expected 10,000 hours, the

170  
031710

~~CONFIDENTIAL~~  
SECRET

value of 5,000 hours will be used. Therefore, the fuel is assumed to operate at  $300 \text{ watts/cm}^3$  for 5,000 hours. Later, some comments will be made on limitations assumed because of lack of enough information on insulators.

In Chapter 7, several cell designs were discussed. If one would have made a weight analysis of the unit cell, then one would have found that the fuel weight was easily the predominate (58%) weight. Outside of the cell, the remaining mass will be the moderator and reflector. Also in the discussion of cell design, the expected efficiency was quoted as 13%. Since the fuel density is very close to  $10 \text{ g/cm}^3$ , one can conclude that the fuel will give 3.9 watts electrical per gram. In order to estimate the fuel required for a reactor, one simply divides power by power density. For example, a 2.0 MW(e) reactor would require 510 kg of  $\text{Mo}^{40}\text{v}/\text{oUO}_2$ . The mass of  $\text{UO}_2$  is 212 kg. This then is the fuel mass required for a 2.0 MW(e) reactor. One can now place a reflector around this fuel and vary the density of the assembly until one gets a critical system. The reflector chosen for this study was 5 cm of Be. The difference between the numbers quoted here and those quoted in Chapter 9 will be mainly due to differences in reflector thickness. In this approach, if one desires a 4.0 MW(e) reactor then the above fuel mass is doubled. In Fig. 8.1, the resultant core radius of a critical system has been plotted as a function of the electrical power. The 2.0 MW(e) case considered above is shown at point A on the curve labelled  $L = 0$ . This curve is for the case of no moderator or a fast reactor. The points labelled on the curve and connected by dotted lines are the lines of constant void fraction. In following the  $L = 0$  curve, as the power is increased, the fuel mass is increased; therefore, the density must be decreased to remain critical.

Another point to be considered is the effect of moderating the reactor. One can take the 2.0 MW(e) fuel mass as given above and mix in some moderator. The moderator chosen is Be. The value  $L = 100$  specified that the ratio of Be atoms to  $\text{U}_{235}$  atoms is one to one hundred. The point B has, therefore, the same fuel mass as point A; however, the Be moderator

1371  
SECRET

CONFIDENTIAL

has been added. One notes that as the value of  $L$  increases, the void fraction of the reactor increases as expected.

These reactor calculations are for idealized spherical cores. There is no power flattening. If one starts at point B, one sees that the void fraction is very high so there is considerable reactivity to be gained simply by increasing the core density. This allows one to make all the compensations needed to go to a power-flattened reactor without much change in the total mass. This approach requires one to stay at rather high power values in order to avoid criticality difficulties. Naturally, a fast reactor will require a higher reactor power than the thermal systems.

Given now the total masses and the electrical power, one can calculate the expected weight to power ratio  $\alpha$ . This is shown in Fig. 8.2 as a function of  $L$  for two power levels. The value of  $\alpha$  at  $L = 0$  is probably on the low side, since the rest of the thermionic cell mass has not been included. At  $L = 100$ , the Be mass is about four times the fuel mass, so this is not a great error. It is obvious from these curves that the moderator has a serious detrimental effect on the specific power. One then asks why moderators should be considered. This returns to problems of materials.

In Chapter 4 there was a discussion of irradiation experiments on  $\text{Al}_2\text{O}_3$  and on some metal-to-ceramic seals. Although there was a few-percent volume expansion noted in the alumina, the seals remained vacuum-tight. The total integrated neutron flux was  $3.1 \times 10^{20}$  nvt. The neutrons counted are for all neutrons with energy greater than 1.0 MeV.

In the reactors being considered here, the moderator is Be. The above experiment was done in the MTR, which is water-moderated. There should be a considerable difference between the two neutron energy spectra. In order to be able to make a rough compensation for this effect, it has been assumed that the damage produced by a neutron is simply proportional to its energy. This proportionality has been normalized to one at 1 MeV. One can therefore use the MTR neutron spectrum and calculate a value

172  
CONFIDENTIAL

CONFIDENTIAL

[REDACTED]

SECRET

which will be called damage flux. This quantity,  $\phi_D$ , is defined as:

$$\phi_D = \int_0^{\infty} \phi \frac{E}{10^6} dE$$

where  $\phi$  is the neutron energy spectrum. With  $t$  the irradiation time, the value obtained for the MTR experiments is

$$\phi_D t = 9 \times 10^{20} \text{ nvt}$$

In the reactor being considered here, the  $\text{Al}_2\text{O}_3$  is expected to run at a little higher temperature than the conditions of the MTR irradiation test. This should allow one to operate at a higher dose rate. Also, since the evidence does not show a limiting condition, the value selected for this study will be increased to  $2 \times 10^{21}$  nvt.

One can now calculate this quantity for the Be-moderated reactors being considered above. Assuming an operating time of 5000 hours, one gets the integrated damage dose for various values of  $L$ . This is shown in Fig. 8.3.

One sees that the assumed extrapolated value crosses the reactor curve at  $L = 100$ . In order to get to a fast reactor ( $L = 0$ ), the extrapolated value must be increased by a factor of 7. For the purpose of this study, the value  $L = 100$  will be used.

Before taking some of these numbers as final, some other interesting observations should be made. What can happen in the future as fuels and insulators are improved? Suppose that an improvement of a factor of two is made in the fuel so that one can operate at  $600 \text{ watts/cm}^3$  instead of the present  $300 \text{ watts/cm}^3$ . Then one could redesign the thermionic cell to obtain this increased performance, and the 2.0-MW(e) reactor now becomes a 4.0-MW(e) reactor. Suppose that the insulator irradiation experiments show that one can go from the present value of  $2 \times 10^{21}$  nvt to  $4 \times 10^{21}$  nvt. One can have the following cases:

173

SECRET

[REDACTED]

031713

- A. 300 watts/cm<sup>3</sup>,  $2 \times 10^{21}$  nvt - present situation.
- B. 600 watts/cm<sup>3</sup>,  $2 \times 10^{21}$  nvt
- C. 300 watts/cm<sup>3</sup>,  $4 \times 10^{21}$  nvt
- D. 600 watts/cm<sup>3</sup>,  $4 \times 10^{21}$  nvt

The curve from Fig. 8.3 has been transferred to Fig. 8.4 and other curves have been added to cover the above examples. The possible operating points are labeled A, B, C, and D. In order to see how these variations effect the value of  $\alpha$ , a new set of curves has been plotted in Fig. 8.5. The same points as above have been labeled on Fig. 8.5. One sees a very interesting point in that improvements in insulators has the same effect as improvements in fuels. A balanced program should take both into account.

As mentioned above, the reactor study shown here will be based on the presently established material limits shown by the label A. From Fig. 8.5 one obtains the value of 0.85 kg/kW(e). Because of a change in the thickness in the Be reflector, the detailed reactor study to be discussed in Chapter 9 will have an  $\alpha$  of 1.13 kg/kW(e). Since this system has had the most work done on it, this will be the final value quoted in the summary.

Another subject to be considered in this lecture is the problem of a shield for equipment. In Fig. 8.6 the damage flux of neutrons leaving the reactor is shown as a function of L. The gamma flux is shown in Fig. 8.7. As in the previous curves, the flux values are almost independent of the reactor design power. Since the value of L has been chosen as 100 and the operating time is to be 5,000 hours, then one obtains for the neutrons a value of  $2.45 \times 10^{20}$  nvt; and for the gammas, the value becomes  $1.4 \times 10^{12}$  Rad.

The other half of the problem is what integrated dose can be tolerated. For fast neutrons a value of  $10^{19}$  nvt seems to be a reasonable value. As for the integrated gamma dose, a value of  $10^{12}$  Rad has been chosen. This rather high value was picked because of some recent work on

031713 174

~~CONFIDENTIAL~~  
SECRET

control rod actuators. Recently, tests on electric stepping motors have completed 10,000 hours of operation at a total dose of  $1.6 \times 10^{11}$  Rad. Actuators have been designed and are under test which are expected to go to a total gamma dose of  $10^{13}$  Rad.

Using the above limiting values, one can calculate shield weights using various materials. If one assumes the material is LiH, then for a reactor of 2 MW(e), the shield would weigh about 100 kg for a reactor of this diameter.

One would now like to make a short summary to show what the total engine weight and specific power will be. As has been mentioned several times before, the reactor weights given in Chapter 9 are shown in Table 8.1. This reactor is expected to produce 20 MW(t). This reactor design is based on the thermionic stacked cell design which was discussed in detail in Chapter 7. The bases of this particular cell design are the fuel and insulator irradiation material testing which was discussed in Chapter 4 and the present lecture. As for the material limitation on the thermionic performance, Chapters 1 and 5 showed that at 10 amps/cm<sup>2</sup> and 0.025 cm spacing, a reactor thermionic cell designed for maximum efficiency is only slightly affected by materials. From these considerations a value of 13% efficiency was derived. Therefore, the above reactor should have an electrical output of 2.6 MW(e). The amount of waste heat to be radiated would be 17.4 MW.

In Chapter 2, the heat pipe radiator optimization was discussed. The value calculated for radiators of about this size was 0.05 kg/kW(t) for a dump temperature of 1200°K. Due to uncertainties in problems of fabrication of the radiator and the possibility of lowering of the operating temperature to a more favorable value for the Be moderator and reflector, this number has been doubled to 0.1 kg/kW(t). Using this value, one obtains the weights shown in Table 8.1. In this present chapter the shield for equipment has been calculated and is also shown in Table 8.1.

175  
SECRET

031710

Table 8.1

## SUMMARY OF COMPONENT WEIGHTS

Reactor core	1913.39 kg
Reactor reflector	1012.52
Equipment shield	100.00
Radiator	1740.00
Controls	75.00
Busbar	303.00
Arc jet	91.00
Lithium tanks	<u>486.00</u>
Total°	5720.91 kg

Jet power is 1.9 MW

$$\alpha = 3.0 \text{ kg/kW jet}$$

In Chapter 3, the weights of the busbar and motor were given and are also shown in Table 8.1. The Li tank weights were also discussed and resulted in 2% tanks. This value appears in Table 8.1. Another important point from Chapter 3 is that the Li arc jet is expected at present to have an efficiency of 75% at 5000 I<sub>sp</sub>. This means that the 2.6 MW(e) value becomes 1.9 MW jet power.

The total weight is 5721 kg which results in a specific power,  $\alpha$ , of 3.0 kg/kW jet power. This value is lower than was expected. In the mission studies to be discussed in Chapter 12, the lowest value considered was 3.5 kg/kW.

This system is designed to operate for 5,000 hours. What would the weight become if one had designed for 10,000 hours? The fundamental problem is connected with the fuel. There has been a considerable amount of discussion on this question, and the answer is not entirely clear; however, it will be assumed here that the fuel which can run at 300 watts/cm<sup>3</sup> for 5,000 hours can also run at 150 watts/cm<sup>3</sup> for 10,000 hours. This assumption says that the fuel can be used to a given energy limit (or

031710

[REDACTED]

SECRET

power density multiplied by time), and this limit is 1.5 MW-hr/cc. The shield and lithium tank also depend on the total available energy of the system.

The weights of other parts of the system depend only on the power as, for example, the busbars and the arc jet. The radiator mass actually varies as  $P^{5/4}$ . The exponent comes about because of the meteoroid penetration probability. One can set down an approximate equation for the mass of the system as

$$M = a Pt + bP^{5/4}$$

and

$$Pt = c$$

or

$$\alpha = \frac{M}{P} = at + bP^{1/4}$$

$$\alpha = at + b\left(\frac{c}{t}\right)^{1/4}$$

Using the values given in Table 8.1 to evaluate the constants, one obtains

$$\alpha = 3.78 \times 10^{-4} t + \frac{9.42}{t^{1/4}}$$

where  $t$  is in hours of reactor operating time. In Fig. 8.8, the predicted value of  $\alpha$  has been plotted as a function of the reactor operating time. For long operating times, the  $\alpha$  becomes very large. At the short operating time, the radiator becomes very large and the  $\alpha$  increases again. In general, one can conclude that one should reduce the reactor operating time to a minimum. This statement naturally leads to some comments on mission studies.

The reactor that has been discussed here has an operating time of 5,000 hours and an  $\alpha$  of 3.0 kg/kW(e). This mission, which will be

177  
SECRET



031710

discussed in Chapter 12, is the manned Mars mission, similar to the STL study for the Nerva reactor. Generally, a nuclear electric propulsion round trip to Mars assumes that the reactor operating time is 10,000 hours. This long operating time comes about because of the method used in most reported mission studies. The method often used is called "variable thrust, power-all-the-way calculation." In this calculation, the reactor is operated all the time; however, the  $I_{sp}$  is varied to change the thrust. Melbourne and Sauer<sup>1</sup> made a very nice study comparing the variable-thrust method to a constant-thrust-and-varying-propulsion-times method. The mission they assumed was a 160-day transfer from earth to Mars. Assuming an  $I_{sp}$  of 5000 sec, one can obtain from their curves the total energy (or power multiplied by time) which is required for various propulsion times. This is shown in Fig. 8.9 along with the variable thrust value. One sees that the total energy requirement is about one-half of the variable thrust case. In Fig. 8.10, the mass ratio of payload plus engine has been plotted as a function of propulsion time. If one assumes the same payload as one obtains from the variable thrust case, one can calculate an  $\alpha$ . This is shown in Fig. 8.11. The  $\alpha$  required has been reduced by 17% from the variable thrust case; however, the operating time has been reduced by a factor of 2. One could add to Fig. 8.11 a curve similar to that given in Fig. 8.8 for some hypothetical engine design but with a variable energy limit. In some cases one would find that the engine could not be designed for the variable thrust case; however, it could be designed for some shorter propulsion time.

The important point from this example is that for a round trip to Mars using a nuclear electric propulsion engine, one does not need a 10,000 hour operating time. An operating life of 5,000 hours is adequate, and in some missions this operating life may still be reduced very considerably.

178  
031710

~~CONFIDENTIAL~~

SECRET

References

1. W. G. Melbourne and C. G. Sauer, Jr., "Optimum Thrust Programs for Power-Limited Propulsion Systems," Jet Propulsion Laboratory Report JPL-TR-32-118, June 1961.

179  
SECRET

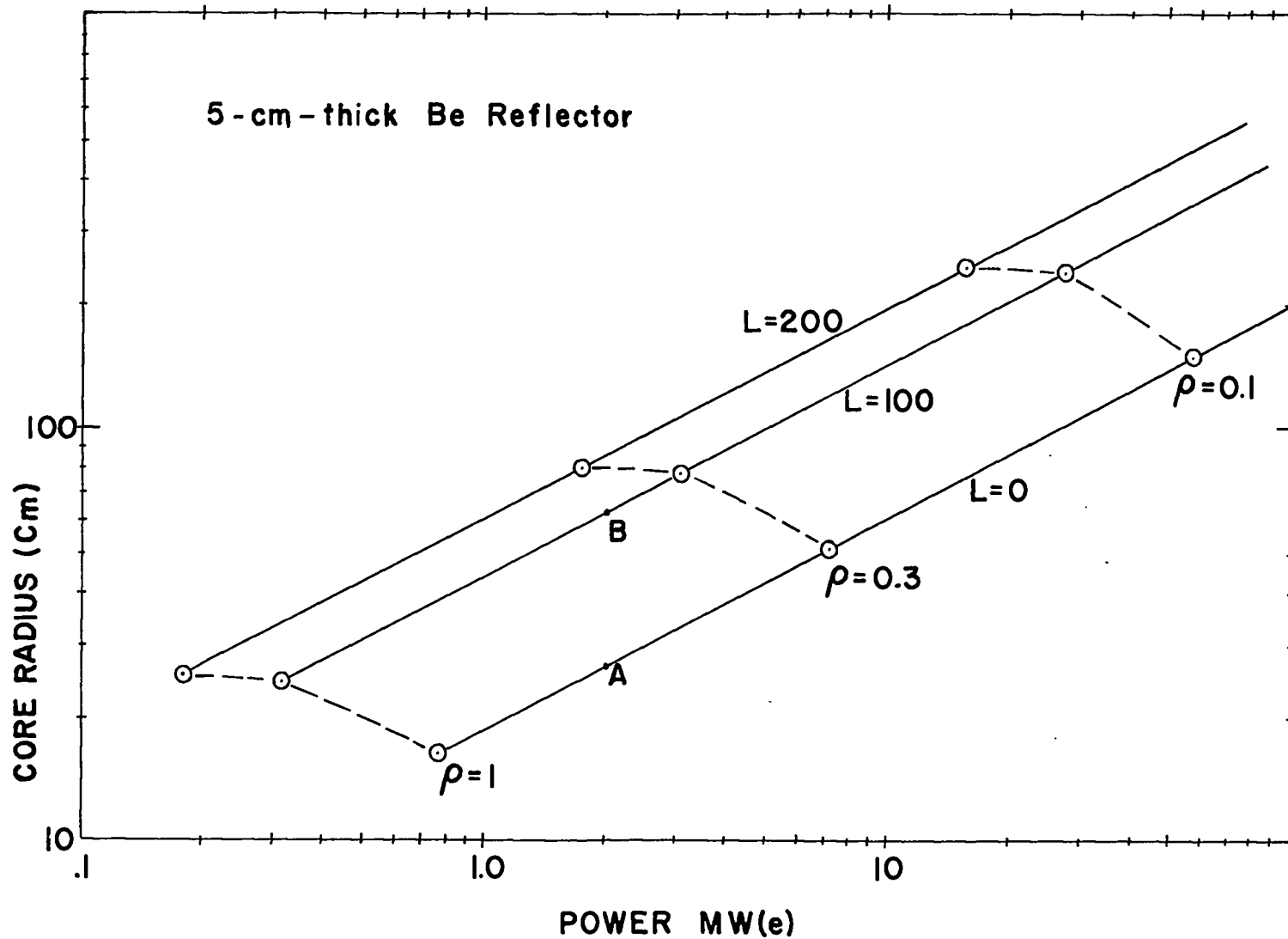


Fig. 8.1 Core radius vs power for various Be/U atom ratio.

~~CONFIDENTIAL~~  
SECRET

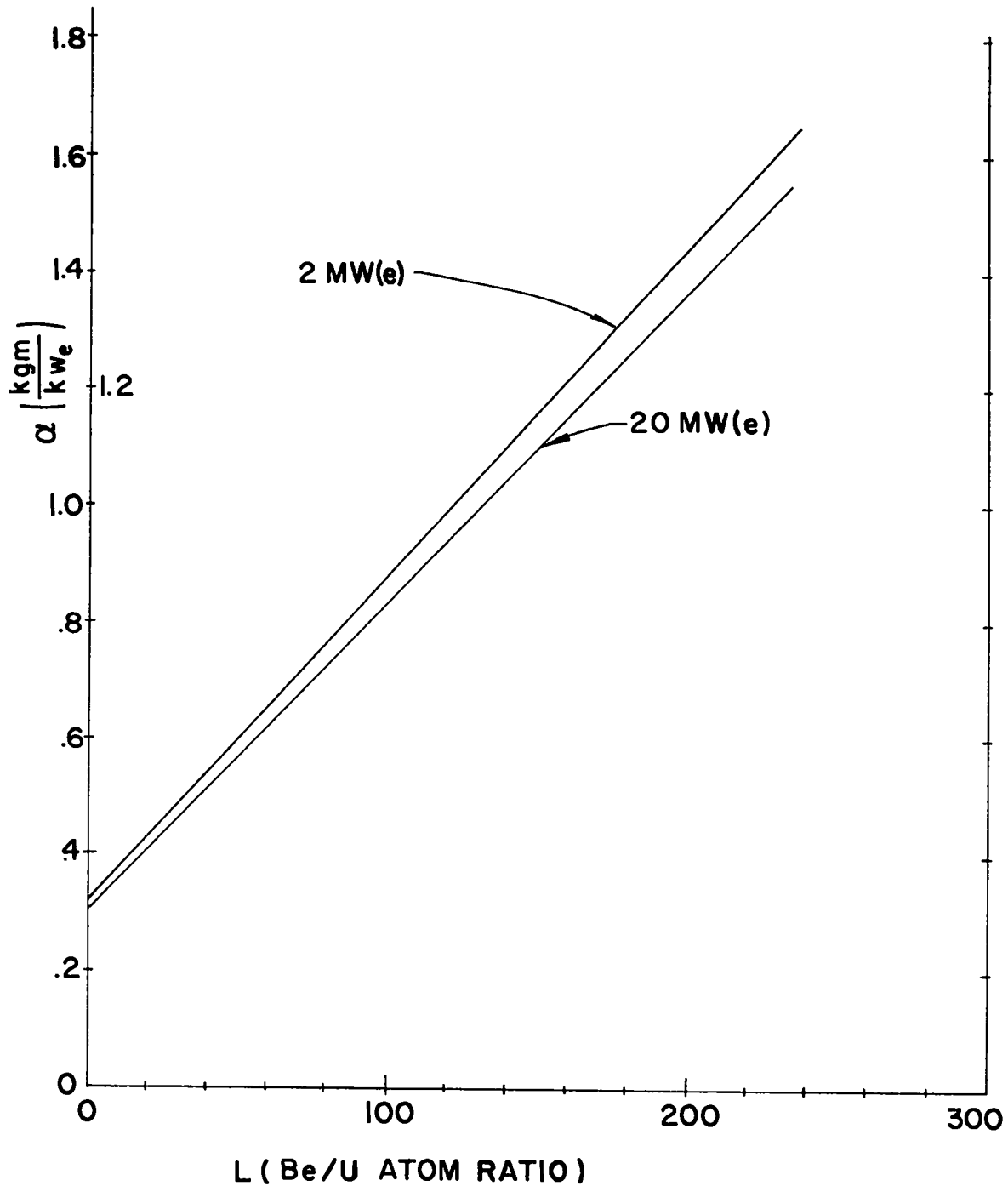


Fig. 8.2 Weight to power ratio vs Be/U atom ratio.

~~CONFIDENTIAL~~  
031713

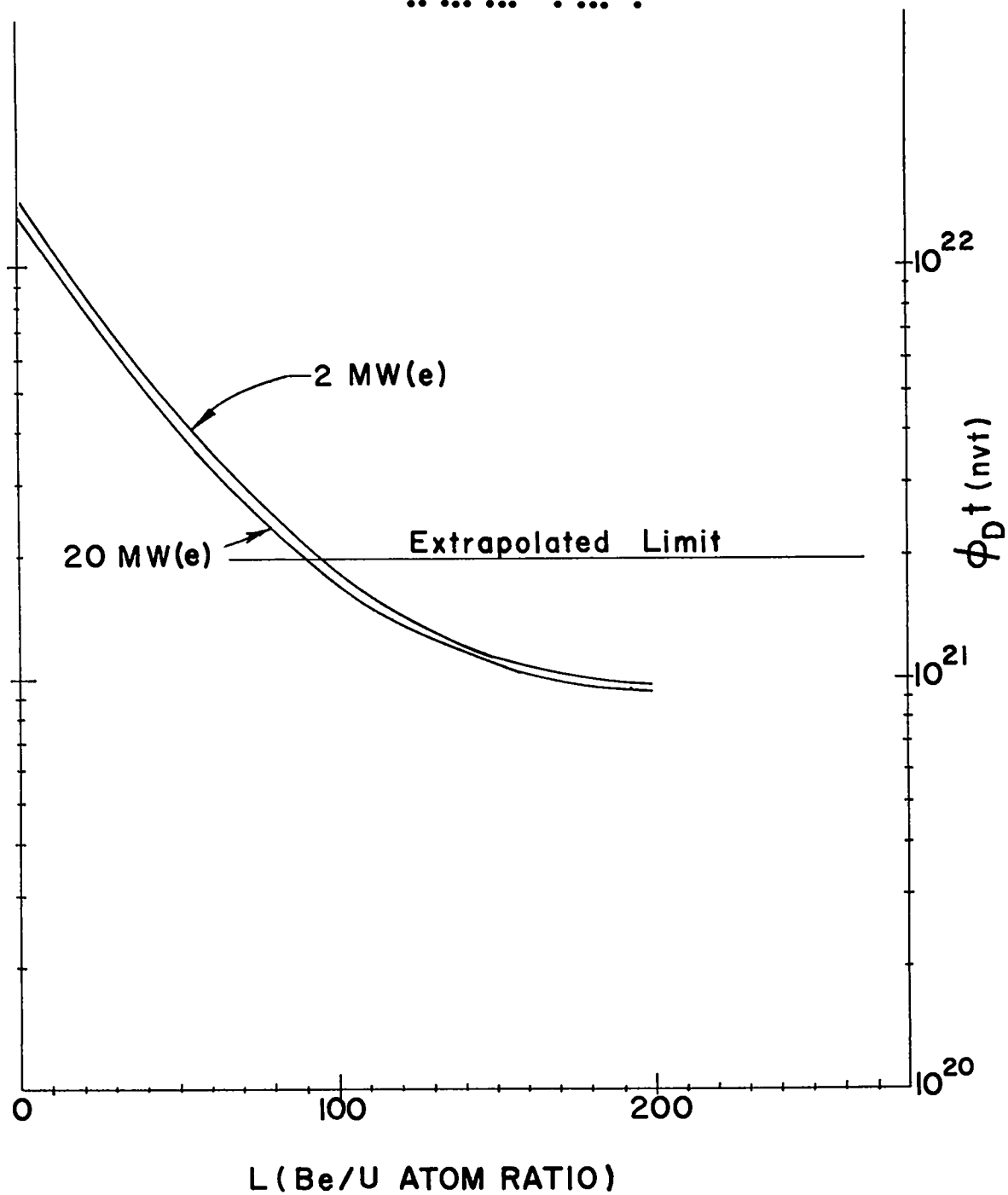


Fig. 8.3 Damage dose vs Be/U atom ratio for various power level.

102  
031713

~~CONFIDENTIAL~~

CONFIDENTIAL

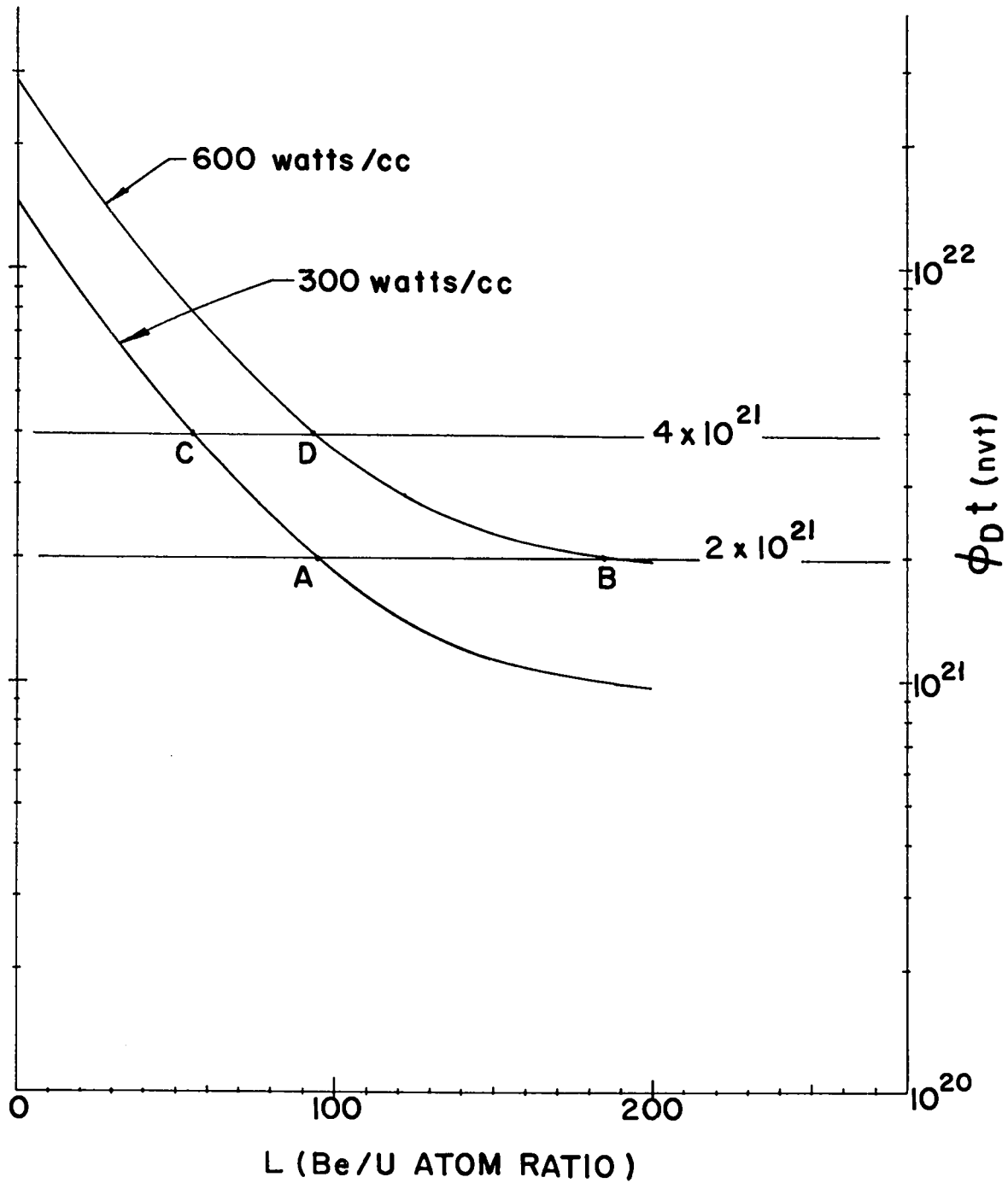


Fig. 8.4 Damage dose vs Be/U atom ratio for various power density in fuel.

~~CONFIDENTIAL~~  
03713

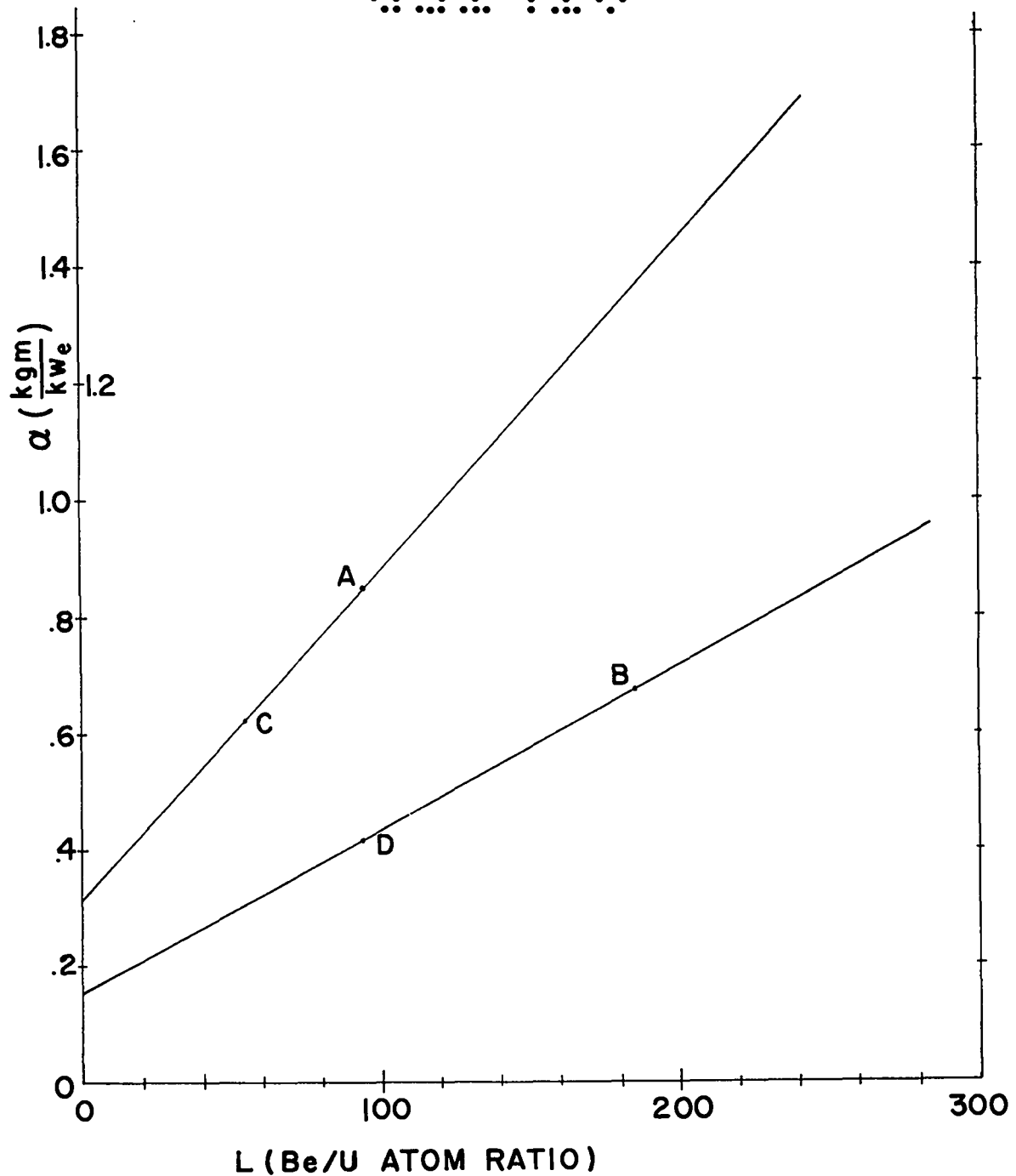


Fig. 8.5 Weight to power ratio vs Be/U atom ratio for various power densities.

184  
03713  
~~CONFIDENTIAL~~  
03713

~~CONFIDENTIAL~~  
CONFIDENTIAL

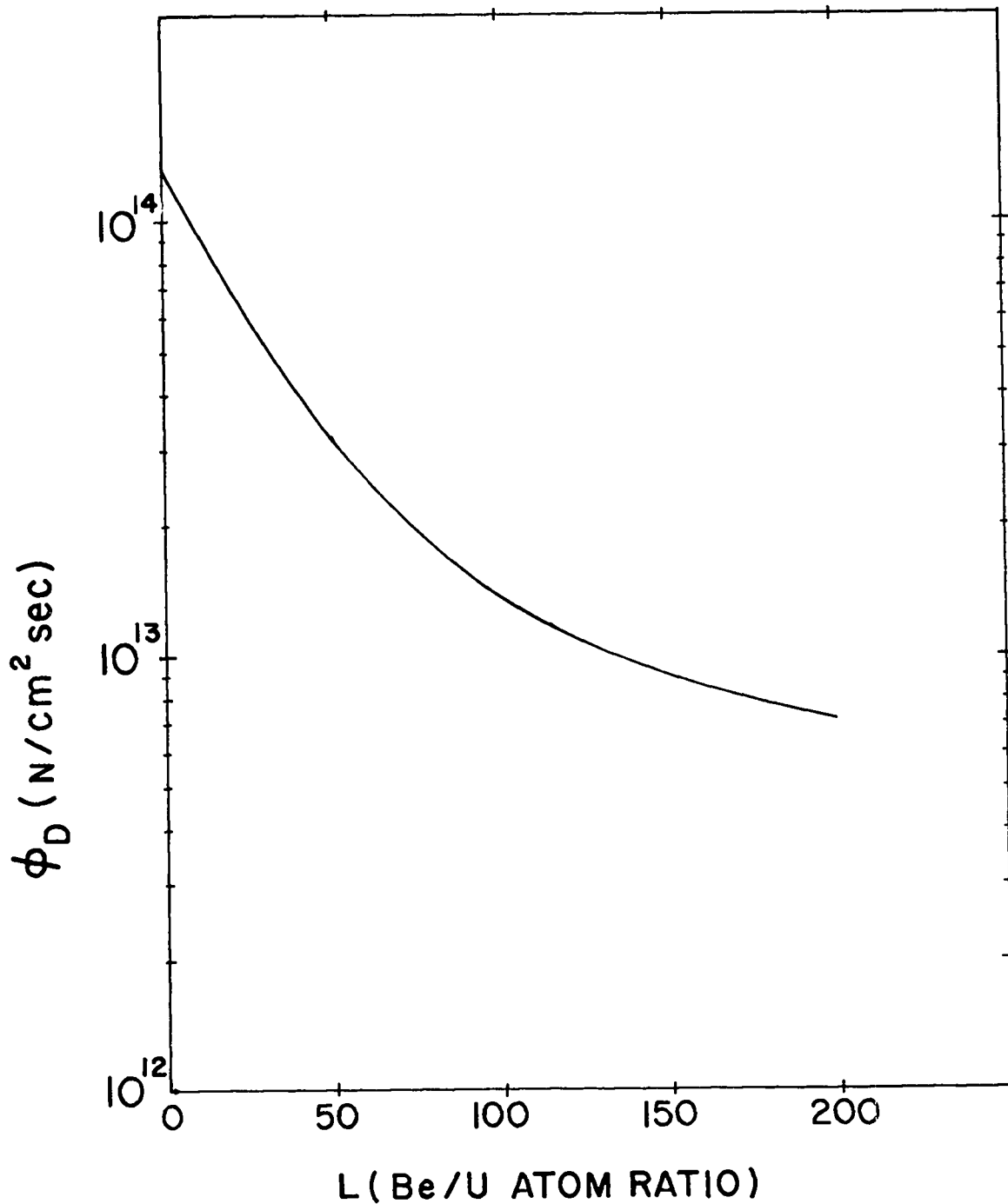


Fig. 8.6 Neutron damage flux having reactor vs Be/U atom ratio.

185  
CONFIDENTIAL



031713

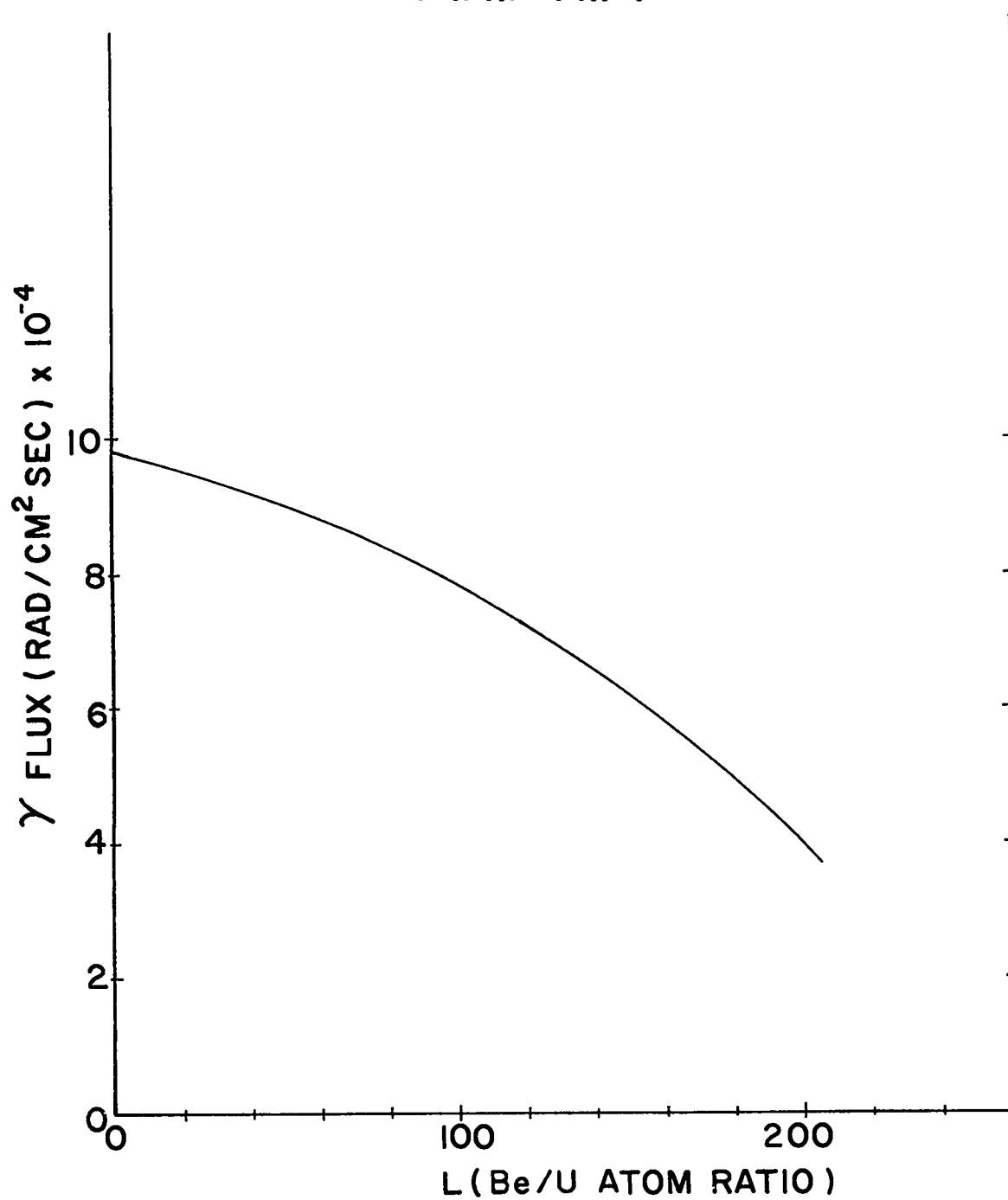


Fig. 8.7 Gamma flux leaving reactor vs Be/U atom ratio.

031713

SECRET

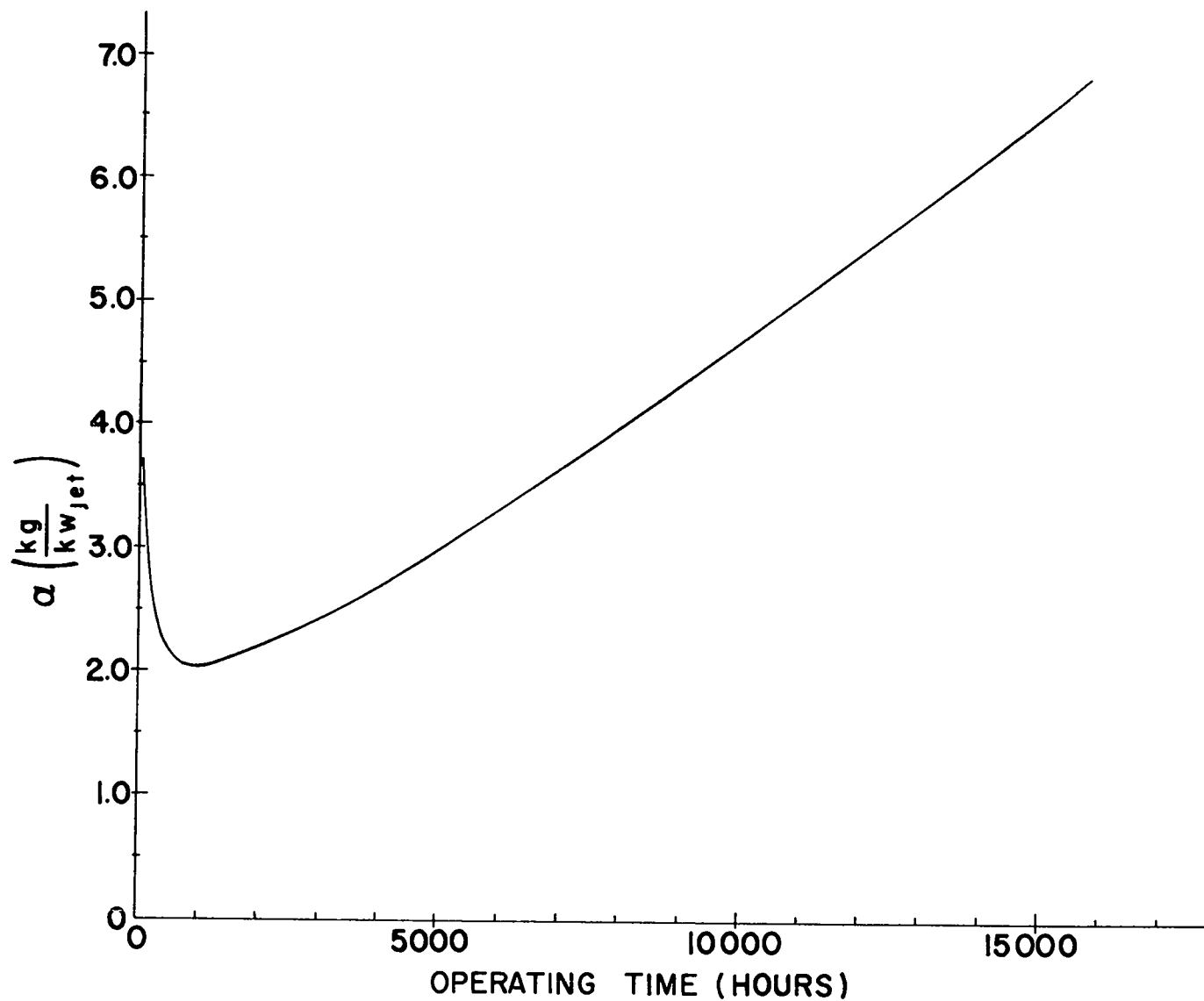


Fig. 8.8 Weight to power ratio of entire engine vs operating time.

SECRET

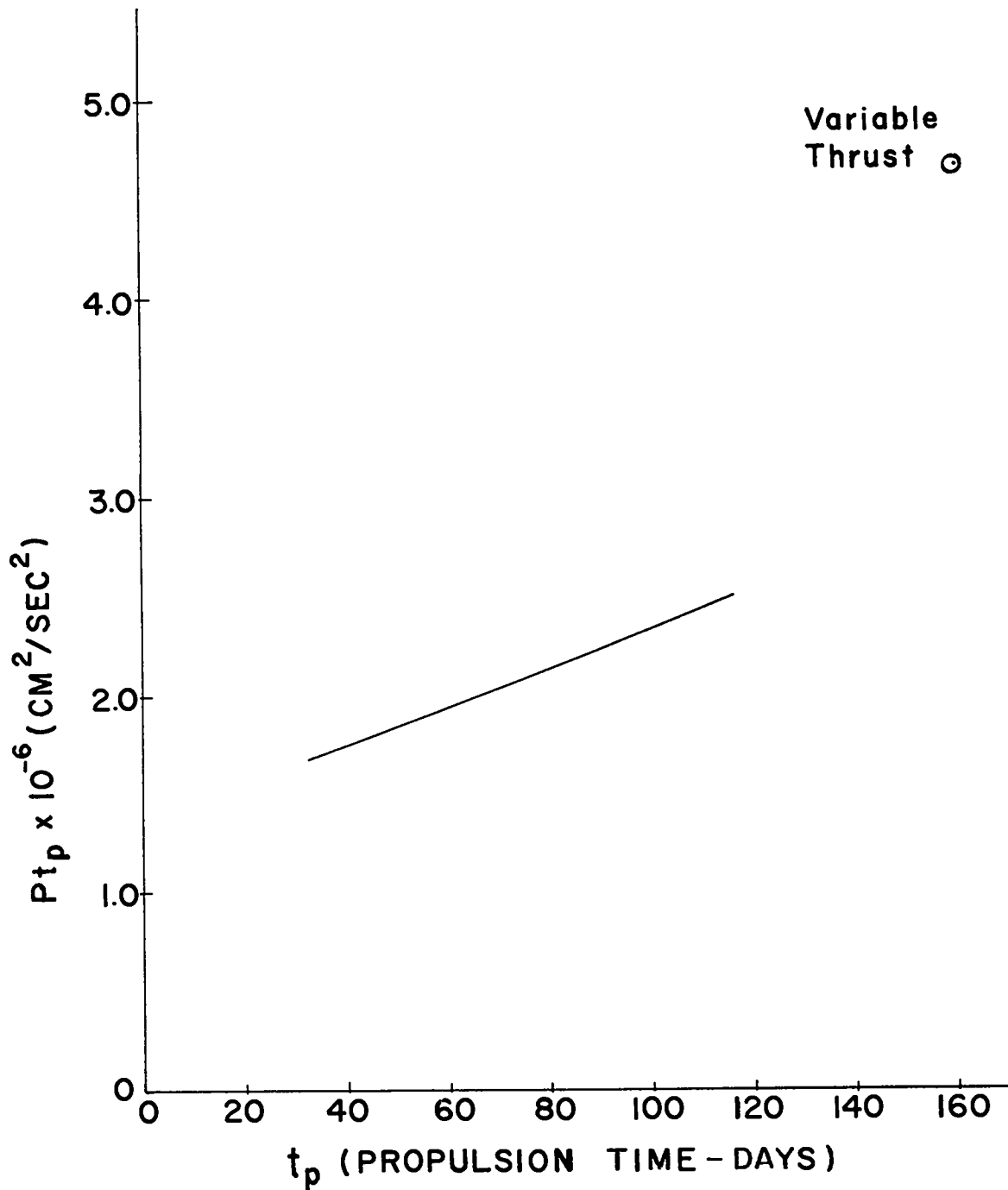
~~CONFIDENTIAL~~  
031713

Fig. 8.9 Total energy given to propellant vs propulsion time.

188  
031713  
~~CONFIDENTIAL~~

~~CONFIDENTIAL~~

SECRET

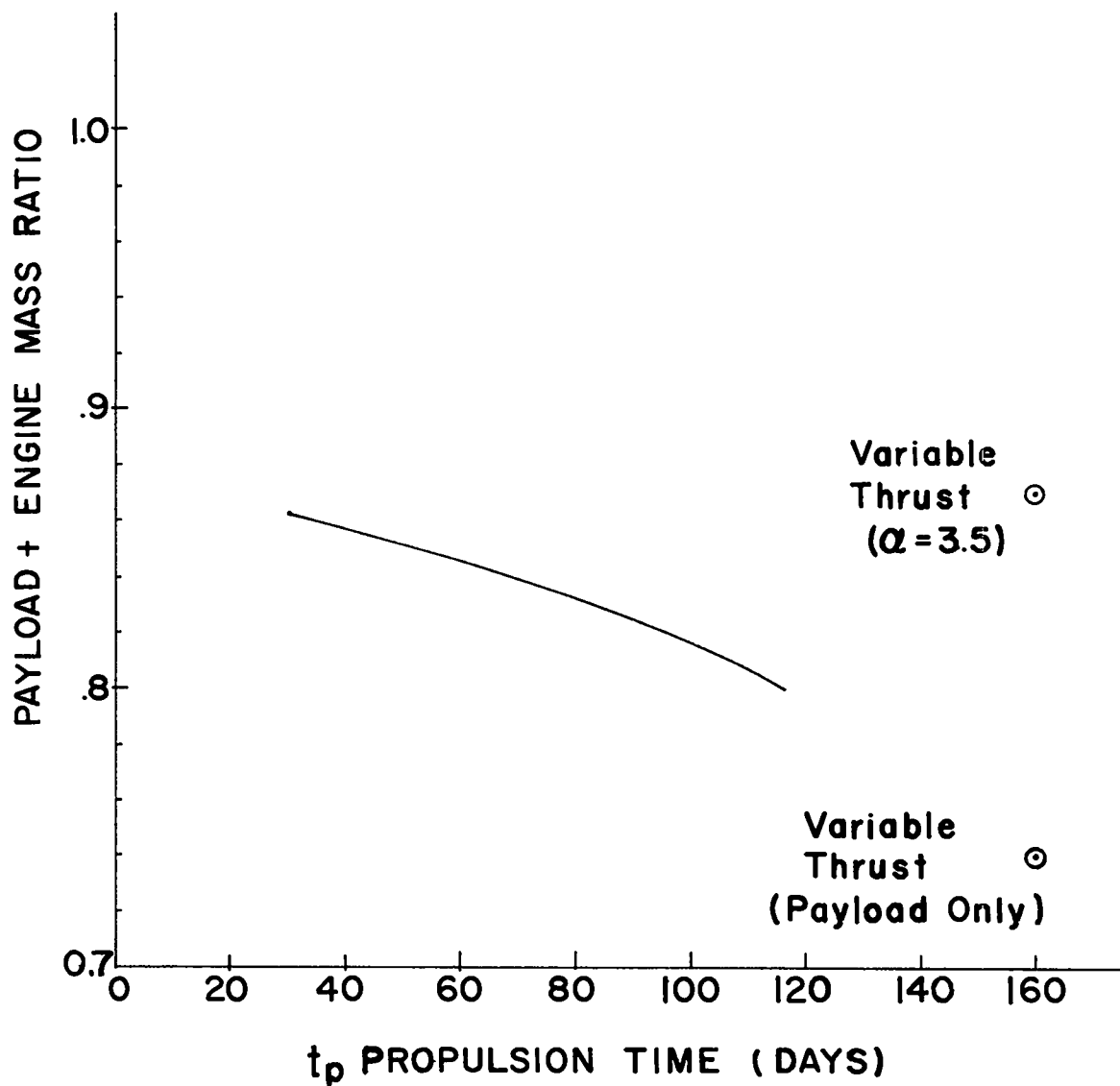


Fig. 8.10 Final mass ratio for various propulsion time.

189  
SECRET

~~CONFIDENTIAL~~

031713

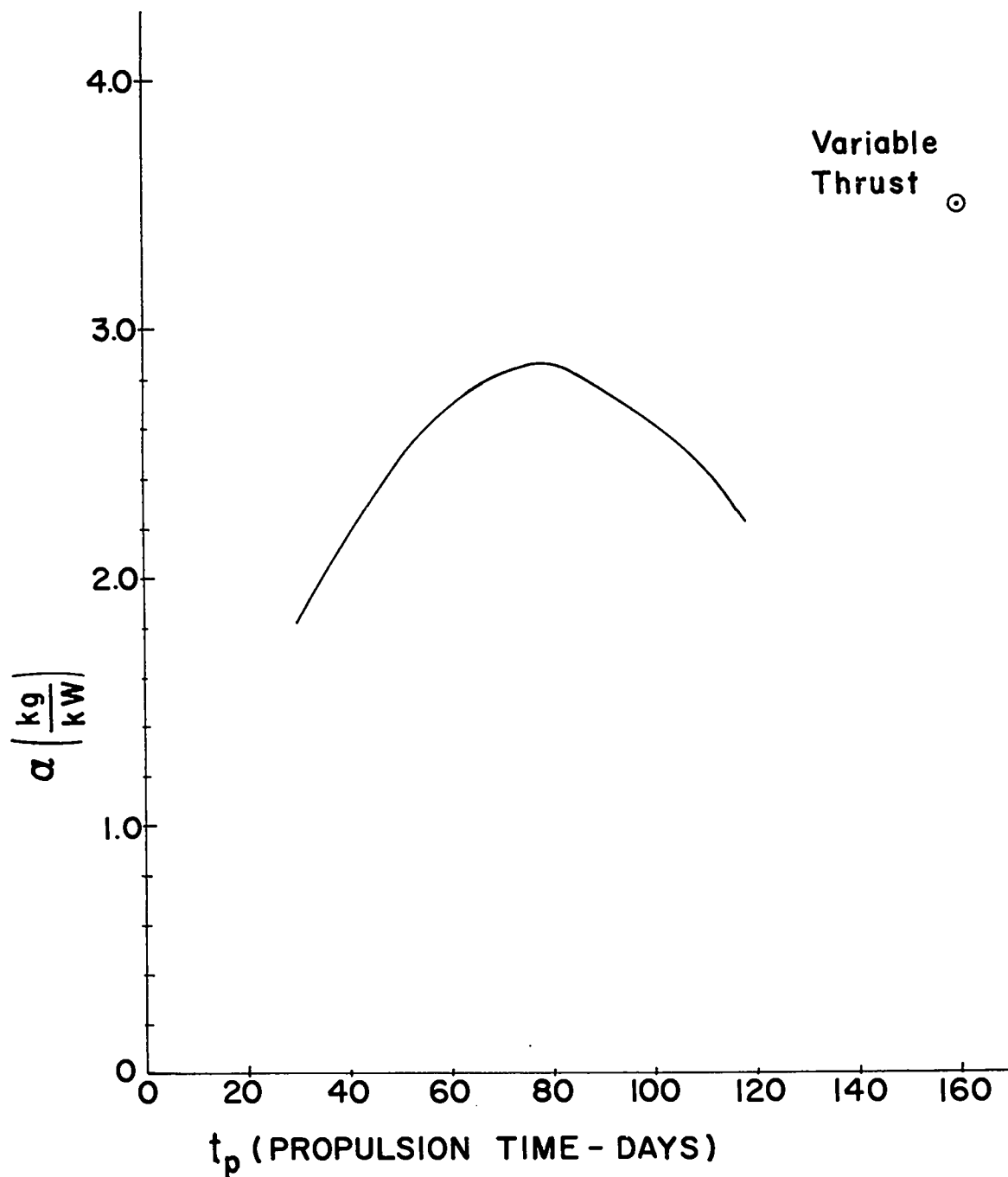


Fig. 8.11 Required weight to power ratio as a function of propulsion time.

190  
031713~~CONFIDENTIAL~~

~~CONFIDENTIAL~~

SECRET

## 9. Thermionic Space Reactors

Richard C. Anderson

Introduction

The thermionic space reactor consists of a cylindrical core, surrounded by a beryllium reflector. The core consists of a number of unit cells, each of which contains a single plasma thermocouple and the coolant and moderator associated with it.

An attractive feature of thermionic reactors is the absence of the external machinery required by conventional reactors to extract electricity. In line with this feature, the reactor is designed to be cooled by heat pipes, thus eliminating the machinery normally required to pump coolants through conventional systems. The coolant material may be either Na or Li<sup>7</sup>.

The moderator is beryllium at 85% of normal density, the 15% void fraction being reserved for heat pipes. There is to be one heat pipe for each two fuel elements.

Three types of plasma thermocouples have been considered. In each case the fuel material is MoUO<sub>2</sub>.\*

In the first type considered, the fuel was in the form of small circular discs. This type of fuel element had two disadvantages: First, the void fraction required for heat pipes was too great and criticality problems developed. Second, the power-flattening problem was more severe than had been anticipated.

---

\*This "standard fuel," referred to below, is defined as Mo<sup>40v</sup>/oUO<sub>2</sub> with fully enriched uranium.

2191  
SECRET

031713

In the second type, the fuel element was in the form of long (50-100 cm) rectangular plates. This design required not only power-flattening from one element to the next, common to all designs, but the additional problem of power flattening within each individual element.

With additional work, the difficulties presented by the first two types of fuel element could probably be overcome; but, instead, effort has been concentrated on the third type, the stacked cell design. The plasma thermocouples in this design have the distinct advantage of being very similar to the types which have been extensively built and tested at Los Alamos and other places. It is with reactors consisting of fuel elements of this type that the remainder of this paper is concerned.

The nuclear calculations for this study have been performed using the DTK program<sup>1,2</sup> which solves the multigroup, angle- and space-dependent neutron transport equations by means of the angular segmentation ( $S_n$ ) method. The calculations were done with 18 groups and the  $S_4$  approximation, using Los Alamos group-averaged cross sections.<sup>3</sup> Non-nuclear properties were calculated by standard techniques. The only calculation of which the details are important is the power calculation, since it has a bearing on what follows. The power calculation is based on the assumption that the system produces 300 watts (total) per  $\text{cm}^3$  of  $\text{MoUO}_2$  fuel material, and therefore depends on the volume of fuel material and not on the U-235 content. Based on the values given in Chapter 7, the efficiency will be assumed to be 13%.

#### Ground Rules

There are six ground rules under which the reactor has been designed. The ways in which they effect the design are discussed below. The six rules established: 1) criticality, 2) fixed power level, 3) maximum damage flux, 4) reflector control, 5) specific mass, and 6) power flattening.

The first criterion, that of criticality, needs no further elaboration.

031713

~~CONFIDENTIAL~~

CONFIDENTIAL

The power level of the system has been fixed at 2.6 MW(e). Given a unit cell design which produces a known amount of power and has a known volume, the dimensions of cylindrical, 2.6-MW(e) cores can be computed and the radii plotted as a function of the heights. Also, from the unit cell properties, the dimensions of critical systems composed of such cells can be estimated and plotted. When the 2.6-MW(e) curve and the critical curve are plotted together (see Fig. 9.1) one of three situations arises: In situation (I) there are two intersections indicating that there are two possible reactors - a short fat reactor and a tall thin reactor. In situation (II) there is no intersection, indicating that a critical 2.6-MW(e) system cannot be achieved with the unit cell as designed. In situation (III) there is a single intersection corresponding to a height-to-diameter ratio near 1. It is this geometry which, for reasons to be pointed out below, is to be desired. If the unit cell design produces situation (I), there are three ways in which the cell may be altered to give situation (III): the void fraction may be increased, the amount of U-235 may be reduced, or the amount of moderator may be reduced. Conversely, situation (II) may be converted to situation (III) by the reverse operations. The analysis of the unit cell by this method does not define the reactor, nor does it necessarily produce a final version of the unit cell; but it does provide a convenient means of evaluating the potential worth of various proposed designs.

The damage flux, as defined in Chapter 8, is a measure of the damage incurred by reactor components as a result of neutron irradiation; the maximum allowable value is based on experimental data. The damage flux in the unit cell is controlled by the amount of moderator, since the more thermal the reactor, the lower the damage. It has been found that a Be/U-235 atom ratio of 100/1 results in a damage flux well inside the maximum acceptable value. It is necessary that the damage flux of the cell be significantly less than the maximum allowable amount, since the damage flux as calculated for a typical unit cell is based on the average power density in the core, while the damage flux of interest is

193

CONFIDENTIAL



031713

the maximum, which cannot be obtained from a unit cell calculation.

In a bare or reflected homogenous core (consisting of identical unit cells) the maximum fast flux, and therefore the maximum damage flux, is at the center of the core.

In the final design of the reactor, it is necessary to utilize cells containing less than the standard amount of U-235. These cells must have a higher flux in order to produce the required power; and, hence, the damage flux in these cells is higher than in those containing standard fuel material. The cells containing the least U-235 are at the center of the core.

The control elements are located in the radial reflector in order to minimize the effect of controls on the power distribution; consequently, it is necessary to place a reflector around the core which is thick enough to contain sufficient reactivity to control the reactor and to accommodate the control elements.

The control system, as visualized, consists of a number of rotating drums, each with a thermal neutron poison on one side. When the poison is rotated in toward the core the reflector is, in part, effectively removed. When the poison is rotated out, the reflector is replaced and the poison removed.

Contributions to the specific mass of various core components, based on 13% efficiency and standard fuel material, are given below:

Fuel pin	0.240 kg/kW(e)
Hardware	0.192 kg/kW(e)
Moderator	0.295 kg/kW(e)
Total core	0.727 kg/kW(e)

The volume of the reflector depends on its thickness and on the core shape. For a given reflector thickness, the volume is minimized when the core height-to-diameter ratio is 1. (This is the first reason for selecting this core shape.)

The contributions to the specific mass of four different reflector thicknesses and the totals for the core and reflector are tabulated below:

194  
031713

[REDACTED]

SECRET

Thickness, cm	5	10	15	20
Specific mass of reflector, kg/kW(e)	0.175	0.384	0.632	0.923
Total specific mass, kg/kW(e)	0.902	1.111	1.359	1.650

A reflector thickness of 10 cm has been arbitrarily chosen. This thickness is too large from the specific mass standpoint, small from the power flattening standpoint, adequate for control, and necessary for criticality. The resulting total specific mass is 1.11 kg/kW(e).

No effort has been made to estimate the contribution for such components as cesium reservoirs, electrical and plumbing connections, etc.

The requirement that the power be as uniform as possible throughout the core at all times is the most severe of the ground rules.

The term "power ratio", as used below has one of two meanings:

1) When the core is treated as a homogeneous medium so that the power density is a continuous function of position, the power ratio is the ratio of the maximum to minimum power densities; or 2) when the core is treated heterogeneously and each unit cell calculated separately, the power ratio is the ratio of power in the maximum power cell to power in the minimum power cell.

There are a number of ways of flattening the power, the most attractive of which is by using the appropriate reflector thickness, referred to below as the optimum reflector. Unfortunately this method is not applicable to the 2.6-MW(e) core for two reasons: 1) The thickness of the optimum reflector increases with increasing core size. For small cores, the optimum reflector thicknesses are in the 5- to 10-cm range. For cores the size of the core under consideration here, the optimum reflectors are in the 15- to 20-cm range, and their use results in an excessively high specific mass; and 2) the minimum power ratio also increases with increasing core size. For small cores, power ratios like 1.1 are easily obtained, but on the 2.6-MW(e) cores the minimum power ratio is about 1.4.

CONFIDENTIAL

The optimum reflector and the minimum power ratio can be reduced in both the radial and axial directions by increasing the void fraction in the core, but the design under consideration is not sufficiently supercritical to permit taking advantage of this feature. The optimum reflector thickness and the minimum power ratio can be lowered in one dimension (and raised in the other) by use of an extreme (e.g. tall, thin) geometry. This technique proved to be of no particular value, since the gains in the one direction were small, and were more than offset by the losses in the other direction. For this reason, a core with a height-to-diameter ratio near 1 appeared to be the most attractive, since it, in a sense, minimized the power flattening problem in both directions simultaneously.

Other methods of power flattening include modifications in the amount of void and moderator in the core. These methods have not been explored. The power flattening beyond that produced by the 10-cm reflector has been accomplished by reducing the amount of U-235 in the unit cell. This can be done in two ways: 1) Use of low enrichment uranium (in  $\text{Mo}^{40}\text{v}/\text{oUO}_2$ ), provides a flat power distribution, but leads to a subcritical system; and 2) use of low- $\text{UO}_2$ -volume-fraction material (with fully enriched uranium) leads to a flat power distribution and a critical system, but these fuel materials are so different from the standard composition that their behavior under irradiation is unknown.

To partially compensate for the problems introduced by the use of low-volume-fraction fuel material, the lowest volume-fraction material has been replaced by low-enrichment material in the reactor design. The power cannot be flattened by using a few, widely spaced volume fractions or enrichments. The power can be flattened completely only by assuming that volume fractions and enrichments in adjacent cells may vary by an arbitrarily small amount. In general, the power ratio will deviate from 1 by about twice the minimum percentage increment in the volume fractions and enrichments. The factor of two is due to combining the axial and radial power distributions.

196  
CONFIDENTIAL

~~CONFIDENTIAL~~

SECRET

The power ratio in the core is a function of time, and the power distribution varies during the life of the reactor, due to two principal effects, burnout and control.

In Fig. 9.2 it is assumed that the power is flat at the beginning of life. At the end of life (5000 hours) the burnout causes the power ratio to increase to 1.05. At the beginning of life, the control poison is rotated inward toward the core. At the end of life it is removed, and a power peak develops in cells nearest the reflector. The power ratio at the end of life, due to the total of both effects is 1.18.

The proper approach is to design for a flat power distribution at the middle of life, and have a power ratio of 1.09 at both the beginning and the end of life.

#### Detailed Design of the Reactor

The reactor which most nearly meets the requirements of the various ground rules consists of 649 fuel elements arranged in a hexagonal lattice, with 15 cells per element. (Here, it is assumed that the heat pipes, provided for by the void fraction in the moderator, lie at the centers of half of the triangles formed by three adjacent elements; this design is the one most closely approached by the mathematical model. The alternative design, in which the fuel elements and heat pipes are all on the hexagonal lattice - every third lattice point being occupied by a heat pipe - would be calculated using the same model, but the approximation would be less close.) The  $\text{UO}_2$  volume fractions range from 26% to 49%, and the uranium enrichments from 51% to 69%. There are a total of 9735 cells producing 2.638 MW(e). The slight excess over the nominal amount of 2.6 MW(e) is due to requirements for integral numbers of cells and symmetry about the core axis. The core height is 97.5 cm and the diameter is 98.1 cm. Figure 9.3 shows the enrichments and volume fractions in the unit cells in the upper right hand quadrant of the core. The weights of reactor components are:

~~CONFIDENTIAL~~  
03713

Core	1917 kg
Reflector	1013 kg
Total	2930 kg
U-235	147 kg

The specific mass is 1.11 kg/kW(e).

The damage flux over 5000 hours is  $2.7 \times 10^{21}$  neutron-Mev/cm<sup>2</sup>. This value is slightly above the lower estimates of the experimental maximum, and well within the values based on higher estimates.

The power ratio, exclusive of the control effects, is 1.06. It is probable that by carrying the calculations through one or two more iterations this could be reduced somewhat. The addition of 9% for control and burnout leads to a total maximum power ratio of 1.15.

The problem of controlling the reactor has been studied only superficially in order to insure that the conditions required to design a control system do indeed exist. The short-range kinetic aspects have not been investigated. The long-range reactivity requirements for control are estimated to be:

Burnout	-1.8%
Temperature change between cold and hot critical:	-0.3%
Fission products (exclusive of Xe <sup>135</sup> , which is to be vented):	-0.2%
Total:	-2.3%

The reactivity worth of the radial reflector is 13.4\$, indicating that there is indeed sufficient control available in the reflector.

#### General Problems

Even the most precise calculations, in the absence of a nearby experiment to which the results can be normalized, can determine the  $k_{eff}$  of the system to within only 2% or 3%; and it is necessary to determine what changes should be made if the reactor turns out to be either slightly overcritical or slightly undercritical.

198  
03713  
~~CONFIDENTIAL~~  
APPROVED FOR PUBLIC RELEASE

~~CONFIDENTIAL~~

SECRET

In the case of overcriticality, the preferred solution would be to replace as many as possible of the unit cells containing low-volume-fraction fuel by cells containing low-enrichment fuel, thus further reducing the material problems associated with low-volume-fraction material.

In the case of undercriticality, the preferred solution would be to raise the power slightly by putting another ring of fuel elements around the core. Alternative solutions, which would raise the specific mass appreciably, would be the addition of moderator or an increase in reflector thickness.

Even if one or more of these modifications must be introduced, it is believed that any reactor based on this conceptual design would differ only slightly from the design presented here.

#### References

1. Bengt Carlson, "Numerical Solution of Transient and Steady State Neutron Transport Problems," Los Alamos Scientific Laboratory Report LA-2260 (1959).
2. C. E. Lee, "The Discrete Sn Approximation to Transport Theory," Los Alamos Scientific Laboratory Report LA-2595 (1962).
3. L. D. Connolly, "Los Alamos Group-Averaged Cross Sections," Los Alamos Scientific Laboratory Report LAMS-2941 (1963).

031713

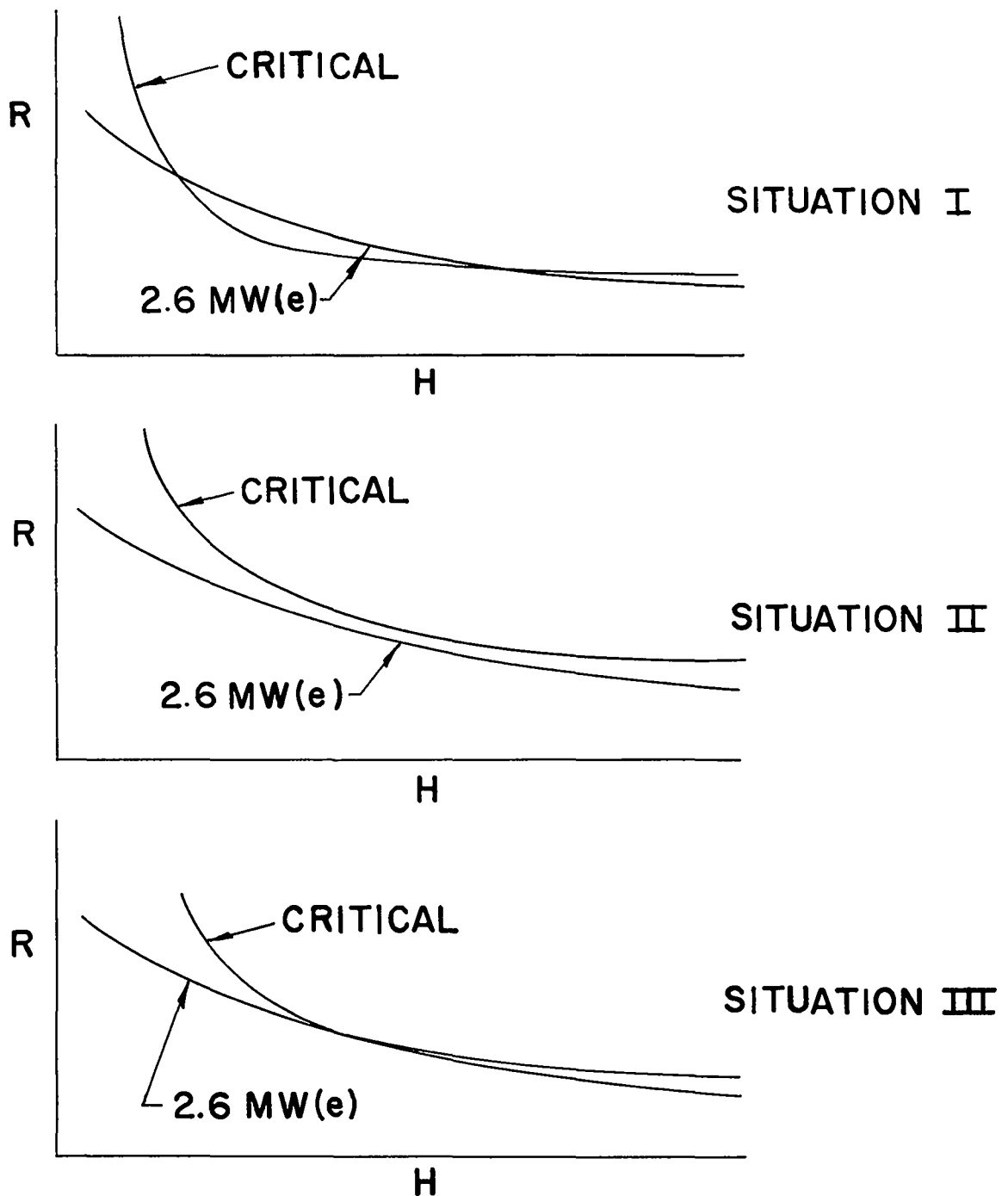


Fig. 9.1 Radius versus height of 2.6 MW(e) and critical cores.

031713

200

SECRET

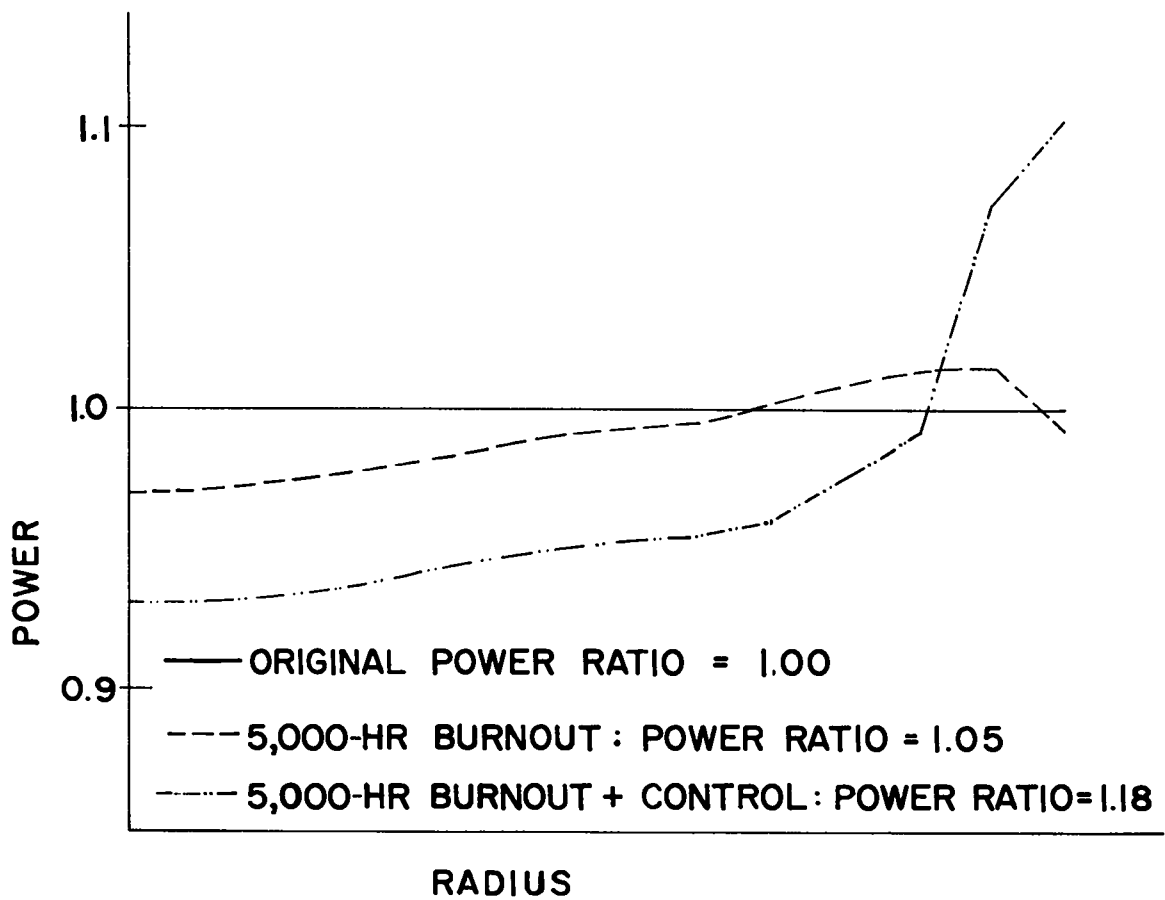


Fig. 9.2. Radial power distributions.



CONFIDENTIAL

03713

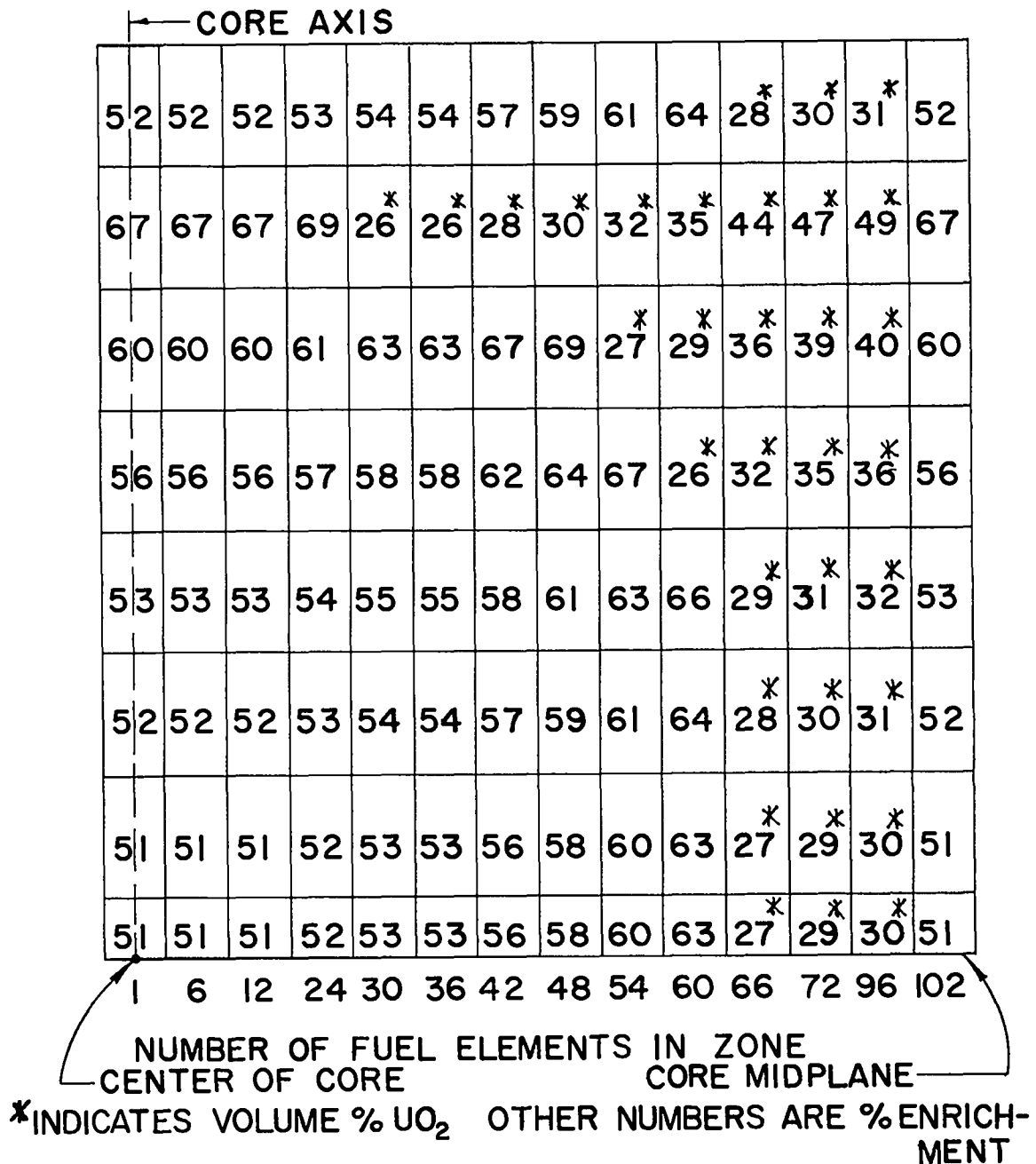



Fig. 9.3. Fuel loading zones in the core.

  
SECRET

## 10. Integrated System

Albert W. Blackstock

In this system study, the modular concept is used; i.e., the system consists of a number of modules assembled together, each containing a thruster, a reactor and a radiator. These modules are connected to a single crew compartment.

Figure 10.1 represents a module without the radiator, since it is so much larger than the other components.

The arc thruster is about 1.7 feet in diameter as well as in length. It radiates the unconverted electrical power and does not contribute to the heat radiated by the main radiator.

The bus bars are made of copper and are 1.2 inches thick, 4.3 inches wide and about 15 feet long. They radiate the heat produced in them both by joule- and gamma-heating. Some weight saving would result from using liquid Na as the bus material, but this may be offset by the weight of plumbing, valves, pumps, etc., that would be necessary. Structural members are also indicated in the figure.

The LiH shield is about 5 cm thick and weighs about 100 kg. The drive rods for the control drums pass through the shield to the drive motors, which are indicated. There may be 35 or 40 control drums in the reflector. The 5 cm of Li is that necessary for an L of 100. Since an average L of 140 was arrived at in Chapter 9, somewhat less shielding would be required. Both reactor and thruster instrumentation and controls are protected by this shield. The bus bars go through the shield to the current header (not shown) which collects the current from the 649 fuel elements. The reactor dimensions, including the shield and 10-cm radial


~~CONFIDENTIAL~~

03713

and end reflectors, are 3.9 feet in diameter by 4 feet in height. A pressure shell, not indicated, surrounds the reactor and is vented to permit fission gases to escape. A thermionic conversion efficiency of 13% was chosen in Chapter 7 as a reasonable figure, which yields 2.6 MW(e) from the 20 MW(th) reactor.

Figure 10.2 shows four modules in a Saturn V 300-mile orbital payload. This figure will serve to illustrate the radiators, each of which is shown joined to a reactor/thruster unit. Each radiator is cylindrical in shape with a frustum of a cone joining the reactor to the cylinder. No folding of the radiators is required. The operating temperature of the radiator is taken to be 1000°K and the emissivity, 0.85. This emissivity can be achieved by a Ni carburizing process which is a standard practice for radiation-cooled anodes of power tubes which operate for about 10,000 hours at temperatures of about 800°C. For this temperature and emissivity, 4.8 watts/cm<sup>2</sup> can be radiated. For the 13% reactor conversion efficiency mentioned, 17.4 MW must be radiated from a 20-MW reactor. This requires 361 square meters or 3880 square feet of area. A 45° half-angle was chosen for the frustum, and the diameter of the cylinder was taken equal to that of the maximum payload diameter for the Saturn V 300-mile orbital vehicle, namely 33 feet. For the required radiating area, the height of the frustum is 14.5 feet and that of the cylinder 26.0 feet, for a total radiator height of 40.5 feet. The outside surface area alone equals the required area. This point will be discussed further later on. These dimensions give an L/D of 1.23, compared to an optimum value of 1 given in Chapter 2.

The heat flux through the end of the reactor is approximately 1500 watts/cm<sup>2</sup>, considerably greater than the 200 watts/cm<sup>2</sup> maximum demonstrated thus far for a heat pipe. To accommodate this heat flux, a single large heat pipe can be used in the transition portion of the radiator. The thickness of the radiator at its point of maximum thickness is determined by calculating the point at which enough heat has been radiated to reduce the heat flux in the radiator to 200 watts/cm<sup>2</sup>. This

  
SECRET

thickness is 3.4 feet. As pointed out in Chapter 2, the thickness of the remainder of the radiator at any point is proportional to the area beyond that point. It is 2.4 feet at the intersection of the frustum and cylinder and tapers down to twice the armor thickness, or about 8 mils, at the end.

For a 456-day mission calculated (Chapter 12), the same time as the STL mission, the weight of a module - excluding structure but including the reactor, reflector, actuator shield, controls, radiator, bus bars, thruster, propellant and tank, and reactor pressure shell - is about 36,000 pounds. Thus, four modules would weigh about 144,000 pounds, which leaves about 96,000 pounds of the Saturn V 240,000-pound, 300-mile orbital capability for other payload and structure. The volume required for the Li propellant at 20°C for four modules in this mission is about 2,800 cubic feet. The volume of the hollow space below the lowest module alone is 21,000 cubic feet, leaving a large volume for tanks, crew compartment, Mars lander, and other payload. In addition to restrictions on payload weight and envelope or volume, limitations on the center of gravity, the nose cone shape, and the load distribution on the booster structure must be considered.

For the reference mission mentioned, a power of 27.9 MW(e) is needed, which requires 11 of the 2.6 MW(e) modules. This would amount to three Saturn V orbital payloads. The initial mass of the ship in orbit is 720,000 pounds. One of the Saturns would, of course, carry only three modules, leaving another 36,000 pounds and a large additional volume for other payload.

Figure 10.3 represents one possible configuration for the 11 modules and a plausible one, it is hoped. The modules are arranged on a circle with a distance between radiators equal to the diameter of a radiator, 33 feet. This results in the reactors being on a circle with a diameter of 234 feet and the diameter of the outer circle is 267 feet. The center circle represents the propellant tank and crew compartment, which are located considerably above the modules. The "spokes" represent structural members.

  
SECRET

031710

The support ring and short members connecting the modules to it permit a module to be jettisoned should its reactor or thruster fail. Perhaps an even number of modules would be better in this respect, and the mission could be redetermined to permit an even number to be used. However, with 11 modules, a jettisoned module could probably be compensated for if the thrusters were properly mounted on gimbals.

Figure 10.4 shows a side or sectional view of the assembly folded so that it is all in one plane, but omitting any modules in between the two shown. The 234-foot diameter is shown, and the distance from any reactor to the crew compartment is 200 feet. As mentioned before, the required radiating area was obtained using only the outside surface of the radiators. However, the radiators will "see" each other to some extent, but this would be compensated for by radiation from the end.

It is desired to use the propellant as reactor shielding during as much of the trip as possible. Individual tanks for each module were considered, but it is difficult to arrange them and the other components so that the remaining propellant always shields the crew. So, a single propellant tank is shown here, which actually may be a cluster of tanks. It is assumed to be a 2% tank. The total propellant mass for the reference mission is 258,000 pounds, which, for Li at 20°C, would occupy a volume of 7,740 cubic feet or 219 cubic meters. For this volume the tank shown, a frustum of a cone which just shields the crew compartments, is about 8 feet high and has a large diameter of 41 feet and a small diameter of 30 feet.

The lower, main crew compartment as shown is a cylinder, 17.5 feet in diameter by 9 feet high, with a volume of about 2150 cubic feet. The water tank provides shielding for the crew during the last few days of the trip, when the propellant tank is becoming empty. During this time the crew is in the upper conical capsule, of 450 cubic feet.<sup>1</sup> The water tank is 3.5 feet deep and contains about 41,000 pounds of water. In Chapter 11 the crew dose during the last part of the trip and shielding arrangements against solar flare and Van Allen belt radiation are

031710  
APPROVED FOR PUBLIC RELEASE

~~CONFIDENTIAL~~

SECRET

discussed. In the configuration shown, insufficient shielding is provided for slow traversal of the Van Allen belts. Another booster, a three-stage Saturn V which can deliver 90,000 pounds to escape, will rendezvous with the ship in high earth orbit, beyond the most intense part of the belts and deliver the flight crew. Still another smaller booster may be required to rendezvous the assembly crew with the three low-orbital Saturn V's, if they cannot go in one of these. But perhaps the assembly crew could go in the one containing only three modules.

In connection with Van Allen belt shielding, the propellant mass in excess of that needed for escape is 240,000 pounds. If this amount of Li is put in a spherical shell  $100 \text{ g/cm}^2$  thick, which is that estimated to be necessary for Van Allen shielding by Moeckel,<sup>2</sup> the volume of the cavity inside is 1110 cubic feet, which is about 90% of the volume of the 1270-cubic feet STL crew capsule, and 2.5 times the 450 cubic feet mentioned previously.

A variant mission is one in which a freighter is sent ahead to Mars, and the manned ship makes a rendezvous with it in a high Mars orbit. Several such missions have been calculated. For this mission eight modules are required for the 420,000 pound manned ship and three for the 240,000 pound freighter. A possible configuration for the return ship, made up of the two combined, is to arrange the eight modules in a circle, 172 feet in diameter, for a spacing of 33 feet between radiators, with a second ring or structure below the support ring for the eight. The three freighter modules are on a 64 foot diameter circle with a 33 foot spacing between them. They dock and couple with the lower support structure attached to the eight modules. They must be lower than the ring of eight modules to achieve a 200 foot separation between the reactors and crew compartment, since they are on a smaller circle. For these dimensions, the arc jets from the upper eight thrusters will not intercept any part of the three lower modules, thereby losing part of the thrust, if the half-angle of the arc cone is less than about  $73^\circ$ .

~~CONFIDENTIAL~~

031710

Another possible arrangement is to arrange the eight modules of the manned ship on a circle large enough for ten, with two vacancies opposite one another. The three freighter modules are arranged side by side in line, with the length of the assembly equal to the diameter of the main ship circle. On rendezvousing, the two outer modules slip into the vacant spaces and the center one is in the center of the circle. All the modules are then at the same height. Extra shielding would be needed for the reactor in the center.

A variation of the configuration shown in Fig. 10.4 is to put the crew compartments and lithium tank below the modules. In this arrangement, the control rod actuator shields, on the lower ends of the reactors, will also provide some personnel shielding from the reactors. With the 11 modules arranged on a 234-foot diameter circle and a 200-foot separation between reactors and crew compartment, the arc jets from the thrusters will intercept no part of the propellant tank or crew compartments if the half-angle of the arc cone is less than  $35^\circ$ .

It has also been suggested that the crew compartment could be towed behind the modules on a long cable. In order to reduce the dose rate from the 11 reactors to  $1/3$  to  $2/3$  Rad per day (as discussed in Chapter 11) with no shielding other than the reactor control rod actuator shields and the solar flare shielding around the crew, a separation of about 42 miles between reactors and crew is necessary.

Now a comparison will be made with STL vehicle.<sup>3</sup> The length of the STL vehicle is 431 feet and the maximum diameter is 99 feet. The maximum dimension of the LASL vehicle is the 267-foot outside diameter. It is interesting to note that the area of the lateral surfaces only of the four STL propellant tanks is equal to the radiating area of 10.5 LASL modules. The total initial weight in orbit of the STL vehicle is 1,969,575 pounds which is more than eight Saturn V 300-mile orbital payloads. The LASL reference mission vehicle initial weight in orbit is 720,000 pounds. The volume occupied by the 11 modules - considering the radiators to be solid instead of hollow inside - plus the two crew

~~CONFIDENTIAL~~

CONFIDENTIAL

compartments, the water shield, and the lithium tank is about 2% less than that of the STL vehicle.

In conclusion, one of the major advantages of the modular concept is the versatility it permits both in the number and in the configuration of the modules for a given mission. A much more detailed study is required to determine the optimum number and arrangement of modules for any specific mission.

#### References

1. Irving M. Karp, "Shielding Requirements for Manned Mars Mission," in NASA TM X-50118, pp. 27-35 (1963).
2. W. E. Moeckel, Exploration of Mars, V. 15 of Advances in the Astronautical Sciences, (American Astronautical Society, New York, 1963), pp. 79-103.
3. TRW Space Technology Laboratories, Final Report Briefing, No. 8423-6018-RL000 (1965).

~~CONFIDENTIAL~~



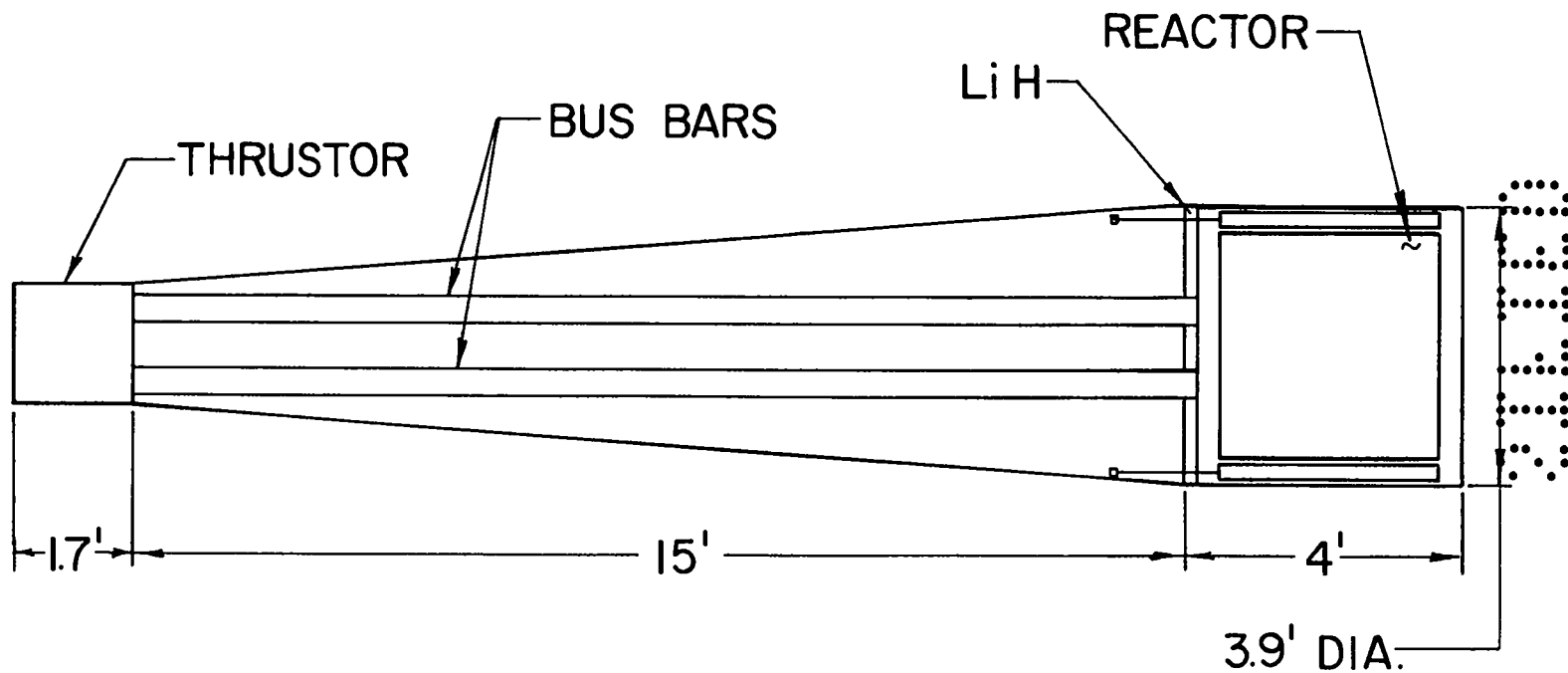


Fig. 10.1 Module without radiator.

FORM 35-11111

1

SECRET

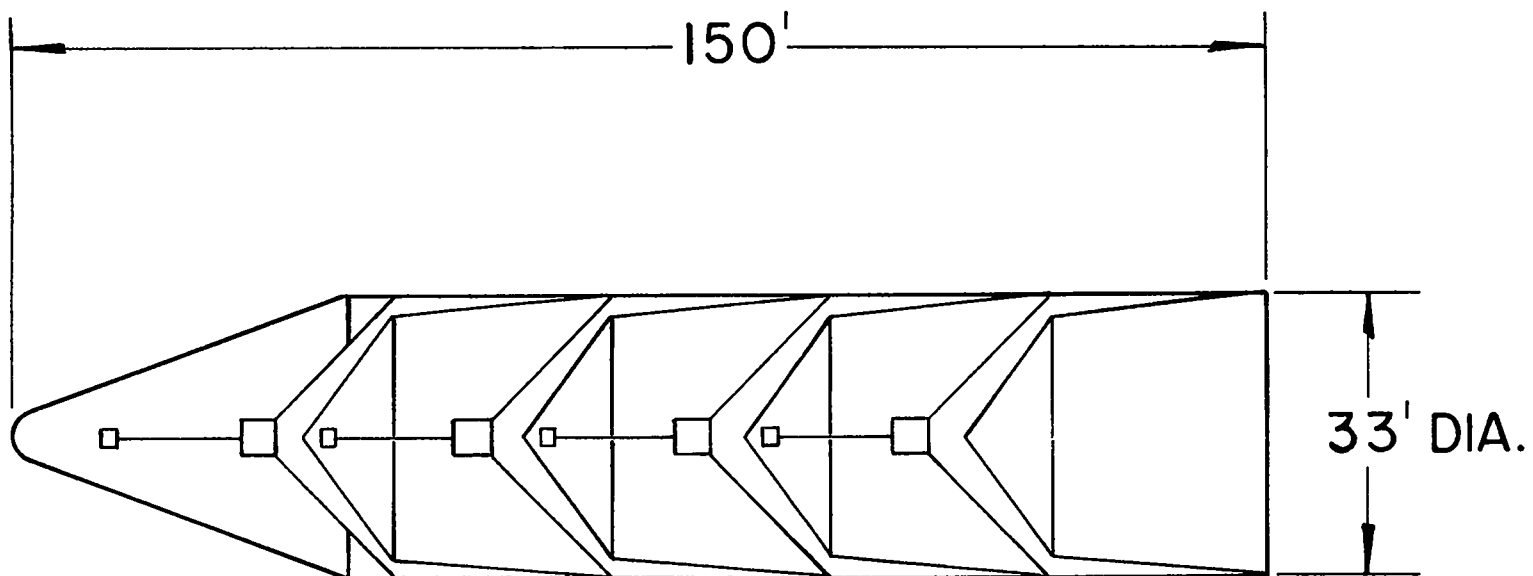


Fig. 10.2 Four modules in Saturn V.

211

~~CONFIDENTIAL~~  
001700

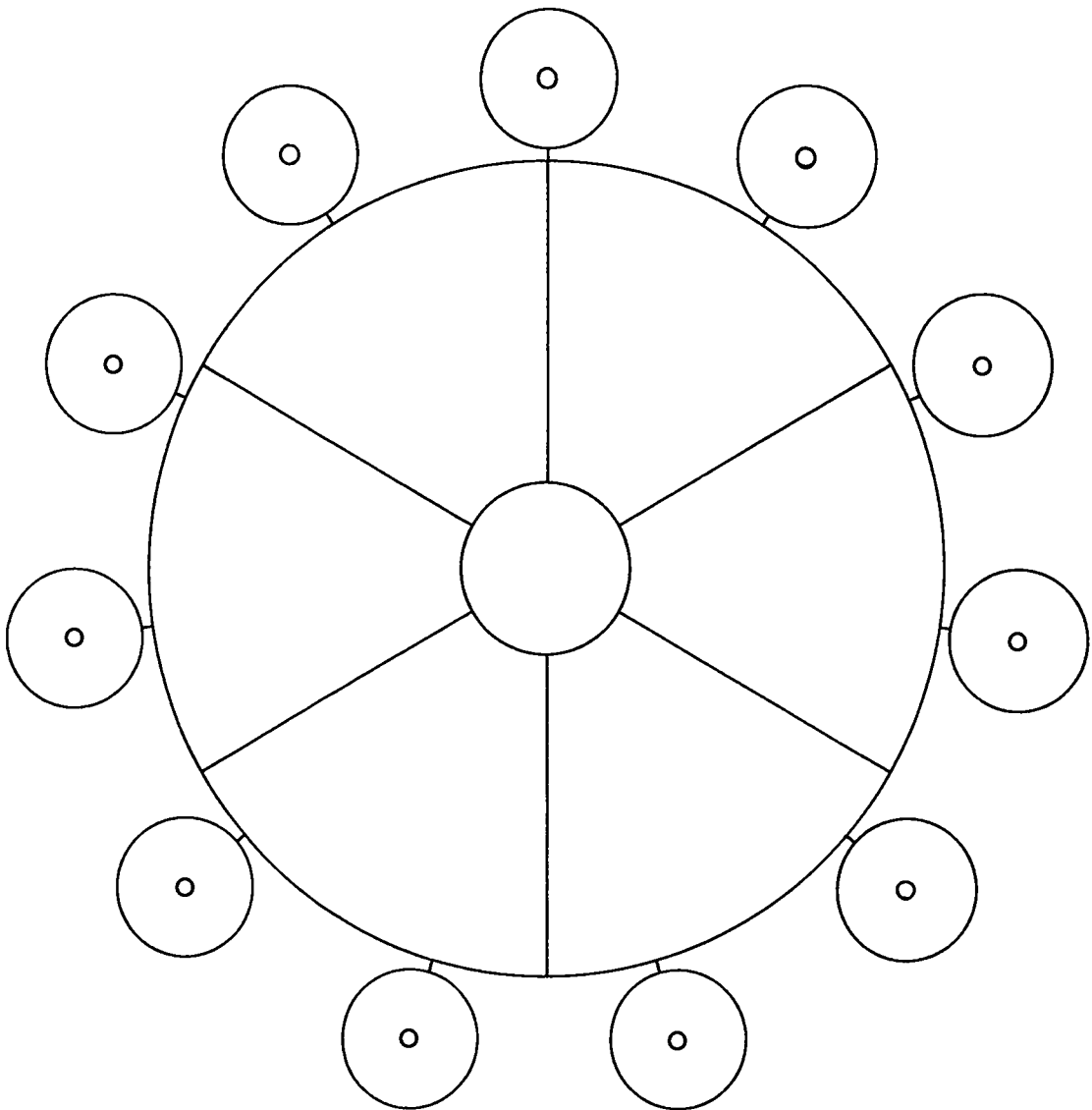


Fig. 10.3 System configuration - top view.

~~CONFIDENTIAL~~  
001700

SECRET

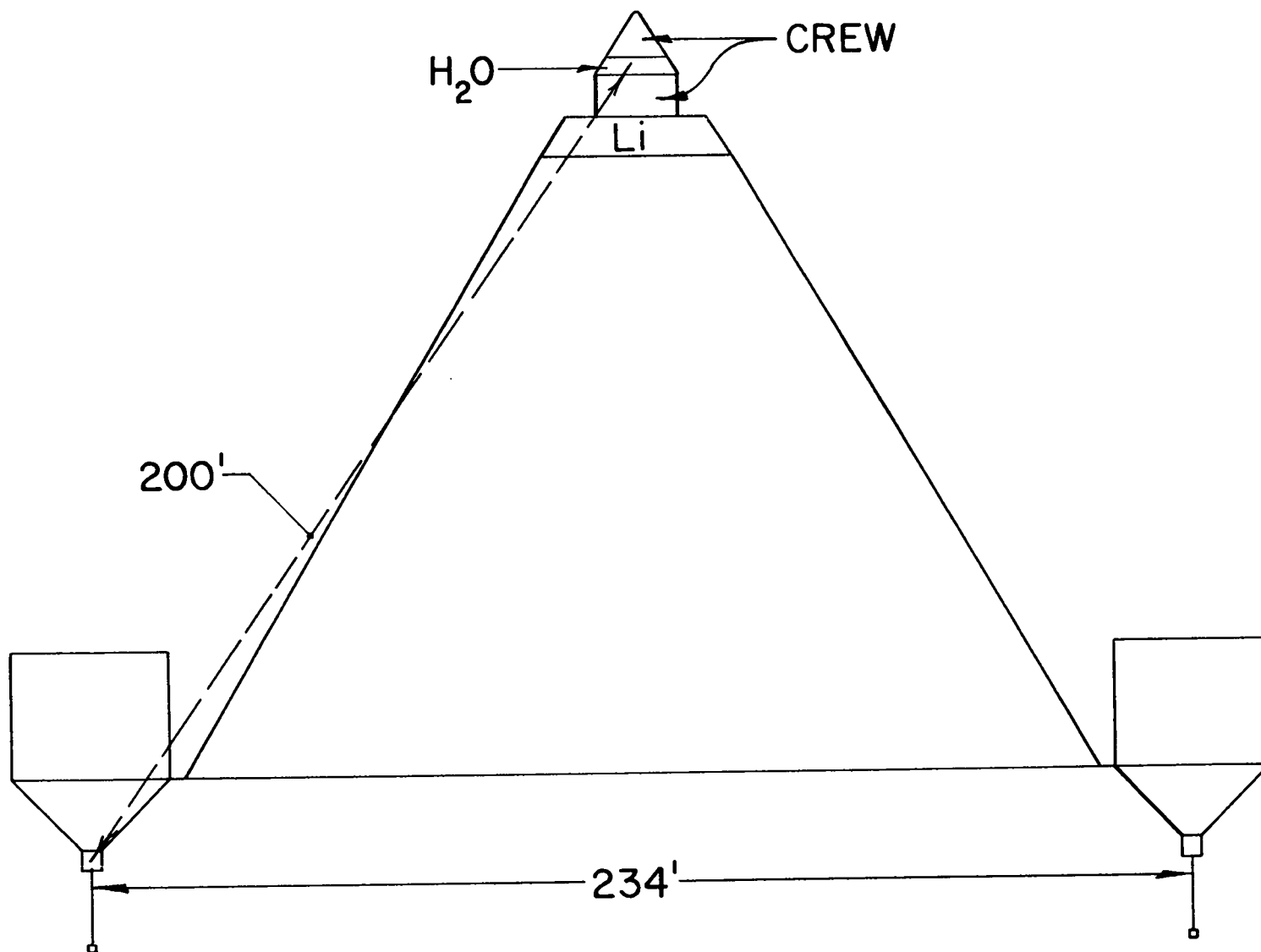


Fig. 10.4 System configuration - side view.

213

CONFIDENTIAL

~~CONFIDENTIAL~~  
03713

## 11. Shielding

Samuel Robert Skaggs

Introduction

Shielding for the manned Mars mission system discussed in these lectures falls into two categories. The first of these is the shielding of the instrumentation and equipment necessary for the operation of the reactor, and the second is the shielding of the spacecraft personnel.

There are four sources of radiation which must be considered in the shielding problem: 1) Van Allen belt radiation, 2) solar cosmic rays, 3) galactic cosmic rays, and 4) radiation from the nuclear power plant. This report illustrates the typical shielding requirements for both equipment and personnel in the radiation flux from these sources.

Equipment Shielding

The proper shielding of the equipment that necessarily must operate near the reactor is of primary concern. These components must operate reliably in a radiation environment for a period of approximately 5000 hours at full reactor power. Included in these components are the various temperature, current, voltage, and pressure sensors; and the control rod actuators. The current and voltage probes appear to present no problem in the radiation field. Recent advances in the development of radiation-resistant integrated circuits have improved the reliability of the electronic components.<sup>1</sup>

Current radiation levels used in the NERVA vehicle tests are the conservative values of  $10^7$  Rad total gamma dose plus the neutron dose.

214

03713

~~CONFIDENTIAL~~

SECRET

Recently, control actuators passed a 90-day exposure in a radiation environment<sup>2,3</sup> for a total gamma dose of  $5 \times 10^9$  Rad and an integrated fast neutron ( $> 1$  Mev) flux of  $2.3 \times 10^{18}$  nvt. Future tests should extend this fast neutron dose to  $10^{19}$  nvt, and it is this value which is used in this report.<sup>4</sup>

The relatively low integrated gamma dose values result primarily from the type of insulation used on the actuators. The use of organic materials such as the polyimides,<sup>5</sup> and ceramics has extended the tolerance limits by 3 to 5 orders of magnitude from the NERVA  $10^7$  Rad value. Ceramic insulation offers the hope of extending the limits as high as  $10^{13}$  Rad. For the purpose of this report, a value of  $10^{12}$  gamma Rad is used as the upper limit.

Critical components near the reactor must be shielded from the fast neutron flux. In general, if enough shielding material is used to reduce the neutron flux to acceptable levels, the gamma flux will fall to an acceptable level. Two schemes exist for the shielding of the actuators. The first scheme is to recess the actuators deep enough in the propellant tank so that the propellant provides the shielding. The second is to build a solid shield specifically for reducing the fluxes to tolerable levels. In this latter scheme, materials such as Be, LiH, and Li have been considered as shielding materials.

In order to arrive at a specific shield weight, the radiations from the reactor were obtained from calculations based on a particular ratio of Be to uranium, and an attenuation factor for the fast neutrons was calculated for various materials. This attenuation factor was then used to determine the shield thickness required to bring the neutron flux down to acceptable levels. From the required shield thickness, the gamma ray attenuation was determined. The attenuation factor required for a tolerable gamma dose was compared with this figure. In most cases, no additional gamma shielding was required. However, where additional shielding was required, an appropriate thickness, always less than 2 cm, of tungsten was inserted to reduce the dose to acceptable levels. A

~~CONFIDENTIAL~~  
03700

right circular cylindrical geometry with the same diameter as the reactor was used to calculate the shield weights. The total shield weight was divided by the reactor power to arrive at a convenient specific weight which is easily included in the  $\alpha$  for the system. In Table 11.1, the specific weights are shown for several moderator-to-fuel ratios ( $L = 0$ , 100, and 200) and the named shielding materials.

TABLE 11.1  
SPECIFIC SHIELD WEIGHT

Reactor Power	Shield Material	Shield weights, kg/kW(e)		
		$L = 0$	$L = 100$	$L = 200$
2 MW(e)	LiH	0.011	0.035	0.016
	Be	0.025	0.087	0.130
	Li	0.011	0.043	0.078
20 MW(e)	LiH	0.009	0.028	0.017
	Be	0.021	0.070	0.056
	Li	0.009	0.035	0.023

From the table, it is evident that the equipment shield will not contribute more than 0.2 kg/kW(j) to the system weight.

#### Personnel Shielding

The intent of this section is to review, within existing knowledge, what radiation levels a man may encounter for a space mission of some 360 to 400 days. Although only the reactor radiation field was of concern in the equipment shielding, the other three sources of radiation must also be considered in the personnel shielding.

Van Allen belt fluxes are as high as  $10^5$  charged particles/cm<sup>2</sup>-sec and consist of both electrons and protons.<sup>6</sup> In the mission under consideration, the space crew is transported through the radiation zone in

~~CONFIDENTIAL~~  
 01100

as short a time as possible, holding the total exposure for two trips through the belts to 10 - 15 Rad.

Giant solar flares present the major non-reactor hazard to manned missions in space.<sup>7</sup> Doses from these flares may range from 25 to 125 Rad per flare. The probability of occurrence of a major solar flare is  $0.14^{+100\%}_{-90\%}$  per week. Detection methods allow approximately twenty minutes to put into effect protective measures before the arrival of the highest energy particles. This is adequate time to rotate the space craft so that the largest mass is in the flare flux path or so that the crew can climb into an adequately shielded closet in the crew compartment.

Galactic cosmic rays are isotropically distributed in space, with an intensity of 2 to 4 particles/cm<sup>2</sup>-sec. Their energies are extremely high, on the order of  $10^{19}$  to  $10^{20}$  eV for the more energetic particles.<sup>8</sup> The dose rates from these cosmic rays is about 0.66 Rad/week.

Present acceptable industrial radiation limits are not practical for most long-term space missions. NASA has established what it considers acceptable radiation limits for space travel which differ from the present industrial limits (see Table 11.2). Briefly, if no short-term dose is greater than 50 to 80 Rad and if there is adequate time to recover from these large doses, an acceptable total trip average dose rate is 1/3 to 2/3 Rad/day. Based on this acceptable dose rate and the dose rates from the other sources mentioned earlier, the contribution from the various sources may be summarized as follows:

<u>Source</u>	<u>Percent of Total Dose</u>
Van Allen belt radiation	5%
Galactic cosmic rays	15%
Solar flare radiation	30%
Reactor radiation	50%

The reactor shielding must, therefore, be sufficient to reduce the fast neutron and gamma dose to approximately half of the total acceptable dose. The thermal neutron flux is adequately attenuated when the proper amount of fast neutron and gamma shield are provided.

01100 217



TABLE 11.2

## MISSION-DOSE-EFFECT TABLE

	<u>1 Hour</u>	<u>1 Day</u>	<u>7 Days</u>	<u>15 Days</u>	<u>30 Days</u>	<u>300 Days</u>
AEC permissible dose	0.0025	0.02	0.1	0.2	0.4	4.0
Dose for one exposure per year	4.0	4.0	4.0	4.0	4.0	4.0
One-time emergency dose	25.0	25.0	25.0	25.0	25.0	25.0
Apollo permissible dose	-	-	54	54	54	54
NASA one-time emergency dose	200	200	200	200	200	200
5-year permissible dose	271	271	271	271	271	271
Maximum dose for no statistically demon- strable effects	25-50	50-100	100-200	150-300	200-300	250-400*
Chronic effects dose - life shortening and possible acute effects	50-100	100-200	200-300	300-400	300-500	300-500*

---

Table of personnel dose - tissue Rads versus mission length.

\*Projected values - no statistical evidence available.

SECRET

A reactor with a dilution ratio of  $L = 100$  with its associated fluxes of  $10^{19}$  nvt and  $10^{12}$  gamma Rad penetrating the equipment shield is chosen for the calculation of the personnel shield. The dose to the crew is primarily from the gamma radiation. The gamma flux is reduced by two means: 1) geometry - allowing about 200 feet between reactor and crew compartment (see Fig. 10.4) and, 2) a composite shield of fuel and other material.

The plasma thruster uses lithium as a propellant. Although lithium is not a very good moderator, there is enough on the spacecraft to be used as shielding. To be sure of a safe return of the crew, however, provisions have to be made for the Mars to earth portion of the trip when most of the lithium will be used up. A composite shield of fuel and LiH, Be, or  $H_2O$  may be used for this purpose. Water is used as the shielding in this study.

Figure 11.1 shows the crew dose as a function of fuel remaining in the tank. The STL NERVA systems study<sup>9</sup> used a 68,000 pound capsule plus 23,000 pounds of shielding. For this study, we use a 51,000 pound water shield as shown in Fig. 11.2. At the end of the Mars to earth transfer about 41,000 pounds (3.5 feet) of additional water shielding is required to adequately shield the crew. These numbers are based on the crew accumulating a total of 80 Rad on the return trip.

Figure 11.2 shows how the water shield can be utilized to its maximum effectiveness. During reactor operation in periods of no flare activity, the water is maintained at a maximum thickness between the reactor and the crew. During periods of maximum solar activity the command module is "immersed". The composite shield mentioned previously is located between the crew compartment and the fuel tank (see Fig. 10.4).

It should be emphasized that this is by no means the final shield configuration. The final shield will be a balance of the equipment location, shield material, and geometry. This study is meant to indicate the magnitude of the shielding requirements.

SECRET

031713

References

1. Missiles and Rockets, Vol. XVI, Number 12, March 22, 1965, pp. 9 and 23. News item from Norden.
2. Irwin Rowe, "Snap Reactor Control Drum Actuators," Paper prepared for the 11th Annual Nuclear Science Symposium, October 28-30, 1964, Philadelphia, Pa.
3. M. Warren, "Irradiation of Snap 10A Control Drum Drive Actuators and Position Sensors," North American Aviation Corp. report NAA-SR-10717, May 15, 1965.
4. Private communication, April 15, 1965:  $7.7 \times 10^{18}$  nvt for 90 days full power operation at 1000°F.
5. D. H. Buckley and R. L. Johnson, "Friction, Wear, and Decomposition Mechanisms for Various Polymer Compositions in Vacuum to  $10^{-9}$  Torr," NASA Lewis Research Center, Cleveland, Ohio, NASA-TN-D2073.
6. W. E. Moeckel, "Electric Propulsion Systems for Mars Missions," in Advances in the Astronautical Sciences, 15, Exploration of Mars, pp. 79-103, American Astronautical Society, 1963.
7. D. L. Dye and M. Wilkinson, "Radiation Hazards in Space," Science, 147, pp. 19-25, Jan. 1, 1965.
8. Proceedings of the Symposium on the Protection Against Radiation Hazards in Space, Gatlinburg, Tenn., November 5-7, 1963, TID-7652, papers: A-1,2,4,6,7; B-3,4,6; C-1,2,3,4,6,7; D-2,5,7; E-1,5,6,8,9; F-1,2,3,4,5.
9. "Mission-Oriented Advanced Nuclear System Parameter Study," Final Report Briefing Charts, NAS-8-5371, February 1965, pp. 39 and 203.

220  
031713

~~CONFIDENTIAL~~  
CONFIDENTIAL

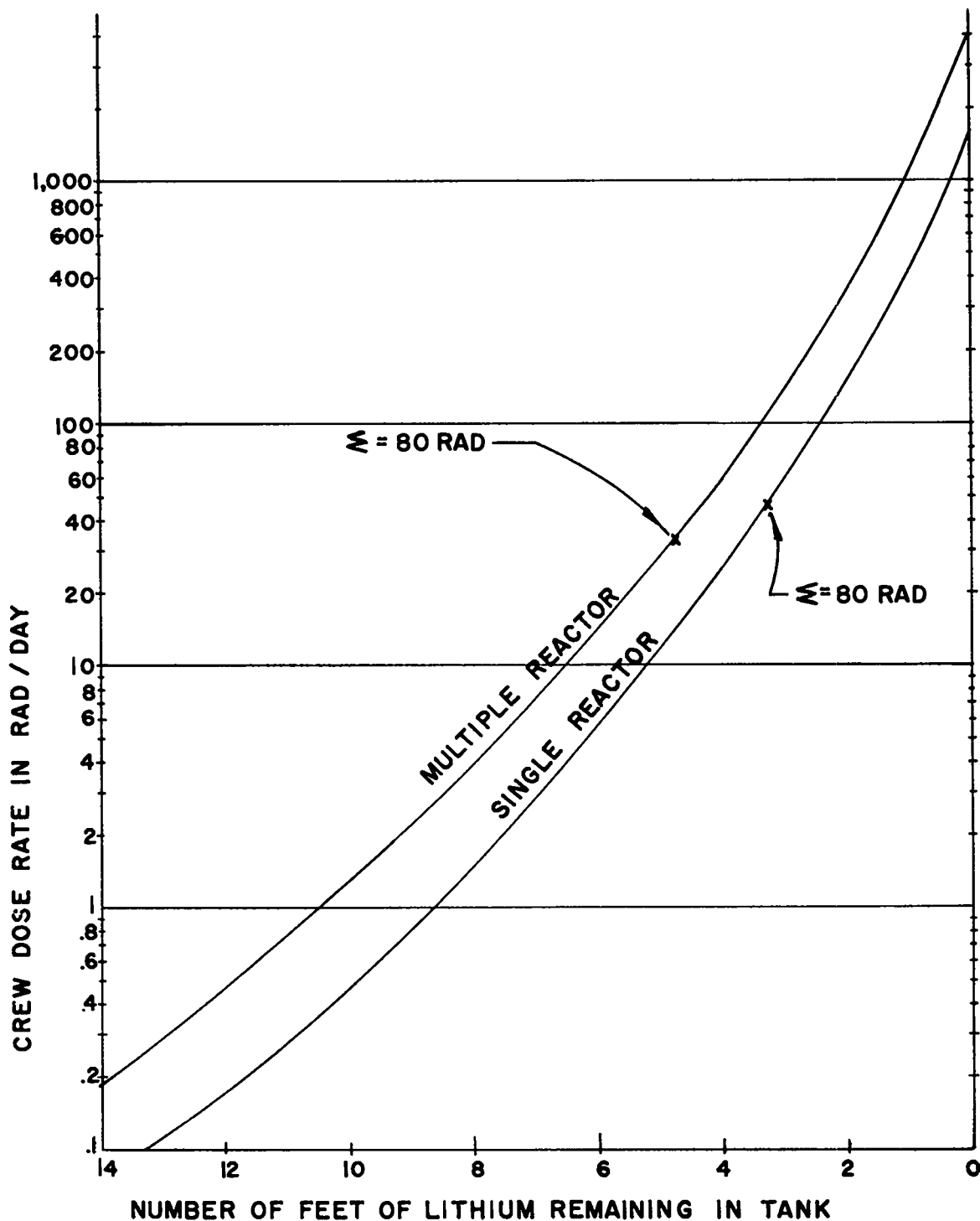


Fig. 11.1 Crew dose vs fuel in tank.

221  
CONFIDENTIAL

~~CONFIDENTIAL~~  
CONFIDENTIAL

~~CONFIDENTIAL~~  
03113

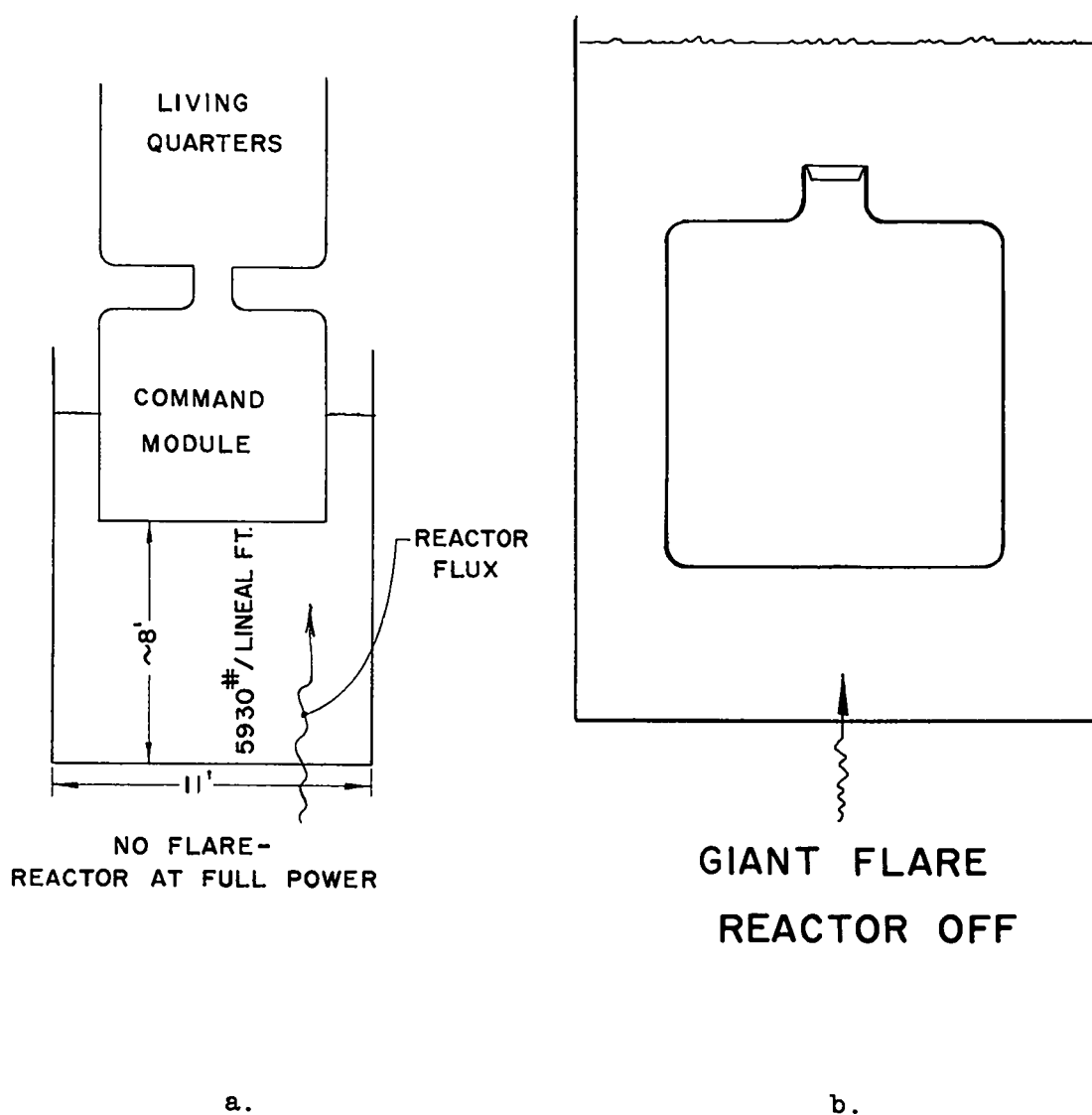


Fig. 11.2 Alternate immersion schemes.

222  
03113

~~CONFIDENTIAL~~

~~CONFIDENTIAL~~  
 21300

## 12. Manned Mars Mission Studies and Propulsion Time Requirements

Ernest W. Salmi and C. Dexter Sutherland

In the standard type of mission calculation performed on Rover reactors and also chemical rockets, one starts with the equation

$$m \frac{dv}{dt} = -c \frac{dm}{dt} \quad (12.1)$$

where  $m$  is the instantaneous mass of the missile, and  $dm/dt$  is the mass of propellant being ejected per unit time with a velocity  $c$ . One can integrate this equation as

$$\int_0^t \frac{1}{m} \frac{dm}{dt} dt = \ln \frac{m}{m_0} = - \int_0^t \frac{1}{c} \frac{dv}{dt} dt$$

It  $c$  is constant, then the right-hand side is

$$\frac{1}{c} \int_0^t \frac{dv}{dt} dt = \frac{v-v_0}{c} = \frac{\Delta v}{c}$$

Then our equation becomes

$$m = m_0 e^{-\frac{\Delta v}{c}} \quad (12.2)$$

The value  $c$  is often written as  $g I_{sp}$ . There exist tables of values of the  $\Delta v$  required for various missions. For example, one can find the  $\Delta v$  required to go from a 300-mile earth orbit to escape, then another  $\Delta v$  for a transfer to a Mars orbit, etc. One can then make a collection of the  $\Delta v$  requirements for a given mission; and, knowing the  $I_{sp}$ , one can

21300  
 23

~~CONFIDENTIAL~~  
03713

calculate the mass ratios for various parts of a mission. Now in this calculation, the  $I_{sp}$  is the variable that depends on the type of propulsion assumed.

The situation in electric propulsion calculations is much different. In this case, the assumption is made that any desired  $I_{sp}$  can be obtained; however, the power is now the limiting factor. Therefore, in addition to equation (12.1) one also has the condition

$$P = - \frac{1}{2} \frac{dm}{dt} c^2 \quad (12.3)$$

Fortunately, (12.1) and (12.3) can be combined in the following way

$$\left( \frac{dv}{dt} \right)^2 = \left( \frac{c}{m} \frac{dm}{dt} \right)^2 = \frac{2P}{m^2} \frac{dm}{dt}$$

or

$$\int_0^t \frac{1}{m^2} \frac{dm}{dt} dt = \frac{1}{m} - \frac{1}{m_0} = \frac{1}{2} \int_0^t \frac{a^2}{P} dt$$

where

$$a = \frac{dv}{dt}$$

It is obvious that one wishes to minimize the right-hand integral so one would always pick the maximum power possible so that it becomes a constant. One can then rewrite this equation as

$$2P \left( \frac{1}{m} - \frac{1}{m_0} \right) = \int_0^t a^2 dt$$

So, given the integral and the power, one can again calculate the various masses. In this case, the  $I_{sp}$  does not enter the calculation. One needs only the power. There exist in the literature tables of this integral for various types of missions. For example, in Fig. 12.1,\* one has the

03713

~~CONFIDENTIAL~~

~~CONFIDENTIAL~~  
 01100

values of the  $\int a^2 dt$  required for escape from both Earth and Mars starting at a 300-km circular orbit plotted as a function of the time to escape.<sup>1</sup> Of course, the longer the time to escape, the lower the acceleration and the smaller values of the  $\int a^2 dt$  required.

There exist similar curves for transfer to the Mars orbit. It should be noted that in these calculations the power is assumed to be constant. The thrust is varied by varying the  $I_{sp}$ . This type of calculation in which one powers all the way is called the variable thrust calculation. This calculation gives one the minimum possible value of  $\int a^2 dt$  for a given mission. Of course, the power-all-the-way assumption results in long reactor operating times which are about 10,000 hours for the manned Mars mission. If one looks over a typical trajectory from Earth to Mars one finds that in the middle part of the trip, the  $I_{sp}$  has been increased to such a high value that the thrust is almost zero. Perhaps the power could be turned off during this period. Melbourne and Sauer<sup>2</sup> have made a comparison between the variable thrust calculation and the case of using a constant  $I_{sp}$  with varying propulsion time. This was done for various Earth-to-Mars transfers, with trip time varying from 40 to 350 days. Figure 12.2\* shows one of their examples of the  $\int a^2 dt$  as a function of trip time for the variable thrust calculation and the constant-thrust, or constant- $I_{sp}$ , varying propulsion time calculation. The  $I_{sp}$  has been assumed to be 5000 seconds. One finds that there is almost a constant 15% between the two calculations. It will be assumed that this 15% correction allows one to go from a variable thrust calculation to a constant  $I_{sp}$  calculation for all the missions discussed later in this lecture.

For the Earth-to-Mars transfer the values of  $\int a^2 dt$  are plotted in Fig. 12.3\* as a function of launch date for various trip times.<sup>1</sup> In these calculations the Earth and Mars orbits are assumed to be co-planar circular orbits. One sees from Fig. 12.3 that for any given trip time, there is an optimum launch date. One can also obtain similar curves for the return trip, and again they also have optimum launch dates.

01100 225



~~CONFIDENTIAL~~  
03113

Unfortunately, for short stay times at Mars, the optimum values do not coincide.

One can take the two sets of curves and assume a 40-day stop at Mars, then both sets of curves can be plotted as a function of launch date from Mars. This is shown in Fig. 12.4. Any vertical line is a possible mission with a 40-day stay at Mars. The solid line is the value of the outbound trip, and the dotted lines are for the return trip. One sees that these curves are symmetrical in time. For more realistic orbit-type calculations, the curves do not come out so exactly symmetrical in time; however, the important feature remains, in that one always has a difficult part and an easy part of the mission.

One is now in a position to calculate a round trip to Mars. Since weights needed for the trip are not the object of this series of lectures, the weights used in this study were taken from the STL study of NERVA.<sup>3</sup> In this study one starts with 8 Saturn V loads of 1,970,000 lb in a 300-mile Earth orbit. One blasts off for Mars and arrives at a 300-mile orbit around Mars with 541,000 lb. One has a 20-day stopover time during which time 2 crew members make a Mars landing using a 79,500 lb lander which also returns the men to the 300-mile orbit. One now has 460,000 lb left in the Mars orbit. Again one takes off from Mars with a resultant 154,000 lb heading towards Earth. The vehicle is on a trajectory that is a fly-by past the Earth. As the vehicle approaches the Earth, the crew climbs into a 42,000 lb capsule which, by chemical rockets, is slowed down to about 15 km/sec as the approach velocity. The total weight is now 14,000 lb. Using aerodynamic braking one finally arrives on Earth with 10,000 lb. The total round trip takes 455 days.

In the STL study the manned capsule was 92,000 lb, of which about 23,000 lb was shield. Later in this calculation the manned capsule and shield will be assumed to have a total weight of 110,000 lb.

In this study using electric propulsion, an  $\alpha$  of 4.0 kg/kW will be assumed for the moment, although the value given in a previous chapter was 3.0 kg/kW. For the moment, the total manned days will be assumed as 456 days.

03113  
225

~~CONFIDENTIAL~~  
SECRET

One starts with one Saturn payload, or 240,000 lb, in a 300-mile orbit. This vehicle is a freighter which contains the Mars lander. This freighter is sent off early. Assuming 35 days to escape and 344 days transfer to Mars, one ends up with 182,000 lb in a high-level orbit around Mars. Of this weight 46,000 lb is engine, 80,000 lb is lander and 56,000 lb is propellant.

While the freighter is on its way to Mars, two more Saturns are placed into a 300-mile orbit. The weight is 480,000 lb. This will become the manned vehicle. This vehicle then takes 30 days to go to a high-level orbit which is past the Van Allen belt. The crew is then sent up to this high-level orbit to meet this vehicle in a fourth Saturn. Taking 264 days, the vehicle arrives at a high-level Mars orbit with a total weight of 319,000 lb. The crew that is going to land on Mars now transfers to the lander. Using the freighter engines they take 10 days to descend into a 300-km orbit and then use the lander for the rest of the trip down and back up to the 300-km orbit. Again the time on Mars is assumed to be 20 days. The freighter engines are again used to take the crew back up to the high-level orbit to the manned vehicle in 10 days. The total time at Mars is 40 days. The total weight expended at Mars is a 80,000 lb lander plus 20,000 lb of propellant. The freighter's engine and remaining fuel are now attached to the manned vehicle, giving a total weight of 401,000 lb. Taking 152 days, one then arrives back at a high-level orbit at Earth with a total weight of 350,000 lb which is made up of a 159,000 lb engine plus 191,000 lb of payload, which is almost the size of one of the original Saturns. How much of this weight is really payload and how much is shields for various purposes is anyone's guess.

A comparison between this study and the NERVA study is difficult at this point. In this case, the manned vehicle ends up with a zero velocity relative to the Earth orbital velocity. In the NERVA study, the crew abandons the ship as it is racing towards the Earth, so that I do not have an equivalent weight for comparison at the moment.

SECRET

~~CONFIDENTIAL~~  
03110

A rather interesting question is how sensitive this mission is to the value of  $\alpha$ . In Fig. 12.5, the payload plus structures and shield are plotted as a function of  $\alpha$ , the curve labeled A is this freighter-type mission. One sees that even at a value of about 7 kg/kW one still delivers back to Earth about 120,000 lb.

Suppose one did not use the separate freighter concept but instead took the freighter with the crew. Then the payload plus structures and shield delivered back to the same Earth orbit is shown by curve B. As one expects for the small values of  $\alpha$  the two payload values are very close; however, for an  $\alpha$  of about 7, the manner in which the mission is performed becomes important.

Another very important point is concerned with the propulsion time: What is the reactor lifetime? For the freighter-type mission, this is shown in the Fig. 12.6. For an  $\alpha$  of 7 one needs only 5,000 hours for this mission. This is considerably shorter than the usually quoted number of 10,000 hours. Next, one sees that as  $\alpha$  is decreased, the payload goes up and the running time goes down, so that for an  $\alpha$  of 3 kg/kW the payload is 220,000 lb and the propulsion time is less than 2000 hours.

Next, one probably does not want to return to Earth with 220,000 lb so one could instead reduce the total manned trip time. The manned capsule in the NERVA study was 92,000 lb. Here we will assume 110,000 lb returned to an Earth high-level orbit. In Fig. 12.7 the manned trip time is shown as a function of  $\alpha$ . This is for the case using a separate freighter. At an  $\alpha$  of 3.0 kg/kW, the time has been reduced to 349 days which is made up of 189 days transfer to Mars, 40 days stay at Mars and 120 days return. In Fig. 12.8, are shown the propulsion times required for this mission. Again 5,000 hours is adequate for an  $\alpha$  of 7 kg/kW; and, as the  $\alpha$  is decreased, the running time is also decreased to less than 2500 hours.

Another mission was also considered. Starting with an initial weight of 1,680,000 lb in the 300-mile Earth orbit, 456 manned days, and a

228  
03110

~~CONFIDENTIAL~~  
CONFIDENTIAL  
SECRET

payload of 110,000 lb returned to Earth, the  $\alpha$  required was about 13 kg/kW.

It is admitted that perhaps the missions studied here are not the best ways of performing the manned Mars mission; however, a few general statements can probably be made concerning this mission. At an  $\alpha$  of about 13 kg/kW, the NERVA system and the nuclear electric system just about break even. As the  $\alpha$  is reduced the nuclear electric performance increases rapidly. At an  $\alpha$  of 7 kg/kW, the performance is extremely good compared to NERVA. Of course, the predicted value given in Chapter 8 is about 3 kg/kW. Therefore, the obvious lesson from this chapter is that a nuclear electric system can do the manned Mars mission faster and with less initial weight than NERVA.

Next, the present 10,000-hour requirement should be reduced below 5000 hours. The people doing mission studies should be very careful about quoting propulsion times because, as shown in a previous chapter, the longer the running time the larger becomes the value of  $\alpha$ . Then from the mission view point, the large  $\alpha$  requires longer running time and around you go again.

It is my belief that the 10,000-hour requirement has been detrimental to the entire nuclear electric propulsion effort. A more realistic value or set of values should be established.

#### References\*

1. C. G. Sauer, Jr., and W. G. Melbourne, "Optimum Earth-to-Mars Round-trip Trajectories Utilizing a Low-Thrust Power-Limited Propulsion System," Jet Propulsion Lab Report JPL-TR-32-376, March 29, 1963.
2. W. G. Melbourne, and C. G. Sauer, Jr., "Optimum Thrust Programs for Power-Limited Propulsion Systems," Jet Propulsion Lab Report JPL-TR-32-118, June 15, 1961.
3. A. R. Chovit, C. D. Kylstra, and R. K. Plebuch, "Defining Nuclear-Rocket Performance," Astronaut. Aeron. 3, p. 36 (June 1965 ).

\*Asterisks in text and in figures indicate work performed by Messrs. Melbourne and Sauer at the Jet Propulsion Laboratory, California Institute of Technology, sponsored by NASA under Contract NAS7-100.

SECRET  
229

~~CONFIDENTIAL~~  
CONFIDENTIAL

~~CONFIDENTIAL~~  
03170

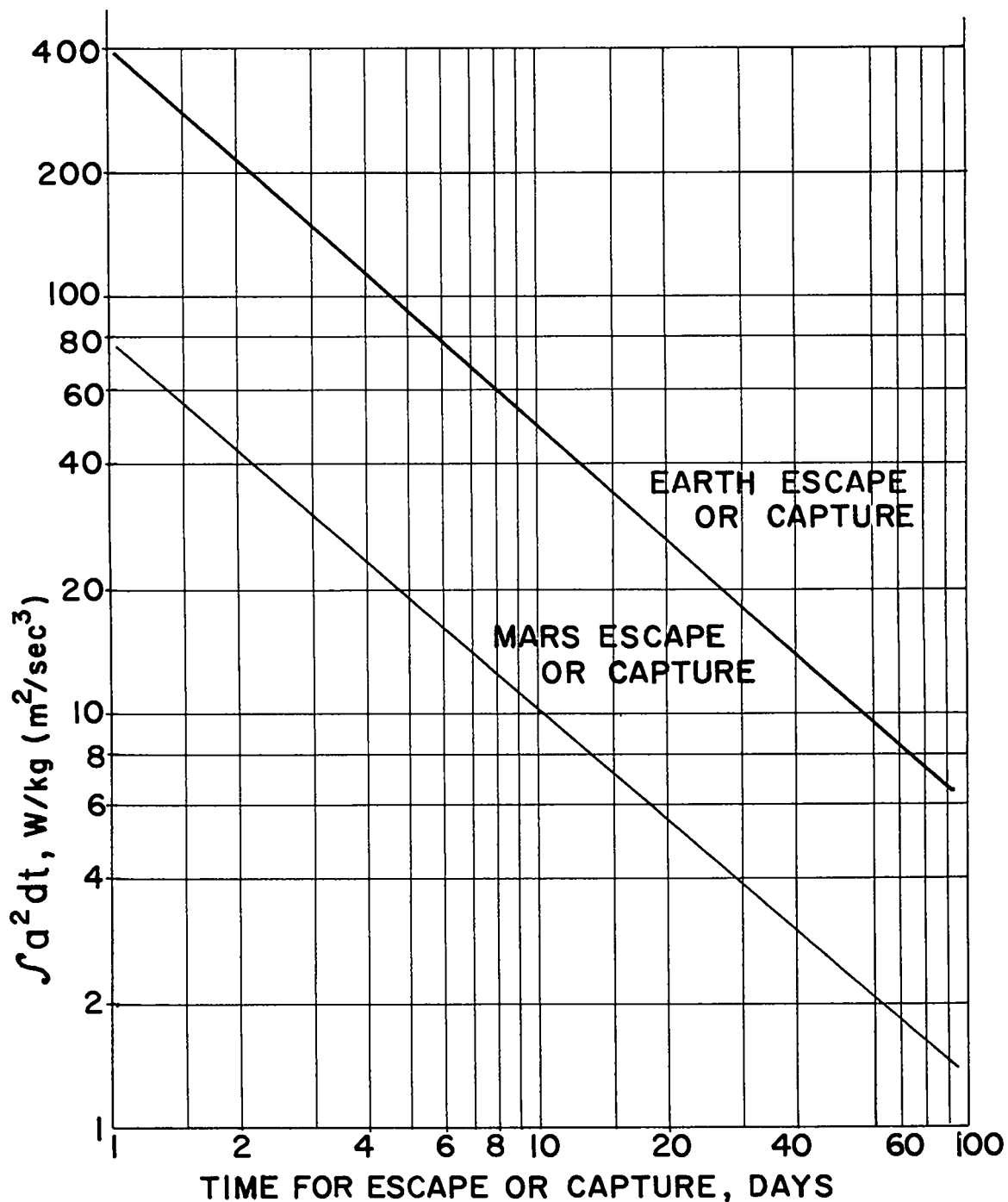


Fig. 12.1\* Earth and Mars:  $\int a^2 dt$  versus escape or capture-time.

03170  
230

~~CONFIDENTIAL~~  
SECRET

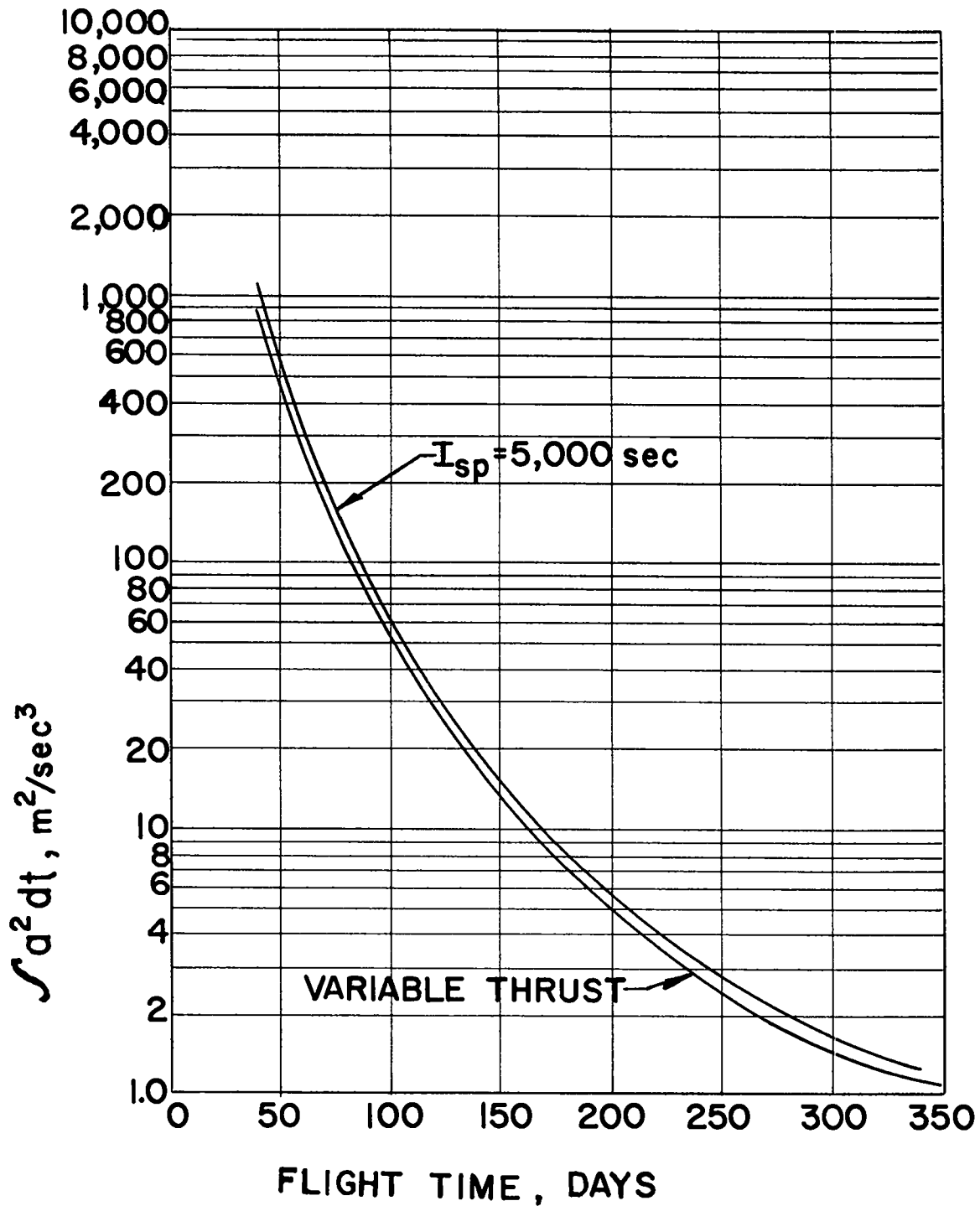


Fig. 12.2\* Flight time versus  $\int a^2 dt$ .

~~CONFIDENTIAL~~

031710

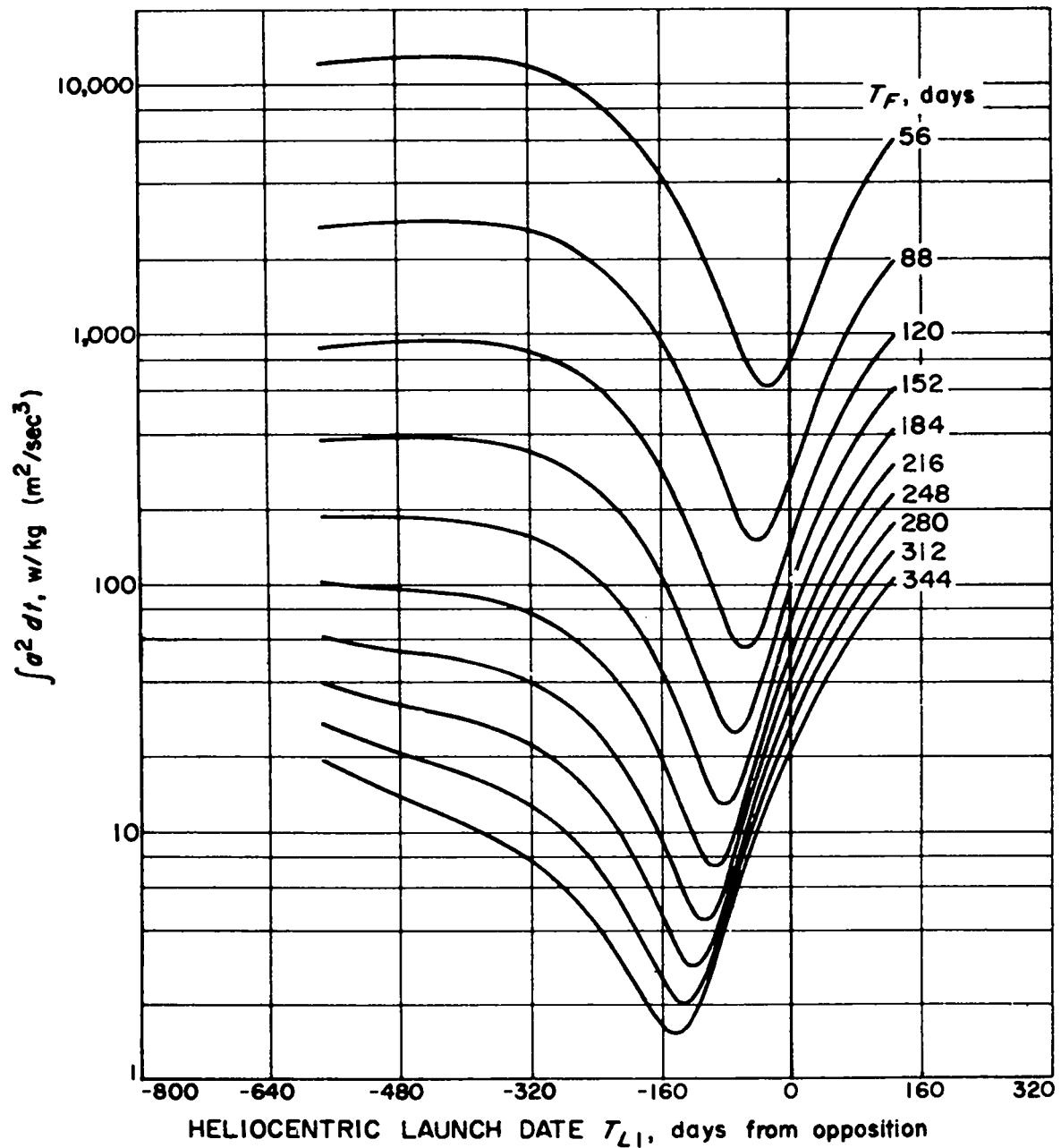


Fig. 12.3\* Heliocentric launch date  $T_{L1}$  versus  $\int a^2 dt$ .

031710 234

~~CONFIDENTIAL~~

SECRET

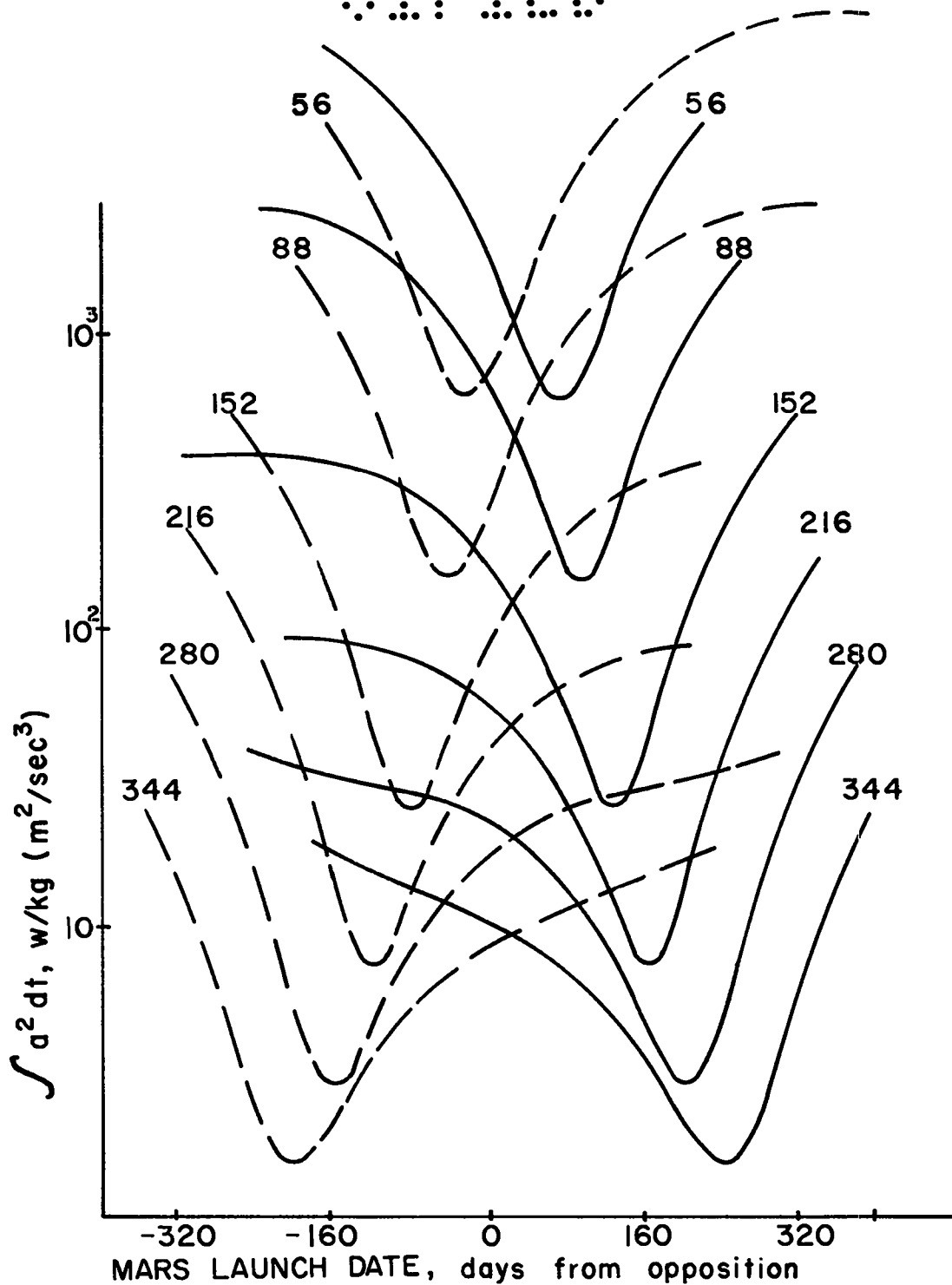


Fig. 12.4 Mars launch date versus  $\int a^2 dt$ .

SECRET



~~CONFIDENTIAL~~  
033413

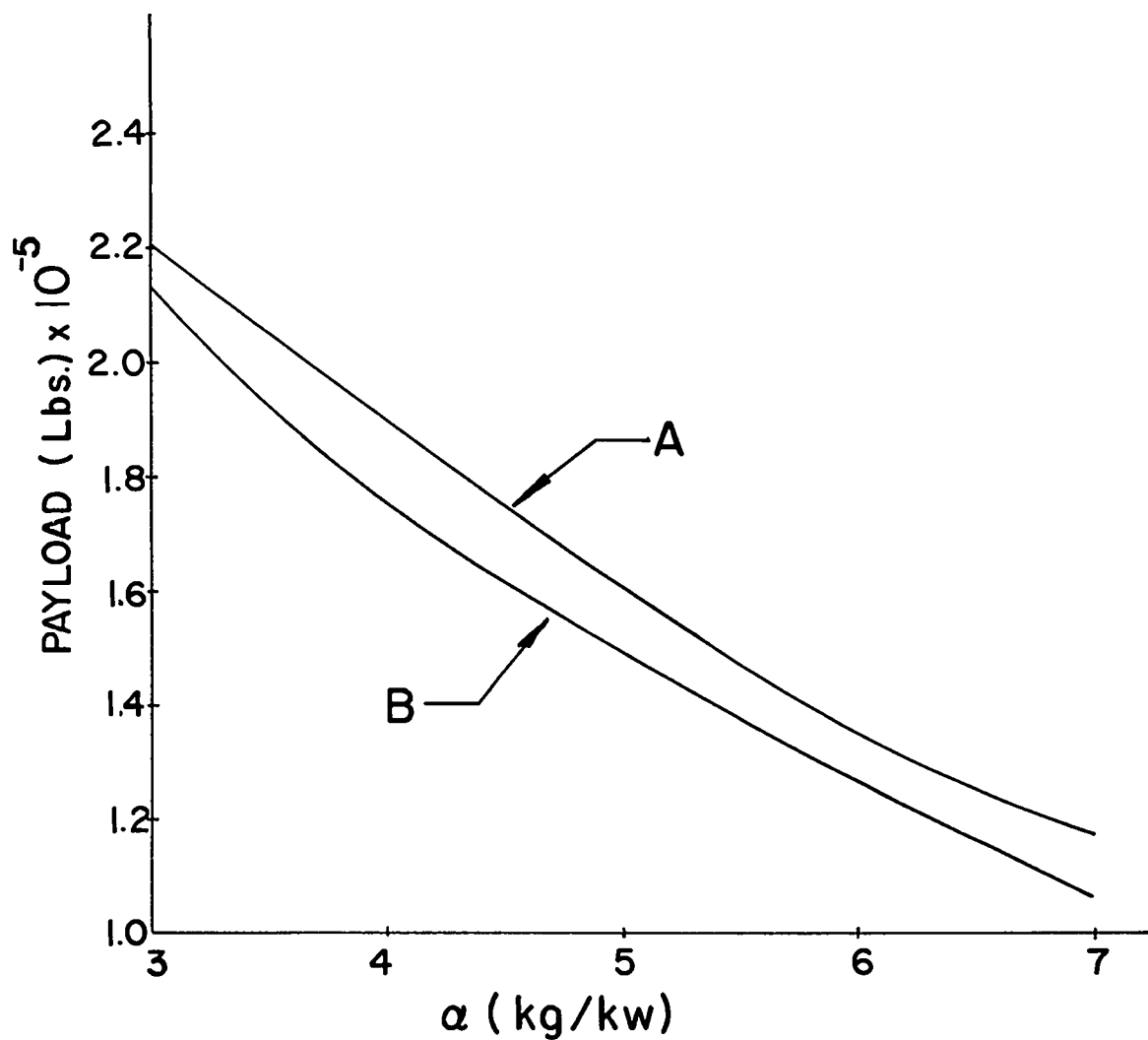


Fig. 12.5 Engine specific mass versus payload

033413 23

~~CONFIDENTIAL~~  
01100

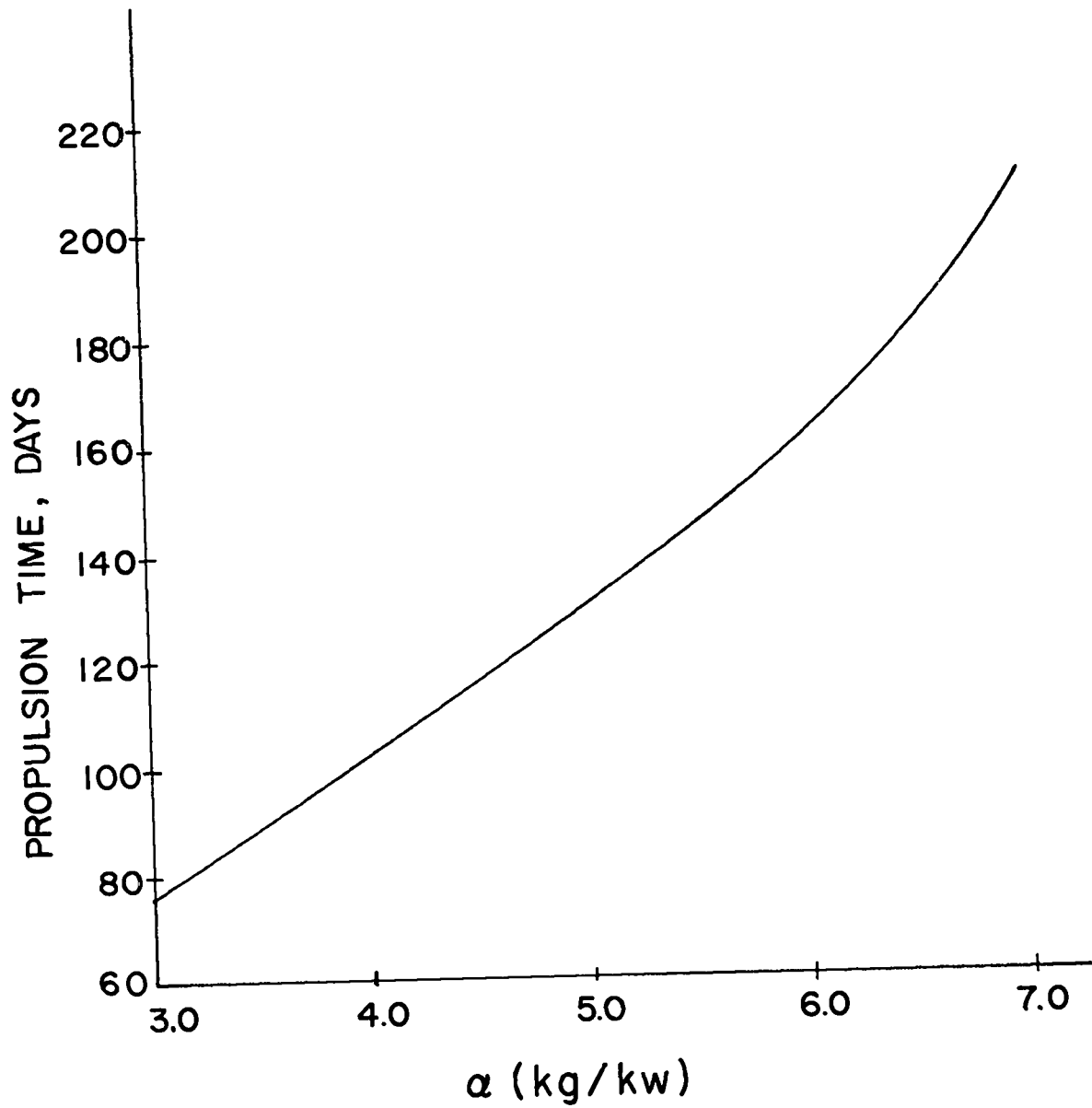


Fig. 12.6 Engine specific mass versus propulsion time.

235  
01100

~~CONFIDENTIAL~~  
APPROVED FOR PUBLIC RELEASE

031712

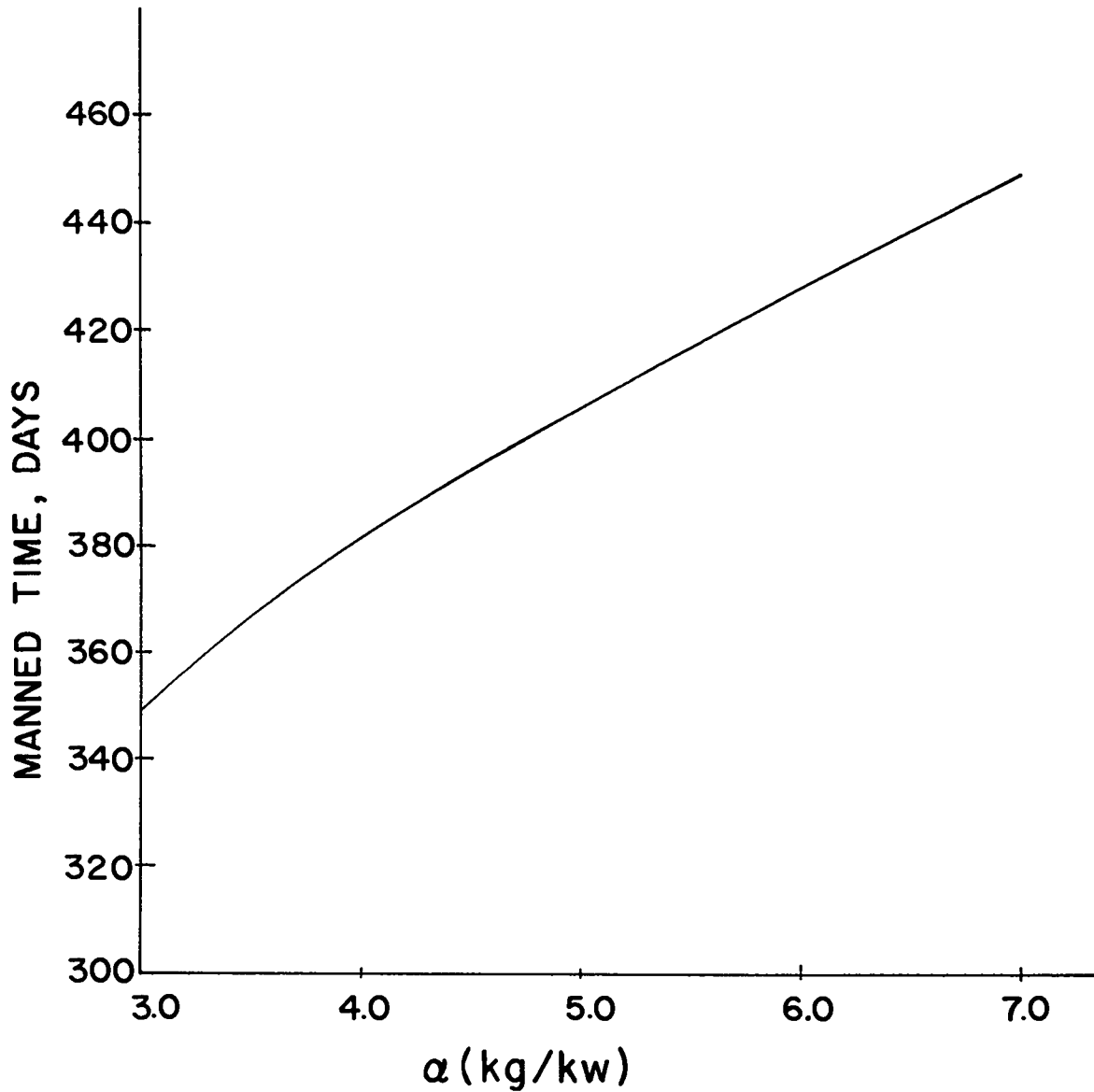


Fig. 12.7 Engine specific mass versus manned time.

031712

235

~~CONFIDENTIAL~~  
21810

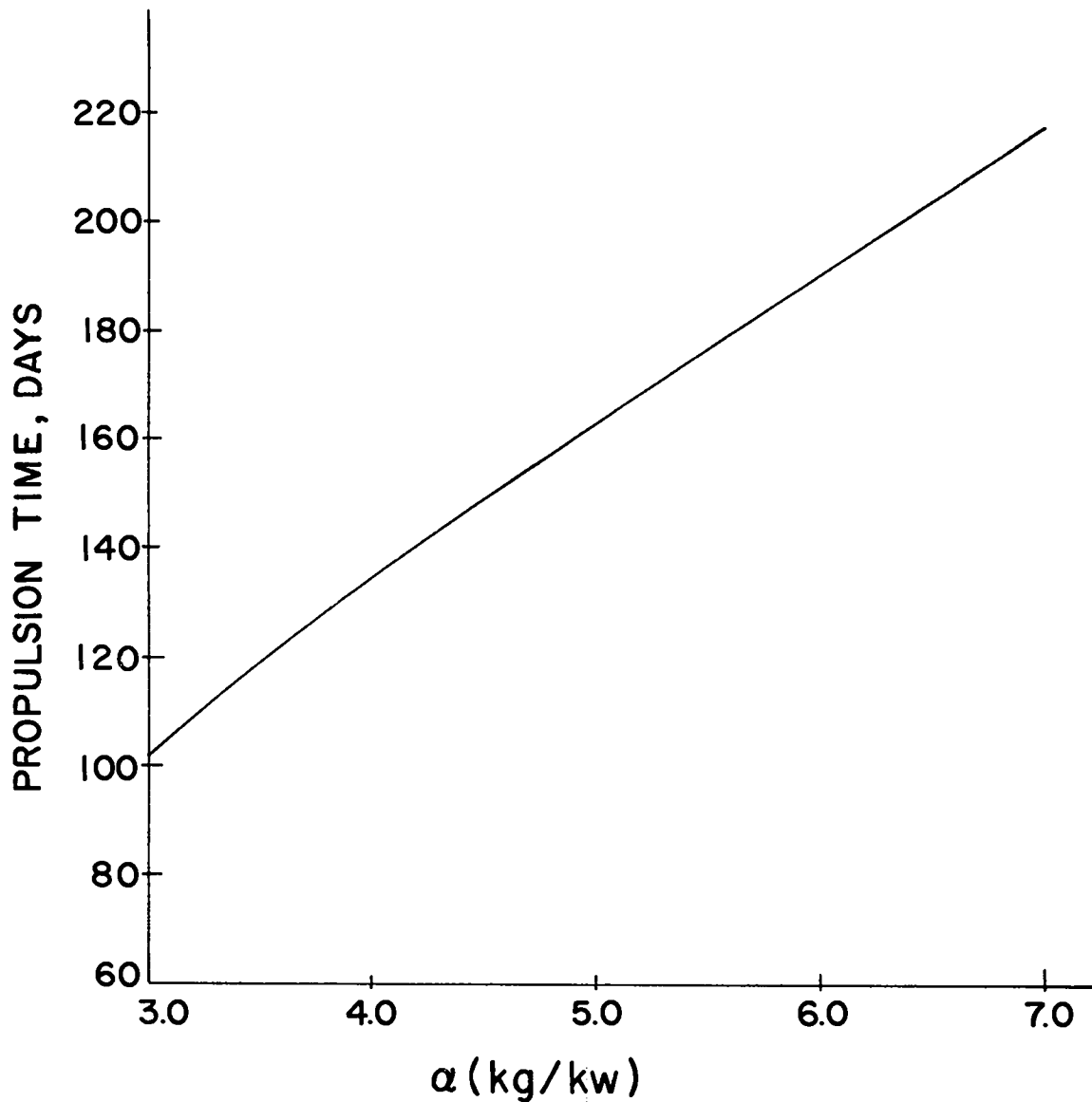


Fig. 12.8 Engine specific mass versus propulsion time.

21810<sup>237</sup>

~~CONFIDENTIAL~~  
03713

## 13. Summary

George M. Grover

In order to acquaint members of N-Division with some of the glowing prospects, and also some of the problems, of thermionic nuclear electrical propulsion for space, N-5 has presented a series of lectures on this subject. The salient points of these lectures are summarized in this chapter.


For this study, a modular concept of space ships is developed. The manned mission to Mars, for instance, requires from 10 to 50 MW of jet power, depending upon the mission time, payloads, etc. We are considering a 2-MW jet engine, reactor, and radiator module. Thus, five to twenty-five such modules must be grouped together to accomplish this mission. Larger modules are possible but from the view of redundancy, economy of development, and flexibility the 2-MW module appears quite desirable.

Arc Jet Engine

The ion or plasma propulsion component of the system is considered first. The output voltage, characteristic of a thermionic reactor, will be around 100 volts. If the engine can use this voltage without transformation, savings in weight of the overall system can be made. Various estimates for power conditioning range from 0.5 to 3 kg/kW(e). This is not a fatal penalty, but certainly it is a serious one. Because of space charge, ion propulsion usually demands high voltages. On the other hand, the recent arc jet experiments indicate promise of an operable

03713<sup>238</sup>

~~CONFIDENTIAL~~

  
SECRET

low-voltage, relatively high-efficiency engine. Most experiments on arc jets have been done using hydrogen. Limitation on pumping of the container creates a great uncertainty in the resulting data. Experiments using condensable vapors, cesium and lithium, are underway at LASL to discover and understand the performance of the arc jet accelerator with and without auxillary magnetic fields. A theory of its operation has been proposed, and the parameters from the theory have been used in this system study. These are, briefly, that a 120-volt, 2.6-MW electrical supply driving a concentric arc using lithium will produce a 5000-second  $I_{sp}$  beam at 75% conversion efficiency.

#### Heat Pipe Radiator

The recent developments in high-temperature heat pipe technology offer the prospect of a completely static system for power generation. The major problem of radiator design is to obtain high reliability of operation despite meteorite damage while maintaining a low overall weight for the power dissipated. Since a heat pipe is a closed and independent system, a multiplicity of the pipes interconnected in series and parallel provides such reliability. The high degree of redundancy offers more than just reliability. It also offers a predictability factor to offset inadequate input information. Suppose, for instance, that the meteorite damage flux is higher than expected. A failure rate can be determined and recovery steps initiated before complete failure occurs.

A design study has been made which indicates that each heat pipe or "cell" in the interconnected radiator optimizes as a cell of height equal to its diameter. The radiator must be composed of an adequate number of these cells to satisfy the redundancy criterion. The minimum size cell is somewhat arbitrary and subject primarily to fabrication limitations. Of course, the cluster of cells must expose a sufficient number of external members to radiate the required energy. The internal cells in the cluster transfer the heat through multiple interconnected

SECRET 239

~~CONFIDENTIAL~~  
03713

paths from the reactor to these surface cells for radiation to space. In the 2-MW module design, 17.6 thermal megawatts must be radiated. Choosing the cell size as 4 inch x 4 inch cubes, one arrives at numbers of cells exposed to the meteorite flux like 20,000 to 30,000. This degree of redundancy allows very thin-walled structures; and, based on this theoretical study, at a temperature of 1200°K a specific weight of 0.05 kg/kW(t) is indicated.

Corrosion studies of heat pipes in this temperature range have been astonishingly successful - the first heat pipe constructed of Nb-1 w/o Zr tubing and wicking with lithium as the working fluid has operated at 1100°C in vacuum for over 4000 hours.

Much more effort must be expended on design studies of cellular heat pipe radiators before exact specifications can be determined. For the purpose of this study, the theoretical number of 0.05 kg/kW(t) was doubled to allow for the uncertain state of knowledge as of this date.

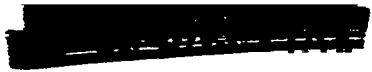
Another approach to the heat dissipation problem is the moving belt radiator. Although this removes the system from the completely static category, the theoretical performance number is in the same ball park as the heat pipe radiator. One approach leads to a value for  $\alpha$  of .05 kg/kW(t) which is the same as the heat pipe radiator  $\alpha$ .

#### Fuel Pin

The heart of the thermionic reactor is the emitter fuel pin. In truth, this does not differentiate it from any other reactor. The fuel must furnish the uranium for criticality, dissipate the fission heat, and accommodate the fission product buildup. In addition, in a thermionic reactor, it must be insulated from other components of the fuel rod, conduct the generated current, and emit electrons either from its surface or a cladding over its surface.

For several years an effort was made to use bare UC ZrC as the fuel. The high uranium density, good electron emission properties, and good thermal and electrical conductivity were assets which this fuel possessed.

03713<sup>240</sup>

  
SECRET

In contrast, the high thermal emissivity, the marginal evaporation rate and, finally, the inability to withstand swelling due to fission product buildup or to vent these products at high burnups have been characteristic of all UC ZrC fuel pins tested at LASL. As a backup, work was also going on using a Mo- $\text{UO}_2$  cermet fuel with a vapor-deposited tungsten coating to prevent  $\text{UO}_2$  evaporation out of the molybdenum matrix. It is this combination which has been found to have excellent qualities as a fuel for a thermionic reactor. The pins are fabricated either by isostatically pressing and sintering or by hot pressing molybdenum and  $\text{UO}_2$  powders. Experiments show that in the resulting matrix; both the molybdenum and the  $\text{UO}_2$  are continuously connected, that is, continuous channels of about  $25\mu$  average diameter permeate the sponge of molybdenum. These channels are not completely filled with  $\text{UO}_2$  and venting of the products can occur.

Specimens of low (9%) and high (13%) initial open porosity have been examined by x-ray photography after 4000 hours of irradiation at 300 watts/cc and  $1800^\circ\text{C}$ . The low-porosity pin showed swelling of less than 5% on the diameter. No swelling could be detected in the three high-porosity samples. After 5000 hours, four other samples were examined in the hot cell. No gross distortion or cracking had occurred. A roughened appearance of the surface could have altered the thermal emissivity. The average swelling on the diameter was 2% for the high-porosity pin and 5% for the low-porosity pins.

The lower range of swelling of the fuel pin could be tolerated in an operating cell. However, further investigation of the effect of porosity and better control of the thickness of the vapor deposited tungsten layer, which varied from 0.002 inch to 0.010 inch in these tests, could lead to further improvement in this component.

With the fuel determined, the integral cell becomes the next area of interest. Only in-pile cells were considered. Until heat can be reliably transferred from the core of a reactor in the temperature range of  $1600^\circ$  to  $1900^\circ\text{C}$ , out-of-pile concepts are not competitive in specific

SECRET



CONFIDENTIAL

03715

power for propulsion purposes. The cylindrical stacked cell was considered in detail, but one should note that other arrangements are possible.

In the in-pile converter concept, insulators are used which must withstand the radiation environment for the life of the reactor. Tests on tungsten-metallized- $\text{Al}_2\text{O}_3$ , vanadium brazed to niobium, ceramic-to-metal seals have been made in the MTR and LAMPRE reactors up to a dose of  $3.1 \times 10^{20}$  nvt (Neutrons of  $> 1.0$  MeV). This was done at a temperature of about  $700^\circ\text{K}$ . At this irradiation level, a small but detectable expansion of the ceramic occurred. The seals, with one exception, were still vacuum-tight but it is impossible to say how much further radiation could have been tolerated. Consideration of this limit of testing was made in the reactor design portion of this study. At this point in the state of testing, a degree of thermalization of the reactor must be provided until a time when further studies of fast flux damage and annealing rates are made.

The "triple layer" insulator, common to all designs of in-pile converters, is a more sensitive region with regard to voltage breakdown at temperature and in a fast flux. Annealing effects at high temperatures should establish a steady state equilibrium with damage, but insufficient information exists to pinpoint the degree of seriousness of the problem. A compensating factor in some stacked cell designs is that this layer need not be vacuum-tight, since it is isolated from the cesium by the seals. Uniform thermal contact over relatively large areas makes this a major fabrication problem.

#### Basic Physics

The basic physics of thermionics conversion is well covered in other sources. There has been a tendency toward closer spacing of diodes to minimize the plasma impedance drop and achieve very high power outputs per square centimeter of emitter area. Unfortunately, these high power densities are obtained at high currents and at a fraction of a volt. Since a practical cell involves voltage drops along the emitter and

03715

~~CONFIDENTIAL~~  
01110

collector as well as in the connecting leads, an analysis of a cell to obtain maximum efficiency operation always places the operating point well toward the open circuit end of the I-V characteristic. In fact, at a 2100°K emitter temperature, the 10 amps/cm<sup>2</sup> - 1 volt region gives the maximum efficiency which is of the order of 13% to 16%. Diode spacing of 10 mils rather than the more difficult 2 to 4 mils spacing is adequate; and, in addition, the I-V characteristics in this low current range are relatively insensitive to the bare work function of the emitter. This was illustrated in Fig. 5.10. Thus, long time changes in the emitter have little or no effect on the cell performance. Another important point is to be found in the desired collector work function. Normally, the lower the collector work function, the better the cell. But with an additional boundary condition requiring high dump temperatures to radiate the waste heat in space, any attempt to improve the performance of the cell by lowering the work function of the collector below about 1.7 volts is frustrated by the formation of a back emission barrier in front of the collector. Thus, nickel, molybdenum, or tungsten wetted with cesium give this value or below; and changes of the bare work function over this range have no effect. Only niobium collectors at the highest dump temperatures are to be avoided, since at the operating cesium pressures the work function is not depressed to the optimum or limit value.

#### Cell Discussion

In view of the discussion above, the operating characteristics of the cell were taken to be 10 watts/cm<sup>2</sup> - 10 amps/cm<sup>2</sup> at 1 volt - at 13% efficiency. The tungsten cladding of the Mo UO<sub>2</sub> fuel is the emitter, and at 2100°K these values are realistic for a diode spacing of 10 mils based primarily on out-of-pile experiments. In-pile performance studies have not covered the range of emitter-collector temperature distribution necessary to confirm these values in detail, but sufficient work has been done to make one feel that these are reasonable values. In the design of the cell, thermal losses and voltage drops must be treated in detail. From the properties of the materials of construction, these losses and

01110<sup>243</sup>

CONFIDENTIAL  
03110

and drops are quite firmly established. One can thus design in detail the stacked cell assembly. Certain design decisions must be made, such as those relating to retention of products in the fuel, venting of these products into the cesium diode space and then to space, or venting the products to free space directly. But, given the fuel characteristics, the design of the stacked rod assembly is completely straightforward. The pin diameter is determined from the balance of power generated and power removed from the surface. The pin length is obtained from a balancing of the voltage drop along the pin, which favors shortening the pin, against the end losses, which favor lengthening the pin. For our parameters and materials, a diameter of one centimeter and a length of five centimeters is about optimum for a single-ended pin support. It can be shown that the collector resistance should equal the pin resistance for maximum specific power of the cell. Thus, the collector thickness is determined.

The collectors are separated from one another by ceramic-to-metal, vacuum-tight seals as shown in Fig. 7.1. Also the collectors must be insulated from the coolant flow, since this coolant is a liquid metal and would short the collectors if no insulation were provided. Since the radial heat flow is relatively large, this insulation layer must be thin and protected, in turn, by corrosion from the liquid metal coolant. Since the insulating layer should be about 10 mils thick, and the outer layer of Nb-1 w/o Zr also 10 mils, vapor deposition of both layers appears to be a feasible method of construction. Stacked cells have been built in various other ways and tested. Only a fabrication study will determine the best design for cells stacked for the length of the reactor.

For 13% efficiency and a fuel power of 300 watts/cc the power out is 39 watts/cc. Since the optimum fuel pin size is about 3.8 cc, each cell produces about 150 watts. For 2.6 MW(e) about 17,300 cells are required. If these are stacked 25 cells to a rod, 692 rods - suitably interconnected - are required for a reactor.

24  
03110

~~CONFIDENTIAL~~  
SECRET

Alternative designs were discussed in Chapter 5. However, 700 rods is not a prohibitive number and, in fact, may be desirable. Interconnections of rods may be made in such a way that failure of a rod does not mean complete inoperability of the reactor. This subject has been explored with respect to single cell interconnections. An extension of this analysis to interconnected rods is desirable. However alternative designs are possible. With the advent of the heat pipe, which can be used in its long tubular form to remove heat from the rod design, other shapes of emitter-collector become feasible. In the form of hollow plates which can act as collectors on their flat surface, the heat is transferred radially to the plate edge and on to radiators. The same rules of power density in the fuel (plus the weight of moderator required for thermalization) hold as for the stacked cell design. Thus in its critical size, the specific power of the reactor is about the same as for the stacked cell reactor, but far fewer individual cells are required per reactor.

#### Scaling Laws

At this point it is expedient to discuss the fast versus the epithermal question, as well as scaling laws and weights derived or assumed for the module.

The fuel we are concerned with, Mo 40 v/o  $UO_2$ , has a density of about 10 g/cc. We have tested this at 300 watts/cc or 30 watts/g for the life of interest - 5000 hours. At 13% cell efficiency we have 3.9 watts/g. Now, why even consider adding moderator which can only increase the total weight without adding to the power output? The reason lies in the state of knowledge of insulator and seal testing. Until further tests are made, we must introduce a degree of thermalization into the reactor design. Relating the test results with the reactor design, using distributed Be within the core, we find that we must now use an  $L (N_{Be}/N_U)$  ratio of about 100 at the present state of the art. This means a distributed weight of Be moderator of about 1.6 times the weight of the fuel.

SECRET

~~CONFIDENTIAL~~  
03110

What happens if we decide we can operate the fuel at 600 watts/cc for, say, half the time? From Fig. 8.5 one can see that there would be some improvement in  $\alpha$  for the reactor but that an even greater improvement in  $\alpha$  is possible if further insulator testing proved that one could allow a faster system. The greatest improvement, of course, is obtained by doing both.

We can list (see Table 8.1) the weights of the components of the system. The shield weight covers only that required for the actuator and sensors and not the shield. It is obvious from this table that if we eliminate all of the moderator from the core, provided the reflector is not drastically altered, the savings in weight of the system results in a reduction in  $\alpha$  from 3.0 to 2.5 kg/kW(e) at a power density in the fuel of 300 watts/cc. It is evident therefore that there is not a large improvement to be gained from going to a fast system from the presently proposed epithermal system.

One further scaling law should be mentioned. This is the dependence of  $\alpha$  on the time of operation. Because of the finite energy available per unit weight of fuel, for long operational times the  $\alpha$  must go up. Also for very short propulsion times which consume the available energy,  $\alpha$  again goes up because of the radiator area increasing very rapidly to obtain a constant meteorite survival probability. Thus a minimum occurs in  $\alpha$ , for our case at a time of 1 to 2 thousand hours.

#### Reactor Calculations

The reactor calculations have been considered in detail only for the stacked rod reactor. The major problem was concerned with flattening the power profiles by variation of the uranium content or enrichment from cell to cell. Thirty variations of either volume fraction or enrichment were required to accomplish this to within  $\pm 1\%$  over the operating life of the reactor. The calculations assumed reflector control and a beryllium-to-uranium ratio of about 100. The cooling of the

246  
03110

~~CONFIDENTIAL~~

SECRET

reactor was assumed to be with heat pipes, and this required 15% of the beryllium volume as void space for the vapor passages.

From these studies it is evident that the 2-MW electrical level in this configuration is a lower limit. Experimental criticality studies may show that a larger power is required. The important point to remember is that if a larger system is required, the power output and the reactor weight both increase and the  $\alpha$  of the reactor remains essentially constant! As long as the power required for the mission under consideration is greater than about 2 MW, one loses only a certain redundancy from the decrease in the number of modules required for the mission; the  $\alpha$  of the reactor remains unchanged.

#### Manned Mission to Mars

Based on the 2-MW jet modular concept, examination of the configuration and trajectories was made for the manned mission to Mars. For comparison, the STL NERVA study was used as a basis for capsule weights, Mars lander weights, etc. The modular concept allows considerable freedom of configuration; and studies of trip times, propulsion times, initial weights in earth orbit, and payloads were made using both a separate freighter plus a manned ship as well as using only one complete ship for the mission.

On examining the shielding problem for the manned mission, we looked at a configuration using eleven modules on a ring with the command capsule 200 feet away on the axis of the ring. The lithium propellant tanks located below the capsule provided shielding for all except the final leg of the mission - returning to the earth capture orbit. The NERVA study had included about 23,000 lb for a solar flare shield, which other reports consider to be somewhat low. We allowed about 45,000 lb of shield which we assumed was in the form of water. This could be relocated relative to the capsule to provide a flare shield with the reactors off or reactor shielding in periods of low solar activity.

SECRET

031710

A number of important points may be learned from these studies. These will be summarized briefly but reference should be made to the pertinent chapters for more details.

For total trip times equal to or less than those required for the NERVA mission, the propulsion times are in range of 2500 to 5000 hours for an  $\alpha$  in the range of 3.0 to 7.0 kg/kW jet. The often-quoted requirement of 10,000 hours operating time for this mission is nonsense when the  $\alpha$  of the system is in this range.

For this mission, four Saturn V's are required to accomplish the Mars mission with payloads, Mars landers, wait times at Mars and total travel times, etc., in comparison to the NERVA study requiring eight Saturn V loads with the added bonus that the entire return ship is captured in a high-level earth orbit.

Constant thrust with optimum coast-period operation, rather than variable thrust, powered-all-the-way operation, makes better use of the always limited energy available from a power source.

With an  $\alpha$  of about 12 kg/kW jet, this mission is comparable with the NERVA mission, and at this level one could question the economics of developing this system. At an  $\alpha$  of 7.0, the mission is easy. So starting with the value of 3.0 for the system described in these chapters, one must ask what factors could cause this to increase past 7 and into the uninteresting region.

One can list a large number of areas in which work must be done to bring this propulsion system into being. The list does not imply any order of priority in which the jobs must be done. These tasks will not go away; but rather, since work is in progress at laboratories in industry as well as in government laboratories, much has been and more will be accomplished in a rather piecemeal fashion.

#### 1) Fuel

Investigation of the effect of such parameters as pin size and coating thickness on swelling; effect of variation of  $UO_2$  content in the molybdenum matrix.

248  
031710

CONFIDENTIAL

2) Insulators

Triple-layer fabrication and evaluation studies; voltage breakdown and leakage resistance as a function of temperature and radiation environment; extension of seal testing to a higher fast nvt.

3) Cells

Understanding and control of cell degradation where it occurs; design and fabrication studies of .010 inch spaced diodes and fission product venting configurations; research on effect of additives on cell performance - both fission product additives for designs in which the products enter the cesium gap and special substances added for easing the fabrication problem by allowing larger diode spacings.

4) Rods

Fabrication studies of stacked cells into rods and design studies of rod interconnections and cesium feed systems.

5) Coolant

Heat transfer rates for large length-to-diameter heat pipes including the wick distribution system for the returning fluid; investigation of an alternate back-up system of multiple liquid metal pumps to move heat from the reactor to the radiator system.

6) Moderator-Reflector

Investigation of canning or cladding of the beryllium of the moderator and reflector both for protection from liquid metal corrosion and to provide structural stability at the elevated temperatures of the radiator system; experimental criticality and flux flattening determinations.

7) Reactor Control

Studies of the number and worth of rods in the reflector, temperature coefficient of the reactor, cooling of the moving components involved, and applicable actuators.

I am sure that this list could be added to extensively "by those skilled in the art", but this should suffice. There are one or more

CONFIDENTIAL



: : : : : : : :

well-known approaches to each of the tasks in the list. It is true that any one of these items could develop into a definite "problem area," but none can be defined in that manner today.

As for the other major components of the system, the radiator and the thruster, our position can be summed up in a few words.

We have a theory of operation of heat pipes and this has resulted in a design configuration consistent with the theory. We do not know how to build this particular configuration in a way which will withstand launching stresses or, in fact, which will even sustain itself in the atmospheric pressure environment at the earth's surface prior to launching. A design compromise is needed to bring the theoretical concept into a fabricable item. To do this in a logical manner, the first step is an experimental verification of the theory and an extension both in experiment and theory to the phenomena occurring at high heat fluxes through walls and liquid filled wicks. This work is underway in N-5.

The thruster also represents a critical area. If it operates modestly close to the expectations assumed for this study, then the system has delightful possibilities. We will have a system in which the impedance of the thruster matches the impedance of the thermionic reactor, and no power conditioning is required. On the other hand, ion propulsion with its high voltage requirement imposes a power conditioning penalty which could cut into the margin on  $\alpha$ . Perhaps if the present arc jet does not work satisfactorily, we will learn enough from the experiments to build one that will.

Finally, as for the reactor itself, what is the problem? It is evident from these lectures that there is really a wide latitude in the value of  $\alpha$  required to do the manned mission to Mars. In fact this margin is sufficient to build into the system a capacity to absorb quite an amount of component degradation and component failure. But how much is required?

Before committing a large effort into this system, one would like to know the payoff but this is tied closely to the failure analysis of

UNCLASSIFIED

230  
03115~~CONFIDENTIAL~~

~~CONFIDENTIAL~~  
SECRET

UNCLASSIFIED

components. To build 100 cells or 100 rods under carefully controlled conditions and test these in a reactor, obtain the mode of degradation and failure, and obtain from these results the effect on  $\alpha$  is, itself, a big effort. One would probably only be satisfied by testing these in a realistic reactor environment (both flux and temperature) and such a reactor does not exist. So the argument is closed on itself - you must make a large-scale effort to determine if the effort is worthwhile. Based on the data presented in these chapters, there is a high probability that such an effort would be worthwhile!

SECRET  
251

~~CONFIDENTIAL~~  
SECRET

UNCLASSIFIED